

# **An Approach for Automated Detection and Classification of Pavement Cracks**

A thesis accepted by the Faculty of Aerospace Engineering and Geodesy of the University of Stuttgart in partial fulfilment of the requirements for the degree of Doctor of Engineering Sciences (Dr.-Ing.)

by

**M. Sc. Bara' Wasfi Al-Mistarehi**

born in Irbid-Jordan

Main referee : Prof. Dr.-Ing. habil. Volker Schwieger  
Co-referee : Prof. Dr.-Ing. habil. Dieter Fritsch  
Date of defence : 18.03.2016

Institute of Engineering Geodesy (IIGS)  
University of Stuttgart  
2017



## Contents

<b>Abstract</b> .....	5
<b>Zusammenfassung</b> .....	7
<b>1 Introduction</b> .....	9
1.1 Motivation .....	9
1.2 Objectives.....	11
1.3 Thesis Outlines .....	12
<b>2 Crack Detection and Classification-An Overview</b> .....	14
2.1 Introduction to Different Types of Flexible Pavement Distresses .....	14
2.1.1 <i>Distress Types</i> .....	14
2.1.2 <i>Severity Levels</i> .....	16
2.2 Data Distress Acquisition Methods .....	20
2.2.1 <i>Manual Acquisition Methods</i> .....	20
2.2.2 <i>Automatic Acquisition Methods</i> .....	21
2.2.2.1 <i>General Characteristics for Different Automatic Acquisition Systems</i> .....	21
2.2.2.2 <i>Examples for Different Automatic Acquisition Systems</i> .....	22
2.2.3 <i>Manual vs. Automatic Data Collection</i> .....	24
2.3 Distress Data Analysis .....	25
2.3.1 <i>Image Processing for Crack Detection- An Overview</i> .....	25
2.3.2 <i>Digital Image Processing</i> .....	26
2.3.2.1 <i>Convolution concept</i> .....	27
2.3.2.2 <i>Edge Detection Filter</i> .....	29
2.3.2.3 <i>Basic Morphological Operations Review</i> .....	31
2.3.3 <i>Image Analysis (Image Interpretation)</i> .....	36
2.3.4 <i>Review of some Global and Local Binarization Techniques</i> .....	39
2.3.5 <i>Partial and Complete Crack Detection Algorithms</i> .....	43
<b>3 Preparation Stages for Crack Extraction</b> .....	56
3.1 Image Enhancement Algorithm (Pre-processing stage) .....	57
3.1.1 <i>Theory</i> .....	57
3.1.2 <i>Experimental Results</i> .....	59
3.2 Thresholding (Segmentation Stage) .....	61
3.2.1 <i>Theory</i> .....	61
3.2.2 <i>Experimental Results</i> .....	68
3.3 Crack Connection (Post Processing Stage) .....	69
3.3.1 <i>Theory</i> .....	69
3.3.2 <i>Experimental Results</i> .....	73
<b>4 Crack Extraction and Classification</b> .....	76
4.1 Contouring Algorithm.....	77
4.2 Binary Mask Detection algorithm.....	79
4.3 Classification Algorithm.....	84
4.4 Experimental Results.....	89

<b>5 Discussion of the Algorithm.....</b>	93
5.1 Advantages of the Total Approach.....	93
5.2 Disadvantages of the Total Approach.....	96
<b>6 Case Studies on Crack Extraction and Classification.....</b>	98
6.1 Data Acquisition.....	98
6.1.1 Data Acquisition System of LEHMANN+PARTNER GmbH .....	99
6.1.2 Data Acquisition System of 3D Mapping Solutions GmbH .....	99
6.1.3 The Data Acquisition System of Unicom-Umap Company.....	100
6.2 General Image Characteristics of the Case Studies.....	100
6.3 Evaluation Criteria.....	102
6.4 Evaluations .....	106
6.4.1 Case Study 1: LEHMANN + PARTNER GmbH.....	107
6.4.2 Case Study 2: LEHMANN + PARTNER GmbH.....	109
6.4.3 Case Study 3: LEHMANN + PARTNER GmbH.....	111
6.4.4 Case Study 4: LEHMANN + PARTNER GmbH.....	114
6.4.5 Case Study 5: 3D Mapping Solutions GmbH.....	116
6.4.6 Case Study 6: Unicom-Umap.....	118
6.4.7 Case Study 7: Unicom-Umap.....	120
6.5 Final Conclusion of the Case Studies .....	122
6.6 Performance Evaluations .....	123
<b>7 Conclusions and Future Directions .....</b>	129
7.1 Conclusion .....	129
7.2 Future Directions and Recommendations .....	130
<b>Bibliography .....</b>	132
<b>Appendices.....</b>	147
Appendix A: Introducing overview of Pavement Distress Data Capturing Systems being used worldwide.....	147
Appendix B: Overview of Some Case Studies .....	150
Appendix C: Some Comparative Studies for Performance Evaluation .....	159
<b>Acknowledgements .....</b>	163
<b>Curriculum Vita .....</b>	165

## Abstract

Considerable developments and improvements have been made in the field of automated crack detection and classification in the last few years. Digital image processing techniques for crack extraction are already widely implemented on large highway maintenance projects. In these projects, automated digital analysis of pavement crack images is mainly applied. Obviously, no standard scenario of digital image processing algorithms for crack extraction and classification identified in the literature is guaranteed to obtain desired results in all crack pavement images cases. Previously, several image processing algorithms for crack detection suffered from various drawbacks in crack detection and classification. A critical shortcoming is that some extrinsic objects, such as lane markings, sidewalks, and railways will be falsely identified individually as crack detection regions. In addition, human intervention is required to some extent. Moreover, some complex types of cracks, such as block types, are particularly difficult to detect. The development of a four-stage approach in this thesis overcomes these weaknesses by developing a new approach that combines and modifies currently existing digital image processing techniques. For the preparation stages, a combination of different morphological operation techniques is employed to correct background illumination. An automatic local adaptive thresholding algorithm is also realized to distinguish between extrinsic objects and pavement cracks.

For the third crack connection stage, an automatic fusion approach is established. This fusion approach is based on a hole-filling algorithm, including the dilation process several times, as well as the connected component algorithm. Furthermore, a complete description is given regarding the different advantages of this integration approach, including filling crack holes, retrieving crack connectivity, as well as reducing noise and distortion of geometrical size and shape of any remaining extrinsic objects. Local automatic analysis is also carried out through this fusion approach, which ignores several extrinsic objects and facilitates crack extraction only.

For the fourth crack extraction and classification stage, an automatic integration approach is implemented. This integration approach is based on the contouring algorithm, the modified binary mask detection algorithm, and the modified classification algorithm. Specifically, this integration approach can automatically extract cracks, determine their severity levels, identify their characteristics, and classify them into different types with a high rate of correctness. This overall fully automatic fusion approach significantly outperforms previous state-of-the-art algorithms. In addition, it introduces a new method for distinguishing block crack type that several previous algorithms have not been able to detect. To obtain a better understanding of the terms of mobile mapping systems theory and digital image processing techniques, a brief introduction is presented on these topics.

Seven real case studies with various scene pavement images from different countries were tested in order to demonstrate the generalizability, efficiency, and improvement achieved with the automation. In addition, the developed algorithms are able to extract and classify cracks either from individual images or geo-referenced continuous images (i.e. mobile mapping data). The overall algorithm is used for testing real pavement crack images. Performance is checked by comparing the results with three well-known previous crack detection algorithms. Within the tests, four case studies contain 96, 94, 95, and 96 images, respectively, which were obtained by LEHMANN + PARTNER GmbH Company in Germany. The images of these four case studies have a resolution of 1920 x 1080 pixels. These images contain different types of cracks, lane markings, and lighting conditions. The developed algorithm delivers an average computation time of 3.8 min and the correctness detection rate for the images is 98.9% to complete crack detection and classification. In addition, one case study contains 336 different continuous crack images, which were captured by 3D Mapping Solutions GmbH Company in Germany too. The images of this case study have different resolutions with numerous extrinsic objects, such as railways, sidewalks, oil spots, and shadows. The developed algorithm exhibits a correctness detection rate for the images of 100% in 16.2 min processing time, and detects and classifies the cracks on around 336 continuous mobile mapping images.

Another two case studies contain two images of a circular street, and 200 images of King Fahd Street, respectively, and were collected by Unicom-Umap Company in Saudi Arabia. The images of these two case studies have a resolution of 2058 x 2456 pixels. These images contain different types of cracks, different extrinsic objects, and other pavement textures (different from the abovementioned German case studies). The developed algorithm delivers an average computation time of 15.6 min, and the correctness detection rate for the images is 100% to complete crack detection and classification.

## Zusammenfassung

In den letzten Jahren wurden beträchtliche Entwicklungen und Verbesserungen im Bereich der automatischen Risserkennung und -klassifizierung gemacht. Digitale Bildverarbeitungsmethoden zur Risserkennung werden in großen Projekten zur Wartung von Fernverkehrsstraßen schon weitgehend eingesetzt. In diesen Projekten wird hauptsächlich eine automatische digitale Analyse von Bildern mit Fahrbahnrisen durchgeführt. Allerdings führt keines der in der Literatur beschriebenen Standardszenarien für Bildverarbeitungsalgorithmen zur Risserkennung und -klassifizierung für jegliche Art von Fahrbahnrisen in allen Fällen zum gewünschten Ergebnis. Bisher wiesen einige Bildverarbeitungsalgorithmen zur Risserkennung bei der Ermittlung und der Klassifizierung der Risse entscheidende Nachteile auf. Als besonders kritisch ist die Tatsache zu bewerten, dass andere Objekte auf der Fahrbahn, wie etwa Straßenbahnmarkierungen, Bordsteine oder Schienen, fälschlicherweise ebenfalls als Rissbereiche identifiziert werden. Außerdem ist bis zu einem gewissen Umfang eine manuelle Nachbearbeitung erforderlich. Darüber hinaus sind einige der komplexeren Rissarten (z.B. netzartige Risse) besonders schwer zu detektieren. Der in dieser Arbeit entwickelte vierstufige Ansatz überwindet diese Schwachpunkte, indem er einige der bisher für die digitale Bildverarbeitung verwendeten Methoden in einem neuen Ansatz modifiziert und miteinander kombiniert.

In der Vorbereitungsphase werden zunächst verschiedene morphologische Bearbeitungsmethoden kombiniert, um die variable Hintergrundbeleuchtung zu korrigieren. Außerdem wird ein automatischer lokaler adaptiver Schwellwertalgorithmus eingesetzt, um zwischen Fahrbahnrisen und Fremdobjekten unterscheiden zu können.

Im dritten Schritt, der Verknüpfung der Risse, wird ein automatischer Verbindungsansatz eingeführt. Dieser zusammenfügende Ansatz basiert auf einem lückenfüllenden Algorithmus, in dem neben einem mehrfach ausgeführten Dilationsprozess auch ein Algorithmus zur Detektion von zusammenhängenden Rissflächen zum Einsatz kommt. Darüber hinaus werden die verschiedenen Vorteile dieses Integrationsansatzes detailliert beschrieben, wie zum Beispiel das Füllen von Lücken in den Rissdaten, die Bestimmung der Konnektivität der Risse sowie die Reduktion des Rauschens und eine Verzerrung der geometrischen Form und Größe bei eventuell verbliebenen Fremdobjekten. Außerdem wird durch diesen Verbindungsansatz eine automatische lokale Analyse durchgeführt, die verschiedene Fremdobjekte ignoriert und lediglich die eigentliche Rissfassung unterstützt.

Während des vierten Schritts, in dem die Risse erkannt und klassifiziert werden, wird ein automatischer Integrationsansatz ausgeführt. Dieser Integrationsansatz basiert auf dem Konturerkennungsalgorithmus, einem modifiziertem Erkennungsalgorithmus mittels binärer Maske und einem modifizierten Klassifizierungsalgorithmus. Dieser Integrationsansatz kann automatisch Risse extrahieren, wobei der jeweilige Schädigungsgrad und die Charakteristika eines Risses bestimmt werden und die Risse mit einer hohen Korrektheitsrate in die zutreffende Typ-Kategorie eingeordnet werden. Dieser allgemeingültige, vollautomatische und gekoppelte Ansatz übertrifft bei Weitem die bisher angewandten Algorithmen. Zudem führt er eine neue Methode ein, mit der auch Netzzrisse detektiert werden können. Das ist bei vielen der gegenwärtig angewendeten Algorithmen nicht möglich. Um einen genaueren Überblick über die im Bereich Mobile Mapping Systeme und digitale Bildverarbeitungsmethoden verwendeten Begriffe zu bekommen, wird dazu ein kurzer Überblick gegeben.

Es wurden sieben Fallstudien mit verschiedenartigen Fahrbahnbildern aus unterschiedlichen Ländern untersucht, um die Allgemeingültigkeit, die Effizienz und die Verbesserung, die durch die Automatisierung erreicht werden, zu demonstrieren. Darüber hinaus kann die hier entwickelte Methode zur Extrahierung und Klassifizierung der Risse sowohl bei Einzelbildern als auch bei georeferenzierten, kontinuierlichen Bildfolgen (z.B. für Mobile-Mapping-Daten) angewendet werden. Der Gesamtalgorithmus wird mit realen Fahrbahnrisen-Bildern getestet. Die dabei erhaltenen Ergebnisse werden mit den Ergebnissen von drei bekannten Risserkennungsalgorithmen bezüglich Leistungsfähigkeit verglichen. Zunächst werden dazu vier Fallstudien, die jeweils aus 96, 94, 95 und 96 Bildern bestehen, ausgewertet. Diese Bilder wurden von LEHMANN + PARTNER GmbH (Deutschland) zur Verfügung gestellt. Die Bilder aus diesen Fallstudien haben eine Auflösung von 1920 x 1080 Pixeln. Sie zeigen

verschiedene Arten von Rissen, Fahrbahnmarkierungen und unterschiedliche Beleuchtungsbedingungen. Der entwickelte Ansatz erreicht für die Risserkennung und -klassifizierung eine durchschnittliche Verarbeitungszeit von 3,8 Minuten und eine Korrektheitsrate von 98,9%. Eine weitere Fallstudie mit 336 kontinuierlich aufeinanderfolgenden Riss-Bildern wurde von der 3D Mapping Solutions GmbH (Deutschland) aufgenommen. In dieser Fallstudie haben die Bilder verschiedene Auflösungen und enthalten zahlreiche Fremdobjekte, wie z.B. Schienen, Bordsteine, Ölflecken und Schatten. Der neu entwickelte Algorithmus weist bei einer Verarbeitungszeitzeit von 16,2 Minuten für die Risserkennung eine Korrektheitsrate von 100 % auf und erkennt und klassifiziert die Risse auf den 336 Mobile-Mapping-Bildern.

Zwei zusätzliche Fallstudien wurden von der Unicom-Umap Company (Saudi-Arabien) zur Verfügung gestellt und enthalten zum einen zwei Bilder einer Ringstraße, zum anderen 200 Bilder der King Fahd Straße. In diesen beiden Fallstudien haben die einzelnen Bilder eine Auflösung von 2058 x 2456 Pixeln. Diese Fotos enthalten ebenfalls verschiedenartige Risse, unterschiedliche Fremdobjekte und Fahrbahnstrukturen, wobei sich letztere von den zuvor erwähnten deutschen Fallstudien unterscheiden. Der neu entwickelte Algorithmus liefert bei einer Verarbeitungszeit von 15,6 Minuten eine Korrektheitsrate von 100 % für die Erkennung und Klassifizierung aller Risse.



---

# 1 Introduction

## 1.1 Motivation

In recent years, crack extraction and classification of actual pavement sections has constituted one of the central subjects in highway transportation applications. Crack detection is a critical aspect of pavement maintenance. It enables knowledge about real pavement cracks in terms of their shapes and types, and informs about optimal maintenance decisions. Therefore, crack detection data archiving and recording is currently widely performed due to a huge increase in traffic volume on roads, differences in weather conditions, and poor asphalt materials. As the Army Construction Engineering Research Laboratory (USACERL), USA, notes (SHAHIN/WALTHER 1990), "More than 560 million square yards of actual pavement sections largely require a methodical objective procedure of determining existing cracks for maintenance priorities and rehabilitation (M&R) strategies". It is clear that crack detection for all pavement sections of all countries should be performed and made easily attainable from the asset manager's perspective. However, many challenges exist in crack detection and classification plans associated with executed data acquisition methodologies, data arrangement and archiving, data analysis, and data verification objectives. Thus, a complete systematic procedure for crack extraction and classification is urgently needed (SHAHIN 2002).

To achieve an effective transportation system, roads have to be well maintained. However, roads in most countries, such as Germany, Jordan, and the Kingdom of Saudi Arabia usually exhibit cracks due to temperature deviations, traffic, etc. Most of these countries' streets need a systematic maintenance procedure based on existing cracks. Pavement crack detection and classification is essential to nearly all aspects of pavement engineering. It is a critical process for roadway agencies to accomplish the tasks of pavement evaluation, performance measurement, maintenance, rehabilitation, and reconstruction of the pavement structure. Network-level pavement management systems require accurate crack data to support sound conclusions regarding where and when to invest in highway maintenance, rehabilitation, and construction. At the project level, crack data is critical to correctly diagnose the causes of pavement deterioration, and therefore is used to select the most appropriate remedial measures.

There have been rapid technological advances in pavement cracking surveys for both data acquisition and data interpretation in the past few years. Although the objective advantages of automated data collection and processing for pavement distress surveys are attractive, many agencies are reluctant to adopt these new technologies, because the data quality is perceived to be relatively low. However, there has been a slow, but growing trend in which more agencies are beginning to realize that as long as a proper balance between data quality and full automation is achieved, the level of error in automation is acceptable.

Manual and automatic are two fundamental techniques utilized to detect pavement crack objects (SHAHIN/WALTER 1990). The collection of cracks and their characteristics can be performed with both techniques. However, due to the specific demands of different maintenance plans and the different properties of both techniques, automatic crack detection technologies are preferable to manual ones. The automated crack detection method is performed with an automatic mobile mapping system, which captures continuous images for pavement crack sections. A few novel mobile mapping systems (commercial systems) provide crack information, such as type, length, and width by using digital image processing and analysis techniques. Since the resolution and precision of the detected cracks are based on the image scale, the latter can be selected easily according to the application needs. However, crack detection using digital image processing and analysis techniques is limited due to crack segmentation problems and limited crack classification criteria. Thus, small cracks might not be sufficiently detected. Therefore, by using high resolution pavement images acquired at a short distance in combination with durable digital image processing and analysis techniques, small cracks can be correctly identified with high correctness rate. Due to the robust suitable

image processing approach for each crack detection stage, crack information, its severity levels, and its characteristics are determined, which can be beneficial for maintenance goals and rehabilitation (M&R) strategies. A drawback of crack detection algorithms is that they sometimes encounter problems due to the irregularities of crack shapes. Typically, these drawbacks are solved by utilizing robust digital image enhancement, thresholding, and crack connection stages, which typically help in order to omit extrinsic objects, and extract and classify different crack shapes efficiently.

Automated road crack data acquisition mobile mapping systems could, thus, constitute a viable tool in pavement maintenance management systems to overcome some of the previously mentioned deficiencies. The automation of algorithms could offer numerous advantages for different countries, some of which may include practicality, capabilities of follow-up, easy-to-use digital functions, and documentation possibilities, planning, monitoring, and management. This automated system will identify and analyse factors that have a profound effect on pavement maintenance management systems. Moreover, it will be able to recommend improvements and suitable engineering guidelines within a particular management framework in order to achieve substantial improvement and predictability.

Various state-of-the-art digital image processing algorithms are modified and integrated as tools for crack processes. This enables crack extraction, which is automatically recorded to the archiving datasets. However, there are significant limitations due to natural pavement images and the crack shapes themselves. These limitations are as follows. At first, no theory of crack segmentation existed, since the segmentation of cracks from pavement images is not a straightforward process. This is considered as a case that is dependent on the available datasets. In addition, extraction and analyzing cracks for numerous kilometres of pavement sections requires an automated thresholding-setting algorithm rather than a fixed threshold algorithm. The former must be able to set threshold levels for each image, separating only the cracks from the remaining image, and take variations in pavement textures into account. On the other hand, the latter algorithm is mainly defined by setting a fixed global threshold for the entire section. Moreover, in most pavement image cases, noise, such as black fan belts and black rubber hoses, poses another common problem. This might be caused by the texture of the pavement surface and the pavement surface roughness. These conditions can generate shadows and small surface holes which can collect oil and other debris. Some of these oil spots' pixel regions have the same intensity values as crack pixel regions, which will increase the difficulty of the segmentation process. Sequentially extrinsic objects, such as lane markings, sidewalks, railways, shadows, different illumination conditions, and occlusions (e.g. buildings, trees, traffic loops) lead to greater post-processing efforts for pavement images. However, with the constantly evolving post-processing algorithms and computation software, these extrinsic objects are more able to be excluded.

It has become more evident that only one individual digital image processing crack detection algorithm is insufficient to guarantee desired results, particularly in cases of complex compound cracks and different pavement textures. Many authors have already suggested several digital image processing algorithms for crack detection and classification. As MICHAEL (1992) states: "A large number of image processing algorithms have been designed for analyzing video images. This is the heart of the problem: there are literally thousands of algorithms available, but many are not suited for one reason or the other. Algorithm selection for image processing system design is still very much an art and not a science. The system tends to be highly nonlinear, and so simply reversing the order in which two processes are applied can drastically change the outcome (the analyzed output). Furthermore, each algorithm tends to have a 'magic number' or two parameter values which must be set (such as gain, window size, etc.), and varying these can also change the outcome. Furthermore, varying the parameters of one processing step can change the effectiveness of the settings of a different processing stage (again, because of the nonlinearities involved). We are looking at the order of 50 such processing steps, all interacting with one another in highly nonlinear and unpredictable ways. Algorithm selection is therefore a formidable obstacle". From this perspective, different digital image processing crack detection algorithms have been attempted.

It is obvious that not only one scenario of digital image processing algorithm for crack extraction and classification can be applied. Consequently, in order to realize results that are improved relative to previous algorithms, a new combination and modification approach of digital image processing techniques for crack extraction and classification is proposed in this thesis. Specifically, it utilizes an improved image created from the original image in order to simplify the extraction of cracks by using algorithms of preparation stages for the cracks' extraction. In this thesis, the overall algorithm for crack extraction and classification is introduced in order to classify cracks into different categories. This integration approach can automatically extract cracks and their characteristics with a high rate of correctness. In addition, this developed algorithm achieves an increase in automation in order to meet the requirements of end-users. Finally, it represents an automatic solution for different shortcomings in previous crack extraction and classification algorithms.

## 1.2 Objectives

The main objective of the thesis is to develop an overall digital image processing algorithm in order to extract and classify cracks automatically, in addition to determine severity levels from continuous geo-referenced pavement images. In particular, this overall algorithm will support highway maintenance applications by determining crack characteristics and including location data recording. This is accomplished by generating comprehensive database attribute structures for cracks' distribution. Therefore, the overall method aims at complementing shortcomings in former crack detection algorithms. In addition to improve both the extraction and the classification of the cracks, this overall algorithm addresses critical areas that need to be inspected deeply, such as solving the automated thresholding-setting algorithm problem to avoid detection errors for many kilometres of pavement sections, analyzing noise regions at higher correctness rates, and generating standard rules based on cracks' geometrical size and shape. This approach must be able to be successfully applied in real environments. To achieve this, several preparation stages have been introduced in order to improve the cracks' original image. Then, an automatic fusion of digital image processing algorithms through certain steps can be followed. This also provides a direct solution for distinguishing between cracks and other extrinsic objects, such as lane markings and sidewalks, and especially in cases of images acquired in different lighting conditions or having different pavement textures or shadows. Furthermore, within this thesis, an implicit determination of cracks' type and their severity levels is proposed.

In addition, this thesis will take advantage of the availability of crack types, their severity levels, and characteristics in the form of dataset structures by recoding this information not only for archiving and preservation purposes, but also for maintenance, rehabilitation, restoration, and reconstruction.

Given the above, the following main contributions are achieved in this thesis:

- Generating improved images from original crack images by combining different morphological operation techniques. The advantage of this combination is that the pavement image background illumination is corrected and converted to standardized uniform background lighting conditions automatically. This operation plays a key role to provide accurate required information for the next thresholding stage.
- Developing an automatic robust local adaptive (dynamic) thresholding algorithm for separating image pixels into classes based on the dynamic automatic window size selection algorithm and automatic contrast determination. The automatic window size selection algorithm takes the length and width of the crack object region into consideration, while the automatic contrast determination algorithm is based on the quality of the pavement image foreground and the type of pavement image background. Thus, this leads directly to taking advantage of the determined suitable threshold results in having a suitable window size in relation to the contrast within the pavement image and retrieving more crack details without loss of its local properties. This holds true especially in the

case of existing extrinsic objects, such as lane markings, sidewalks and railways, by changing their pixel intensities to become background pixels during the robust automatic threshold stage.

- Presenting a fully automatic fusion approach for the post-processing stage based on a hole-filling algorithm that includes several dilation processes and labelling a connected components algorithm by means of a colouring scheme. This integration approach can fill crack holes, retrieve crack connectivity, reduce noise, and display a coloured indicator for each crack region. This is particularly useful in cases of noisy pavement images that are occupied partially by lane markings, sidewalks, railways, different lighting conditions, shadows, and other extrinsic objects. In addition to improving crack connectivity and hole-filling, the distortion of geometrical size and shape of any remaining extrinsic objects can be successfully addressed by this fusion approach. Furthermore, any common denominators, such as linear geometrical shapes between these extrinsic object regions and crack regions, are removed with this integration approach. Thus, this fusion post-processing approach for crack detection applications can facilitate accurate crack extraction and classification, in which several linear extrinsic objects can be ignored.
- Presenting and developing an automatic integration approach for the crack detection stage based on the contouring algorithm, the modified binary mask detection algorithm and the modified classification algorithm. This combination approach can automatically specify the exact location of cracks in the original image, modify binary ellipse mask detection based on geometrical size and shape for cracks' region, extract cracks, determine their severity level and characteristics, and then classify it them into different types. The advantage of generating a modified binary ellipse mask is that an implicit determination for corrected crack regions can be successfully achieved without any noise regions. This latter mask holds in several cases of noisy pavement images, including partial lane markings, sidewalks, railways, different lighting conditions, shadows, and other extrinsic objects that are considered as major obstacles in several previous algorithms. In addition, to improve the crack extraction process, the drawback of complex compound crack classification, such as the block crack type, can be solved by the modified classification algorithm. This latter algorithm enables determination of whether the available crack is the main crack or a branch of a block crack type, which provides very good a priori knowledge for perfect classification by means of crack orientation angle and number of crack branches. Moreover, the overall algorithm enables extracting and classifying cracks and their severity levels from continuous geo-referenced images. Overall, the algorithm significantly outperforms previous algorithms.
- Introducing an overall fully automatic fusion method based on integration and modification of existing digital image processing techniques for crack extraction and classification, which are used to detect cracks under different pavement textures and different lighting conditions.

### 1.3 Thesis Outline

This dissertation is organized into seven chapters that offer a description of the overall approaches and the utilized tests. Chapter 1 presents the background and the motivation of this research, the objectives of the study, and the thesis organization. Chapter 2 briefly reviews flexible pavement distress types and previous algorithms' techniques for extracting and classifying cracks and their corresponding shortcomings. Particularly, an overview of the most widely used algorithms and already obtained results are specified, with special attention being paid to the weaknesses of these methods.

The fusion algorithm of the preparation stages for crack detection from pavement images is presented in Chapter 3. The aim is to create improved images with a limited amount of noise and extrinsic objects. In Chapter 4, details about the modified integration algorithms are given starting with two algorithms for extracting crack regions exactly and deleting noise regions absolutely using modified binary ellipse detection masks. These provide precise crack characteristic information for

each crack region. Then, a modified classification approach based on crack orientation angle and number of crack branches is described. Furthermore, experimental results are given using an actual case study to prove the efficiency of the presented approaches. In addition, algorithm advantages and drawbacks are presented in chapter 5.

Chapter 6 presents a selection of various case studies from different countries with different pavement textures and different illumination conditions. In addition, this chapter presents the mobile mapping systems that have been used for data acquisition, the algorithm methodologies that have been utilized, the shortcomings that have been solved, and the obtained results that are compared with previous algorithms. Finally, Chapter 7 summarizes the major contributions achieved, presents conclusions, and proposes several directions for future research.

## 2 Crack Detection and Classification - An Overview

The need for crack detection and classification is continuously increasing. Crack detection has become financially manageable in diverse fields and applications, such as pavement evaluation, performance measurement, maintenance, and rehabilitation. Specifically, crack detection and classification remain desired for network-level pavement management systems. The requirements are mainly specified for several applications, recording, capabilities of follow-up, highway documentation possibility, archiving, and updating. Under these requirements, the approach for crack detection and classification comprises some well-known steps: introduction to different types of flexible pavement distresses, data distress acquisition methods, and distress data analysis, including digital image processing, image interpretation, related algorithms, and an overview of binarization methods. In this chapter, an overview of the most relevant methods to solve the tasks in this thesis is given from different viewpoints.

### 2.1 Introduction to Different Types of Flexible Pavement Distress

#### 2.1.1 Distress Types

Generally, large structures, such as pavements or skyscrapers, are constructed with sensitive materials. These materials exhibit distress after construction because of loading, environmental conditions, and aging. The distresses are presented in the form of surface cracking in most situations. The focus of this thesis is on one of these structures, asphalt pavement. In this section, the leading types of pavement distress are described in detail. Moreover, the central typical indicators associated with each type of pavement distress are given. The definitions comply with those found in German regulations of the Road State Determination Manual (FGSV 2006).

- a. **Cracking** is defined as an individual (single) crack or a network of cracks (Block type) or a crack accumulation. Individual (single) cracks may be distributed in several directions as either vertically, horizontally, or transversely. In a network cracks are connected to one another, similar to a net, with the size being diverse. A network of cracks is classified as a block type. Open and sealed cracks are equally considered. The indicator for crack detection is represented by the area of the cracking region. If there is a problematic distinction between network cracks, crack-accumulations and individual (single) cracks for the same feature, it will be considered an individual (single) crack. Figure 2.1 illustrates the types of cracking.



Figure 2.1: Cracking (FGSV 2006).

- b. **Patching** is an area of damaged road surface that is restored by repairing. The indicator for patching is represented by the area of the patching region. Full-surface layer repairs over the entire lane width, with a total length of more than 20 m, are not considered patch-

es. There are two types of repairs for patching, either laid-on patching or pickled patching/excavation:

1. Laid-on patching: This is defined as an opposite part to the road surface area. It is thin, not flat, and higher than the surrounding road area.
2. Pickled patch/excavation: This is defined as a part of the surface restored by roadway construction. Its surface is infinitely adjusted in height equal to the level of other road surfaces (be-laid layer). Figure 2.2 illustrates patching.

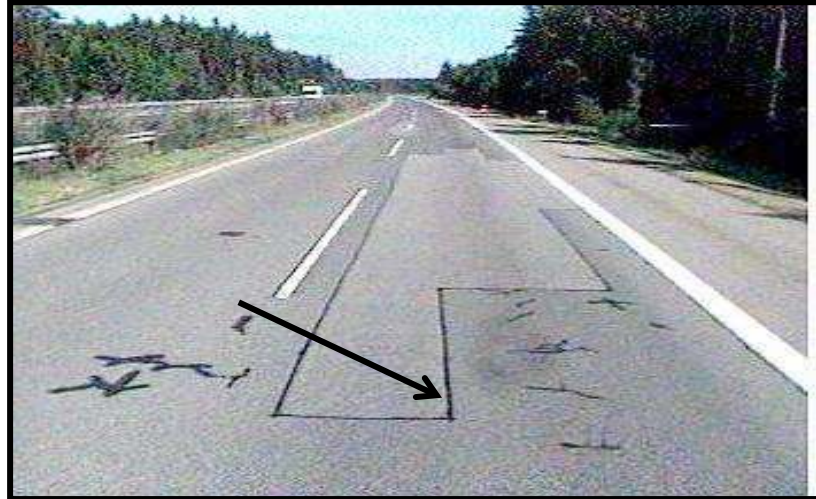


Figure 2.2: Patching (FGSV 2006).

- c. **Out-Breaks (Potholes)** are the detachment of the road surface parts due to traffic, weather, etc. The indicator for out-breaks is represented by the area of the pothole region. Figure 2.3 illustrates out-breaks.



Figure 2.3: Out-breaks (potholes) (FGSV 2006)

- d. **Open Work Seams** are defined as a fine, not connected gap between two asphalt layers. The indicator for open work seams is represented by the sum of length [m]. The affected length by open labour seams is calculated. A problematic distinction exists between individual (single) cracks, network cracks, crack accumulation and open work seams. Open work seams are usually straightforward. They occur in the longitudinal direction due to the limited width of the paver during the installation of the roads. At the same time, open work seams may occur in the transverse direction due to different asphalt layer installation. Therefore, the separation is based on the observer. Figure 2.4 illustrates open work seams.



Figure 2.4: Open work seams (FGSV 2006).

- e. **Binder Enrichment** is the escape of bituminous binder on the road surface. The indicator for binder enrichment is represented by the area of the binder enrichment region. Figure 2.5 illustrates binder enrichment.

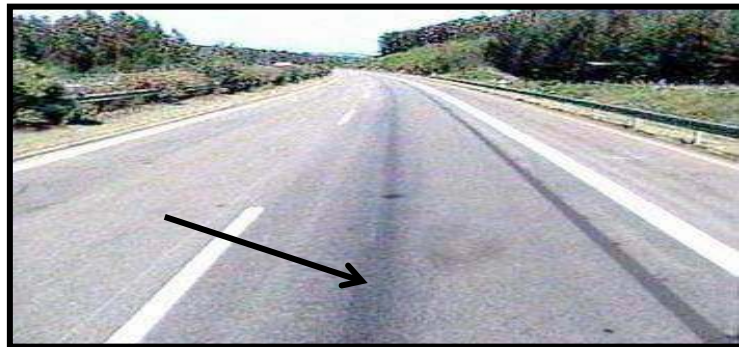


Figure 2.5: Binder enrichment (FGSV 2006).

The framework of this thesis is constrained to extract and classify cracking types, their severity levels, and their characteristics only. This is done due to their correspondence to the types of distress on the available datasets of pavement images in this thesis.

### 2.1.2 Severity Levels

The severity level for a distress is a ranking index that divides the condition of distress into three types based on different ranking criteria. The three types of severity levels can be categorized into low, medium and high, based on the observer. Studies in distress detection procedures (SHAHIN 2002) have confirmed several indicators for detection. Table 2.1 displays the overall indicator regarding each type of distress. The general factors that control the severity level of several cracks are (SHAHIN/WALTER 1990):

1. Width of cracks,
2. The status of a crack; if it is filled or not,
3. Presence of random cracks around the main crack region,
4. The situation and appearance of the area around the crack itself,
5. Depth and diameter are considered as control factors in the case of evaluating pothole severities only.

Severity levels are evaluated based on several factors, as mentioned above. All of these factors are based on the observer's evaluation (non-automatic way). There are no standard specifications and no standard methods for controlling the severity level. Every road authority has its own method and own specifications based on the country and available data sets (SHAHIN 2002). For example, in the U.S. there are specification guides for the severity level evaluation on pavement maintenance management, for roads and streets, using the PAVER System Manual (SHAHIN 2002). On the contrary, in Germany,



severity level assessment and evaluation is determined by state value  $ZG$  and the normalized state value  $ZW$  (FGSV 2006).

Table 2.1: Indicators for distresses detection

Types of distress ( ZTV ZEB-STB_1 2006 )	Indicators for detection	Severity level (SHAHIN 2002)	Severity level ( FGSV 2006 )
Cracking	Surface area unit (length and width)	Based on the observation either low, medium, or high, unrelated to depth	Based on the state value and normalized state value determination
Patching	Surface area unit (length and width)	Based on the observation either low, medium, or high, unrelated to depth	Based on the state value and normalized state value determination
Outbreaks (potholes)	Pothole area unit (diameter)	Based on the depth of potholes	-
Open work seams	Sum of length	Based on the observation either low, medium, or high, unrelated to depth	-
Binder enrichment	Surface area unit (length and width)	Based on the observation either low, medium, or high, unrelated to depth	-

State value  $ZG$  is defined as a quantitative expression of state parameter described by state attributes (e.g., rut depth at 2 m bar or in % unit in the case of cracking and patching). Table 2.2 shows scaling parameters for motorways and federal highways outside of town-asphalt construction. Table 2.3 illustrates scaling parameters for federal highways inside of town-asphalt construction.

The normalized state value  $ZW$  is defined as a dimensionless value ranging from 1.0 (excellent) to 5.0 (worst). The state value is transferred via the normalization function to the normalized state value. Table 2.4 shows the normalization functions for the normalized state value calculation (FGSV 2006).

Based on the German regulations of the Road State Determination Manual (FGSV 2006), all state values refer to a section evaluation length of 100 m. The traffic lane is divided into three lanes (FGSV 2006). Theoretically, the normalized state value must be calculated for the asphalt tracks per metre for one-third of a traffic lane. The observer must give a grade value ranging from 1.0 (excellent) to 5.0 (worst) for every 1.0 m of 100 m. This procedure must be repeated for all section lengths. Afterwards, the average and standard deviation values are calculated based on the defined default of the normalized state value. This procedure gives an indicator for the normalized state value. Regarding the state value for cracking types, it is represented by the affected cracking area ratio (%). The affected cracking area ratio is calculated by dividing the number of grid covered with cracking by the total number of grid in the section evaluation. Then, the result must be multiplied by 100%. The traffic lane is divided into three sub-lanes, with each sub-lane width being 3.0 m. The length of the each sub-lane is 100 m (FGSV 2006). Each sub-lane is divided into equal grids. Each grid dimension is (1 x 1) m<sup>2</sup> (FGSV 2006). Therefore, the area of each sub-lane is 300 m<sup>2</sup> (300 grids). Figure 2.6 displays a sketch of an evaluation section.

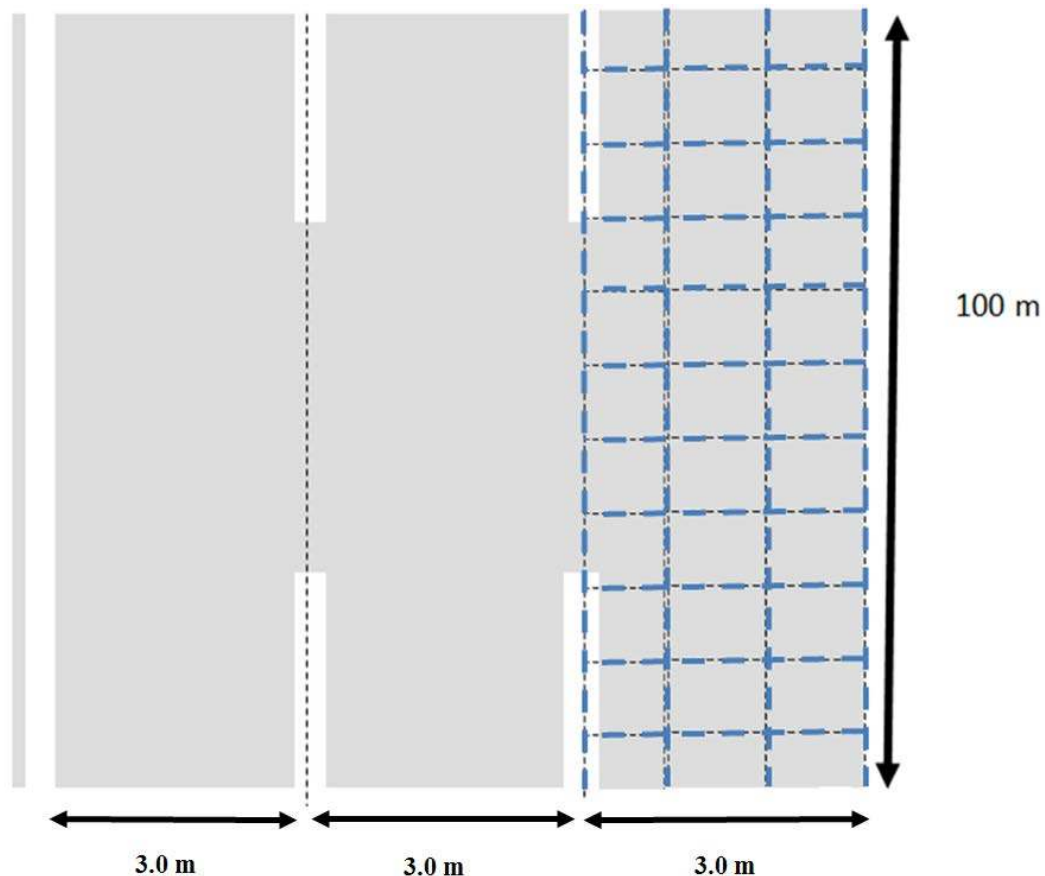


Figure 2.6: Sketch of the evaluation section.

Table 2.2: Scaling parameters for motorways and federal highways outside of town-asphalt construction (FGSV 2006)

State value <i>ZG</i> ( FGSV 2006 )	Normalized state value <i>ZW</i>		
	<i>ZW</i> =1.5	Warning value <i>ZW</i> =3.5	Threshold value <i>ZW</i> =4.5
Cracking (affected area ratio) (%)	1%	5%	10%
Patching (affected area ratio) (%)	1%	10%	15%

The measurements of the state value are transformed in the process, as shown in Table 2.4, for the normalized state value calculation, using the normalization functions. The normalization condition of the individual characteristics, or indicators, via normalization functions are currently fixed by three parameters on the value scale as the following (FGSV 2006):

1. The normalized state value  $ZW=1.5$  is equivalent to the tolerance of acceptance for the flatness characteristics;
2. The normalized state value  $ZW=3.5$  is denoted as warning value and describes the state whose attainment is a matter of intense scrutiny to analyse the causes of poor conditions;
3. The normalized state value  $ZW=4.5$  is denoted as threshold value and describes a condition in which the initiation must be examined by a structural or traffic restricting measure.

The tolerance value of 1.5, the warning value of 3.5, and the threshold value of 4.5 are determined by the particular requirement level of street segments and characterized by functional classes. This is especially important for visualization of the state assessment and evaluation, and making maintenance decisions. The different classes (functional portions) are defined as follows:

(1): If  $ZG < 1.5$ , and  $ZW = 1.0$ , this functional portion is good. The severity level of the cracking region is low (weak). There is no need for maintenance,

(2): If  $1.5 \leq ZG < 3.5$ , and  $ZW$  is calculated using the normalization function (Table 2.4). The severity level of the cracking region is medium. It needs maintenance to some extent,

(3): If  $3.5 \leq ZG < 4.5$ , and  $ZW$  is calculated using the normalization function (Table 2.4), the functional portion lies in the critical range between the threshold value and the warning value. The severity level of the cracking region is high (strong). The decision-maker must be cautious of this functional part, as it needs maintenance to some extent,

(4): If  $ZG \geq 4.5$ , and  $ZW = 5.0$ , this functional portion is bad (poor). The threshold value is exceeded, and the severity level of the cracking region is very high (very strong). This section must be repaired and needs maintenance. Figure 2.7 shows generalized cases of the normalization functions with the fixed points.

Table 2.3: Scaling parameters for parameters for federal highways inside of town-asphalt construction (FGSV 2006)

State value $ZG$ ( FGSV 2006 )	Normalized state value $ZW$		
	$ZW=1.5$	Warning value $ZW=3.5$	Threshold value $ZW=4.5$
Cracking (affected area ratio) (%)	1%	15%	25%
Patching ( affected area ratio) (%)	1%	15%	25%

Table 2.4: Normalization functions for the normalized state value calculation (FGSV 2006)

Functional portion ( FGSV 2006 )	State value $ZG$	Normalized state value $ZW$
(1)	$ZGI=1.5$ value $ZG < 1.5$	1.0
(2)	$ZGII=3.5$ =warning value $1.5 \leq ZG < 3.5$	$1.5 + 2.0 * (ZG - ZGI) / (ZGII - ZGI)$
(3)	$ZGIII=4.5$ =threshold value $3.5 \leq ZG < 4.5$	$3.5 + (ZG - ZGII) / (ZGII - ZGIII)$
(4)	$ZGIII=4.5$ =threshold value $ZG \geq 4.5$	5.0

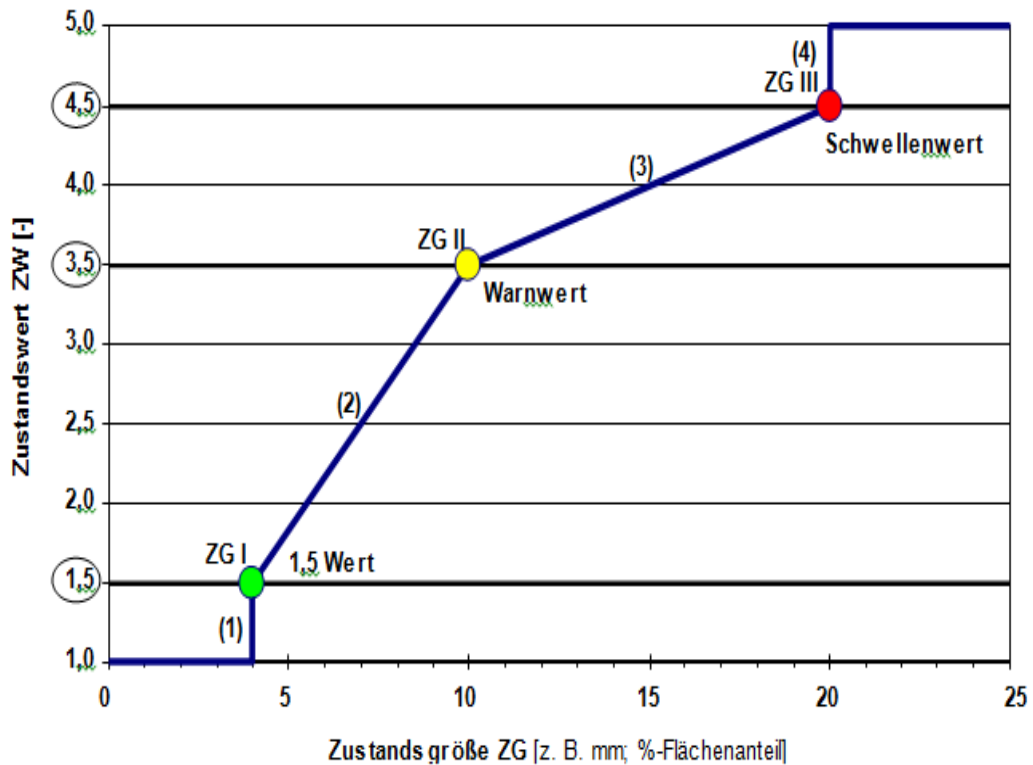


Figure 2.7: Generalized cases of the normalization functions with the fixed points (FGSV 2006) (Translation: 1,5 Wert/ 1.5 Value; Warnwert/ Warning Value; Schwellenwert/ Threshold Value; Zustandswert (ZW)/ Normalized state value (ZW); Zustandsgröße (ZG) [z.B. mm; %-Flächenanteil]/ State Value (ZG) size [e.g. mm, % area ratio])

## 2.2 Data Distress Acquisition Methods

Data collection, data verification, and data analysis are considered the three major subjects for any ideal pavement management system. The majority of the necessary information for pavement administration is provided by effective pavement surveys. For any vital pavement project, the following are considered the most important requirements: a quantified condition of networks, more precise and attainable information, forecasting the maintenance and rehabilitation requirements, setting the rehabilitation and maintenance priorities, tracking interpretation treatments, prediction of the pavement evaluation, and assigning funding. Therefore, it is important to acquire precise pavement condition data, in an effective and secure way, in order to ensure a credible analysis and interpretation system (GONTRAN ET AL. 2003, MOHAJERI/MANNING 1991, CLNE ET AL. 2003).

### 2.2.1 Manual Acquisition Methods

A walking survey is considered a well-known approach for implementing manual pavement condition surveys. This survey approach is done by specialists who are able to extract the crack and evaluate the pavement severity level according to the fixed identification criteria. The specialists select roads having distress, after which the selected roads are divided into branches, which are a single entity and have a distinct function. The selected branches, divided into smaller components, are called sections (AL-MISTAREHI ET AL. 2012). The following factors are considered when dividing branches into sections:

1. Pavement structure: the structural composition (thickness and materials),
2. Traffic: the volume and intensity of traffic,
3. Construction history: the pavement sections should have the same construction history,
4. Pavement rank: the functional classification (arterial, collector, local),

5. Drainage facilities: the drainage facilities and shoulders should be consistent throughout the pavement section (SHAHIN/WALTER 1990).

The selected pavement sections are divided into sample units with an area of  $233 \pm 93 \text{ m}^2$  (SHAHIN/WALTER 1990). The minimum number of sample units to be surveyed is determined based on the total number of sample units and the pavement condition index (PCI) standard deviation. This is assumed to be 10 for asphalt surfaced pavements (Figure 2.8). For example, if the total number of sample units is 80 and PCI standard deviation for flexible pavement is 10, the number of sample units to be surveyed will be 12. Different instruments, for instance, a hand odometer or tape, are used to measure the distress length, width, and area. The distress inspection is conducted by walking over the sample unit, measuring the distress type and severity, according to the distress manual, and recording the data on the flexible pavement survey sheet. One data sheet is used for each sample unit throughout the field inspection procedure. Afterwards, the detailed report of the extent, amount, and severity for each distress existence is introduced. This approach is time-consuming and labour-intensive (ALMISTAREHI ET AL. 2012).

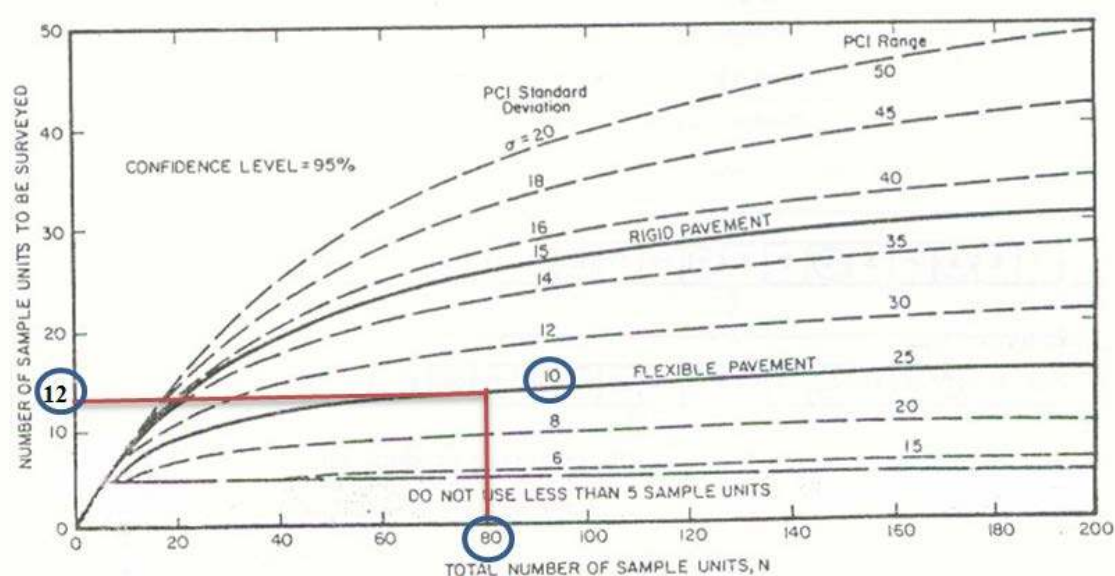


Figure 2.8: Selection of the minimum number of sample units (SHAHIN/WALTER 1990).

## 2.2.2 Automatic Acquisition Methods

### 2.2.2.1 General Characteristics for Different Automatic Acquisition Systems

Automated survey methods are completed using vehicles, traveling at highway speeds, to gather data. These automated vehicles are called mobile mapping vehicles. Different forms of automated pavement survey vehicles are obtainable worldwide with various data collection techniques. Mobile mapping vehicles have a general structure and characteristic, according to sensors and capability. This general structure consists of different sensors, such as cameras, laser scanners, inertial measurement units, global positioning system receivers, distance measurement units, inclination odometers, accelerometers, and lighting units. There are also different types of cameras, for example, charge-coupled device CCD cameras, video cameras, line scan cameras, panoramic cameras, and macro-picture cameras (surface cameras). Moreover, there are different types of laser scanners, such as Sick LIDAR scanners, Riegl (VMZ 450) laser scanner, Leica (P20) laser scanner, Faro laser scanner, and laser profilometers. The selection of one camera or laser type over another is based on the application. A large range, with several usages and applications, exploit automated mobile mapping acquisition systems. Some of these applications are utilized for highway distress rating and estimation, pavement distress and airport runway distress, tunnels, and bridge fields. The framework of this thesis is constrained to describe mobile mapping systems that are developed for distress data collection. Different road mobile mapping systems have the capability for distress data collection. This capability varies from one system to another. Different examples of automated acquisition systems will be presented in the following section.

### 2.2.2.2 Examples for Different Automatic Acquisition Systems

Identification of the different types of distress and connecting them to their corresponding causes is the major key to having an effective road surface assessment. As a matter of fact, digital imaging, using vision cameras, is the most well-known method for automatically gathering road data. After this is used, a suitable technique is exploited for storing and processing continuous pavement images. A video logging technique has been adopted by some commercial systems, such as VIASAT (SCHWARZ ET AL. 1993) and GeoVAN (GEOVAN 2014). These acquisition systems composite different sensors, like cameras, inertial measurement units, global positioning system receivers, and lighting units. The general denominator between these systems is that one or more cameras are fixed, along with archival equipment, for recording 2D images of the road surface. Another disposition needs a setting of two cameras separated by a baseline distance for collecting stereo images. The 3D information is then computed, based on the latter two stereo images and camera calibration information, using epipolar geometry. Once the global positioning system receiver information is incorporated with the video data to generate a GIS database of the road surfaces, it is expected to develop a road network assignment and pavement maintenance and management (HE 2002). Some of these imaging-based systems can acquire and process images for providing distress information, for instance, crack patterns, length, width, counts, areas, and sometimes depth (GONTRAN ET AL. 2003). One drawback of pure video-based systems is their disadvantage in differentiating dark areas not caused by pavement distress, such as shadows, oil spots, and tire marks (CHENG ET AL. 1999). In addition, shadows and poor lighting are considered another main problem that can be overcome by providing additional lighting systems or by capturing images at night (MCGHEE 2004).

Due to the complication of automatic object discrimination, an alternative solution is the semi-automatic object detection. The major rule of the latter system is that object discrimination is utilized manually, by human intervention. Subsequently, accurate locations of objects and automatic detection are carried out by the system. For example, extraction and location of a vertical lined object from mobile image sequences has been proposed by TAO (2000). In addition, predicting the approximated location of the objects is done using a map data set in another approach. After that, several algorithms, such as line clustering, feature corresponding, and line reconstruction, are utilized for exactly detecting the object existence and its location from the image.

In general, several commercial fully-automated and semi-automated surveying systems have been investigated thoroughly in the U.S. transportation departments. The term "system" identifies an instrumented mobile vehicle with fixed sensors, hardware, and software for representing and reducing distress data from miscellaneous sensor data which is collected by a data acquisition subsystem (MEIGNEN ET AL. 1997).

For example, the Pavement Distress Analysis System has been the predominant test system utilized by long-term pavement performance programs. This system consists of different sensors, such as cameras, inertial measurement units, global positioning system receivers, distance measurement units, inclination odometers, and lighting units. The latter one supplies a semi-automated approach by permitting a human operator to manually choose a distress and its severity level. The digitized images are considered input data files; whereas, ASCII format files, with reduced distress data, are represented as outputs.

In addition, the Video and Sensor Playback System is called Pathview I, and Digital Playback Workstations are called Pathview II. These acquisition systems are developed by Pathway Services, Inc. Four cameras, global positioning system receivers, five lasers, and various sensors are integrated as a data acquisition subsystem. This last subsystem is called Pathrunner. Automated detection and classification of roughness, rutting, faulting, and texture are achieved by the software subsystem. Human intervention is strongly required for the cracks' estimation. Detailed information is recorded on PATHVIEW (2014).

Another pavement inspection digital imaging system has been developed by International Cybernetics Corporation. This system consists of different sensors, such as progressive scan charge-coupled devices CCD cameras, inertial measurement units, global positioning system receivers, barometers, inclination odometers, and lighting units. The system can detect cracks from images and needs only minimal human intervention, unlike the former ones. More information about this system is reported in IC (2014).

A typical solution to produce images from 3D laser profiles, and then extract cracks, is utilized by a pavement scanner profile system. This system is called Roadview 3D, developed at Mandi Communication, Inc. This system consists of different sensors, such as cameras, laser scanners, inertial measurement units, global positioning system receivers, and lighting units. Crack resolution up to 3 mm is obtained for a 4.2 m wide image (MANDLI 2014)

A fully automated system known as Wisecrax has been developed by Roadware Group ARAN, Inc. (ARAN 2014). Around eight agencies use this system for analysing pavement cracks. The general structure of the ARAN system consists of different sensors, such as video cameras, laser scanners, two or more charge-coupled devices CCDs, inertial measurement units, global positioning system receivers, and accelerometers. In the task of planning, two continuous video cameras, covering the survey lane, are fixed by two beams in the back of the vehicle. These two cameras are black and white charge-coupled devices (CCD) and face perpendicularly to the pavement surface. A regular pavement surface coating the required lane is composited from simultaneous images from two cameras and successive images from one camera. The latter system permits the cameras to collect images without shadows at 80 km/h. The crack correspondence process is implemented by using the WiseCrax product. The latter one is able to identify each crack, its beginning and end location, using an x-y coordinate system, its length, its width, and its orientation. Finally, a crack map is created, and a statistical report is also prepared, through the crack correspondence process. The crack map is associated with attributed tables displaying the start and end point of the crack, the length, the width, and the orientation (WANG/ELLIOT 1999). As published, this system has the capability for fully automated detection and classification of crack types. However, this system possesses some drawbacks and shortcomings regarding data acquisition and data processing (WANG/ELLIOT 1999).

The LEHMANN + PARTNER GmbH Company in Germany utilized the S.T.I.E.R mobile mapper system (Note: S.T.I.E.R is not an abbreviation, it is an artificial name) (LEHMANN+PARTNER 2014) This S.T.I.E.R mobile mapper system consists of different sensors, for example, panorama colour cameras, surface cameras, laser scanner, Applanix POS LV 420 positioning system, and lighting units. This mobile mapping vehicle is used for surveying the longitudinal and transverse evenness, measuring texture, and 3-dimensional road surface, as well as recording surface images (LEHMANN+PARTNER 2014).

The Mobile road mapping system MoSES (Mobiles Strassen-Erfassungs-System) is used by the 3D Mapping Solutions GmbH Company in Germany. This system is comprised of a 3D mapping multi-camera module, powerful high performance kinematic laser scanners, a receiver of the global positioning system, an inertial navigation system, and a distance measuring instrument. The system can collect panoramic views along roadways (3D-MAPPING 2014).

A group of digital cameras, a receiver of the global positioning system, an inertial navigation system, and a distance-measuring instrument are fixed on the Unicom-Umap Company vehicle-Saudi Arabia. This system is called VISAT™ (Video Images, INS System and GPS Satellites) mobile mapper system. The system can collect images along roadways (UNICOM-UMAP 2014). VISAT™ has been developed at the University of Calgary in the early 1990s and was among the first terrestrial MMS at that time. Recently, an improved version was developed by Absolute Mapping Solutions Inc, Calgary, Canada. The system's hardware components include an Inertial Navigation System (INS), a dual frequency GPS receiver, 6 to 12 digital colour cameras, and an integrated Distance Measurement Instrument (DMI), and the VISAT™ system controller. The camera cluster provides a 330° panoramic field of view (CHENG ET AL. 2008).

In the last few years, several high-quality MMS techniques have been presented and amended quickly. Distress View 3D (GIE 2014) utilizes a laser vision system. This system contains lasers, cameras, global positioning system receivers, an inertial navigation system, and lighting units. Distress View 3D (GIE 2014) produced a map to demonstrate the left and right rut sign of a 2D colour image as a model of 3D sensors that assist the image data. JAVIDI ET AL. (2003) shows an improvement for ARAN work (ARAN 2014) by measuring 3D-depth. In particular, a phase-shifting digital interferometry-based approach is introduced for developing ARAN outputs. The principle is utilized by projecting multiple laser beams on a charge-coupled devices (CCD) camera, and after that, notices the deviation patterns for 3D-coordinates reconstruction, using holography. In LAURENT ET AL. (1997), a multi-scanner synchronized system for measuring dense 3D coordinates is presented. This latter approach is a nearly real-time solution for a high speed mobile mapping vehicle. In addition, it is eligible to produce an output binary image with 255 (bright) pointing non-distress areas, and zero (dark) representing distress areas. It is called a road inspection system. It is developed by the National Optics Institute, Canada. Examples of other systems can be mentioned, such as the presentation of a system consisting of six sensors for high speed and resolution scanning to produce binary crack maps (BURSANESCU/BLAIS 1997), and the use of both 2D and 3D approaches in a universal survey for road data-capturing methods summarization (TAO 2000). Moreover, ABUHADROUS ET AL. (2004) presents an approach to scan road surfaces in general with all extrinsic objects, such as traffic and trees. After that, extraction range points associated with road edges and centres then employ feature triangulation for indicating roads curves, and terrain hilliness without recovering geometrical details of surface pavement distresses is presented.

The Ministry of Transport, Japan Highway Public Corporation, and Road Management Agents have been using a road surface condition survey vehicle for measuring cracks, ruts, and flatness (vertical asperities) for some time. This measuring vehicle is known as "ROADMAN". It consists of different sensors, such as cameras, inertial measurement units, global positioning system receivers, distance measurement units, and lighting units. Finally, preparing the result report of the road surface condition is done for the purpose of reasonably and effectively managing and preserving the road pavement (HISASHI/TATSUHIDE 2000).

According to the above information, all of these commercial systems share the same goal of collecting accurate pavement condition data. Additional details about different automated pavement survey vehicles (commercial systems), worldwide, are reported in Appendix A.

### 2.2.3 Manual vs. Automatic Data Collection

Generally, in crack detection applications, two approaches are utilized for data capturing. These methods are the manual collection and the automatic collection. The former demands are expensive, labour-intensive, hazardous, subjective, and difficult to manage; whereas, the latter technique is safe, not labour-intensive, objective, integratable with a management system, and can complement the individual weaknesses of the former one (WANG/ELLIOT 1999).

In a comparative study of data obtained by a mobile mapping system (MMS) and ground truth observations (manual method), LEE ET AL. (1991) concluded that the data obtained by an MMS was of "reasonable" accuracy. The conclusion was not based on any statistical analysis, nor was a definition of "reasonable" accuracy provided. MASTANDREA ET AL. (1995) reported an accuracy of 5 to 10 centimeters for various inventory elements collected by a MMS. They did not report on the evaluation methodology or data elements used in the evaluation or provide analysis details. EL-SHEIMY (1996) compared the accuracy of descriptive data obtained with a MMS to ground truth observations. His findings indicated that errors in digital measurements increased with increasing distance between the object and the camera. However, EL-SHEIMY (1996) does not provide information on the identity and size of the measured inventory elements or on the number of observations made on the elements. In a test of crack identification and classification, ARAN (2014) compared the accuracy of its photogrammetric software package for crack identification with the long term pavement performance (LTPP) procedure and found them comparable. However, there was no similarity in crack classification (block, fatigue, transverse, longitudinal wheelpath, and edge) in the two methods.



In another test, ARAN (2014) also shows that its photogrammetric software package was able to automatically classify collected data on pavement cracks into the LTPP categories. However, there was no indication if the classification was correct. Not all comments were positive (KHATTAK ET AL. 2000); Florida state reported that “the results from real time pavement distress analysis from images [are] far from accurate.”

In summary, the literature indicates that accuracy of the manual method depends on the surface composition and continuity between the point of observation and the target object. Literature on the accuracy of descriptive data obtained by MMSs is insufficient to judge whether MMSs provide accuracy comparable to the manual method. Not all agencies are satisfied with the results of automation. Some reported that improvements are needed in the quality of images provided, as well as in the data reduced from those images. Most statistical analyses show that the accuracy of descriptive inventory data depends on the method of collection and that the manual method provides slightly more accurate data (KHATTAK ET AL. 2000).

Regarding time-consumption, data collection by MMSs is speedier in the field compared with the manual method. However, data processing and extraction of descriptive data from digital images with photogrammetric software packages takes more time in the office as compared with the manual method. The total time consumed by the manual method was less than the time required by MMS methods. In addition, costs of automated pavement condition data collection and processing vary greatly depending on specific items addressed and on logistics. Full-featured collection and processing will average more than \$30 per lane-km and may reach \$125 per lane-km or more in urban, high-traffic areas. The distance traveled to collect data is also a significant factor in determining costs (MCGHEE 2004).

After collection of the pavement data, using the techniques described above, distress data analyses usually follows. The data are analysed manually or automatically based upon standard criteria which vary from country to country. In this thesis, the focus will be on the automatic distress data analysis. This portion will be implemented by using digital image processing techniques in the following section.

## **2.3 Distress Data Analysis**

The main idea of this approach is to detect cracks automatically, derive reliable crack measurements, and classify cracks into different categories by means of photogrammetry. It utilizes image processing analysis to recover crack surface information through different image processing techniques (LUHMANN ET AL. 2006). An intensive review of image processing techniques is presented by FRYER ET AL. (2006), ATKINSON (1996), LUHMANN ET AL. (2006), and other textbooks on digital image processing (BATTIATO ET AL. 2002).

### **2.3.1 Image Processing for Crack Detection- An Overview**

The framework of this thesis is focused on cracking types and how to detect cracking types using digital image processing techniques. The cracking types of this thesis are detected from pavement images, and therefore digital image processing techniques are used rather than other techniques. A thorough review of image processing techniques is presented by LI ET AL. (1991), KOUTSOPOULOS/ DOWNEY (2006), CHOU ET AL. (1994), and other algorithms on digital image processing for cracking detection (CHENG/MYOJIM 1998, JAVIDI ET AL. 2003, DAVID/JOE 2005, YING/SALARI 2009, TEOMETE ET AL. 2005). The requirements for any cracking detection procedure, using digital image processing techniques, are presented as follows:

- (a) Image with clear cracks and good resolution,
- (b) low noise level.

Studies in digital image processing techniques (BUGAE/YAXIONG 2003, MASER 1987, CHOU ET AL. 1994, JAVIDI ET AL. 2003, SEAN/STEVENS ON 1998, WANG/HARALICK 2002) have confirmed several digital image processing procedures which are based on different concepts as follows:

- (a) The definition of the digital image processing concept is pixel intensity, brightness levels (contrast), and their distribution. This concept is considered as a base for different previous algorithms; (see LI ET AL. 1991, MASER 1987, KOUTSOPOULOS/DOWNEY 2006, JAVIDI ET AL. 2003, RABABAAH ET AL. 2005). This digital image processing concept is explained in more detail in section 2.3.2.
- (b) The definition of the convolution concept is used during the image enhancement stage for some algorithms (MOHAJERI/MANNING 1991). The convolution concept, its function, its process, and its effect on pixel intensities are explained in more detail in section 2.3.2.1. The image enhancement stage definition is explained in more detail in section 2.3.5.
- (c) An edge detection filter, such as the Sobel Edge Detection Filter, is used as a tool for crack extraction during the segmentation stage (see LI ET AL. 1991). This edge detection filter, its equations, and its principle work are explained in more detail in section 2.3.2.2.
- (d) Basic morphological operation reviews are presented in HSU ET AL. (2001). They address the main problems during the post-processing stage, and the available solutions using the hole pixel initial algorithm (flood filling operation). The morphological operations and their principles are displayed in more detail in section 2.3.2.3. The post-processing stage definition is explained in more detail in section 2.3.5.
- (e) Any crack detection algorithm must include four stages: preprocessing stage, segmentation stage, post-processing stage, and crack extraction and classification stage. These stages have been proposed in the literature (see HSU ET AL. 2001, SALARI 2012, CHOU/SALARI 2012, TEOMETE ET AL. 2005). Every stage has a definition, problems, and concepts regarding image analysis (image interpretation). These stages concerning image analysis (image interpretation) are explained in more detail in section 2.3.3.
- (f) Some global and local binarization techniques, (e.g., NIBLACK 1985, SAUVOLA/ PIETIKAKINEN 2000, YING/SALARI 2009) have been previously used to threshold pavement images successfully. These techniques are explained in detail in section 2.3.4.
- (g) Several crack detection algorithms have been developed, but many of them experience some problems (CHOU ET AL. 1994, LE ET AL. 1990, CHOU/SALARI 2012, TEOMETE ET AL. 2005, RABABAAH ET AL. 2005). These partially and completed crack detection algorithms are explained in detail in section 2.3.5.

In the above mentioned material, the main steps of distress data analysis are described in detail. Moreover, the steps of image interpretation are briefly introduced, and the main typical challenges associated with each step are given. In addition, the related algorithm research and binarization overviews are introduced.

### **2.3.2 Digital Image Processing**

The digital image processing term refers to many concepts, such as expansion, rectification, reduction, geometrical editing, and assembly that can be utilized on images. This thesis is essentially interested in image preprocessing and image analysis (interpretation). The result of the former one is an image ready for analysis. This image seems to be similar to the original one or is significantly different. Where the aim of image pre-processing is to prepare an image, the result of the latter one is almost always the measurement and classification of some features of the original image. In other words, the latter aims to demonstrate an image that quantifies and qualifies some of its features.

In general, any digital image must be formed of different discrete points of tone (or brightness). These tone levels represent different shades of gray or coloured tones. To create a digital image from a continuous-tone image, the latter continuous-tone image will be sampled and quantized through a sampling process. The aim of the sampling process is to test the intensity of the continuous-tone image at certain locations (LUHMANN ET AL. 2006).

The digital brightness value of each sample is specified during the quantification process. A sample term in a digitized image is pointed to a pixel. Figure 2.9 illustrates the image coordinate system and the pixel numbering convention, where  $(x, y)$  are the coordinates for each pixel associated with its location in the digital image. The pixel number and the line number are denoted by  $x$  and  $y$ , respectively.

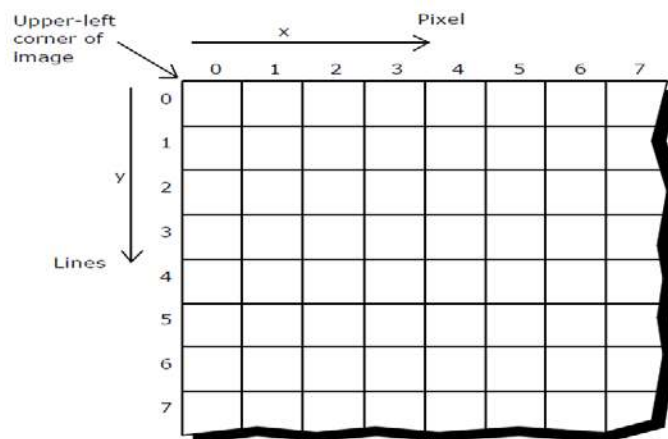


Figure 2.9: The pixel numbering convention (GIRARDELLO 2002 and HOWE/GLEMENA 1987).

In order to understand the image processing concept, the basic notion of photogrammetry needs to be introduced. The convolution concept, edge detection filter, morphological image processing operations, and morphological operations for holes filling, must be defined in advance.

### 2.3.2.1 Convolution Concept

Convolution can be generally described as an integral summation of two component functions. Convolution measures the amount of overlap as one function is shifted over the other. The convolution at a point is the product of the two functions that occurs when the pulse is moved over the point. When actually taking the convolution of two functions, one function is flipped with respect to the independent variable before shifting, and a change of variables from  $t$  to  $T$  with respect to facilitate the shifting operation. In one dimension, the mathematical definitions of convolution in discrete and continuous time are indicated by the "\*" operator (SEAN/STEVENSON 1998).

If  $f$  and  $g$  are functions in  $t$ , then the convolution of  $f$  and  $g$  over a finite range  $[0, t]$  will be represented by equation (2-1) below:

$$[f * g](t) = \int_0^t f(T)g(t - T)dT, \quad (2-1)$$

where

- $f * g$  : convolution of  $f$  and  $g$  under the integral over a finite range  $[0, t]$ ,
- $f(T)$  : function of  $T$  under the integral,
- $g(t - T)$  : reflection of  $g(T)$ , shifted by an amount  $t$  on the  $T$  axis.

ATKINSON (1996) defines convolution requirements as follows: (i) The first input array is usually a gray level image; and (ii) the second input array is called the kernel. This latter image must be significantly smaller as compared to the former one, and must also be two-dimensional. Figure (2.10) illustrates the definition of a matrix and a kernel at a single coordinate; the complete convolution is found by repeating the process until the kernel has passed over every possible pixel of the source matrix.

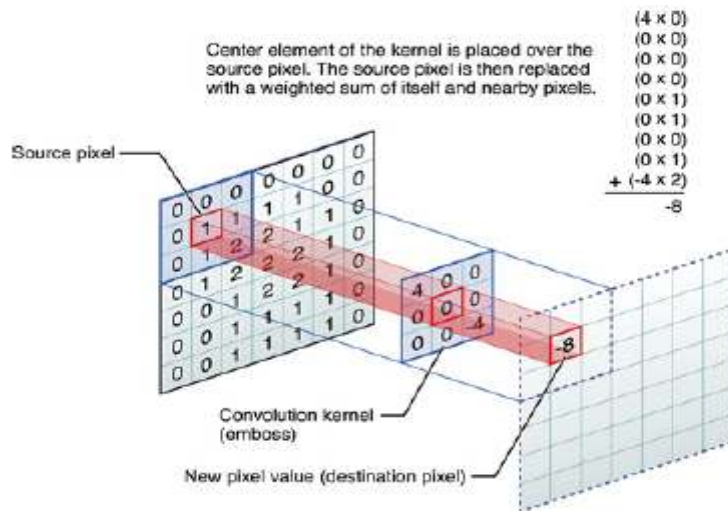


Figure 2.10: A single location in a 2-D convolution (ATKINSON 1996).

LUHMANN ET AL. (2006) summarizes the convolution process as follows: (i) moving the kernel over the image, generally starting from the top left corner, through all of the positions where the kernel must be fit within the image boundaries; and (ii) each single output pixel must be associated with each kernel position. The value is computed by multiplying the kernel value and the underlying image pixel value for each of the cells in the kernel, and then adding all of these numbers together. Therefore, the convolution is given mathematically by:

$$V = \frac{\sum_{i=1}^q (\sum_{j=1}^q f_{ij} d_{ij})}{F}, \quad (2-2)$$

where

- $f_{ij}$ : the coefficient of a convolution kernel at position  $i, j$  (in the kernel),
- $d_{ij}$ : the data value of the pixel that corresponds to  $f_{ij}$ ,
- $q$ : the dimension of the kernel, assuming a square kernel (if  $q=3$ , the kernel is  $3 \times 3$ ),
- $F$ : either the sum of the coefficients of the kernel, or 1 if the sum of coefficients is 0,
- $V$ : the output pixel value, if  $V$  is less than 0,  $V$  is clipped to 0.

With respect to object detection, the most important feature of a smoothing convolution operator is that it must not shift the object position. Any shift introduced by a preprocessing operator would cause errors in the estimates of the position and possibly other geometric features of an object. In order to cause no shift, the transfer function of a filter must be real. A filter with this property is known as a **zero-phase shift convolution filter**. This filter does not introduce a phase shift in any of the periodic components of an image (no geometry change). In principle, there are three types of phase response that a filter can have: zero-phase, linear phase, and nonlinear phase (BATTIATO ET AL. 2002). In the following, a general overview will define only the **zero-phase shift convolution filter**, as others lie beyond the scope of the current research.

### Zero-Phase Shift Convolution Filter

The zero-phase shift convolution filter is characterized by an impulse response that is symmetrical around zero. The actual shape does not matter, only that the negative numbered samples are a mirror image of the positive numbered samples. When the Fourier transform is taken of this symmetrical

waveform, the phase will be entirely zero (Figure 2.11, b). Figure 2.11 illustrates the definition of zero-phase shift convolution filter.

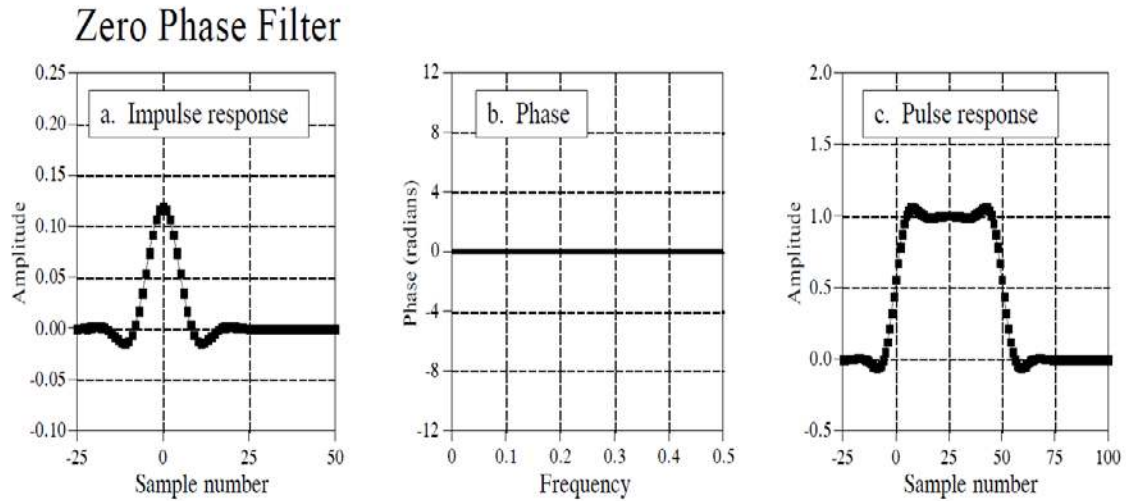


Figure 2.11: (a) A zero-phase shift filter has an impulse response that has left-right symmetry around sample number zero, (b) A zero-phase shift filter has a frequency response that has a phase composed entirely of zeros, (c) zero-phase impulse responses are desirable because their step responses are symmetrical between the top and bottom, making the left and right edges of pulses look the same (ATKINSON 1996).

In conclusion, the advantage of the zero-phase shift filter is that it does not introduce a phase shift in any of the periodic components of an image (no geometry change). This advantage is important in the case of crack detection. The disadvantage of the zero-phase shift filter is that it requires the use of negative indexes, which can be inconvenient to work with. Zero-phase filtering can be achieved by running the filter  $H(z)$  twice: first in reverse time, followed by a second application in forward time. The two-stage filtering procedure (LUHMANN ET AL. 2006) is as follows:

1. Signal sequence is given and known as follows  $n = 0, 1, \dots, N - 1$
2. Reverse-time filtering is performed to produce the filtered sequence as follows  $y_{rev}(n), n = 0, 1, \dots, N - 1$
3. Forward-time filtering of the signal sequence  $\{y_{rev}(n)\}$  is performed.

### 2.3.2.2 Edge Detection Filter

In principle, the boundary between two regions, where a large variation in intensity takes place, is called an edge. An edge can be derived using digital image processing by first enhancing the input image, and then using a thresholding scenario for output image binarization. In order to obtain precise edge detection, several edge enhancement filters must be utilized for locating sudden changes in intensity profiles. Not surprisingly, several utilizing local derivatives or gradient operator applications must be completed using edge enhancement filters. Extraction edges of gray scale images have different properties in this manner: (i) edge direction must be orthogonal with considerable intensity change in the neighbouring pixels; and (ii) each edge must have a unique direction and magnitude.

In conclusion, the edge, or more accurately the ramp, is defined as a considerable variation of intensity between two pixel value areas of a specified size. Extensive summaries of edge detection methods are given, for example, by FRYER ET AL. (2006), ATKINSON (1996), LUHMANN ET AL. (2006), and other textbooks on digital image processing (BATTIATO ET AL. 2002). In the following, a general overview will define only the Sobel Edge Detection Filters, as others lie beyond the scope of the current research.

### Sobel Edge Detection Filter

A special preset 3\*3 non-linear edged enhancement filter is called the Sobel Edge Detection Filter. A mathematical form of the Sobel function is given by equations (2-3), (2-4), and (2-5), respectively. In principle, the convolution of the image with a separable, small, and integer valued filter, in both vertical and horizontal directions, is utilized for the Sobel operator production. One of the Sobel operator advantages is that it is comparatively inexpensive in terms of computation time, due to its fixed size. In addition, the Sobel operator enables to produce comparatively crude gradient approximations, particularly for high frequency changes through the image. A mathematical form of the kernel mask computations is given by equations (2-8) and (2-9), correspondingly. Moreover, the convolution process involves the original image (equation 2.10) and two 3\*3 kernel masks for estimating derivative approximations of both horizontal and vertical changes, which are given mathematically by equations (2-6) and (2-7), respectively (LUHMANN ET AL. 2006):

$$G_{ij} = \sqrt{G_x^2 + G_y^2}, \quad (2-3)$$

$$G_x = F_{i+1,j+1} + 2F_{i+1,j} + F_{i+1,j-1} - (F_{i-1,j+1} + 2F_{i-1,j} + F_{i-1,j-1}), \quad (2-4)$$

$$G_y = F_{i-1,j-1} + 2F_{i,j-1} + F_{i+1,j-1} - (F_{i-1,j+1} + 2F_{i,j+1} + F_{i+1,j+1}), \quad (2-5)$$

$$G_x = f_x * F, \quad (2-6)$$

$$G_y = f_y * F, \quad (2-7)$$

$$f_x = \begin{bmatrix} -1 & 0 & 1 \\ -2 & 0 & 2 \\ -1 & 0 & 1 \end{bmatrix}, \quad (2-8)$$

$$f_y = \begin{bmatrix} 1 & 2 & 1 \\ 0 & 0 & 0 \\ -1 & -2 & -1 \end{bmatrix}, \quad (2-9)$$

$$F = \begin{bmatrix} \vdots & \vdots & \vdots & \vdots & \vdots \\ \cdots & F_{i-1,j-1} & F_{i-1,j} & F_{i-1,j+1} & \cdots \\ \cdots & F_{i,j-1} & F_{i,j} & F_{i,j+1} & \cdots \\ \cdots & F_{i+1,j-1} & F_{i+1,j} & F_{i+1,j+1} & \cdots \\ \vdots & \vdots & \vdots & \vdots & \vdots \end{bmatrix}, \quad (2-10)$$

where

$f_x$ : kernel mask in x-direction,

$f_y$ : kernel mask in y-direction,

$G_{ij}$ : magnitude of gradient,

$G_x$ : magnitude of gradient in x-direction,

$G_y$ : magnitude of gradient in y-direction,

$F$ : matrix of gray values of image,

$F_{ij}$ : gray value of the investigated pixel,

$i, j$ : coordinates of the pixels which are investigated,

$F_{i-1,j-1} \dots F_{i+1,j+1}$ : gray values of the surrounding pixels.

### 2.3.2.3 Basic Morphological Operations Review

Morphology expression is derived from biology. The main idea of this operation is to study the structure of objects within an image. It is defined as a group of different non-linear operations exploiting the shape, and relatively ordering pixel values, inside of an image. There is no relationship between morphological operations and numerical pixel values. These latter points indicate that morphological operation can be utilized for processing binary images (black 0's and white 1's pixels) and also gray-scale images (black 0's and white 255's pixels) (DROOGENBROECK/TALBOT 1996). A small shape template is often required for morphological operation implementation. This template is known as a structuring element. This structuring element is expressed as a binary image with a value of zero or one. It must be considerably smaller than the image being proposed, yet have the same size and shape as the objects which are to be analyzed. Therefore, the structuring element has various shapes based on the object shape, such as a line, disk, square, and diamond. In general, there are two types of structuring elements: (i) flat structuring element (origin at the center with symmetrical unit height); and (ii) non-flat structuring element (continuous intensity variation, which is seldom utilized). In principle, any type of structuring element must be located in all possible positions within an image. Then, it must be compared with the neighbouring pixels. Several morphological operations have been proposed in the literature, some of which must be checked to determine whether the structural element "fits" within the neighbourhood; whereas, others will be utilized if the structuring element "hits" or intersects the neighbourhood (Figure 2.12).

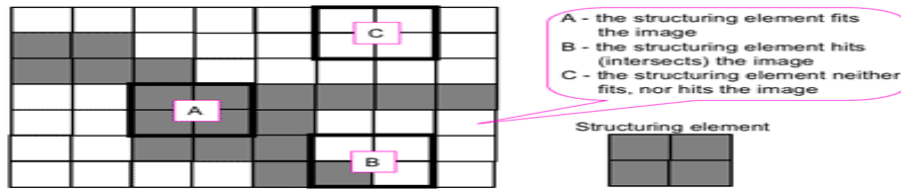


Figure 2.12: Structural element concept (EFFORD 2000).

Various essential functions, based on Boolean operations for binary images, are presented for morphological image processing (DROOGENBROECK/TALBOT 1996).

#### The Dilation Process

The idea of this process is to lay the structuring element  $B$  on the image  $A$ . This structuring element  $B$  is then moved across image  $A$  in the same way as in convolution. However, the concept of dilation is different from convolution. The dilation process is mainly performed in two steps (DROOGENBROECK/TALBOT 1996):

1. If there is a synchronization between any "white" pixel in the image and origin of the structuring element, there will be no variation and movement to the next pixel presented,
2. If there is a synchronization between any "black" pixel in the image and origin of the structuring element, variation will be utilized by making a black for all pixels covered by a structuring element in the image.

A mathematical form of the dilation process is given by equations (2-11), (2-12) and (2-13). Figure (2.13) illustrates the dilation process effect, in which all black pixels of the original image will be kept, any image boundaries will be widened, and any small gaps will be removed by filling.

$$E = A \oplus B, \text{ is the dilate of image } A \text{ by structuring element } B. \quad (2-11)$$

$$E(x) = \begin{cases} 1, & B \text{ hits } A \text{ at } s \\ 0, & \text{otherwise} \end{cases} \quad (2-12)$$

$$A \oplus B = \left\{ s \mid \left( (\hat{B})_s \cap A \right) \subseteq A \right\}, \quad (2-13)$$

where

- $A$  : input image,
- $B$  : linear structure element,
- $(\hat{B})_s$  : reflection or translation of structural element  $B$ , which overlaps at least some portions of  $A$  by vector of shift  $s$ ,
- $s$  : vector of shift (pixels),
- $A \oplus B$  : set consisting of all structuring element origin locations, where the reflection or translation of  $B$  overlaps at least some portion of  $A$ .

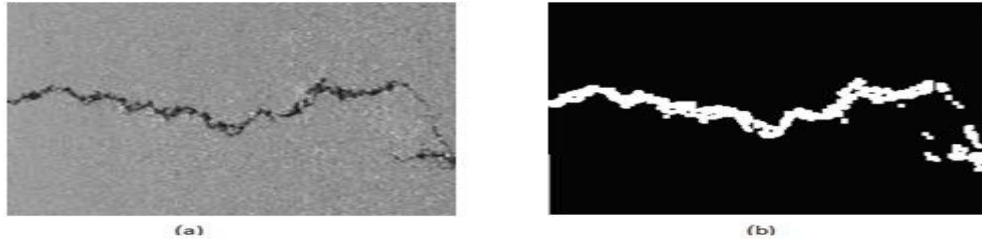


Figure 2.13: Example of the dilate: a. original image  $A$ ; b. resultant image:  $A \oplus B$

### The Erosion Process

The concept of this morphological operator is the same as the dilation process in a sense. On the contrary, converting pixels' colour to white and not black is the major difference between this process, as compared with the former one. When a structuring element is moved across an image, the erosion process is fundamentally utilized in two steps (DROOGENBROECK/TALBOT 1996):

1. If there is a synchronization between any “white” pixel in the image and the origin of the structuring element, there will be no variation and movement to the next pixel introduced,
2. If there is a synchronization between any “black” pixel in the image and the origin of the structuring element, in addition a minimum of one “black” pixel in the structuring element over a “white” pixel in the image, then variation will be performed by changing the “black” pixel in the image (associated to the location on which the origin of the structuring element falls) from a “black” colour to a “white” colour.

A mathematical form of the erosion process is presented by equations (2-14), (2-15), and (2-16), respectively (DROOGENBROECK/TALBOT 1996). Figure (2.14) shows that only the pixels synchronizing with the structuring element origin will be kept.

$$E = A \ominus B, \text{ is the erosion of image } A \text{ by structuring element } B. \quad (2-14)$$

$$E(x) = \begin{cases} 1, & B \text{ fits } A \text{ at } s \\ 0, & \text{otherwise} \end{cases} \quad (2-15)$$

$$A \ominus B = \{s | ((B)_s) \subseteq A\}, \quad (2-16)$$

where

- $A$  : input image,
- $B$  : linear structure element,
- $(\hat{B})_s$  : reflection or translation of structural element  $B$ , that overlaps at least some portions of  $A$  by vector of shift  $s$ ,
- $s$  : vector of shift (pixels),
- $A \ominus B$  : set of structuring element origin locations, where the reflected or translated  $B$  has no overlap with the background of  $A$ .



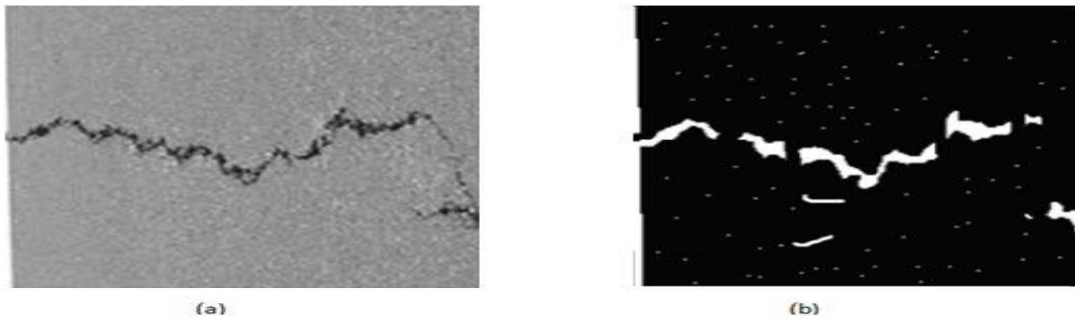


Figure 2.14: Example of the erosion: a. original image  $A$ ; b. resultant image:  $A \ominus B$

### The Morphological Reconstruction Concept

One of the most important morphological operations is usually the morphological transformation, which includes two images and a structuring element. This morphological concept is referred to as morphological reconstruction. LUHMANN ET AL. (2006) define morphological reconstruction as follows: (i) morphological reconstruction is utilized using two images; one image is called a marker and includes the beginning points for transformation. The second image is called a mask constraining transformation; (ii) the morphological reconstruction process relies on the characteristics of the mask image and must be continued until the mask image values do not change (peaks of the mask image will become flat); (iii) morphological reconstruction requires the structuring element to identify connectivity; and (iv) there are two types of morphological reconstruction, i.e., either by exploiting the dilation process (opening by reconstruction) or by investigating the erosion process (closing by reconstruction).

VINCENT (1993) summarizes the opening by reconstruction algorithm in sequential steps as follows:

1. The input image must first be eroded before using it as a marker. So, the marker is the resultant eroded image.
2. The number of openings by reconstruction of an original input image  $A$  is expressed as the reconstruction  $A$  by dilation from the erosion size  $n$  of  $A$ . The final dilation result is the reconstructed image (Figure 2.15). Mathematically opening by reconstruction is given by:

$$O_R^{(n)}(A) = R_A^D[(A \ominus nb)], \quad (2-17)$$

where

- $A$  : is the mask (original input image),
- $b$  : is the marker (the resulted eroded image),
- $n$  : are the erosion times,
- $R_A^D$  : reconstruction  $A$  by dilation process,
- $O_R^{(n)}(A)$  : the product of opening by reconstruction operation,
- $(A \ominus nb)$  : denotes  $n$  erosion times of  $A$  by  $b$ .

The idea of closing by the reconstruction approach is similar to the opening by the reconstruction concept discussed previously. VINCENT (1993) introduces the closing by reconstruction algorithm in two steps:

1. The complementary image obtained from the opening by reconstruction is used as a marker for closing by reconstruction implementation.

2. The number of closing by reconstruction of an image  $A$  is utilized as the reconstruction by erosion of  $A$  from the dilation size  $n$  of  $A$ . Mathematically closing by reconstruction is presented by:

$$C_R^{(n)}(A) = R_A^E[(A \oplus nb)], \quad (2-18)$$

where

- $A$  : is the mask (the resulted image from opening by reconstruction),  
 $b$  : is the marker ( complementary of resulted opening by reconstruction image after dilation),  
 $n$  : are the dilation times,  
 $R_A^E$  : reconstruction  $A$  by erosion process,  
 $C_R^{(n)}(A)$  : the product of closing by reconstruction operation,  
 $(A \oplus nb)$  : denotes  $n$  dilation times of  $A$  by  $b$ .

In relation to the previously stated, closing by the reconstruction process has been demonstrated by complementing the image as a marker, obtaining the opening by reconstruction as a mask, and then finally complementing the final result after reconstruction.

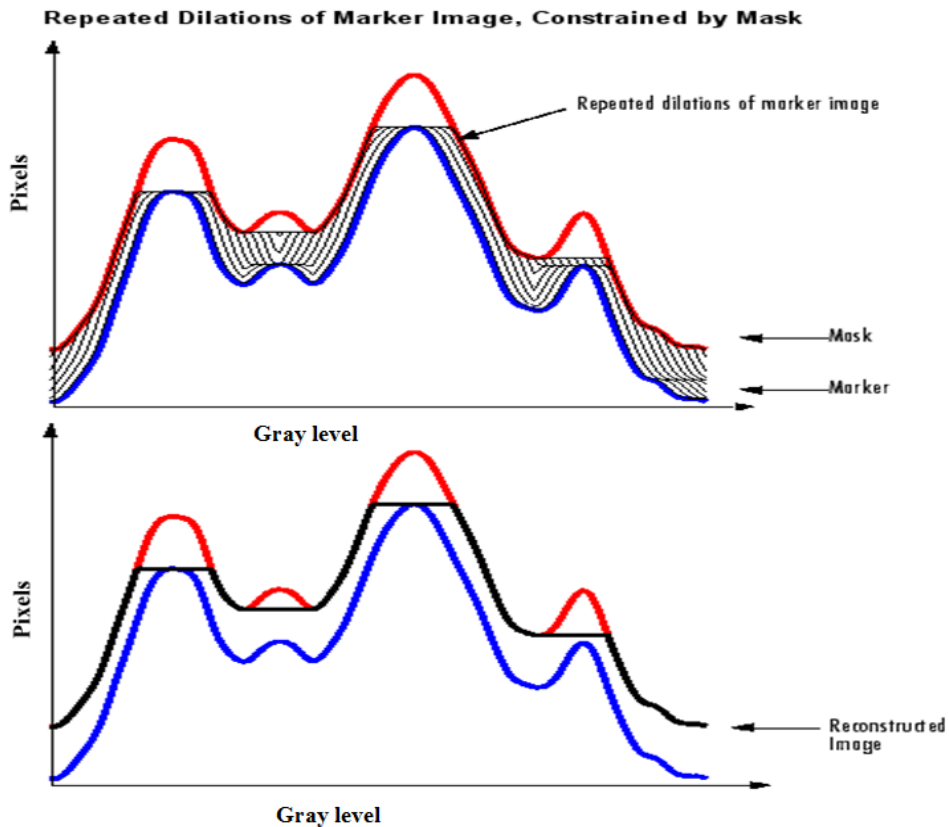


Figure 2.15: Opening by reconstruction algorithm (MATLAB 2014).

Figure 2.15 illustrates an original image  $A$  (red colour) as a mask. The resultant eroded image is considered through the marker  $b$  (blue colour). The opening by reconstruction is implemented by dilation  $A$  from the erosion times  $n$  of  $A$  (black curves colour). This procedure will be repeated until no changing of the mask image ( $A$  [red colour]) values occurs. In other words, all peaks of the mask image will become flat. Therefore, the final dilation reconstructed image with flat peaks is denoted in the black colour (the last black curve colour) as shown in Figure 2.14.

## The Morphological Operations for Holes Filling Concept

A background region encompassed by linked boundaries of foreground pixels is usually referred to as a hole. The focus of this thesis is particularly on morphological reconstruction using dilation algorithms for filling holes. So, two morphology reconstruction filling operations can be presented according to GONZALEZ/WOODS (2008):

### Hole-Pixel Initial Algorithm (HPIA)

The idea of this algorithm is an approach for region filling. GONZALEZ/WOODS (2008) introduce this filling approach as follows: (i) it relies on a cluster of dilations, intersections, and complementations by starting with point  $p$  inside of the border; (ii) the main target of this algorithm is to fill the entire region with black. Therefore, the starting point  $p$  must be assigned to a value of “black”; (iii) the assumption of this algorithm is that the “white” colour is labelled for all background (non-boundary) regions, so this algorithm will fill the background with a “black” colour; and (iv) this algorithm will be continuous until it reaches  $G$ .  $G$  demonstrates the object number within the images (number of iterations), and  $(x, y)$  represent the pixel coordinates of object  $i$ . Therefore, vector  $\mathbf{P}$  is considered an initial vector for this algorithm; see equations (2-19) and (2-20), respectively:

$$\mathbf{P} = \{I_i | i = 1, 2, \dots, G\}, \quad (2-19)$$

$$\mathbf{I}_i = \{(x_j, y_j)\}, j \text{ is number of holes in object } i \quad (2-20)$$

The drawback of the hole pixel initial algorithm is that it requires the beginning points for each hole inside of each object, within the image, and this is unsuitable for real-time applications. It is time-consuming and requires human involvement during the primary step. This drawback is solved by using an automatic way of Matlab (GONZALEZ/WOODS 2008) to find the beginning points for each hole. In conclusion, this algorithm can fill holes inside of objects successfully after a specified number of epochs and stop when no change of  $\mathbf{X}_G$  value will be recorded. Mathematically, the hole pixel initial algorithm is given by equation (2-21) (GONZALEZ/WOODS 2008):

$$\mathbf{X}_G = (\mathbf{X}_{G-1} \oplus B) \cap A^c, \text{ for } G = 1, 2, 3, \dots \quad (2-21)$$

where

- $P$  : initial vector of the algorithm,
- $B$  : symmetric structuring element,
- $\cap$  : intersection operator,
- $A^c$  : complement of original input binary image  $A$ ,
- $\mathbf{X}_G$  : product of the algorithm at iteration step  $G$ ,
- $\mathbf{X}_{G-1}$  : vector at iteration step  $G-1$ .

By analyzing equation (2-21), if  $\mathbf{X}_G = \mathbf{X}_{G-1}$ , then the algorithm ends. The filled set and its boundary will be utilized by a set union of  $\mathbf{X}_G$  and  $A$ , where finally the  $\mathbf{X}_{G-1}$  set will be included in all of the holes. Sequentially, the intersection process with the  $A$  complement at each epoch will keep the outcomes within the required region (GONZALEZ/WOODS 2008).

### Border Image Initial Algorithm (BIIA)

The idea of this approach is more effective for filling holes. This algorithm depends on the morphological reconstruction concept discussed previously. GONZALEZ/WOODS (2008) introduce these algorithm steps as follows: (i) a binary image is assumed as  $A(x, y)$ ; (ii) a marker image is presented as having 0 everywhere, excluding boundaries. Boundaries must have a value of  $1 - A(x, y)$ . Mathematically, the initial value for this approach is given by equation (2-22); (iii) next, several iterations will be realized and repeated by equations (2-23) and (2-24), respectively; and (iv) as any morphological reconstruction process, this algorithm will be terminated when there is no change in the mask image (flat peaks appear).

$$b(x, y) = \begin{cases} 1 - A(x, y), & \text{if } (x, y) \text{ is a border pixel of } A \\ 0 & \text{otherwise} \end{cases}, \quad (2-22)$$

where

$b(x, y)$ : the marker,  
 $A(x, y)$ : binary input image (mask).

$$O_R^{(n)}(A^c) = [R_{A^c}^D(b)]^c, \quad (2-23)$$

$$R_{A^c}^D(b) = D_A^{(G)}(b), \quad (2-24)$$

where

$A^c$ : the complement of the original input binary image,  
 $b$ : the marker,  
 $R$ : morphological reconstruction operation,  
 $A$ : mask of original binary image,  
 $D$ : dilation,  
 $G$ : objects number within images (number of iterations) until  $b^G = b^{(G+1)}$ ,  
 $n$ : the erosion times,  
 $O_R^{(n)}(A^c)$ : the product of opening by reconstruction operation.

The product of opening by reconstruction operation will produce a final binary image output equal to  $A$  with all the holes filled. The border image initial algorithm also generates a speed factor problem. This hindrance is associated with different reasons as follows: (i) this algorithm must be started from the border and will extend one pixel at a time from a boundary. Therefore, it needs several epochs for finding the final binary output image with all of the holes filled, while the number of epochs relies on the image size (dimensions); and (ii) another reason for this speed problem is in the case of the image not containing any objects. In this case, the algorithm will consume a large amount of time (GONZALEZ/WOODS 2008).

This thesis will define no more morphological operations, since this lies beyond the scope of this research. Further definitions of other morphological operations and algorithms can be found in DROOGENBROECK/TALBOT (1996) and other textbooks on digital image processing.

### 2.3.3 Image Analysis (Image Interpretation)

Image analysis is not the same as image processing. The basic aim of image analysis is to realize, measure, and classify image objects. Image analysis for crack detection is utilized during three categories as follows:

1. segmentation (thresholding stage),
2. crack connection (post-processing stage),
3. crack extraction and classification (detection stage).

Segregation of individual objects for measuring their pertinent brow is realized during the segmentation stage. The type of objects to be isolated (detected) are based on the image analysis target. Brightness, texture, colour, and shape properties may be measured through the segmentation stage (CHOU ET AL. 1994).

Crack connection (post-processing stage) is considered an optional stage based on the image analysis requirements. The latter stage is usually followed by the classification stage. To some extent, comparisons between the extracted measured features are done during the classification stage. In principle, the comparison is implemented as follows (CHOU ET AL. 1994):

1. Specifying which object features are needed to classify cracks
2. Specifying the allowance degree (how close the measurement must be to the instituted criteria). The aim is to classify crack features into different classes. Different classes (groups) are generated for crack feature assignment. This process is based on how the crack feature measurements match with the setup criteria.

Regarding crack classification in general, several classification approaches have been proposed in the literature; see HSU ET AL. (2001), SALARI (2012), CHOU/SALARI (2012), TEOMETE ET AL. (2005). There are no general specifications or methods for all crack cases. Every road authority has its own method and own specifications. These differ from one country to another due to their relationship with the pavement texture type.

Over the last 15 years, different image processing algorithms for pavement distress analysis were presented by different algorithms. Although a large amount of attention has been paid to this domain, in the literature there is still no single system of algorithms that is considered to be the best path for crack detection and classification. There are many complexities involved which are associated with crack detection and classification problems. These difficulties are summarized as follows (GERARDO ET AL. 2004):

1. Pavement construction materials have a lot of variability
2. Different shapes and alignments of cracks exist
3. Different extrinsic objects exist on the road pavement surface, for example, tire marks, paint, shadows, oil spots, mufflers, traffic loops, etc. All of these extrinsic objects create an object occlusion problem.

A perusal of literature would strongly confirm that there are possibly from 20 to 200 groups of crack detection and classifications being executed by different investigators. The performance of each set of algorithms is checked by looking at the results and applying them (empirical way). Moreover, due to the variance of pavement textures, this situation creates a need for any proposed set of algorithms to be examined on comprehensive sections of different pavement textures (HEROLD ET AL. 2008). In conclusion, different sets of algorithms were developed. Possibly, some of these algorithms systems are more effective as compared to others, but in principle, none are recommended as superior (HEROLD ET AL. 2008). Most of the previous algorithms used digital image processing techniques for crack detection. Digital image processing and analysis for crack detection can be divided into four sequential stages: pre-processing, segmentation, post-processing, and feature extraction and classification. In general, segmentation and feature extraction/classification, and the problems associated with them, are of great interest throughout different recent research works. However, pre-processing and post-processing stages are considered as preparatory stages (optional stages) for segmentation and feature extraction/classification stages, respectively. In some cases, segmentation may be utilized without having any pre-processing, i.e., it is based on the original image's nature. The same issue exists for post-processing, as feature extraction/classification may be done without having any post-processing processes. This matter depends on the nature of the resultant images from the thresholding stage. Finally, feature extraction/classification is related to each other. Classification is impossible unless feature extraction is done (JIAN 2002).

### **Segmentation Definition and Problems**

Over the past years, segmentation has represented a critical task for pavement image processing, as it is a fundamental issue in order to measure and distinguish cracks successfully. Isolating the cracks from the remaining extrinsic objects and noise is done during the segmentation stage, if the cracks are not successfully separated. The cracks will not be measured precisely without segmentation (KELVIN ET AL. 2007).

In fact, no direct straightforward approach is known to the author for segmentation, and therefore no notion of segmentation is available. As HARALICK/SHAPIRO (1985) has stated: "Image segmentation techniques are basically ad hoc and differ precisely in the way they emphasize one or more of the de-

sired properties and in the way they balance and compromise one desired property against another.” In general, MICHAEL (1992) claims that segmentation is the same as binarization. To some extent, this assumption is not true because the segmentation may be done on grayscale images, without switching to a binary image. For all anyone knows, algorithms for crack detection and classification are utilized by converting gray-scale images into binary images. However, working with binary images has different utilities. As JAMES (1988) has expressed: "If you can obtain a suitable binary image showing the required object, then there is a wide range of techniques which you can use to enhance the image and extract features that make classification possible. Binary image processing is easier from both the theoretical and practical point of view. Binary images are more amenable to analysis because they have clear-cut properties, such as boundaries, areas and shape. We can ask questions about the shape of a binary object because it has well-defined boundaries. Questions about the shape of an object in a gray level image depend on where we decide its edges are." Overall, obtaining a satisfying binary image constitutes the most challenging issue during binary processing. As JAMES (1988) has indicated, “This can be 99% of the real image processing/ recognition problem.”

To obtain an appropriate binary image, it is necessary to select a convenient threshold. Sequentially picking a suitable threshold is considered a problematical task for pavement images. According to the experiences of automated commercial systems, any commercial automated image processing system must have a threshold-setting algorithm integrated into it. Moreover, a superior threshold value for each image must be recommended by this threshold-setting algorithm. This threshold value should be able to isolate only the cracks from the rest of the pavement images. In addition, variations in the pavement images must be considered by using a changeable threshold rather than a fixed one. In fact, this is one reason why some threshold setting algorithms are more effective than others. The histogram method is the most common and simple approach for setting a threshold automatically (KITTLER/ILLINGWORT 1985).

By analysing Figure 2.16, it can be seen that the brightness levels of the pavement surface are lighter than the brightness levels of the cracks. Therefore, the histogram (Figure 2.16-left) has two peaks, and the threshold will be located in the valley between them. In the final resultant binary image, the cracks will be displaced as black, and the rest of the pavement image as white (or vice versa). In actuality, most of the cracked pavement image histograms do not have just two obvious peaks (Figure 2.16-right). It is obvious from this kind of brightness level distribution that the setting threshold value will be more complicated. Although it is possible to have several trial and error techniques, it is not a logical approach for any automated system (KITTLER/ILLINGWORT 1985).

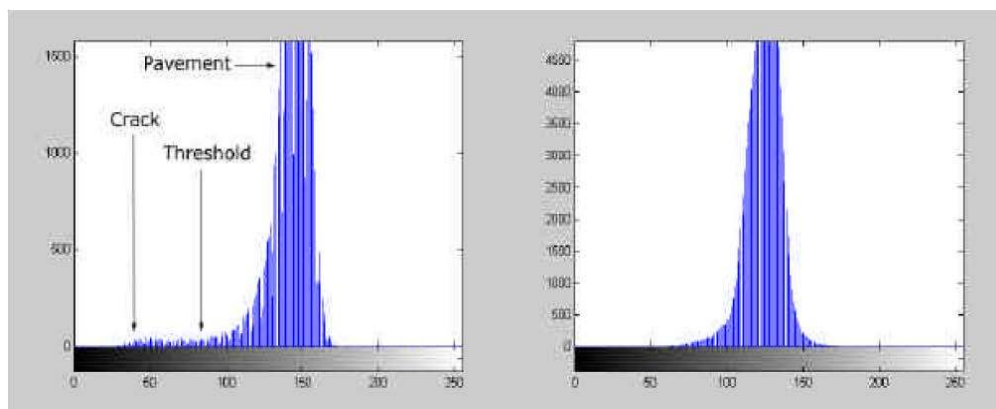


Figure 2.16: Histogram showing two types of intensity distributions (GIRARDELLO 2002 and HOWE/GLEMENA 1987).

Several significant problems associated with the segmentation stage were recorded as follows: (i) current pavement images contain a broad zone of gray levels. Thus, the contrast is considered as one of the techniques for crack recognition. There is a variance of the contrast level between pavement surface and the crack. In most cases, cracks must be darker than the rest of the pavement image. In the other cases, it is unattainable to detect cracks from the rest if the contrast is too low. Several research works tried to solve this problem by adjusting the non-uniform background illumination, using different averaging algorithms; and (ii) the other common problem with pavement images is noise. The

appearance of noise is due to multiple factors: (a) texture of the pavement surface; and (b) shadows and small holes in the surface, such as oil spots and other debris, that are generated due to the pavement surface roughness. A median filter is used as an efficient solution for removing each small spot of noise (KOUTSOPOULOS/DOWNEY 2006). It is worth mentioning that there are several kinds of noise (e.g., black fan belt or piece of black rubber hose) that are not deleted by the median filter. The reason for this is because the size and colour (brightness levels) of the black fan belt or the black rubber hose's pixels are similar than the size and colour (brightness levels) of the pavement cracks. These types of noise will appear as lying adjacent to the cracks. Consequently, from an empirical point of view, it is impossible to cut them out during the segmentation stage. As can be seen in Figure 2.17, a black rubber hose is located adjacent to the cracks (Figure 2.17-right). This creates a problem from the image processing side, in contrast to a human rater. The latter one can distinguish between a hose and cracks; whereas, the former one will deal with the hose in the same way that it deals with other black pixels in the binary image. In conclusion, the hose will be detected as a possible crack. In order to solve this problem, some mechanisms must be included to remove the hose from consideration, although it may not be deleted from the black pixel class. The characteristics for crack differentiation during the classification stage may be utilized as a possible mechanism to exclude the hose from a crack. From this point of view, some operations can be used for large-sized noise removal; however, in the same instance, narrower cracks will also be removed (KITTLER/ILLINGWORT 1985).



Figure 2.17: Two noisy binary images (GIRARDELLO 2002 and HOWE/GLEMENA 1987).

### 2.3.4 Review of Some Global and Local Binarization Techniques

Recent research work has demonstrated that different binarization approaches can be used to extract objects from pavement images, as well. OTSU (1979) presented a threshold selection approach. The aim of this approach is to automatically select an optimal threshold for image segmentation. This is completed to increase the quality of separation. Several methods have been introduced in the literature. The histogram of the image will be divided into two probability distributions. The objects will be represented by one probability side of the distribution, while the background will be represented by the other side. These methods are based on the maximum entropy algorithm (KAPUR ET AL. 1985, NIBLACK'S 1985). YANOWITZ/BRUCKSTEIN (1989) proposed an approach for threshold surface calculations. This approach is executed by a gradient map of the image. The latter approach's aim is to mark an object boundary for the local threshold determination. Histogram-based global thresholding techniques are used by SOLIHIN/LEEDHAM (1999) and LEEDHAM (2003) in order to define a new class of histograms. These techniques rely on a two-phase thresholding approach of foreground, background, and a fuzzy area. A histogram-based binarization algorithm is used for multi-scale texture segmentation and spatial cohesion constraints, e.g., pavement images. This latter algorithm is used automatically by MOTWANI ET AL. (2004) for crack detection from various pavement sources. Seriously degraded and very low quality gray scale pavement images, with a great deal of noise, will be binarized using a local (adaptive) threshold method (YANG/YAN 2000). SAUVOLA/PIETIKAKINEN (2000) proposed an approach for adaptive image binarization. This algorithm deals with a pavement image as a bundle of different components, such as noise, background, and the rest of the image. RANDOLPH/SMITH (2008) show different overviews of binary domain approaches. They demonstrate that filters will extract edges and enhance pavement images to be of a finer quality. Simple and complex pavement images were tested by the algorithm by WU/AMIN (2003). This last algorithm works well, using multi-stage global thresholding followed by local spatial thresholding. FAN ET AL. (2003) investigated wavelet coefficient correlations to exchange the segmentation phase with a diffusion process. This algorithm succeeds to deal with noisy pavement images.

Several high-quality techniques have been introduced and improved rapidly. BARTOLO ET AL. (2004) presented Bernsen's algorithm as a tool for pavement image binarization. This algorithm is able to deal with poor quality images, e.g., inhomogeneous shadow background. So, it is considered a precise binarization method without any user-defined interaction. A digital image binarization scheme is presented by GATOS ET AL. (2004). This algorithm scheme is implemented as the follows: (i) low-pass Wiener filter is used during the pre-processing stage; (ii) Niblack's approach is done during the segmentation stage; and (iii) a post-processing quality and connectivity step is done lastly. MEHMET/SANKUR (2004) show different overviews of most image thresholding methods, such as histogram shape, measurement space clustering, entropy, object attributes, spatial correlation, and local gray-level surface for pavement images. The performance measures of these thresholding methods are compared in MEHMET/SANKUR (2004). BIENIECKI/GRABOWSKI (2005) present a comparative study between global and local thresholds. This comparative study is implemented with a suitable window size (the window size definition is explained in more detail in chapter 3, section 3.2.1). Local feature thresholding algorithm and quad-tree decomposition for pavement sub-regions are adapted by (AKIHITO/SAITO 2005). GATOS ET AL. (2004) report a segmentation-free recognition procedure and closed cavity regions for old pavement images. A novel alternative binarization algorithm and a new thresholding technique for pavement image interpolation is introduced and compared against existing algorithms, see LEEDHAM (2003), JI ET AL. (2005). A survey by KAVALLIERATOU/ANTONOPOULOU (2005) extensively compares the most widely used pavement image binarization methods. These methods utilize the fact that the pixels representing cracks do not exceed 10% of the total number of pixels for the entire image. In fact, some algorithms are usually based on robust adjustment techniques (e.g., BURGOYNE ET AL. 2007, BADEKAS/PAPAMARKOS 2007). These latter techniques used binarization algorithms for degraded pavement images, and can differ successfully between crack images and non-crack images by different mechanisms.

Several other well-known methods in the literature have been employed to test the same collections of pavement images for comparison. These methods include Niblack's method (NIBLACK'S 1985), Sauvola's method (SAUVOLA/PIETIKAKINEN 2000), and beamlet transformation for crack detection (YING/SALARI 2009). These methods are chosen because either they have been previously used for threshold pavement image successfully, or they were designed to extract textual information from its application (WU ET AL. 2005). In the following, a general overview of these well-known methods is presented.

### **Niblack's Method (Local Thresholding by NIBLACK'S 1985)**

A significant advantage of this representation is that it suggests the use of a local adaptive method for threshold surface computations. According to equation (2-25), Niblack represents the threshold value for a pixel, with a fixed neighbourhood window as a linear relationship of mean and standard deviation of the neighbourhood pixels with a constant gradient of  $v$ . Thus, this method is utilized by moving a window across the image. The local mean and standard deviation must be calculated for each centre pixel in the window. Similar to the corresponding method, two factors affect the algorithm performance as follows: (i) window size (a small window leads to a loss of details, on the contrary, a large window leads to high computation cost); and (ii) parameter  $v$  (which is critical in terms of how the algorithm can select a suitable  $v$  to separate the object well). The following equation explains the threshold determination:

$$T(x, y) = m(x, y) + v \cdot \sigma(x, y), \quad (2-25)$$

where

- $m(x, y)$  : mean gray level of the pixels within the window,
- $\sigma(x, y)$  : standard deviation of these pixels within the window,
- $T(x, y)$  : Niblack's threshold,
- $v$  : user defined parameter that is used to adjust the percentage of total pixels that belong to foreground object, especially in the boundaries of the object.  
A value of  $v = -0.2$



Then, from equation (2-26), the pixel class is evaluated as follows:

$$\omega(x, y) = \begin{cases} \omega_f, & f(x, y) < T(x, y) \\ \omega_b, & p(x, y) \geq T(x, y) \end{cases}, \quad (2-26)$$

where

- $\omega(x, y)$  : pixels intensity of image after threshold,
- $f(x, y)$  : gray level intensity of each pixel  $(x, y)$  in the original image,
- $T(x, y)$  : threshold calculated by Niblack's method using equation (2.25),
- $\omega_f$  : foreground pixels intensity,
- $\omega_b$  : background pixels intensity.

### Sauvola's Method (Local Thresholding by SAUVOLA/ PIETIKAKINEN 2000)

Sauvola's algorithm (SAUVOLA/PIETIKAKINEN 2000) is considered as an adjustment of Niblack's algorithm. This algorithm shows a good interpretation for pavement images of complex conditions, e.g., the background contains a light texture, large variations, and uneven illumination. The main difference between Niblack's algorithm and Sauvola's algorithm is that the latter one uses a dynamic range of the standard deviation  $\sigma$  rather than a fixed one, like the former algorithm. Sauvola's algorithm can select a threshold value based on image properties using equation (2-27) as follows:

$$T(x, y) = m(x, y) \cdot \left( 1 + v \cdot \left( 1 - \frac{\sigma(x, y)}{\sigma} \right) \right), \quad (2-27)$$

where

- $m(x, y)$  : mean gray level of the pixels within the window,
- $\sigma(x, y)$  : standard deviation of these pixels within the window,
- $T(x, y)$  : Sauvola's threshold,
- $v$  : constant with usual value  $v=0.1$ ,
- $\sigma$  : constant with usual value  $\sigma=128$  (it depends on the number of gray values).

Equation (2-26) above is used for pixel class determination.

The parameter  $v$  is used to adjust the percentage of total pixels that belong to the foreground object.  $\sigma$  is referred to as the maximum gray value standard deviation obtained over all of the neighborhoods (window). It is considered a dynamic range of standard deviation. In conclusion, although different methods of image thresholding exist, which may be applied for crack detection of pavement images, all of them require some user-defined parameters. Thus, the studied algorithms are inappropriate for an automated crack detection interpretation system. Niblack's and Sauvola's algorithms utilize a parameter  $v$ . The value of parameter  $v$  must be determined directly from an image's nature. However, the requirement for the single parameter  $v$  hinders the automation process. Moreover, determining the intensity for each point within a specified window is adverse for speed.

### Beamlet Transformation for Crack Detection

The concept of beamlet transformation was first introduced by DONOHO/HUO (2001) as a tool for multi-scale image analysis. In general, the beamlet transformation is the collection of line integrals along the set of all beamlets. Beamlet transformation for crack detection is defined as a simple dyadic organisation of all crack line segments at different locations, orientations, and scales (YING/SALARI 2009). This principle is used as a tool to detect and extract linear crack edges with high accuracy.

For digital images, the beamlet transformation is a measure of the line integral in the discrete domain. The beamlet transformation for all the points along the beamlet is defined using equation (2-28), where the beamlet transform  $Tf$  of function  $f$  is defined as follows:

$$Tf(x, y) = \sum_{x, y} f(x, y) \phi(x, y), \quad (2-28)$$

where

- $T f(x, y)$ : beamlet transformation of function  $f(x, y)$ ,  
 $(x, y)$ : pixels coordinates,  
 $f(x, y)$ : gray level intensity of pixel  $(x, y)$  in the image,  
 $\phi(x, y)$ : weighting function of each pixel  $(x, y)$  in the image.

The weighting function of each pixel is calculated using equation (2-29) by:

$$\phi(x, y) = \frac{l_n}{\sqrt{L}}, \quad (2-29)$$

where

- $\phi(x, y)$ : weighting function of each pixel  $(x, y)$  in the image,  
 $l_n$ : length of a segment in each square pixel on the beam,  
 $L$ : total length of the beam.

The total length of the beam is calculated using equation (2-30) by:

$$L = \sum l_n, \quad (2-30)$$

The steps for executing the beamlet transformation to detect cracks are implemented as follows (YING/SALARI 2009):

- a. The image must be divided into smaller rectangular windows;
- b. Build a beamlet dictionary: a beamlet dictionary is defined as a dyadically organized library of line segments at a range of locations, orientations, and scales which give a multi-scale approximation to the collection of all line segments. For single scale beamlet transformations, all windows have the same dimension, and thus the same beamlet structures. Therefore, the dictionary needs to only be calculated once, and can be used for all of the windows. For each beamlet, the following database must be registered as follows:
  - i. The coordinates of the pixels that are located on the beam must be specified,
  - ii. Each segment of the beam must record its corresponding length  $l_n$ ,
  - iii. The total length of beamlet  $L$  is computed,
  - iv. The weighting of the corresponding pixels are calculated based on (ii) and (iii) results using equation (2-29),
  - v. The beamlets dictionary is saved.
- c. The beamlet dictionary is executed iteratively for each small window after completing its building and storing. Next, the beamlet, which provides the maximum value, is selected if its value exceeds a pre-defined threshold value. This beamlet will represent cracks within the window (Figure 2.18). Figure (2-18) displays the beamlet transform as a weighted sum of pixel values along the shaded line that the beamlet traverses.

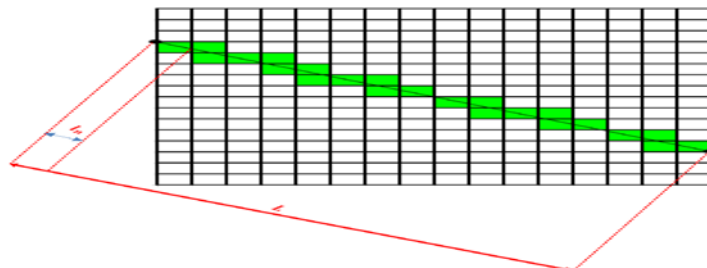


Figure 2.18: Beamlet transform is a weighted sum of pixel values along the shaded line (YING/SALARI 2009).

### 2.3.5 Partial and Complete Crack Detection Algorithms

Several image processing algorithms for crack detection have been developed; however, many of them, which are dependent on approximation algorithms, face some challenges. Therefore, automated analysis and pattern recognition are highly appropriate for pavement surveying. In general, the required approach is to collect pavement images using cameras mounted on a moving vehicle. Next, special software is utilized to identify and quantify the pavement distress from these images. During the previous two decades, the numbers of research projects concerning the development of automated pavement inspection systems has increased significantly. In most of the developed algorithms, pavement images are processed to extract crack information during four stages as follows (Figure 2.19):

1. Image enhancement (pre-processing) stage: Pavement images are composed of background, noise, and cracks. The noise on the image, objects on the road, the pavement patterns, and the non-uniform backgrounds, cause difficulties for crack detection and even fail the threshold process. In order to recognize distress with fidelity on the road surfaces, many algorithms have been developed to eliminate noise and normalize the background. e.g., histogram equalization, contrast, morphological operations algorithms, and the multiply factor method.
2. Thresholding (segmentation stage): Thresholding is a technique used to separate objects from the background. Since cracks are always darker than their surroundings, the threshold value should be of relatively low intensity. Usage of more than one thresholding mechanism value gives a dynamic approach to crack extraction.
3. Crack connection (post-processing stage): The binary images extracted from pavement images are usually noisy. The cracks in the binary images are discontinuous, and there are two reasons for this discontinuity of the cracks: firstly, the reality of the shape of the cracks itself, and secondly, the discontinuity due to the segmentation process in the previous thresholding stage. In order to obtain continuity of linear cracks, the discrete linear crack points need to be connected. In addition, in this stage, the remaining noise is reduced, and all of the cracks holes are filled using different morphological operation algorithms, hole filling algorithms, and connected components algorithm.
4. Crack extraction and classification (detection stage): Some of the resultant images from the post-processing stage are still being affected by noise, so the processing methods in this stage are able to extract linear cracks alone by setting a threshold to the crack size. Linear cracks will be detected, and the remaining noise will be eliminated. Then, according to length, width, and orientation, linear cracks are classified into different categories by using different methods.

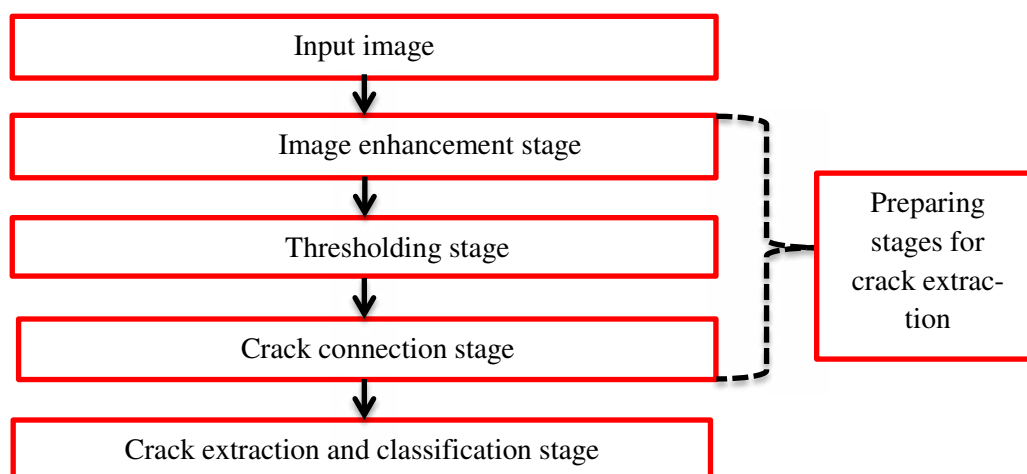


Figure 2.19: Workflow for the combination of general stages to extract crack information.

This section will focus on partial and complete crack detection algorithms. Every crack detection algorithm includes four stages as mentioned previously. Every stage is realized using different methods. Figure 2.20, 2.21, 2.22, and 2.23, respectively, present a workflow for the used methods of each stage, with respect to different algorithms. All of these algorithms will be explained in detail later in this section.

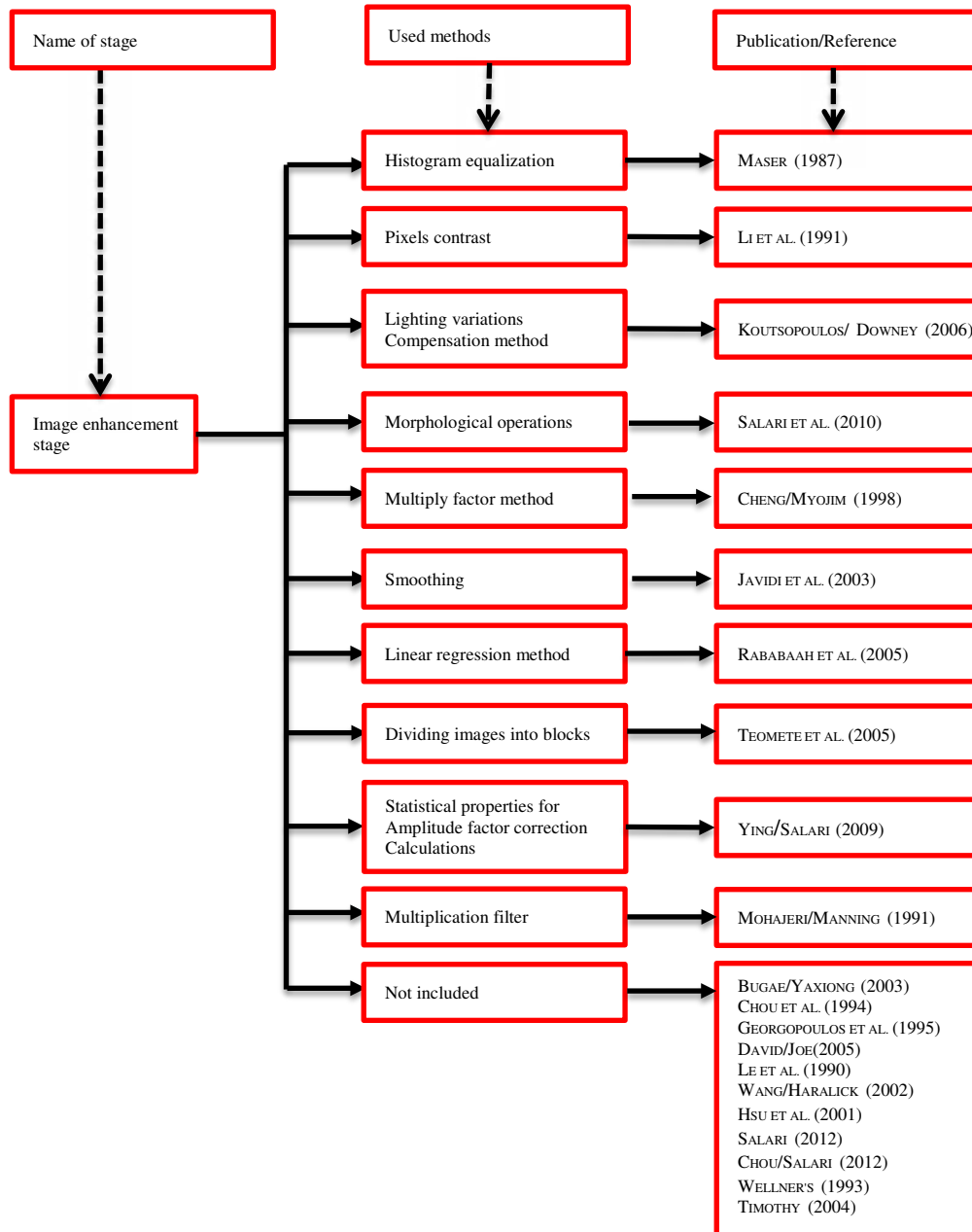


Figure 2.20: Workflow for the used methods of image enhancement stage with respect to different algorithms.

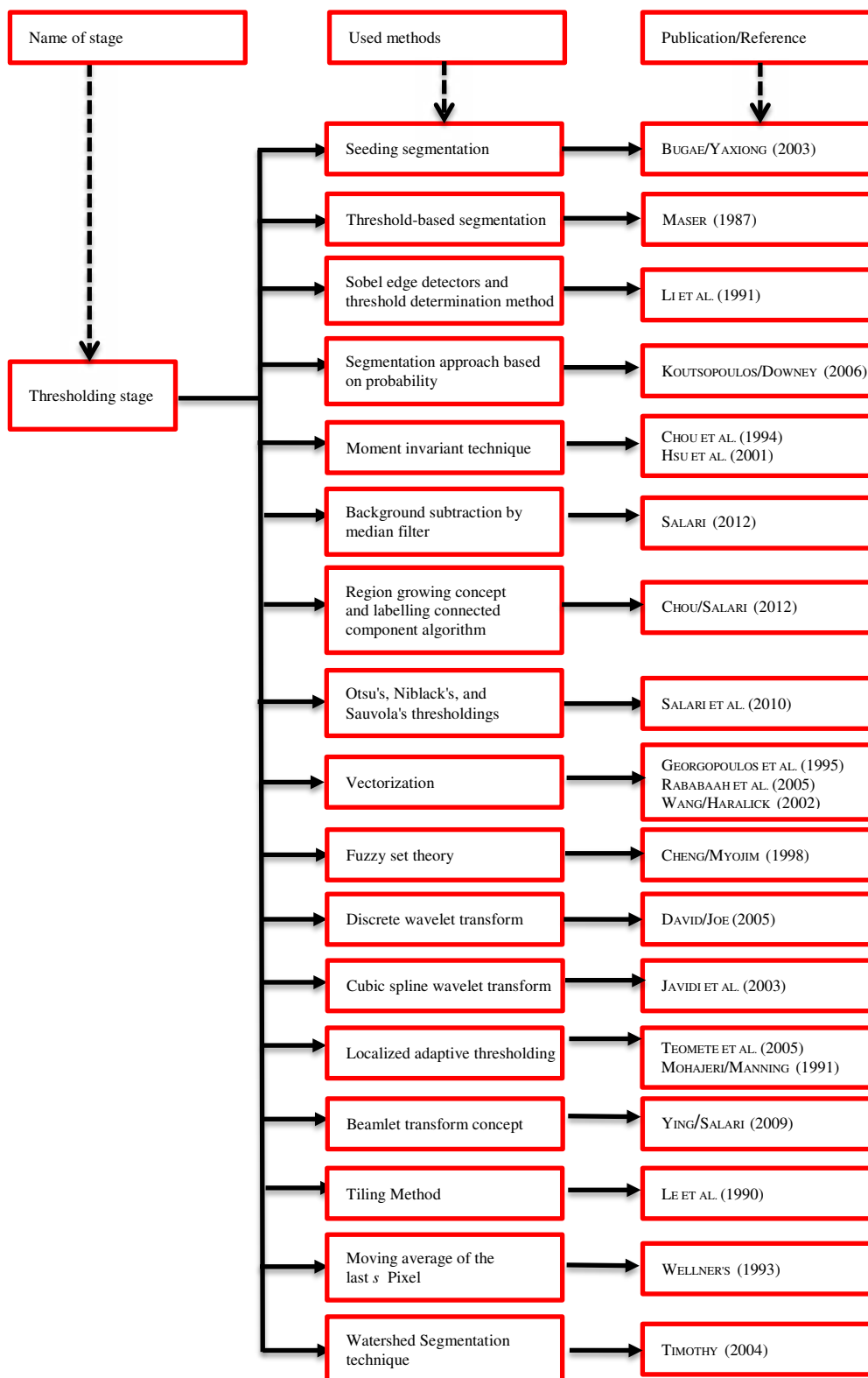


Figure 2.21: Workflow for the used methods of thresholding stage with respect to different algorithms.

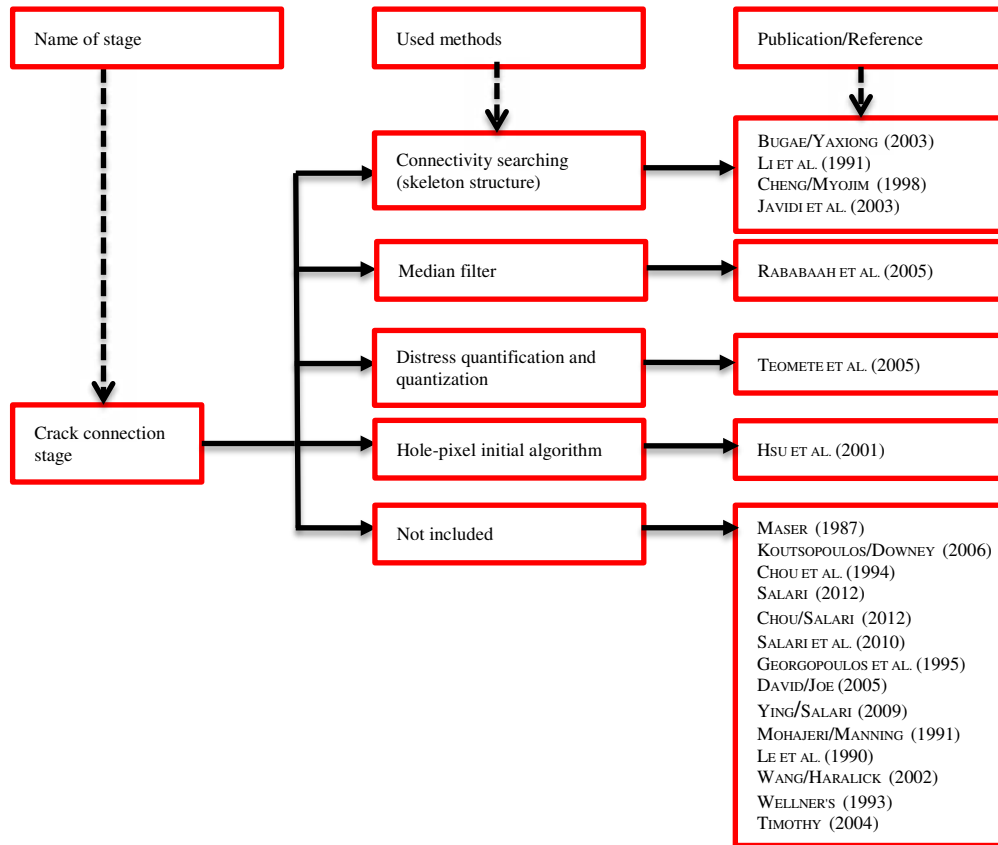


Figure 2.22: Workflow for the used methods of crack connection stage with respect to different algorithms.

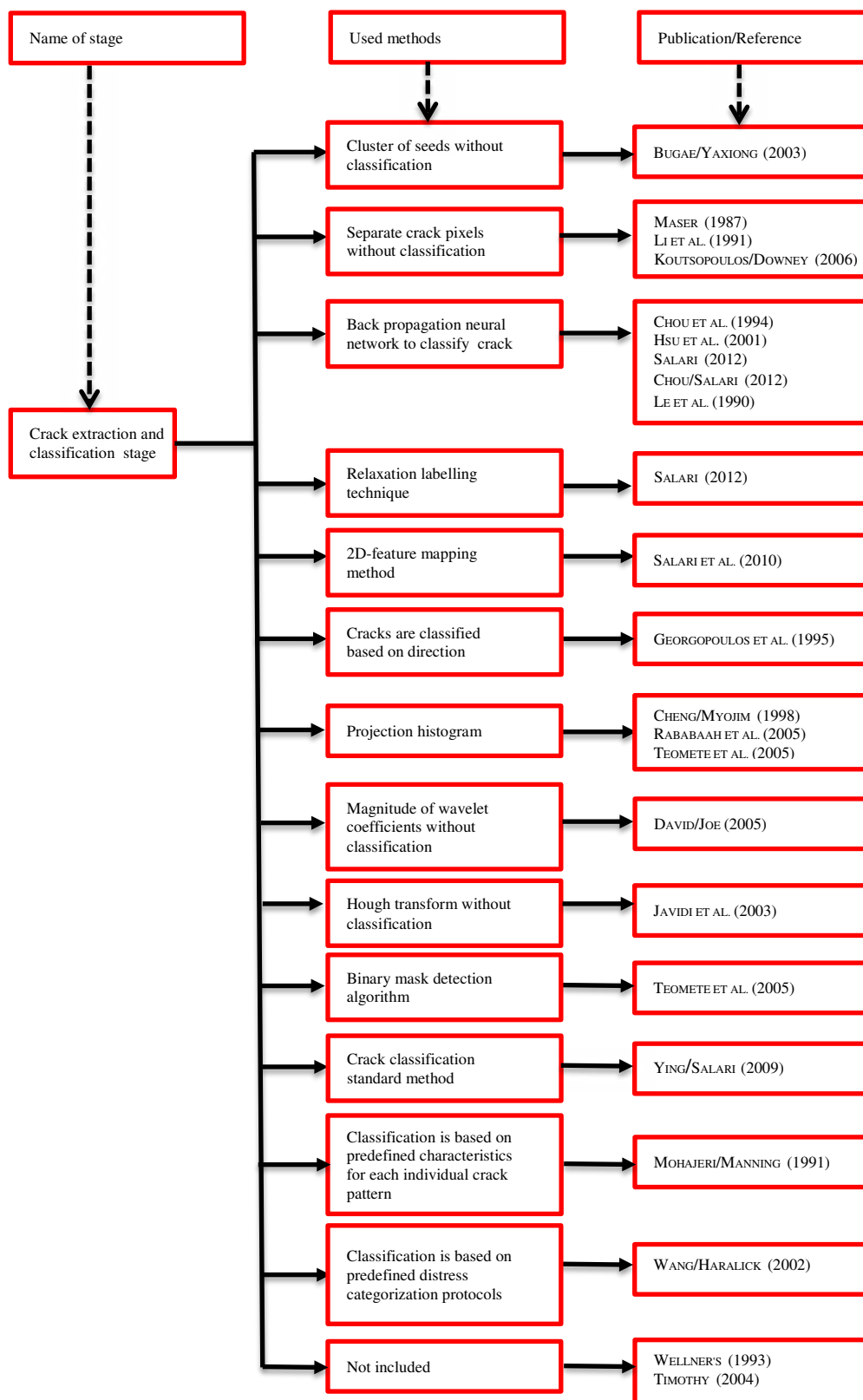


Figure 2.23: Workflow for the used methods of crack extraction and classification stage with respect to different algorithms.

BUGAE/YAXIONG (2003) developed a customized image processing algorithm for pavement cracking inspection. The image enhancement stage is not included in this algorithm. The image is divided into small cells during the thresholding stage. Each cell is investigated and classified by determining if there is a crack inside. For this reason, local parameters are defined. Connectivity searching (cluster of seeds continuity) is done during the crack connection stage. Obviously, after verification, a cluster of seeds is identified as a real crack. This real crack must stratify the seeding algorithm characteristic during crack extraction and the classification stage. The BUGAE/YAXIONG (2003) algorithm produced false seeds (noise) in different cases. Firstly, the road sections are occluded by shadows. This is due to the nonexistence of image enhancement (pre-processing stage). Secondly, the road sections contain cracks of illuminated background. Moreover, this algorithm cannot classify cracks. Due to these disadvantages, this algorithm is considered to be an incomplete procedure.

MASER (1987) used the histogram equalization technique during the image enhancement stage. This image processing technique is investigated for image contrast adjustment. This method increases the global contrast obviously in cases of close contrast images. During implementation of this technique, the most frequent intensity values will be distributed effectively on the histogram. Therefore, the lower local contrast areas will gain a higher contrast. This means that the overall contrast of the entire image will be improved during the image enhancement stage. MASER (1987) separated crack pixels using a threshold-based segmentation method during the thresholding stage. The crack connection stage is not included in this algorithm. In addition, MASER (1987) separated crack pixels with a lot of noise during the crack extraction and classification stage. It should be noted that the Maser algorithm cannot distinguish between cracks and road markings. Furthermore, the resultant images still have noise. Therefore, this algorithm cannot classify cracks. For these reasons, it is considered to be an incomplete procedure.

LI ET AL. (1991) utilized the contrast between pixels in the image enhancement stage. A Sobel Edge Detector (described previously in section 2.3.2.2) is used to filter out the edges during the thresholding stage. Then, LI ET AL. (1991) modified the threshold determination method. The basics of this threshold determination method are developed by KITTLER/ILLINGWORT (1985). LI ET AL. (1991) modified the threshold value depending on statistical characteristics of crack pixel clusters and local thresholding. The assumption of this algorithm is that noise clusters had a perimeter of less than 20 pixels. Therefore, the selection of threshold values is done iteratively. This threshold value is different from one image to another one. The positive characteristic of this algorithm is its ability to connect crack segments using connectivity searching. This is done during the crack connection stage. In addition, the final result of this algorithm will form a continuous cluster of crack pixels during the crack extraction and classification stage. Alternatively, some disadvantages exist, as follows: Firstly, the LI ET AL. (1991) algorithm cannot deal with complex compound cracks with noise clusters of more than 20 pixels. Secondly, the algorithm cannot classify cracks. Therefore, this algorithm is considered to be an incomplete procedure.

KOUTSOPOULOS/DOWNEY (2006) proposed a lighting variation compensation method by subtracting an average of a few non-distress images from the same series during the image enhancement stage. For segmentation, instead of using ordinary binary segmentation, which assigns a value of one to object pixels and a value of zero to background pixels resulting in a binary image, a different approach is suggested. It assigns values from 0 to 3 to each pixel based on its probability of being an object pixel. Background pixels are drawn from the Gaussian distribution. Object pixels are drawn from a similar distribution with a lower mean and a higher variance. The threshold that meets various criteria can be obtained from these two distributions during the thresholding stage. The aim of this algorithm is to separate crack pixels from the background pixels during the crack extraction and classification stage. The crack connection stage is not included in this algorithm. However, this algorithm does not work correctly because the extracted thresholding value responded to the cracks and lane markings together. These line markings need to be eliminated as false positives. Moreover, this algorithm cannot classify cracks. In conclusion, this algorithm is considered to be an incomplete procedure.



CHOU ET AL. (1994) used moment invariants from different types of distress to obtain features during the thresholding stage. The image enhancement and crack connection stages are not included in this algorithm. Additionally, back propagation neural networks were used to classify the features during the crack extraction and classification stage. A back propagation neural network is used to classify the type of distress based on Hu's moments (HMs), Zemike moments (ZMs), and Bamieh moments (BMs). The back propagation neural network of this algorithm deals with 18 nodes (four BMs+7ZMs+6HMs+1Bias) in the input layer, 17 nodes in hidden layers, and seven nodes in the output layer. This approach can classify cracks into seven types: longitudinal, transverse, combined, right and left, diagonal (edge cracks), alligator, and no crack. Moment invariants are shown to be feasible for pavement crack classification. The negative sides of this algorithm occur due to different reasons as follows: Firstly, the irregularity and fuzzy shape of the pavement cracks themselves will lead to the loss of moment invariant properties. Then, the feature extraction will not have been performed well. Secondly, the extraction's irregular and fuzzy features are used as inputs to the neural networks. The weaknesses of these extracted features affect the neural network classification rate. Therefore, the classification rate will be satisfactory, but not perfect. In conclusion, this algorithm is considered a complete procedure with some negative aspects. These negative sides depend on the case studies.

In general, two-dimensional image patterns will be minimized into feature vectors, e.g., translation, scale, and the rotation of an object in an image, using moment invariant techniques during the thresholding stage. The hole-pixel initial algorithm (HPIA) is implemented in order to fill all of the object holes during the crack connection stage. This is usually followed by a crack extraction and classification stage in which the extracted features of the segmentation stage will be considered as input to the neural network (HSU ET AL. 2001). The back propagation neural network technique classifies cracks into: longitudinal, transverse, netted (alligator & block), and cavities (potholes). Based on the desired end-product, the accuracy of the final classification results was 85%. Image enhancement is not included in this algorithm. This algorithm cannot distinguish between cracks and lane markings. Therefore, it is considered as a complete algorithm with some problems and defects. To some extent, the crack detection problem is still unsolved. Nevertheless, there are several other algorithms which are able to detect and classify cracks, see SALARI (2012), CHOU/SALARI (2012), SALARI ET AL. (2010). These algorithms are considered as complete algorithms with some problems and defects. These algorithms face obstacles, such as pavement images with shadows and pavement images with lane markings. For example, SALARI (2012) proposed an algorithm based on background subtraction by a median filler during the thresholding stage. Image enhancement and crack connection stages are not included in this algorithm. This algorithm employed relaxation labelling techniques and neural network training to classify distresses as longitudinal cracks, transversal cracks, or potholes during the crack extraction and classification stage. CHOU/SALARI (2012) suggested an algorithm based on using a region growing concept and labelling connected components algorithm. These algorithms are able to differentiate road surface from the background region and separate cracks from the road surface during the thresholding stage. The definition, evaluation, and concepts regarding labelling connected components algorithm are explained in detail in chapter 3, section 3.3.1. Image enhancement and crack connection stages are not included in this algorithm. This algorithm used Neural Network Training to classify cracks into four categories: block cracks, longitudinal cracks, transverse cracks, and no crack during the crack extraction and classification stage. SALARI ET AL. (2010) offered an algorithm to remove non-uniform illumination effects using morphological operations during the image enhancement stage. Otsu's, Niblack's, and Sauvola's thresholding algorithms are implemented during the thresholding stage. Additionally, 2D-feature mapping was used to classify cracks into four categories: alligator cracking, block cracking, longitudinal cracks, and transverse cracks, during the crack extraction and classification stage. Afterwards, the extracted cracks will be printed on the original image using a contouring algorithm (JONES 1971). Image enhancement and crack connection stages are not included in this algorithm.

GEORGOPOULOS ET AL. (1995) proposed a method in which the distress can be represented by a set of vectors approximating the crack composing the distress (vectorization) during the thresholding stage.

The direction vectors are then grouped into two categories: horizontal and vertical. Finally, the cracks are classified based on their direction during the crack extraction and classification stage. The image enhancement and crack connection stages are not included in this algorithm. Although this algorithm works well, there are some defects in the case study of having different pavement textures. Therefore, this algorithm is considered as a complete procedure with some complications.

According to CHENG/MYOJIM (1998), a viable crack extraction method exists that comprises four stages: (i) using a multiple factor method in the image enhancement stage. This method is implemented by dividing pavement images into rectangular windows. The mean value for each window is computed. Then, the mean value of each window is converted to a target value by a multiplier. The latter one is different from one window to another. Finally, a decision will be made based on the presence of a sudden drop of illumination. If a sudden drop exists within a window, the window is classified as a crack window, and the mean value of the window must be exchanged by the average of neighboring windows. (ii) fuzzy set theory is implemented during the thresholding stage. The crack membership values of the pixels are established by mapping the fuzzified image to the crack domain. (iii) skeleton structure (connectivity searching) is used to review the connectivity of the darker pixels during the crack connection stage. Finally, (iv) the cracks are classified using the image projection algorithm during the crack extraction and classification stage. The algorithm examines the peaks of the projection vectors in order to determine the type of cracks. The results of classification will appear as follows: (1) If a peak exists in the vertical projection vector, the crack is classified as longitudinal; (2) if the peak exists in the horizontal projection vector, the crack is classified as a transverse crack; (3) if the peak exists in the diagonal direction, the crack is classified as diagonal; and (4) if four peaks exist in all four direction projections, the crack is classified as an alligator crack. However, the algorithm is considered as a complete procedure with two defects. Firstly, this algorithm is limited and can be prone to failure, especially in the case of large-sized images. The reason for this is that the algorithm is set as a classical pixel based approach. Reviewing and linking cracks, pixel by pixel, is quite time-consuming. Secondly, the multiple factor method does not execute any reactions in the pre-processing stage, if the cracks cross more than one window.

As a consequence, the identification of corresponding crack objects requires a robust extraction algorithm which is insensitive to illumination and scale differences, e.g., wavelet transformation. A wide variety of crack extraction algorithms have been proposed and investigated in the literature, e.g. DAVID/JOE (2005), JAVIDI ET AL. (2003). DAVID/JOE (2005) addressed the discrete wavelet transformation during the thresholding stage. Various frequency sub-bands will be generated for each pavement image. Moreover, the grade of distress without classification will be displaced based on the quantity of wavelet coefficients during the crack extraction and classification stage. The image enhancement and crack connection stages are not included in this algorithm. This algorithm has an important disadvantage because it fails in cases of pavement texture variance. For this reason, this algorithm is considered to be an incomplete procedure. Further methods exploit the knowledge of wavelet transformation. JAVIDI ET AL. (2003) presented a smoothing concept as a tool for image enhancement during the pre-processing stage. Then, they introduce a cubic spline wavelet transformation during the thresholding stage. The partial derivatives along x and y of a two-dimensional smoothing cubic spline wavelet function are defined. Next, the noise of the background will be eliminated, and the main cracks will be extracted by evaluation of the development across scales related to the wavelet transformation maximum. Moreover, connectivity searching for extracted cracks is done during the crack connection stage. In addition, the number of prevailing cracks is quantified without classification by using the Hough transform. This is done during the crack extraction and classification stage. The Hough transform technique is not very delicate to noise, has a possibility to deal with segmented images, and is invariant to non-uniform illumination, scaling distortions, and shadows. In fact, this method is limited and inflexible, especially in the case of having varied pavement textures. This leads to the determination that this algorithm is an incomplete procedure.

In the computer vision community, fully automated reconstruction methods, modifications of pixel intensities, noise reduction elimination, and separating cracks from the rest of the image have been reported extensively; see RABABAHAH ET AL. (2005), GEORGOPOULOS ET AL. (1995), TEOMETE ET AL. (2005). The usage of linear regression techniques for the image enhancement stage was described by

RABABAAH ET AL. (2005). The thresholding process is suggested by GEORGOPOULOS ET AL. (1995). The crack is represented by a set of vectors approximating the crack (vectorization) during the thresholding stage. In addition, a default 3-by-3 size median filter is utilized during the crack connection stage. The types of cracks are classified by computing a mean value of intensities for each row. Finally, the cracks are defined as either horizontal or vertical, based on the TEOMETE ET AL. (2005) description during the crack extraction and classification stage. To some extent, this algorithm is considered to be a complete procedure with some problems and defects. The shadows problem is still unsolved from this algorithm side. Importantly, the absence of some parts of the cracks in the case of shadows and in noise existence due to checking the cracks pixel by pixel, are likely to occur during algorithm implementation.

Due to the above factors, the complete automation of crack detection remains an open topic of research, particularly in the case of complex compound cracks. Therefore, a semi-automatic method might still be needed for crack detection, see TEOMETE ET AL. (2005), YING/SALARI (2009). TEOMETE ET AL. (2005) presented an algorithm based on dividing images into blocks, determining sub-block sizes in pixels, and noting the pixel intensities during the image enhancement stage. Localized (adaptive) thresholding is done by computing relative mean values of intensity for each row during the thresholding stage. TEOMETE ET AL. (2005) suggested a method for distress quantification and quantization effectively from the Long Term Pavement Performance Program. The Long Term Pavement Performance Program was set up for pavement data collection. It is represented as a part of the Strategic Highway Research Program (SHARP). During the crack connection stage, the images must be cropped from 2048 x 3072 to 256 x 256. Finally, during the crack extraction and classification stage, a binary mask detection algorithm is implemented to define the region of interest. The binary mask must be defined in two ways as follows: (i) either based on colour and intensity values using several trial and error techniques (setting threshold to the crack size); and (ii) further automated methods to exploit the knowledge of the shape. These methods require pre-defined conditional statements for the binary mask shape (square, rectangle, and ellipse). The established binary mask must move over the binary image objects. When the conditional statements are satisfied, the binary mask will be projected to define a region of interest. The characteristics of the extracted objects will be known from the geometrical characteristics of a binary mask shape. Then, a projection histogram is applied for crack classification as either horizontal or vertical cracks (TEOMETE ET AL. 2005). This method is considered to be a complete procedure with some problems and defects based on the available data sets. The reason for this is due to some drawbacks related to some parts of the algorithm. One of these disadvantages is that the algorithm cannot identify complex compound cracks clearly. In addition, the algorithm is very sensitive to noise (TEOMETE ET AL. 2005).

YING/SALARI (2009) presented an algorithm for crack detection and classification. Statistical properties for pavement distress images were investigated for amplitude factor correction calculation. This factor is important to correct background illumination during the image enhancement stage. The beamlet transformation concept was introduced by DONOHO/HUO (2001). This concept is used during the thresholding stage for extraction of linear objects. Beamlet transformation is able to detect all of the line segments at various locations, orientations, and scales. Finally, the crack classification standard method is utilized during the crack extraction and classification stage. This method is based on two factors: (i) if the crack shape has branches, it will be classified as a block type, irrespective of crack orientation; and (ii) if the cracks do not have branches, the orientation angle is calculated as an angle between the horizontal axis toward the crack segments (start and end point of each crack) in the clockwise direction. This orientation angle is used to control the classification, in which the classification will be as the following: (a) if the orientation for the majority of the crack pixel regions is greater than or equal to  $60^\circ$ , it will be classified as a vertical individual crack; (b) if the orientation for the majority of the crack pixel regions is smaller than or equal to  $30^\circ$ , it will be classified as a horizontal individual crack; and (c) if the orientation for the majority of crack pixels region is smaller than  $60^\circ$  and greater than  $30^\circ$ , it will be classified as a transverse individual crack. The crack connection stage is not included in this algorithm. It is worth noting that there are limits of angles with horizontal axes (such as  $30^\circ$  and  $60^\circ$ ) for classification. YING/SALARI (2009) used these numbers based on predefined conditional statements for classification. In conclusion, this algorithm is considered to be a complete procedure with some problems and defects. The disadvantages are that this method cannot distinguish

between cracks and lane marking. Additionally, some parts of noise may appear based on the available data sets.

MOHAJERI/MANNING (1991) present a system for crack detection. This system is given as an automated trail of pavement administration. The multiplication filter is utilized in the image enhancement stage. The latter one will be used to remove noise and increase the rise of crack features in the resultant images. In the thresholding stage, dynamic (adaptive) thresholding is used for better segmentation. A different histogram distribution will be drawn for each image. This part will be done for the best threshold selection. The characteristics of each individual crack pattern are used to classify cracks in different categories. This is done during the crack extraction and classification stage. The crack connection stage is not included in this algorithm. This approach is determined to be a complete algorithm with some problems. It can classify cracks into different types: longitudinal, transverse, block, and alligator. In addition, it can register the length, width, and area of the crack region. However, this algorithm can be prone to failure in some cases, e.g., the pavement images have oil spots on the ground. In conclusion, this algorithm is considered to be a complete procedure with some problems and defects.

LE ET AL. (1990) offered the tiling method as a possible approach for the thresholding stage. The image data will be minimized through the tiling method into a matrix of 0 and 1. A tile of the original image is expressed as a matrix cell, and then the decision if the given tile includes a crack feature or not is reported. Each cell is fixed to 1 or 0 according to the results of the latter process. A simulator is defined to create generated synthesized images. The real pavement images are used for system examination. In the crack extraction and classification stage, neural networks are scrutinized using different approaches for image impersonation. The first technique is the image-based technique. The entire set of tiles of the original image is turned on using the latter technique. For example, if the size of the image is: (600\*600) and the size of the tile is (20\*20), then a vector of  $(600/20)*(600/20)$  entries=900 entry is created. Therefore, the matrix symbolizing the image will have a dimension of (20\*20) filled of 1's and 0's. Then, the neural network will be applied to see every single tile of the original image. Finally, the pattern will be detected using neural networks. The second technique is called the histogram-based technique. The outputs from this technique will be horizontal and vertical histograms. The latter one is created by counting the number of 1's in both horizontal and vertical directions of the resulting matrix. Neural networks will be run by inserting only two vectors for a training step. Neural networks will classify cracks into different types based on the allocation of the number of cracked objects cumulative in vertical and horizontal vectors. Taking the same example above, neural networks will deal with 30 vertical and 30 horizontal (=60) entries. Furthermore, the third is called the proximity-based technique. It is a simple and fast approach. Consequently, this technique calculates proximity values by taking the variance between the adjacent cells in the histogram. A proximity value is calculated for the vertical histogram. In addition, another proximity value is computed for the horizontal histogram. Finally, neural networks will use three-node input layers only as the following: one proximity value from the horizontal histogram, one proximity value from the vertical histogram, and the third one will be the number of cracked tiles in the image. The classification results were: 70.2% for the image-based technique, 75% for the histogram-based technique, and 95.2% for the proximity-based technique. Therefore, the latter technique is the best and can be considered as a lower cost approach when compared to the former ones, since it utilizes just three values for image depiction. Finally, this system can classify two types of cracks as either vertical or horizontal. The image enhancement and crack connection stages are not included in this algorithm. However, this system can be prone to failure in the case of both alligator and block cracks. Thus, it is considered to be a complete algorithm with some problems and defects.

Some automated algorithms, e.g., WANG/HARALICK (2002), rely on an automated system qualified for gathering and anatomizing high-resolution digital images in real-time. The analytical description of distress characteristics were used as a tool for differentiation between any cracks from other non-distress noises. In the thresholding stage, a vectorization concept is implemented to link the detected cracks. Finally, a distress database is built for storing the location, orientation, crack indices, and the size of each crack. In the crack extraction and classification stage, cracks are detected based on predefined distress categorization protocols. Image enhancement and crack connection stages are not in-

cluded in this algorithm. It is worth noting that this algorithm can be prone to failure. As a result, various external objects, e.g., oil spots, lane markings, tree shadows and unclearness may be included in the road pavement surface. This approach cannot distinguish between these extrinsic objects and the cracks themselves; therefore, this algorithm is considered to be a complete algorithm with some problems and defects.

WELLNER (1993) utilizes knowledge of the intensities of the surrounding pixels around the current pixel. The average value is computed around each required pixel. In other words, an approximate moving average of the last  $s$  pixel seen is calculated while traversing the image. Next, a comparative study is implemented during the thresholding stage. If the intensity value of the current pixel is lower than the average, the current pixel is adjusted to black; otherwise, it is adjusted to white. A significant advantage of such a representation is that it allows the ability to maintain hard contrast lines. This algorithm is low cost with minimal labor, as it needs only a single pass through the image. The disadvantages are related to the moving average and the distribution of pixels in all directions. Particularly, the neighbourhood pixels are not distributed equally in all directions. The moving average is not considered to be a perfect representation of the surrounding pixels at each phase. Image enhancement, crack connection and crack extraction, and the classification stages are not included in this algorithm. Therefore, this algorithm is considered to be an incomplete procedure (BRADLEY/ ROTH 2007).

TIMOTHY (2004) presents a thresholding and evaluation algorithm, which is called the watershed segmentation technique. This technique attempts to enhance the textured area into a three-dimensional space during the thresholding stage. The latter one will have different forms of textures that will have different heights. This technique determines if there are two regions linked without flooding. The shortcoming of this algorithm occurs due to its noise sensitivity, particularly in the case of large areas. This algorithm will ignore cracks within wear and polishing areas. The reason for this is based on probability only. This leads it to remove some false positives. Image enhancement, crack connection, crack extraction, and classification stages are not included in this algorithm. In conclusion, this algorithm is considered to be an incomplete procedure.

In summary, each crack detection algorithm mentioned above has some missing stages, missing points for each stage, problems, and defects. These missing points are considered as critical areas for further research. Each crack detection algorithm mentioned above requires further research. Table 2.5 summarizes the algorithms, their statuses (complete or incomplete), the missing stages within the algorithms, missing points for each step, problems associated with the algorithm. As a logical follow-up, the algorithm to be developed will be based on the ability to achieve more correct results for the detection and classification of pavement cracks from continuous pavement images.

Table 2.5: Conclusion for each crack detection algorithm, its status, and its missing points

<b>Algorithm name</b>	<b>Status of algorithm incomplete or complete (conclusion)</b>	<b>Missing stages within algorithm</b>	<b>Missing points and problems associated with the algorithm</b>
BUGAE/YAXIONG (2003)	Incomplete	Image enhancement and crack classification stages	<ul style="list-style-type: none"> <li>– Shadow problem</li> <li>– Illuminated background</li> <li>– Crack classification</li> </ul>
MASER (1987)	Incomplete	Crack connection and crack classification stages	<ul style="list-style-type: none"> <li>– Lane markings problem</li> <li>– Noise problem</li> <li>– Crack classification</li> </ul>

<b>Algorithm name</b>	<b>Status of algorithm incomplete or complete (conclusion)</b>	<b>Missing stages within algorithm</b>	<b>Missing points and problems associated with the algorithm</b>
LI ET AL. (1991)	Incomplete	Crack classification stage	<ul style="list-style-type: none"> <li>– Complex crack detection</li> <li>– Crack classification</li> </ul>
KOUTSOPOULOS/DOWNEY (2006)	Incomplete	Crack connection and crack classification stages	<ul style="list-style-type: none"> <li>– Lane marking problem</li> <li>– Crack classification</li> </ul>
CHOU ET AL. (1994)	Complete with some problems and defects	Image enhancement and crack connection stages	<ul style="list-style-type: none"> <li>– Irregular shape of cracks affects neural network classification rate</li> </ul>
GEORGOPOULOS ET AL. (1995)	Complete with some problems and defects	Image enhancement and crack connection stages	<ul style="list-style-type: none"> <li>– Different pavement texture problem</li> </ul>
CHENG/MYOJIM(1998)	Complete with some problems and defects	-	<ul style="list-style-type: none"> <li>– It cannot work in the case of large-sized images or if the crack crosses more than one window</li> </ul>
DAVID/JOE(2005)	Incomplete	Image enhancement, crack connection and crack classification stages	<ul style="list-style-type: none"> <li>– Different pavement textures problem</li> <li>– Crack classification</li> </ul>
JAVIDI ET AL. (2003)	Incomplete	Crack classification stage	<ul style="list-style-type: none"> <li>– Different pavement texture problem</li> <li>– Crack classification</li> </ul>
RABABA AH ET AL. (2005)	Complete with some problems and defects	-	<ul style="list-style-type: none"> <li>– Shadow problem</li> <li>– Noise problem</li> </ul>
TEOMETE ET AL. (2005)	Complete with some problems and defects	-	<ul style="list-style-type: none"> <li>– Complex crack detection</li> <li>– Noise problem</li> </ul>

<b>Algorithm name</b>	<b>Status of algorithm incomplete or complete (conclusion)</b>	<b>Missing stages within algorithm</b>	<b>Missing points and problems associated with the algorithm</b>
YING/SALARI (2009)	Complete with some problems and defects	Crack connection Stage	<ul style="list-style-type: none"> <li>– Lane marking problem</li> <li>– Noise problem</li> </ul>
MOHAJERI/ MANNING(1991)	Complete with some problems and defects	Crack connection Stage	<ul style="list-style-type: none"> <li>– Oil spots problem</li> <li>– High pavement texture problem</li> </ul>
LE ET AL.(1990)	Complete with some problems and defects	Image enhancement and crack connection stages	<ul style="list-style-type: none"> <li>– Alligator and block crack detection</li> </ul>
WANG/HARALICK (2002)	Complete with some problems and defects	Image enhancement and crack connection stages	<ul style="list-style-type: none"> <li>– Lane marking problem</li> <li>– Oil spot problem</li> <li>– Shade problem</li> </ul>
HSU ET AL. (2001)	Complete with some problems and defects	Image enhancement stage	<ul style="list-style-type: none"> <li>– Lane marking problem</li> </ul>
SALARI (2012)	Complete with some problems and defects	Image enhancement and crack connection stages	<ul style="list-style-type: none"> <li>– Lane marking problem</li> <li>– Shadow problem</li> </ul>
CHOU/SALARI (2012)	Complete with some problems and defects	Image enhancement and crack connection stages	<ul style="list-style-type: none"> <li>– Lane marking problem</li> <li>– Shadow problem</li> </ul>
SALARI ET AL. (2010)	Complete with some problems and defects	Crack connection stage	<ul style="list-style-type: none"> <li>– Lane marking problem</li> <li>– Shadow problem</li> </ul>
WELLNER'S (1993)	Incomplete	Image enhancement, crack connection, crack extraction and classification stages	<ul style="list-style-type: none"> <li>– Crack classification</li> <li>– Pixel distribution problem during thresholding stage</li> </ul>
TIMOTHY (2004)	Incomplete	Image enhancement, crack connection, crack extraction and classification stages	<ul style="list-style-type: none"> <li>– Crack classification</li> <li>– Noise problem</li> </ul>

### 3 Preparation Stages for Crack Extraction

In Chapter 2, it was shown that combining digital image processing and analysis techniques can be useful to some extent for overcoming individual difficulties associated with crack detection and classification. This is done in order to reach reliable and improved results in almost all operative conditions. At the same time, it is clear that several image processing methods for crack detection face numerous obstacles and problems. In addition, some of them are incapable of delivering correct measurable facts, and usually lead to irregularities in crack aspects. From this perspective, a flexible fusibility process which can ensure correctness and homogeneity in the results is urgently needed.

The main challenge for the integration of a digital image algorithm is the selection of a suitable approach for each crack detection stage. This suitable approach can achieve the desired goals for each stage in terms of high correctness rate, ease-of-use, and low level of user involvement. The algorithm's goal is to extract and classify cracks of pavement images automatically. Generally, any automatic approach should use image processing algorithms as a tool for crack detection.

This thesis presents a uniform algorithm for processing digital pavement images. This algorithm is based on a combination of different image processing techniques and some modifications of previous algorithms, especially during the threshold stage. Specifically, this thesis presents a threshold-setting algorithm. This threshold-setting algorithm sets the optimal threshold value for each pixel in the image. This adaptive local threshold is able to separate all of the cracks, and only the cracks, from the remainder of the image. Then, for the purpose of improving the threshold results, this thesis employs some combinations of crack connection processes. This general strategy aims to remove the remaining noise, check the cracks' continuity, and fill all of the crack holes. Moreover, it provides an accurate crack image ready for the crack extraction and classification stages. In these ways, the abovementioned preparation stages pave the way for better crack extraction and classification.

As a result, the algorithm of this thesis yields an increase in automation and updating, represents a solution for preparation stages in order to extract cracks from sequence pavement images, and results in detailed crack information with different pavement textures. In the following, a detailed description of the algorithm is given in order to introduce all of the used methodologies. As presented in figure 3.1, the algorithm is divided into the following steps.

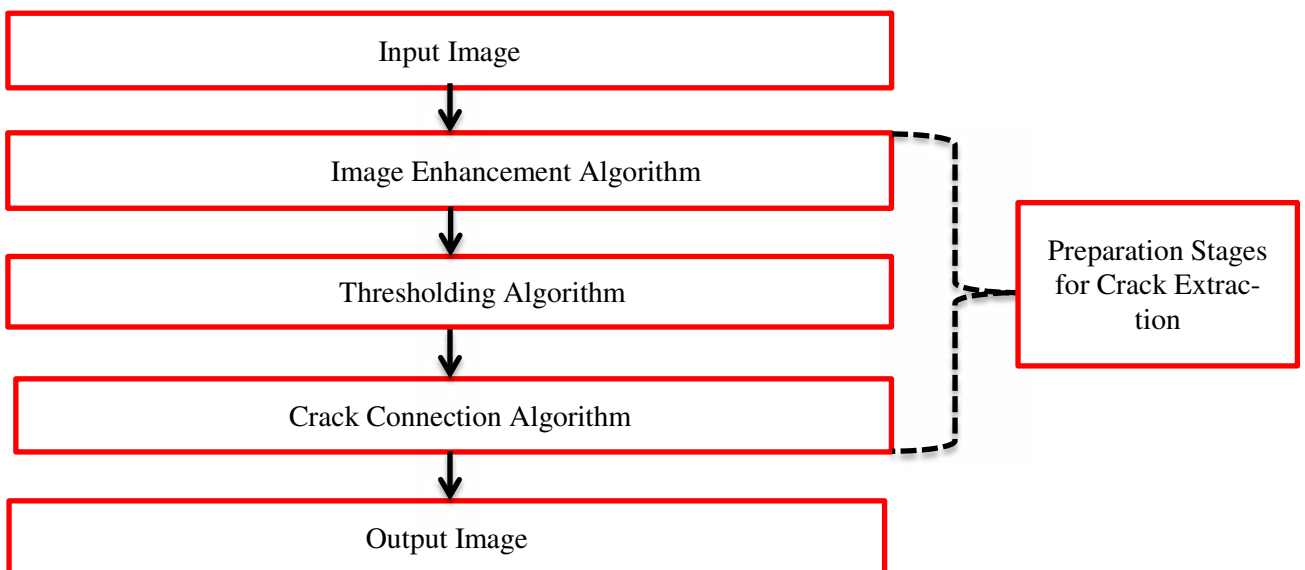


Figure 3.1: Workflow for the combination of different algorithms during preparation stages.



## 3.1 Image Enhancement Algorithm (Pre-processing stage)

### 3.1.1 Theory

The reason underlying this first stage is that the pavement images are collected under different lighting situations. This creates the need for correction of background illumination. This stage is optional, as previously described in Chapter 2, based on images' nature. As a consequence, conversion of all of the acquired images to standard background conditions requires a robust corrected illumination algorithm, which is insensitive to illumination and scale differences, and employs region properties (CHENG/MIYOJIM 1998). A wide variety of background illumination correction algorithms have been proposed and investigated in the literature, (e.g., SINGH/GARG 2011, LI ET AL. 2011, LIU ET AL. 2009, RADIM ET AL. 2011). Generally ACHARYA ET AL. (2009) addressed the histogram equalization algorithm. GONZALEZ/WOODS (2008) proposed the contrast enhancement algorithm, which extends the histogram equalization algorithm to fully accept invariant local image illuminations. SINGH/GARG (2011) reported that combinations of morphological operation techniques significantly outperform state-of-the-art methods, such as the histogram equalization (ACHARYA ET AL. 2009), the contrast enhancement (LIU ET AL. 2009), and statistical properties of pixels brightness method (CHENG/MIYOJIM 1998). As an example of this, histogram equalization can hardly correct background illumination to 60%, while combinations between morphological operation techniques can correct background illumination to 80% and higher. Furthermore, SINGH/GARG (2011) illustrates that most scenes with negligible or moderate pavement images that are corrected with histogram equalization are also corrected with morphological operations (usually with fewer lighting conditions). Nevertheless, when the pavement images are obtained with strong illumination and shadows, histogram equalization and other methods fail, while a combination of morphological operation techniques continues to work. Thus, a combination of morphological operation techniques has been selected for the application in this thesis.

So, as a first stage, this thesis employs an algorithm for combining different digital morphological operations to automatically and accurately adjust lighting for pavement images. This algorithm starts by an erode operation of digital images based on selecting a suitable structure element. The black pixels will be turned to white. Then, the original image will be modified using the eroded image with the help of opening by the morphological reconstruction algorithm. The resultant image must be subject to a dilation process, in which the black pixels will be retained and any boundary will be widened automatically. After this, closing by morphological reconstruction will be implemented to form a complete detailed representation of a modified image scene.

The image enhancement algorithm of this thesis can be divided into the following steps, as presented in figure 3.2.

1. **Erode Operation:** The essential erode function, based on Boolean operations for binary images, is utilized for morphological image processing (DROOGENBROECK/TALBOT 1996). This operation is described in more detail in Chapter 2, section 2.3.2.3. The erode operation will be applied to the original image. The implementation of this operation utilizes the linear structural element. The selection for this type of structural element is performed to preserve crack shapes. The erode operation provides the achievable results into a better state, i.e., good image appearance and noiselessness, which yields an improvement in the output of the algorithm presented in this thesis.
2. **Opening by Reconstruction:** The original image and the eroded image are combined using the opening by the reconstruction process. The opening by the reconstruction process is implemented based on VINCENT (1993), as illustrated in Chapter 2, section 2.3.2.3. Furthermore, this thesis makes the process work optimally by setting the original image as a mask and the eroded image as a marker. For this purpose, opening by reconstruction is implemented between the mask and marker several times through the dilation process. The

operation will be continued automatically until all of the peak values in the mask image become flat. The final image of this operation will help in obtaining similar intensity values, as well as reducing illumination differences.

3. **Dilate Operation:** As previously reported in more detail in Chapter 2, section 2.3.2.3, the dilate was described as one of the Boolean operations for binary images (DROOGENBROECK/TALBOT 1996). Consequently, the use of this operation offers an important advantage, i.e., instead of using the intensity values of the resultant opening by the reconstruction image, the latter image will be applied to a similar operation of erode using linear structural elements. This results in expanding every boundary and extracting information about them from the resultant image.
4. **Closing by Reconstruction:** Closing by reconstruction has been used for illumination correction and smoothness. In addition, it enables converting the image to a suitable form for the segmentation stage. This thesis follows an operation that is somewhat analogous to VINCENT (1993), as it is illustrated in detail in Chapter 2, section 2.3.2.3. This operation will be implemented using the same concept as the opening by the reconstruction process. The complementarity of the resultant dilated image is employed as a marker, while the resultant opening by the reconstruction image is utilized as a mask. The aim of this operation is to remove all of the peaks from the resultant opening by the reconstruction image through a continuous erosion process. Moreover, the intensity values of the complementary result are closed by the reconstruction image, which is recorded and locally illuminates the surface at a very narrow range. This may result in missing some features which are not visible at the narrow range (GONZALEZ/WOODS 2008). Sometimes, the effect of this pre-processing stage is displayed in the appearance of the final resultant image from this stage implementation in terms of smoothness; whereas, for other pavement image cases, there is no obvious effect in the image. However, this does not mean that this stage is not helpful, because in both cases the pixels' intensities are changed to be homogeneous and the background illumination is corrected, as well. Thus, this operation plays a key role in providing correct information for the next thresholding stage.

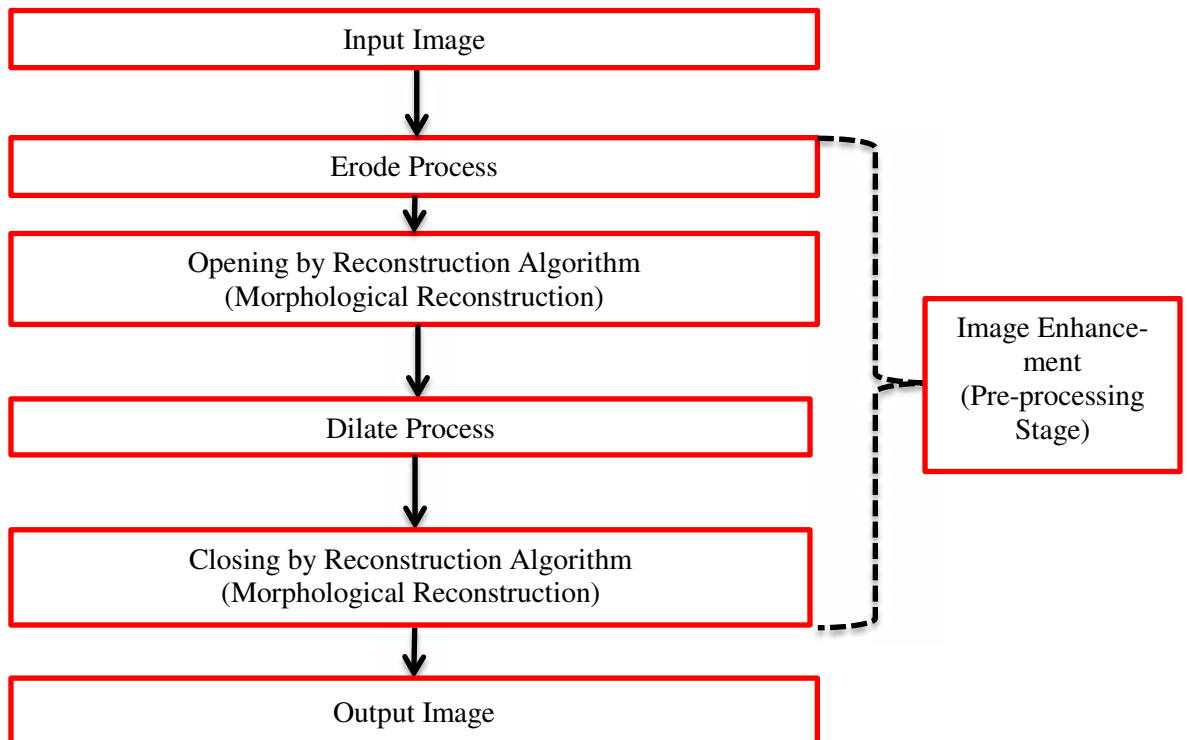


Figure 3.2: Workflow for the combination of morphological operation during the image enhancement stage.

### 3.1.2 Experimental Results

In order to show the results of this study, the developed algorithm was applied to exemplary pavement images of different streets in Germany, which were obtained from LEHMANN + PARTNER GmbH Company. S.T.I.E.R mobile mapper system has been used for capturing image sequences (Chapter 6; figure 6.1). The original image (figure 3.3-left) has a resolution of 1920 x 1080 pixels. This image contains two crack alignments, moderate pavement texture, and different lighting conditions. In the following, an evaluation of all pre-processing steps is presented. Since all of the figures below are not visible, a kind of inversion is performed for exemplary visualization. The pavement images will be displayed in white colour instead of black colour.

**Erode Operation:** Inspired by the positive results of using the erode operation (figure 3.3), a binary image was generated from the original image.

**Opening by Reconstruction:** The opening by reconstruction is a combination of corrected illumination produced by both marker and mask images. Then, the final resultant image is displaced after removing peaks of background illumination (figure 3.4).

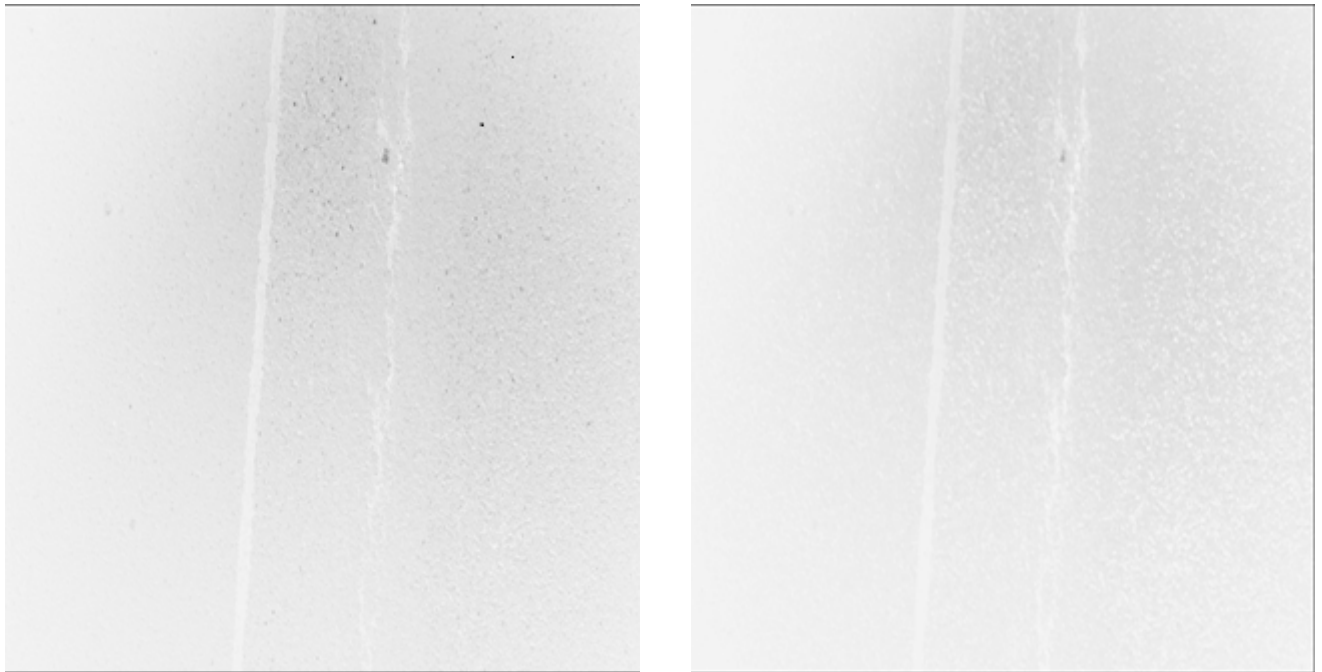


Figure 3.3: LEHMANN + PARTNER GmbH dataset, original image (left), the resultant binary image after erode operation (right); (inverted illustration).

**Dilate Operation:** The object boundaries are expanded by the dilation computation (figure 3.5). Additionally, the holes are filled, and the black pixels are retained. Comparing figure 3.5 with figure 3.4, it can be seen that there is no difference in appearance. However, the values of the pixel intensities are changed to become more homogenous, and this is important to obtain a good result for the closing by reconstruction (the following step).

**Closing by Reconstruction:** Once the complementary resultant closing by the reconstruction image is determined, this image will be smoother than the original image. At that time, the target of the pre-processing stage is realized. The intensities of the final resultant image are used as an input for the thresholding stage without any illumination effect. This is done in order to improve the results in terms of correctness (figure 3.6).

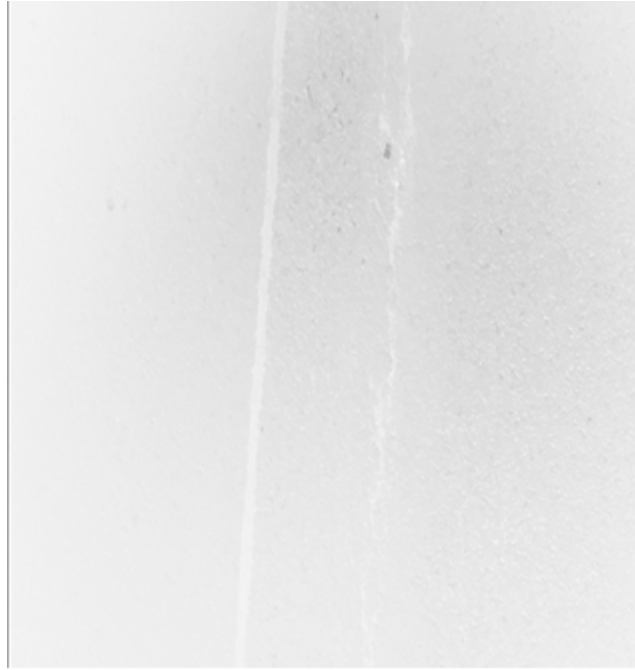


Figure 3.4: LEHMANN + PARTNER GmbH dataset, the resultant image after applying opening by the reconstruction process; (inverted illustration).



Figure 3.5: LEHMANN + PARTNER GmbH dataset, the resultant image after applying the dilate process; (inverted illustration).

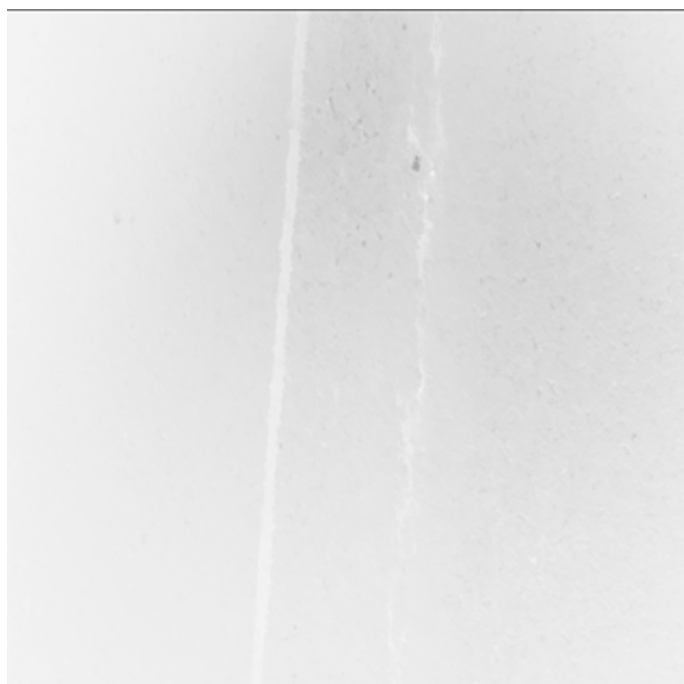


Figure 3.6: LEHMANN + PARTNER GmbH dataset, the resultant image after applying closing by the reconstruction process; (inverted illustration).

## 3.2 Thresholding (Segmentation Stage)

### 3.2.1 Theory

In section (3.1), the integration and combination of different morphological operations during the pre-processing stage deliver images with a uniform distribution of illumination. Then, as a second stage, the threshold setting algorithm requires a robust dynamic automated algorithm. This algorithm is insensitive to noise and obstacles, and employs region properties (TRIER/TAXT 1995). A wide variety of thresholding algorithms have been proposed and investigated in the literature (e.g., TSAO ET AL. 1994). Generally, LE ET AL. (1990) addressed different types of global fixed threshold algorithms, which include the simple image statistic method (KITTLER/ILLINGWORTH 1985), the between class variance method (OTSU 1979), the entropy method (KAPUR ET AL. 1985), the moment preserving method (TSAI 1985), and the quadtree method (WU ET AL. 1982). These algorithms work correctly in the case that the gray-level distribution histogram contains distinctively separated peaks corresponding to the objects and background. TRIER/TAXT (1995) proposed the local adaptive dynamic threshold algorithms, which extend the global fixed algorithm using local properties. The principle of local adaptive dynamic thresholding is dependent on the selection of an individual threshold for each pixel based on the range of intensity values in its local neighborhood. It works for segmenting an image whose histogram does not contain distinctive peaks (TSAO ET AL. 1994). TRIER/TAXT (1995) reported that the local adaptive dynamic threshold algorithms significantly outperform other methods, such as global fixed threshold algorithms, in the case of pavement images, such as the simple image statistic method (KITTLER/ILLINGWORTH 1985), the between class variance method (OTSU 1979), the entropy method (KAPUR ET AL. 1985), the moment preserving method (TSAI 1985), and the quadtree method (WU ET AL. 1982). For example, the method proposed by TSAI (1985) can extract crack objects to 30%; whereas, Wellener's local adaptive threshold method (WELLENER 1993) can detect the same cracks up to 80% and higher. Furthermore, TSAO ET AL. (1994) illustrates that most scenes with pavement images of high texture and gradient that are thresholded with global fixed thresholding methods are also thresholded with dynamic local adaptive thresholding methods (always with a higher extraction correctness rate). Nevertheless, when pavement images are obtained with a lot of shadows, strong illumination gradients, or do not

undergo any pre-processing stage, global fixed threshold methods will certainly fail, while local adaptive dynamic thresholding continues to work. In addition, pavement crack images have different characteristics, such as: (i) the number of foreground pixels is much smaller than the background pixels; (ii) the image background is likely to contain a higher variance due to inhomogeneous pavement texture and different light intensities; and (iii) a histogram of the gray-level distributions will show a large peak corresponding to the background gray-levels and a smaller peak corresponding to the foreground gray-levels, such as cracks, manholes, and markings, as shown in figure 3.7. This makes it difficult to establish a single threshold which will correctly identify the crack pixels. Thus, local adaptive dynamic thresholding has been selected for application in this study.

The threshold setting algorithm (adaptive or local dynamic thresholding) can be defined by a simple extension of Wellener's method (WELLENER 1993). Accordingly, a convolution concept (ATKINSON 1996) is introduced, and its parameters are estimated. This concept is implemented by using the mean statistical operator within a  $ws$  window of pixels around each pixel. This takes advantage of the determined suitable threshold results in having a suitable window size in relation to the contrast within the image. This is usually followed by a Sobel Edge Detector to extract the edges of cracks clearly. Alternatively, after using the Sobel Edge Detector, the approach of this thesis is to use the extracted object correspondences to cracks and to other noise as input for the post-processing stage. The approach of this thesis consists of the following steps, as shown in Figure 3.8.

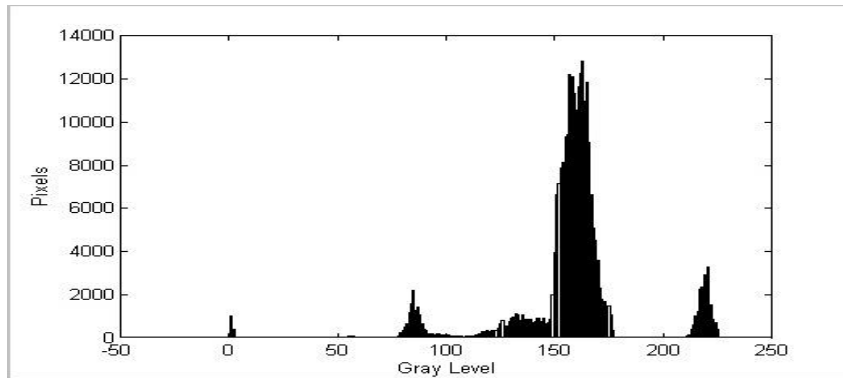


Figure 3.7: Gray-level distribution histogram for an image (MILSTEIN 1998).

**1-Adaptive Thresholding Algorithm:** As presented in section (3.1), the first stage delivers an image with a uniform distribution of illumination. On the other hand, local adaptive thresholding is created for each pixel in the image. This threshold is utilized to evaluate the pixel.

The general threshold definition can be expressed using equation (3-1) as follows:

$$T = T [x, y, g(x, y), f(x, y)], \quad (3-1)$$

where

- $f(x, y)$  : the gray level of point  $(x, y)$  in the original image,
- $g(x, y)$ : some local property of this point described below,
- $T$  : threshold value.

$g(x, y)$  is considered as one of the most important factors in threshold computations around a specified point. When the value of this factor is 0, then  $T$  is considered as a simple fixed global threshold. However, this factor is based on the environment around a specified point, in order to take the effect of noise and lighting into account. Sometimes, this factor is represented by some local property around the specified point  $(x, y)$ . The local property around the specified point  $(x, y)$  is computed by mean gray-level, max gray-level, or min gray-level, or the average between max and min gray-level in a predefined environment (CHOW/KANEKO 1972).

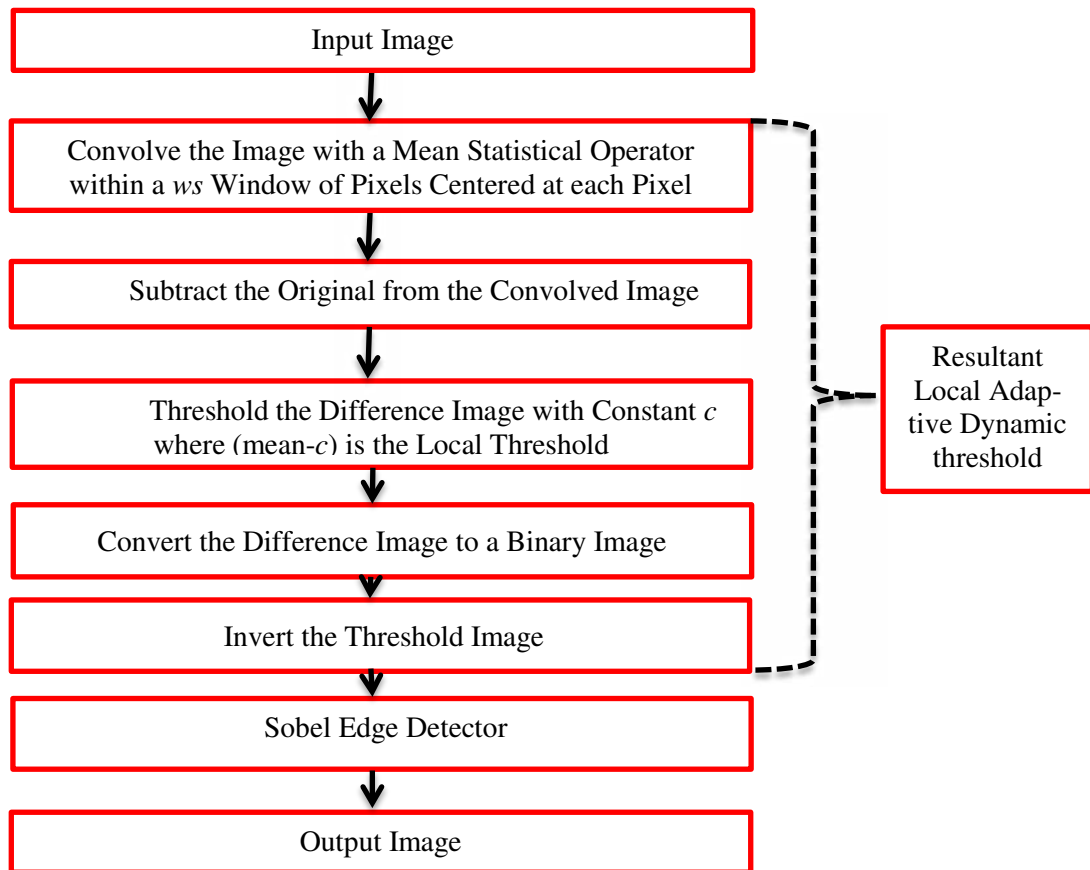


Figure 3.8: The general workflow for segmentation (thresholding stage).

Consequently, according to Chapter 2, section 2.3.5, Wellener's algorithm (WELLNER 1993) exploits the knowledge of the intensities for the surrounding pixels around the current pixel. The average value is computed around each required pixel. In other words, an approximate moving average of the last  $s$  pixels seen is calculated while traversing the image. Then, a comparative study is implemented during the segmentation stage. If the intensity value of the current pixel is lower than the average, the current pixel is adjusted to black; otherwise, it is adjusted to white. A significant advantage of such a representation is that it allows maintaining hard contrast lines. This algorithm is also of low computational cost because it only needs a single pass through the image. The disadvantages are related to the moving average and distribution of pixels in all directions. Particularly, the neighbourhood pixels are not distributed equally in all directions. This means that the moving average is not considered as a perfect representation of the surrounding pixels at each phase (BRADLEY/ROTH 2007). In conclusion, the use of this Wellener's method fails in the crack extraction process due to the abovementioned disadvantages. Therefore, in this thesis, the approach modifies and extends Wellener's method by computing the average of  $ws$  window of pixels centered in each pixel using the convolution concept instead of calculating a running average of the last  $s$  pixel seen. This extension and modification offers important advantages. Specifically, it is direct, easy to code, and the computed average is superior for comparison; thus, it is reliable that all of the neighboring pixels around the centered pixel within the window are distributed in all directions. In other words, this modification can overcome many problems of the Wellener's algorithm. Moreover, after the local threshold average value is computed iteratively for each pixel in the image, the image will undergo some mathematical digital image processing operations (i.e., binarization, subtraction, inversion) as described above in figure 3.8. Finally, a comparative study is executed automatically between the intensity value of the specified pixel and the threshold average percent value. The aim is to produce the final resultant local adaptive dynamic threshold image as follows: if the intensity value of the specified pixel is less than the threshold average percent, the pixel is considered as a background pixel (black pixel); otherwise, the pixel is considered as a foreground pixel (white pixel).

In order to evaluate the performance of the adaptive thresholding algorithm for this study, it is obvious that the window size  $ws$  and the constant  $c$  are the most important factors affecting the adaptive thresholding algorithm execution. This creates a need to explain in more detail the definition, evaluation, and the effect of window size  $ws$  and constant  $c$ , respectively in the following.

### Evaluation of the window size $ws$

The correctness rate with which the image pixels are classified by the algorithm is based on the size of the windows being used. If the environment of the window is too small, this will result in noisy appearance, some foreground pixels being misclassified as background, and introduce the possibility of insufficient data, as shown in (figure. 3.9-2<sup>nd</sup>line-right). On the other hand, large window sizes yield the poorest results due to being adversely affected by the illumination gradient, more computationally effort than the threshold using smaller windows, and local characteristics of the pixel neighbourhood will be lost. Thus, the larger window may capture gray-level contrasts that are unavailable in the pixel neighbourhood. This will affect the threshold value. In addition, the misclassification of foreground and background pixels will occur due to the manipulated threshold value (figure 3.9-2<sup>nd</sup>line-left).

Finding a suitable window size is still a critical task in the research community. Several approaches have been developed and presented, but still rely on a small group of images. In particular, a broad variety of window size selection has been proposed and investigated in the literature (e.g., BARTOLO ET AL. 2004). KAMEL/ZHAO (1993) utilized  $(2ws + 1) \cdot (2ws + 1)$  size neighbourhoods centered at the four points and  $ws$  represents an approximate assumed value for the width of the detected edge for all dataset images as a fixed value. The algorithm requires user pre-defined parameters, i.e., the width  $ws$ . TRIER/JAIN (1995) proposed Eikvil's method, which is based on smaller window  $ws$  and larger window  $wl$ . The  $ws$  and  $wl$  selection is performed manually for each image. Furthermore, these parameters cannot be fixed to a particular value like KAMEL/ZHAO'S (1993) assumption because these parameters are related to each image's properties. PAPAMARKOS/GATOS (1994) used a fixed 9\*9 window size to perform pixel class within the image. YANG/YAN (2000) reported that the dynamic window size algorithms significantly outperform the other methods, such as using a fixed window size (e.g., BULEN/MEHMETS 2004, BARTOLO ET AL. 2004).

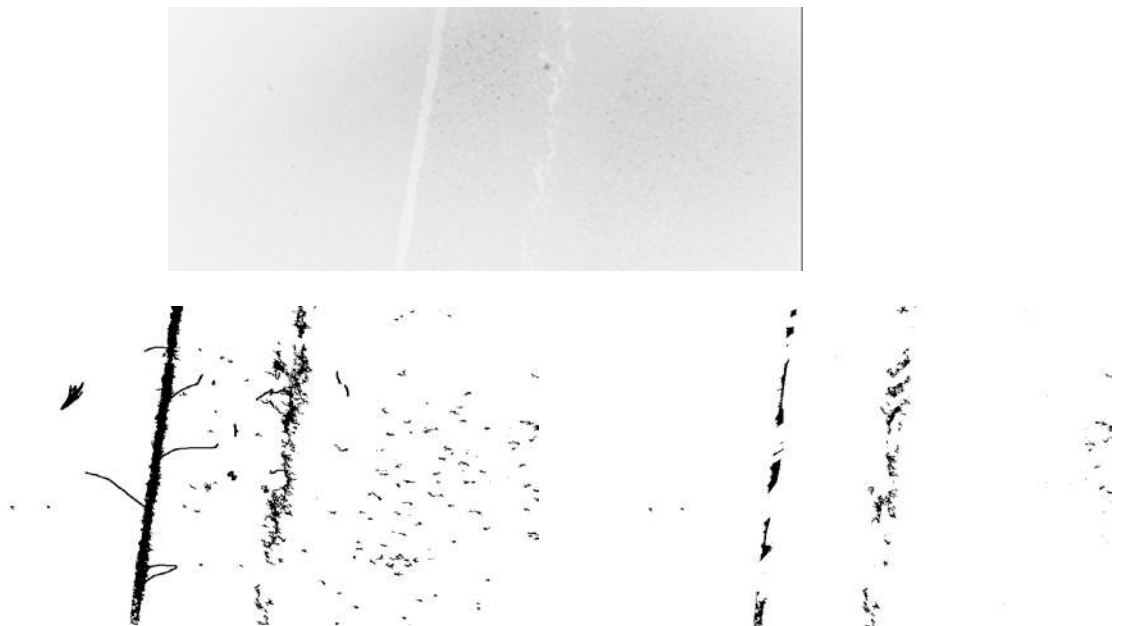


Figure 3.9: Adaptive thresholding algorithm: original image (inverted illustration) (1<sup>st</sup> line); using  $ws=170*170$ ; (2<sup>nd</sup> line-left); using  $ws=50*50$  (2<sup>nd</sup> line-right).



For example, YANOWITZ/BRUCKSTEIN (1989) used a fixed single window size with a correctness rate of 65% for crack detection; whereas, YANG/YAN (2000) can detect the same cracked objects to 80% by using the dynamic window size algorithm. Furthermore, different methods for threshold pavement images exist. These methods all require some user-defined parameters, such as window size. Therefore, these algorithms are not suitable for automated crack detection application. Thus, this thesis employs the algorithm by YANG/YAN (2000) in order to automatically and accurately determine window size without prior knowledge.

The YANG/YAN (2000) algorithm for window size determination is carried out as follows: (i) the image will be divided into  $N \times N$  regions, where  $N=4, 5, 6, 7, 8$ ; (ii) the gray-level histogram distributions will be drawn on partial regions in the image in order to detect higher local contrast regions (chosen regions); and (iii) if  $N$  is even, two diagonal directions are assumed for regions, but if  $N$  is odd, horizontal and vertical directions are supposed for regions, as shown in Figure 3.10.

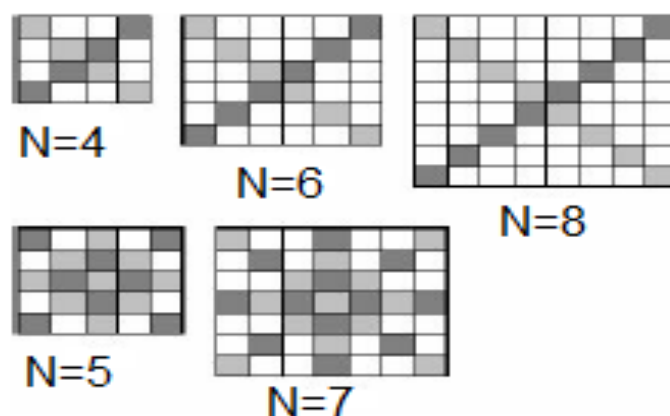


Figure 3.10: The divided regions on which gray-level histogram analysis will be performed (BARTOLO ET AL. 2004).

The frequency of gray-level histogram is computed in horizontal and vertical directions if  $N$  is odd, and on two diagonal directions if  $N$  is even over the chosen regions from (ii) step; (iv) zero-phase shift convolution filter (described in chapter 2, section 2.3.2.1) will be performed if  $N$  is odd (5,7) over the chosen regions, this filter does not shift the crack position (no geometry change); and (v) the evaluation of the window size for the image will be derived from gray-level histogram information, in which the window size of the given image is expressed as the region length having the highest frequency of pixels.

However, the advantages of this algorithm are that the calculated region lengths in the horizontal and vertical directions will reverberate the window size in the region. Since region lengths are calculated in the horizontal and vertical directions, the window length and width will reflect the length and width of the object in the region, respectively. For example, region lengths obtained from a region having a horizontal crack line would reflect the length of the crack line in the horizontal region length and its width in the vertical region length. Thus, the average window size would reflect a measure of the length and width of cracks in the selected regions. This guarantees that the selected window size is largely sufficient to contain an appropriate exemplification of the cracks without losing the local characteristics of the window. Furthermore, this strategy yields a reduction of human intervention during the entire process and represents a direct solution for window-size selection. On the other hand, if the study deals with a pavement image having complex background patterns, variable illumination, or very poor quality, it is recommended to apply the global thresholding technique before applying the YANG/YAN (2000) algorithm for window size determination. In figure 3.11, the final threshold result for one image after suitable window size selection is displaced. By analyzing this figure compared with figure 3.9, the results indicate an improvement in crack appearance compared to the results of figure 3.9. It is obvious that the correct window selec-

tion provides a correct crack appearance without loss of local crack properties. It is indeed correct that there is still some noise, but it is less compared to figure 3.9. Further post-processing operations will improve the crack detection correctness rate by removing the remaining noise.

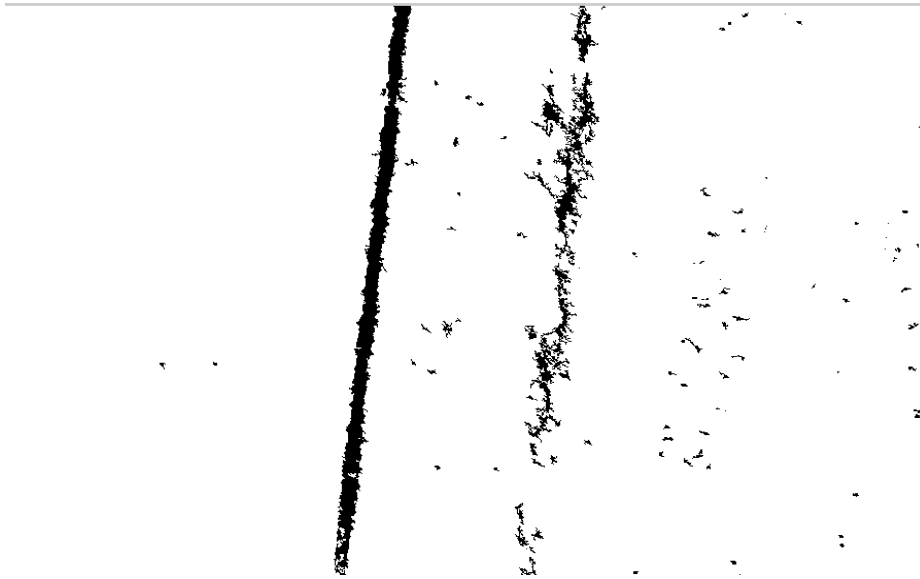


Figure 3.11: Adaptive thresholding algorithm after applying the YANG/YAN (2000) algorithm for window size determination ( $ws=120*120$ ).

### Evaluation of the constant $c$

The performance of the adaptive threshold algorithm is also based on the constant  $c$ . This constant represents contrast within the image. The contrast is represented by different lighting intensities within the image. The natural pavement image contains several light intensities due to different textures. So, the contrast grades across the image will vacillate continuously. Thus, this creates a need to determine a value to control the lighting fluctuation and its effect on crack detection results. The value of  $c$  will be computed adaptively. Finding a suitable contrast value  $c$  is still a debated issue in the research community. In fact, a broad variety of contrast value  $c$  selections has been proposed and investigated in the literature (e.g., NIBLACK 1985, SAUVOLA/PIETIKAKINEN 2000). NIBLACK'S (1985) utilized empirical user-defined parameters as fixed values for adjusting total pixels that belong to foreground objects. The algorithm requires a user pre-defined parameter, i.e.,  $c$ . It reflects the contrast within the image. SAUVOLA'S/PIETIKAKINEN (2000) proposed a constant, usually with a value of  $c=0.1$ . The  $c$  selection is done empirically. BARTOLO ET AL. (2004) and TRIER/JAIN (1995) reported an automatic solution for determining the value of  $c$ . This algorithm significantly outperforms other methods, such as using a fixed empirical contrast value (e.g., NIBLACK 1985, SAUVOLA/PIETIKAKINEN 2000). Moreover, different methods for thresholding pavement images exist. All of these methods require some user-defined parameters for contrast determination. Therefore, these algorithms are not suitable for automated crack detection application. Thus, this thesis employs an algorithm developed by BARTOLO ET AL. (2004) and TRIER/JAIN (1995). This algorithm proposes a solution for the determination of  $c$  which is based on two properties: the quality of the image foreground and the type of the image background. If an image background contains high textures, the value of the  $c$  must be larger than that chosen for images having a homogenous background. This is necessary, as the value of  $c$  is sufficiently large to capture the contrast between the background pixels. In fact, the largest value of  $c$  is controlled by the quality of the image foreground. For example, if the study deals with pavement images having a mixture of pixel classes in the entire background, the  $c$  value must be adequately large for classification mixture windows. On the contrary, pavement images having a low difference between the gray levels of the foreground and background require smaller values of  $c$ . So, the algorithm is realized as follows: (i) dividing each image into smaller regions. In this thesis, the images are divided into 16 equal-

sized regions. This division is adopted based on the existing data sets to meet the requirements for the previous step. (ii) The contrast within each region is utilized for  $c$  determination using equation (3-2) below. (iii) This method must be performed iteratively until different values of  $c$  are calculated for all image regions.

$$c = Z_{max} - Z_{min} , \quad (3-2)$$

where

- $c$  : contrast within the region,
- $Z_{max}$  : maximum intensity value within the region,
- $Z_{min}$  : minimum intensity value within the region.

Table 3.1: Some results for  $c$  and  $ws$  with respect to different pavement texture images

Pavement Image	Contrast range $c$	Window size $ws$
Dark shadow image	$45 \leq c \leq 55$	50*50
Low pavement texture image	$10 \leq c \leq 30$	20*20
Moderate pavement texture image	$20 \leq c \leq 50$	30*30
High pavement texture image	$35 \leq c \leq 66$	50*50

Table 3.1 displays the contrast range and window size with respect to different image cases. These results show the largest window size obtained for dark shadow images or high pavement texture images; whereas, the images with low or moderate pavement texture have the smallest window size.

## **2-Sobel Edge Detection Filter.**

This thesis uses the Sobel Edge Detection filter based on LI ET AL. (1991). They used this edge detector to filter out the response of edges during the segmentation stage. This filter achieved highly correct results. The mathematical side and functions related to this edge detector are explained in detail in Chapter 2, section 2.3.2.2. In fact, a review of the literature identifies different types of edge detection filters. For example, first-order differential filters, which include Sobel, Prewitt, and Roberts filters, and second-order differential filters, including Laplacian, and second-order directional derivatives (LUHMANN ET AL. 2006). Each edge detection filter has its own properties and principles for work. For example, Prewitt and Sobel gradient operators work well on images with sharp edges. They are suitable in the case of cracks generally where the lighting and overall imaging environment is tightly controlled. At the same time, the results of applying the Roberts operation will highlight changes in intensity in vertical, horizontal, and diagonal directions. This is suitable in the case of longitudinal cracks, transverse cracks, and alligator cracks. However, it is worth noting that there are some disadvantages of these first-order differential filters. For example, the Roberts filter suffers greatly from sensitivity to noise. In addition, the Sobel filter and Prewitt filter do not tend to work well in the case of "natural simple" images, such as images with simple cracks. In these cases, the need for applying second-order differential filters can sometimes be used as a more robust edge detector, such as the Laplacian filter. One distinct advantage of the Laplacian filter is that it does not rely on a threshold to separate the edge pixels from the rest of the image. It is considered as an isotropic operator (i.e., it detects edges in any direction). Even though the Laplacian filter offers some important advantages, it suffers from major susceptibility to image noise. The presence of any noise within the image is the cause of a fair amount of "streaking" (LUHMANN ET AL. 2006).

All of these edge detection operators usually do not lead to a robust solution, especially if the imaging environment is not tightly controlled. Moreover, all of them are sensitive to noise based on available datasets. Due to the abovementioned reasons, the choice of a suitable edge detection operator is actually case-dependent. In this application, the Sobel Edge Detector filter is utilized. This choice is based on different factors, such as: (i) the advantages of this filter, and how it works (described above in more detail); (ii) it is precisely based on the previous algorithms and a literature

review of all related works (LI ET AL. 1991); and (iii) based on the empirical tests of this study for available data set images, the results of the Sobel Edge Detector were the best compared to other filters.

### 3.2.2 Experimental Results

To assess the results, the second stage in the developed algorithm of this thesis was also applied to the dataset of pavement images for different streets in Germany. S.T.I.E.R mobile mapper system (LEHMANN + PARTNER GmbH Company) has been employed for capturing image sequences. The image (figure 3.12) has the same characteristics previously described in Chapter 3, section 3.1.2. In the following, an exemplary visualization for all threshold stages is presented.

#### **Adaptive Thresholding Algorithm and Sobel Edge Detector Implementation**

Using the adaptive thresholding algorithm (described above), the approach of this thesis successfully creates binary crack images. The results are shown in figure (3.12-1<sup>st</sup>line). The window size is selected automatically. In addition, the constant value is set up to take different lighting and illumination levels into consideration. The cracks have been extracted from corresponding images, but the crack edge boundaries are unclear. To address this, the approach of this thesis applies the Sobel Edge Detector in particular for boundary specification, and it is found to work well. The edge boundaries are extracted for the cracks, as well as for noise (Figure3.12-2<sup>nd</sup>line). This is essential for the flow in the later post-processing stage.

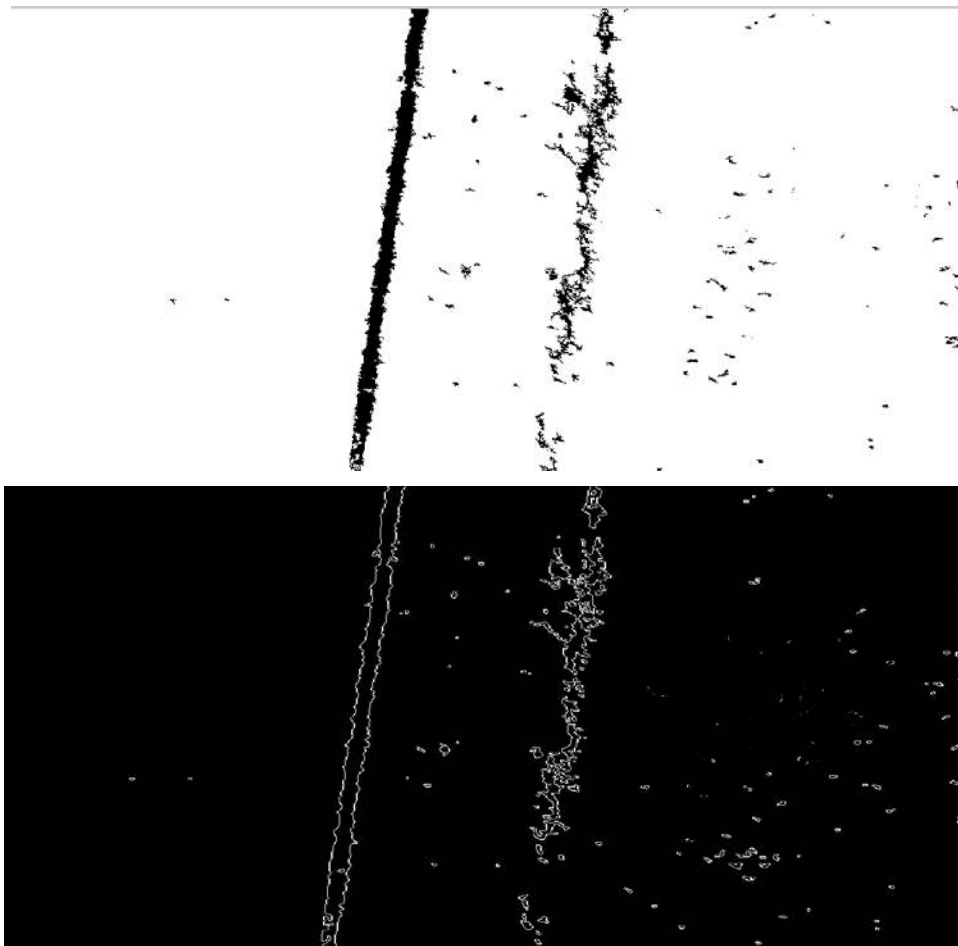


Figure 3.12: Results for thresholding (segmentation stage); the resultant image after applying the adaptive thresholding algorithm (1<sup>st</sup> line); the resultant image after applying the Sobel Edge Detector (2<sup>nd</sup> line).

### 3.3 Crack Connection (Post-processing stage)

#### 3.3.1 Theory

In section (3.1), pavement images were processed in order to correct background illumination, not taking into account the goal of crack extraction from the images. The resultant corrected images are employed then to extract crack outputs, as presented in section (3.2); whereas, all images are converted efficiently into binary images. Using different integration and combination of morphological operation during the pre-processing stage with the help of the adaptive thresholding algorithm can lead to: (i) noise due to the pixel intensity change, some background pixels displaced as foreground pixels; (ii) crack discontinuity (this occurs due to two reasons: firstly, the real shape of the cracks themselves, and secondly the discontinuity due to segmentation operations during and threshold stage); and (iii) holes inside of the crack regions. In order to overcome these problems and improve the results, an integration algorithm for the post-processing stage of this thesis has been developed.

A review of the literature clearly indicates that this post-processing stage is implemented by only a few of the algorithms. Most of the crack detection algorithms exclude this stage. This cancellation happens due to different reasons: (i) it is unnecessary from their perspective; (ii) it may be incorporated in the next stage (crack detection) or previous stage (the threshold stage); and (iii) in addition, to some extent, some of the algorithms (partially procedures) do not take care of classification and everything related with it. Nevertheless, various post-processing algorithms have been proposed and investigated in the literature, (e.g., BUGAE/YAXIONG 2003, LI ET AL. 1991, CHENG/MYOJIM 1998, JAVIDI ET AL. 2003, RABABAAH ET AL. 2005, TEOMETE ET AL. 2005, HSU ET AL. 2001). Generally, no standard method is implemented for the post-processing stage. The selection of one method over another is based on the relevant requirements and goals, and is case-dependent on the images' nature. BUGAE/YAXIONG (2003) addressed the seeds cluster algorithm. RABABAAH ET AL. (2005) proposed the median filtering algorithm. Median filter can delete noise and small narrow cracks regions. These small narrow cracks regions have the same intensity values as the noise. So RABABAAH ET AL. (2005) reported that the median filter strongly fails in the case of crack detection. HSU ET AL. (2001) reported the hole pixel initial algorithm (flood-filling algorithm), which can fill crack holes and connect cracks together to 75%. The skeleton structure was introduced by CHENG/MYOJIM (1998). Connectivity searching provides an accurate result for crack connection (JAVIDI ET AL. 2003, LI ET AL. 1991). In addition, when the pavement images are comprised of high texture, some post-processing algorithms, such as the seeds cluster algorithm, median filter and other methods, fail; whereas, the hole pixel initial algorithm (flood-filling algorithm) continues to work. Thus, this point must be considered when determining which hole-filling algorithm is suitable for application in this study.

Thus, the post-processing algorithm of this thesis is based on a combination process between the hole-filling algorithm and the labelling connected components algorithm. This integration of both algorithms provides correct results. This combination can fill crack holes. Moreover, this enables an implicit determination of cracks within images. This determination is performed by dividing pixel images into classes with different colours through the labelling connected components algorithm. Finally, these different classes enable the approach in this thesis to convert the image into a form that is ready for classification. One advantage of this algorithm is that it retrieves crack connectivity. Another advantage is that dividing image pixels into classes by the labelling connected components algorithm can reduce image information related to pixel intensities. Specifically, instead of dealing with all pixel intensities randomly, the approach of this thesis can deal with identical, or nearly identical, intensity values for each class. This matter will be better when crack classification is done. Furthermore, this integration approach reduces human involvement to a minimum during the entire process.

The post-processing algorithm of this thesis can be divided into the following steps, as presented in figure 3.13.

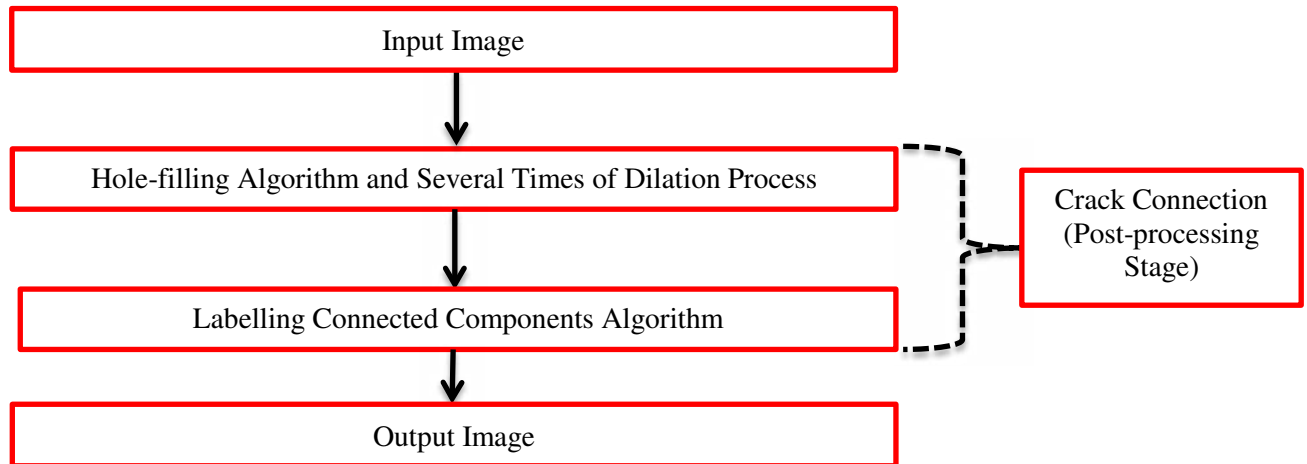


Figure 3.13: Workflow for the combination of different algorithms during the crack connection stage.

The general workflow can be divided into the following steps (figure 3.13):

### **1. Hole-filling Algorithm**

As presented in Chapter 2, section (2.3.2.3), two hole-filling algorithms have been proposed and investigated in the literature, e.g., the hole pixel initial algorithm (HPIA) algorithm and the border image initial algorithm (BIIA) (GONZALEZ/WOODS 2008). Generally, there is a difference of work principles between the hole pixel initial algorithm and the border image initial algorithm. The latter possesses a disadvantage with respect to computational speed, since this algorithm begins from the object border. Then, it will be expanded one pixel from the border. This process must be continued until all holes are filled. Sometimes, it needs 100 epochs based on the image dimensions. In addition, this algorithm will be utilized irrespective of whether or not the input image has an object. So, this algorithm wastes a lot of time, and the final-filling holes suffer from missing details; whereas the disadvantages of the former are related to having the starting point for each hole in each object in the image. This matter is quite complex, so it needs human involvement during the fundamental stages in order for the final filling holes to be accurate (GONZALEZ/WOODS 2008). HSU ET AL. (2001) reported that the hole pixel initial algorithm (flood-filling algorithm) strongly outperforms other methods, such as the connectivity searching (JAVIDI ET AL. 2003) and the skeleton structure (CHENG/MYOJIM 1998). For example, the hole pixel initial algorithm (flood-filling algorithm) can fill crack holes and connect cracks together to 75%; whereas the seeds cluster algorithm can fill crack holes and connect cracks together to 30% and lower. Nevertheless, when the pavement images are comprised of high texture, as mentioned previously, some post-processing algorithms, such as the seeds cluster algorithm and other methods, fail; whereas the hole pixel initial algorithm (flood-filling algorithm) continues to work. Thus, in this thesis, based on previously described properties, previous algorithms, and literature review, the hole pixel initial algorithm and the border image initial algorithm have been tested for crack hole filling. A comparative study is implemented to select the best algorithm based on the available datasets. After this, the best hole-filling algorithm (hole pixel initial algorithm) is investigated, accompanied by several dilation processes that were described previously in Chapter 2, section 2.3.2.3. A disk-structuring element is used during this dilation process. This operation plays a key role to facilitate the distinction between crack and other extrinsic objects during the next detection stage.

### **2. Labelling Connected Components Algorithm**

This step is designed, at first to accurately and quickly divide binary image pixels into connected components (CC). The connected component process is performed on the hole-filling binary image to segment its pixels into smaller connected components (CC). All of the pixels in each connected component have the same intensity values (0 or 1) due to the binarization. So, the division process is based on two factors: (i) the pixel connectivity; and (ii) the pixel intensities. Firstly, the connec-

ted components (CC) process has been completed, and all of the pixels have been separated into different groups (figure 3.14-1<sup>st</sup>line left). Secondly, the labelling connected components algorithm is run for each group of pixels. The latter is labelled with two possibilities: (i) by gray-level value (value labelling), such as 1,2,3,...etc., (figure 3.14-1<sup>st</sup>line right); or (ii) by colour (colour-labelling), such as one colour for the background as an isolated connected component, and a fixed colour for each foreground connected component (figure 3.14-2<sup>nd</sup>line). The labelling connected components algorithm is performed based on the connected components of the pixel, which are assigned to GONZALEZ/WOODS (2008).

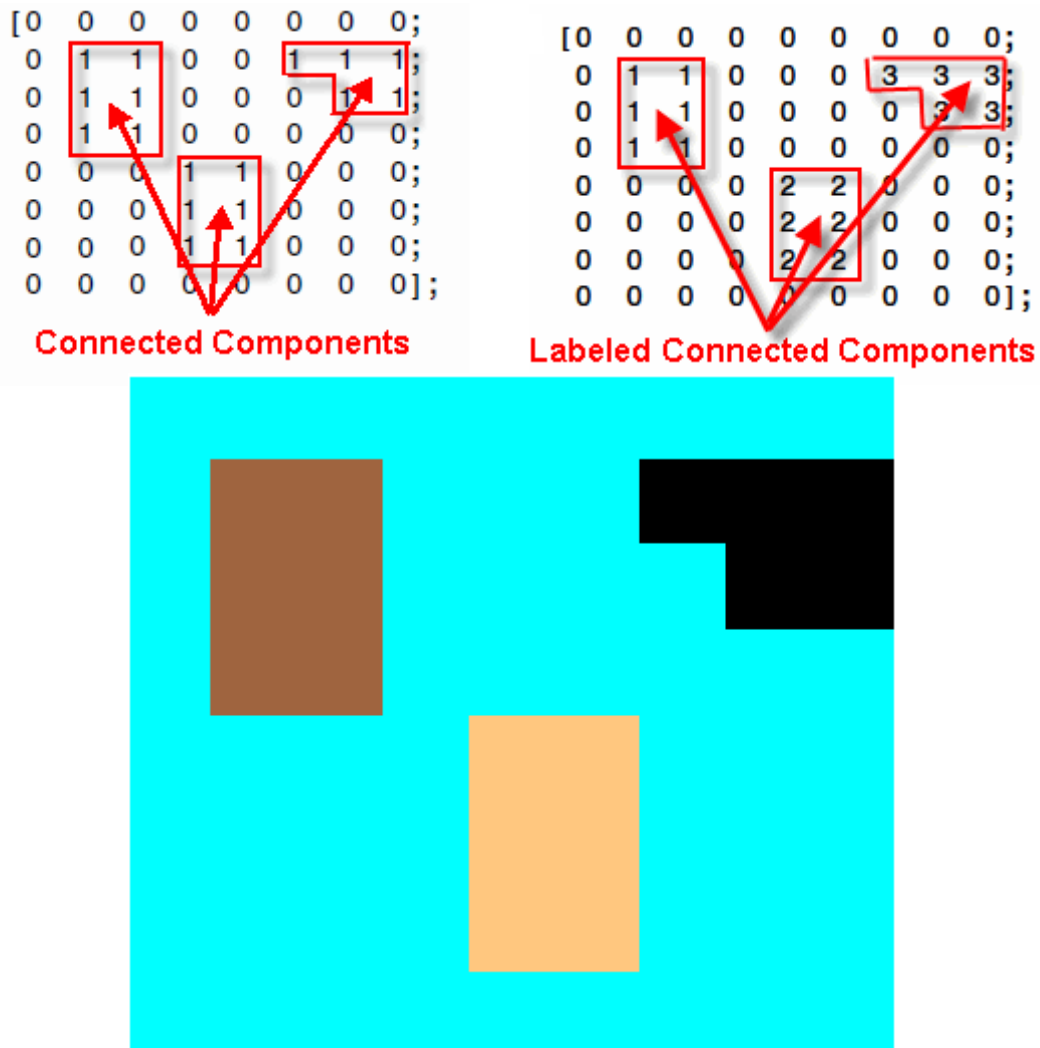


Figure 3.14: Labelling connected components algorithm during the post-processing stage; connected components (1<sup>st</sup> line-left); labelling connected components (value-labelling) (1<sup>st</sup> line-right); labelling connected components (colour-labelling) (2<sup>nd</sup> line) (MATLAB 2014).

In particular by dealing with various connected components in an image instead of random foreground and background black and white pixels, the processing time can significantly decrease. A coloured connected component image is the output of this step, and it is used as a heuristic for the crack appearance and the rest of the noise.

The labelling connected components algorithm is realized for connected region detection in binary or coloured images. So, if the labelling connected components algorithm is incorporated into an image analysis system, several kinds of data will be operated (SAMET/TAMMINEN 1988). Similar approaches are introduced in the literature to divide images into different regions in order to guide image classification and analysis, such as the relaxation labelling technique (SALARI 2012). Others were used for robust threshold images, such as the region growing concept and the labelling connected components algorithm (CHOU/SALARI 2012, SAMET/TAMMINEN 1988, CHEN/LEEDHAM

2005, WU/AMIN 2003). In addition, the labelling connected components algorithm reveals the structure of all equivalent classes by assigning a unique label or colour to each class. Thus, this will lead to reduced classification errors and time. In addition, the labelling connected components algorithm is critical for any automated image analysis enforcement. Finally, it serves to guide the process of classification to deal with different pixel equivalent classes instead of attempting to classify each white pixel as a crack or noise alone. This can simplify and speed up the classification stage. The approach of this thesis follows the labelling connected components algorithm having some analogy with CHOU/SALARI (2012). This connected components algorithm is utilized mathematically in equation (3-3) as follows:

$$X_G = (X_{G-1} \oplus B) \cap A, \text{ for } G = 1, 2, 3, \dots \quad (3-3)$$

where

- $B$  : symmetric structuring element,
- $\cap$  : intersection operator,
- $A$  : input binary image,
- $X_G$  : the product of the algorithm at iteration step  $G$ ,
- $X_{G-1}$  : the vector at iteration step  $G-1$ .

As in equation (3-3), the connected components algorithm is executed on the hole-filling binary image. The algorithm finished at iteration step  $G$  when  $X_G = X_{G-1}$ . The algorithm uses the union set to collect structure data that supply a good representation of the equivalent classes. The intersection at each iteration with the hole-filling binary image constrains the results inside of the region of interest only. The connected components algorithm represents a good exemplification of how a morphological process can be exploited to meet the requirements.

In this study, the application of the connected components algorithm is realised as follows:

- (i) Assume eight-connected pixels, which are defined as a neighbour to every pixel that touches one of their edges or corners. These pixels are linked vertically, horizontally, and diagonally. Each pixel with coordinates is represented as a neighbour to the pixel  $(x, y)$  (figure 3.15). It is worth noting that the approach of this thesis selects eight-connectivity due to the available dataset image nature. This approach could also be expressed as e.g., north-east, north, north-west, and west of the actual pixel (assuming eight-connectivity).

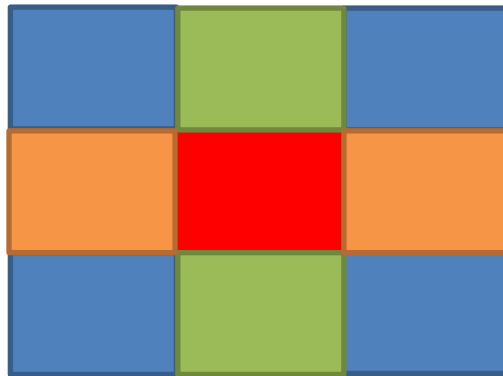


Figure 3.15: Assuming eight-connectivity during the crack connection stage.

Figure 3.15 shows eight-connected pixels around the central pixel (red square), which are defined as neighbors to the central pixel (red square) that touches one of their edges or corners. These pixels are linked vertically (green squares), horizontally (orange squares), and diagonally (blue squares).



- (ii) The connected component is built by scanning a binary image pixel-by-pixel from top to bottom and from left to right. This process is done in order to specify connected pixel regions that have the same set of intensity values ( $I$ ).
- (iii) The connected component regions are formed by eight-connectivity checks around each pixel. The question then arises: Does the pixel to the left have the same intensity value as the actual pixel? If the answer is yes, this pixel is put in the same connected component region of the current pixel. If the answer is no, this pixel is out of the connected component region of the current pixel. This question must be repeated over all pixel neighbours during eight-connectivity. The algorithm continues this approach. Finally, this approach will generate connected components whenever necessary.

After this, the resulting connected components must be labelled through the labelling connected components algorithm. This algorithm is realised as a two-pass algorithm. The aims of the first-pass algorithm are as follows: (1) assign temporal labels for every pixel; and (2) store equivalence classes. On the other hand, the aims of the second-pass algorithm are as follows: (1) find the smallest label within each equivalence class; (2) replace each temporary label for each pixel within the equivalence class by the smallest label; and (3) display the different equivalence classes by different gray-levels form or different colours, where one unique label and colour are assigned for each equivalence class.

The first-pass labelling algorithm is realized as follows:

- (i) Scan the image by moving along a row until it comes to element  $h$ .
- (ii) If element  $h$  is not the background ( $h$  symbolizes the pixel to be labelled for which  $I=1$  [white not black]); when it is true, the following steps must be performed:
  - a. Examine the neighbours of  $h$  that have been obverted in the scan.
  - b. If there are no neighbours (all neighbours are 0 [black]), specify a new label to  $h$ .
  - c. If only one neighbour has  $I=1$ , specify its label to  $h$ .
  - d. Otherwise, if more than one of the neighbours have  $I=1$ , find the neighbours with the smallest label and specify it to  $h$ . Then, record the note of equivalence between neighbour labels. After completing the first-pass labelling algorithm, the equivalence label pairs are recorded and saved into equivalence classes.

The second-pass labelling algorithm is utilized as follows (GONZALEZ/WOODS 2008):

- (i) Scan for each element of the image data by column, and then row, and identify if element  $h$  is in the background or not.
- (ii) If it is not in the background, the following steps must be performed:
  - a. Find the smallest label within the equivalence class that concludes element  $h$ .
  - b. Relabel element  $h$  with the smallest equivalence class label.
  - c. Display the final results, in which each equivalence class has its unique value and its unique colour.

It is worth noting that the background is consumed to specify the remarkable elements from the foreground. In the case of ignoring the background, the two-pass algorithm will deal with the background as another coloured region, similar to this study's application.

### 3.3.2 Experimental Results

In order to show the results of this thesis, the algorithm was applied to the dataset of pavement images for different streets in Germany. S.T.I.E.R mobile mapper system (LEHMANN + PARTNER GmbH Company) has been employed for capturing image sequences. The image (figure 3.16) has the same characteristics previously described in Chapter 3, section 3.1.2. In the following, an exemplary visualization for all of the workflow of the post-processing stage is presented.

### Hole-filling Algorithm

Since the processing time has not yet been taken into account, the hole pixel initial algorithm (HPIA) and the border image initial algorithm (BIIA) have been tested in this thesis in order to ensure good robustness for crack hole filling. A comparative study is implemented to select the best algorithm based on the available datasets. Finding better crack hole filling and crack connectivity constitute an important issue, especially in the case of having high pavement texture images. The nature of these latter images have numerous obstacles, such as aggregate size, the binder size itself, and black rubber hose. All of these obstacles will appear as noise. Sometimes these obstacles (noise) affect the hole-filling algorithm's behaviour. In fact, this impact is based on how the algorithm is performed, in which some hole-filling algorithms may deal with these obstacles as cracks and fill the holes between them. In addition, some parts of the crack regions will be missed; whereas, another hole-filling algorithm will perform successfully in crack hole filling and crack connectivity. The conclusion is that the choice of the hole-filling algorithm is actually case-dependent (figure 3.16).

Accordingly, figure 3.16 shows that there are differences in the results of applying the border image initial algorithm with respect to the results of applying the hole pixel initial algorithm. The associated resultant image by the latter algorithm might be more useful than the first one. The former one can be prone to failure due to different reasons, such as: (i) it fails to connect some parts of the crack regions; (ii) it cannot fill some holes inside of the crack regions; and (iii) there are some missing parts of the crack regions. Although the hole pixel initial algorithm cannot reduce noise, it can, to some extent, fill crack holes and check connectivity successfully. In conclusion, the hole pixel initial algorithm followed by several iterations of the dilation process is adapted in this study's application (AL-MISTAREHI/SCHWIEGER 2015).

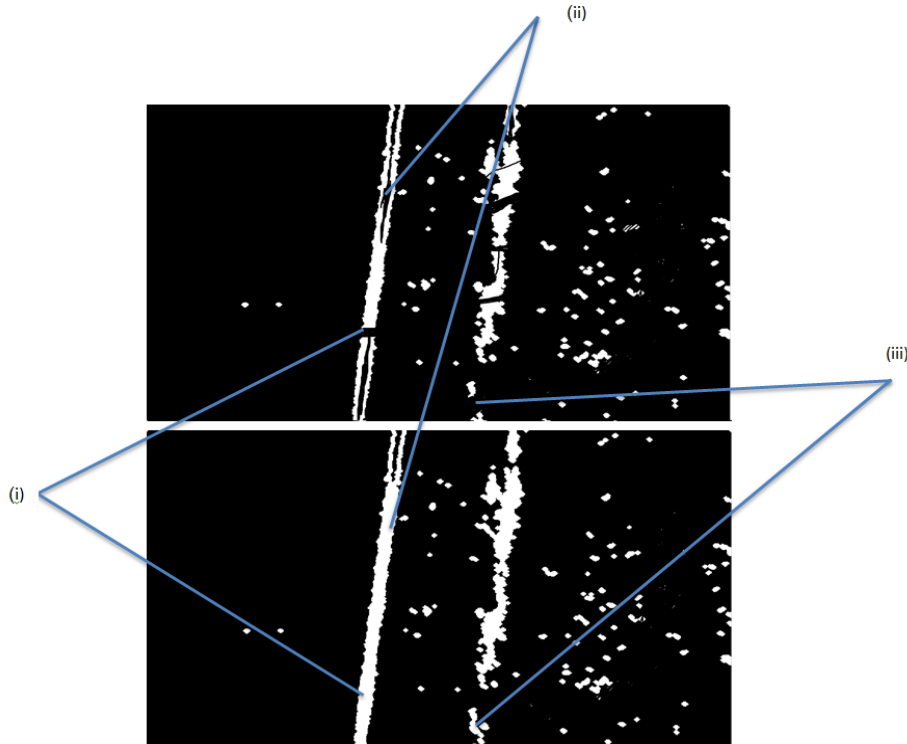


Figure 3.16: Results for hole-filling algorithms (post-processing stage); the resultant image after applying the border image initial algorithm (1<sup>st</sup> line); the resultant image after applying the hole pixel initial algorithm (2<sup>nd</sup> line).

### **Labelling Connected Components Algorithm**

Once the resultant image from the hole-filling algorithm is realized, the division of the binary image into regions can be solved automatically by using the labelling connected component algorithm. The labelling connected component algorithm results are considered as a final preparation step before the crack extraction and classification stage (figure 3.17).

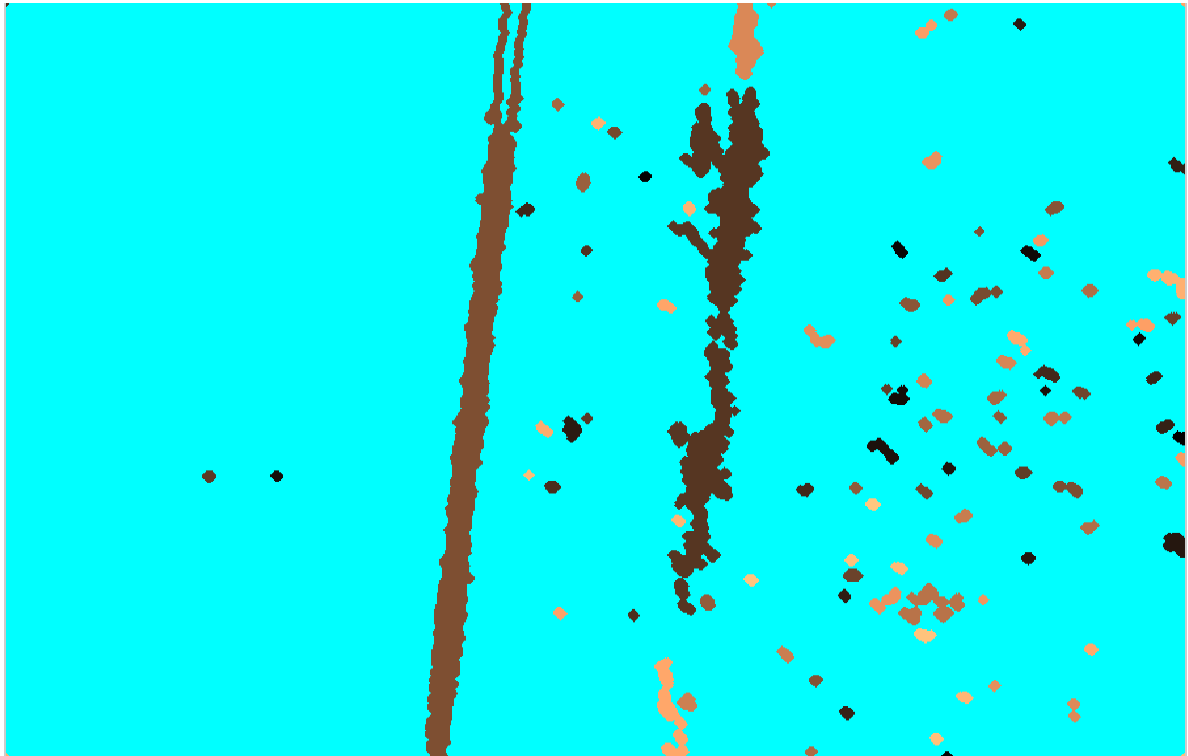


Figure 3.17: Results for the labelling connected components algorithm (post-processing stage).

Figure 3.17 illustrates that different connected components are assigned different colours. Each colour represents a connected component region (equivalence class) with the same, or nearly the same, intensity values. For example, all backgrounds have one colour and the cracks have another colour due to different intensity values. These results are sufficient as a final preparation step before the crack extraction and classification stage (detection stage) due to different reasons, such as: (i) the crack regions are clear with distinctive colours (instead of dealing with the original unclear crack gray-scale images); (ii) the holes and gaps inside of the crack regions are filled; and (iii) the cracks' connectivity is adequate, to some extent. In fact, it can be seen from Figure 3.17 that there are some noise connected component regions which have the same colour as the crack connected component regions. This means that some noise intensities have the same, or nearly the same, intensities as the crack intensities. This creates a challenge for the next detection stage (crack extraction and classification) regarding how the algorithm presented in this thesis will be able to distinguish between cracks and noise based on the intensity factor only. This creates a need to insert another factor, rather than intensity, to overcome this problem (AL-MISTAREHI/SCHWIEGER 2015).

## 4 Crack Extraction and Classification

Crack extraction and classification, as the task of detecting different crack types from different pavement texture images, is still an active topic of transportation research, e.g., (SALARI 2012). A complete detailed representation of cracks' surfaces is required for any application, for instance, pavement evaluation, performance measurement, maintenance rehabilitation, and reconstruction of pavement surfaces. Manual crack detection systems may provide an accurate representation of crack surfaces. However, due to field survey limitations, such as time consumption, high labour effort, and dangerous and low repeatability level, manual crack detection systems are not sufficient to produce full crack sense coverage. Automatic crack detection systems are more suitable for crack detection coverage than the former manual detected methods.

Most well-known crack detection algorithms are executed by the integration of digital image processing approaches. These approaches are considered to be the most suitable tool for the crack detection target. As presented in Chapter 3, in order to simplify the crack detection task from an original gray scale pavement image, several categories of preparation stages, such as the pre-processing stage, thresholding stage, and post-processing stage, have been exploited; see (TRIER/TAXT 1995; CHOU/SALARI 2012, BIENIECKI/GRABOWSKI 2005). Each preparation stage is realized by a combination of different digital image processing algorithms styles. The aims of all of the preparation stages are as follows: (i) conversion of the original gray scale crack image to an easier form for crack detection; (ii) elimination of several distributing information from the original gray scale image, such as shadows during the pre-processing and thresholding stages due to binarization; and (iii) production of a coloured image with different equivalence classes instead of dealing with random intensities of black and white images. In fact, if anyone looks roughly on the final resultant image from all of the preparation stages, the cracks will be represented as a coloured connected component region in addition to remaining noise. Some noise connected component regions have the same colour as cracks connected component regions' colour. This means that some noise intensities have the same or nearly the same intensity as the crack intensities. This creates a challenge to introduce a powerful algorithm. This algorithm enables one to find other criteria in addition to cracks' intensities. This criterion will help for crack extraction (AL-MISTAREHI/SCHWIEGER 2015).

Direct crack extraction and classification from pavement images based on the combination of different image processing techniques, and some modifications of previous algorithms, are presented. The algorithm of this thesis suggests applying the contouring algorithm (SALARI ET AL. 2010; JONES 1971). This contouring algorithm specifies exactly the location of the crack in the original image. Then, for the purpose of extracting cracks, this study modifies the binary mask detection algorithm based on the geometric relationship for crack regions (TEOMETE ET AL. 2005). This modification strategy aims to extract cracks and their characteristics. Furthermore, this study uses the crack classification method (YING/SALARI 2009) for an implicit determination of the type of cracks and their characteristics in the final resultant images.

In principle, the algorithm's goal for this study can extract and classify cracks of pavement images automatically, not manually. In the following, a detailed description of the algorithm is given in order to introduce the completely used methodologies. As presented in Figure 4.1, the algorithm of this stage is divided into the following steps.

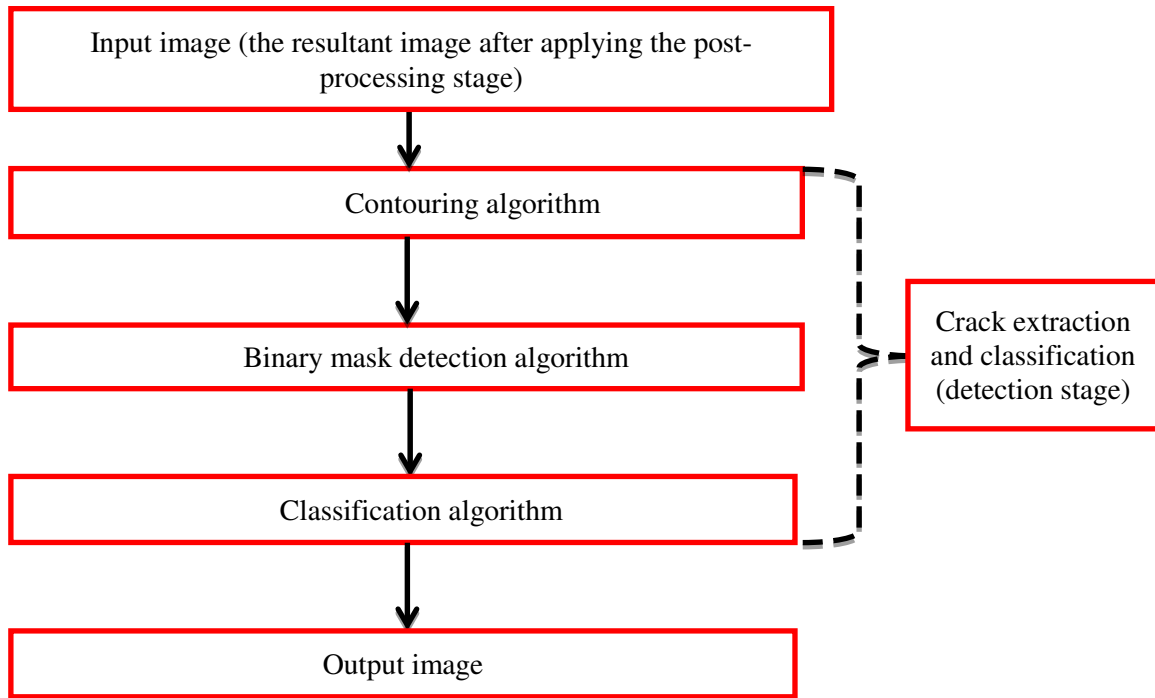


Figure 4.1: Workflow for the combination of different algorithms during the detection stage.

## 4.1 Contouring Algorithm

A wide variety of the most common contour tracing algorithms for different applications have been proposed and investigated in the literature, e.g., JONES (1971), ARAMINI (1980), BRUSS (1977), COTTAFAVA/LEMOLI(1969), ERMLER ET AL. (1976), FISHER (1981), HECKMAN/MEYER(1980), BATCHA/REESE(1960), and WALDEN (1972). Generally, SOSS (2003) addressed the square tracing algorithm. TOUSSAINT (1997) proposed the Moore-neighbour tracing algorithm, which cannot be based on the same stopping criterion as the square tracing algorithm, to fully accept invariant image patterns and terminate. TOUSSAINT (1997) introduces border tracing by radial sweep, while PAVLIDIS (1982) presented the Pavlidis' algorithm. In particular, the most evident contouring algorithm is investigated using triangular procedures (JONES 1971). The other methods, such as the square tracing and Moore tracing algorithms, possess a number of shortcomings which cause them to fail in tracing the contour of huge patterns; this is due to their size of connectivity (TOUSSAINT 1997). SALARI ET AL. (2010) utilises the contouring algorithm for printing cracks on the original image. SALARI ET AL. (2010) reports that applying contouring algorithms outperforms significantly over the drawbacks of other methods, such as the border tracing by radial sweep (TOUSSAINT 1997) and Pavlidis' algorithm (PAVLIDIS 1982), e.g., border tracing by radial sweep ignores holes present in the pattern. Although, the contouring algorithm by SALARI ET AL. (2010) can successfully trace the contour around the crack regions, taking holes into consideration.

Furthermore, SALARI ET AL. (2010) illustrates that if the crack pavement images are connected within eight connectivity patterns, some contouring algorithms, such as the square tracing algorithm, fail to extract the contour around the crack regions (usually fewer contouring algorithms can accomplish this). Thus, this application based on the literature adapts applying the contouring algorithm by JONES (1971) and SALARI ET AL. (2010). This contouring algorithm is able to compute and draw contour lines around different regions in the original image. These regions are considered as the probable regions to have cracks. The contouring algorithm's aim is to automatically specify the probable crack locations in the original image. This will be helpful to extract the real crack measurements from the original images after detecting them. This is done instead of measuring cracks' properties from coloured connected components images. In other words, the contouring algorithm is used as a tool for projecting all of the coloured equivalence classes (probably crack regions) on the original image.

Then, the overall algorithm for contouring (JONES 1971, SALARI ET AL. 2010) is described as follows:

1. Define the feature e.g. cracks.
2. Find the minimum and the maximum gray values (colour)  $f_{min}, f_{max}$  over the feature.  $f$  represents the gray values "colours". The gray value  $f$  is interpreted as the third dimension of the coordinate system "heights".
3. Identify the existing contour level  $e$ , where  $e$  is defined as the lowest contour level to be drawn within range  $[f_{min}, f_{max}]$ .
4. If  $f_{min} \leq e \leq f_{max}$  then go to step (5), or else go to step (7).
5. Dash the contour over the feature.
6. Save the contour.
7. If not all the features are handled, then consider the next feature and go to step (2), or else go to step (8).
8. Connect the contours that have the same level.
9. Scheme the contours.
10. Compute the contour lines data structure matrix as a two-row matrix using linear interpolation. The previous described overall contouring algorithm is summarized in detail in Figure (4.2).

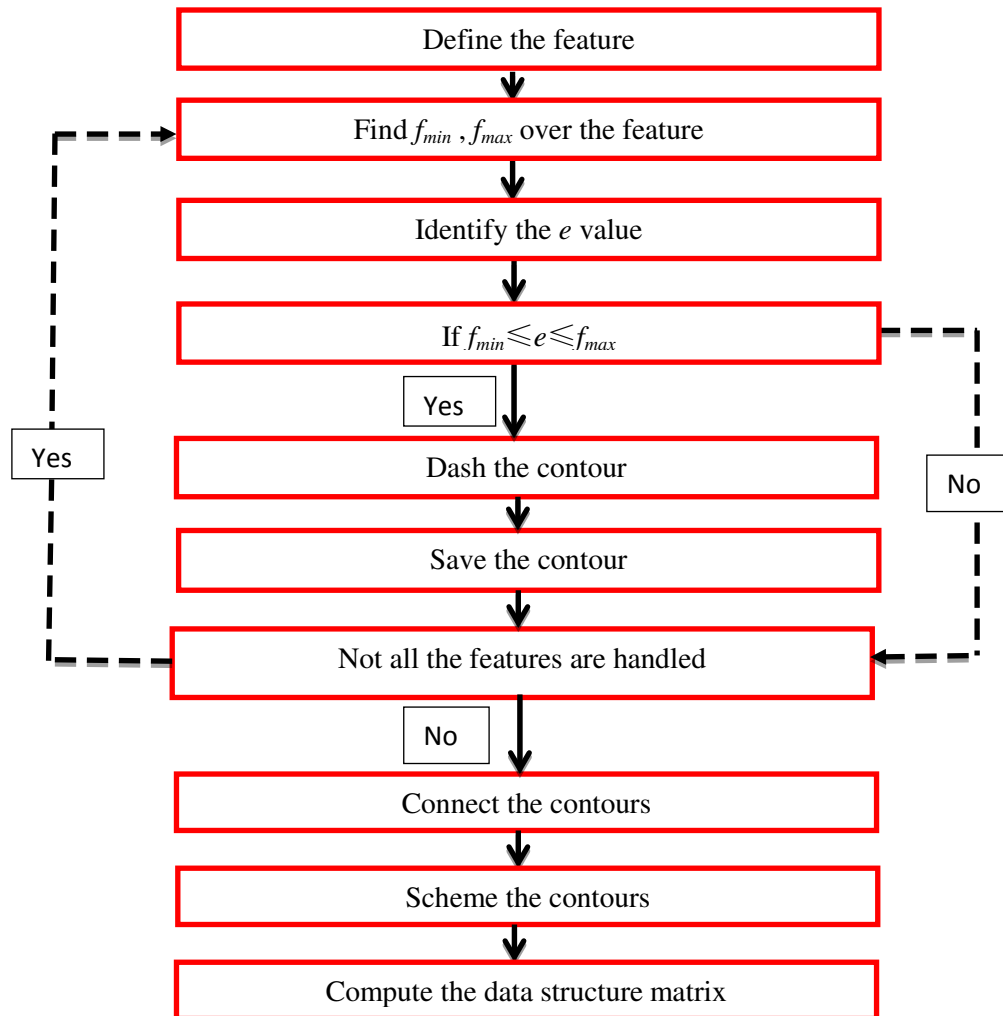


Figure 4.2: Workflow for the contouring algorithm during the detection stage.

In conclusion, the contouring algorithm specifies all contour lines using this matrix. The first row of the column contains the labelled contour value in the map. The value below this is the number of

vertices in the contour line. The remaining columns contain the  $(x, y)$  coordinates for each vertex in which the contour crosses over them (Figure 4.3).

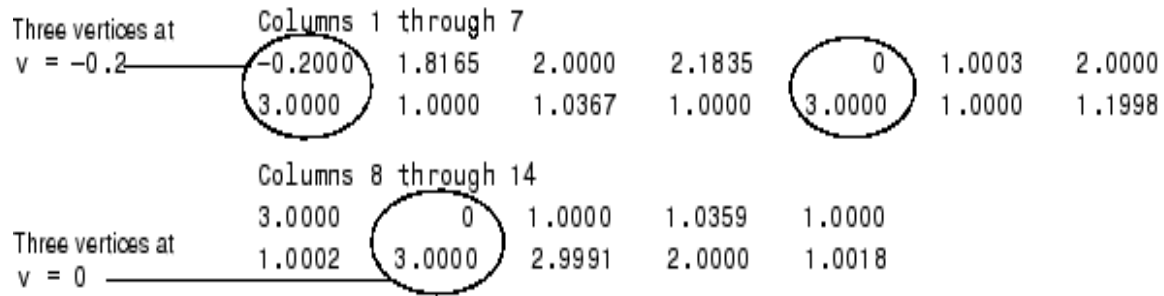


Figure 4.3: Example of the contour matrix for three vertices (MATLAB HELP, 2012<sup>n</sup>).

By analyzing Figure 4.3, the contour line crosses over nine vertices (edges), and the labeled contour value for first three vertices is equal to  $(-0.2000)$ . The  $(x, y)$  coordinates for the first three vertices were  $(1.8165, 1.0000)$ ,  $(2.0000, 1.0367)$ , and  $(2.1835, 1.0000)$ , respectively.

## 4.2 Binary Mask Detection Algorithm

The resultant contouring images indicate different probable crack regions (green colour regions). Some of them are related to actual cracks, and others are related to noise. As a consequence, the discrimination between cracks and noise requires a robust extraction algorithm, which employs region shape properties instead of being based on the intensities only (TEOMETE ET AL. 2005). A wide variety of crack classification algorithms have been proposed and investigated in the literature, e.g., (CHOU ET AL. 1994, GEORGOPOULOS ET AL. 1995, CHENG/MYOJIM 1998, LE ET AL. 1990, RABABAAH ET AL. 2005). Generally, all of these classification algorithms are considered a complete procedure with some problems and defects. Some of these problems are summarized as follows: (i) loss of invariant properties of cracks in the case of different pavement textures; (ii) absence of some parts of cracks in the case of shadows; (iii) incapacity to distinguish cracks from noise due to similar intensities; (iv) incapability to differentiate cracks from marking lines; and (v) inability to identify cracks from other extrinsic objects (LE ET AL. 1990). The reasons for all of these problems are as follows: (i) inadequate preparing stages before the crack extraction and classification stage; and (ii) most crack extraction methods are based on the pixel intensity values, and unfortunately some noise regions have the same intensities as the crack regions. This issue will affect the classification rate.

TEOMETE ET AL. (2005) proposes the binary mask detection algorithm. This binary mask detection algorithm is able to detect reliable crack regions by different approaches. One approach is completed by setting a threshold to the crack size using several trials and errors; whereas, the second approach investigates the shape of crack regions. The latter approach of this algorithm can detect crack regions automatically. TEOMETE ET AL. (2005) report that the binary mask detection algorithm significantly outperforms other classification methods in terms of the incapacity to distinguish cracks from noise due to similar intensity. So, the binary mask detection algorithm (second approach) inserts a shape factor besides the intensity for crack extraction successfully. Thus, the binary mask detection algorithm (second approach) has been selected for this thesis application with some modifications and extensions. This extension has an important advantage to preserve crack connectivity for classification. Moreover, the modified binary mask algorithm can ignore noise regions. To some extent, this modified binary mask algorithm performs successfully in extracting characteristics of the crack regions from the geometric characteristics of the binary mask shape. Moreover, these crack characteristics play a key role to provide the correct crack type in the next step.

As a result, the modified binary mask algorithm achieves an increase in automation. It represents a straightforward solution for crack extraction and results in detailed crack structures, with high

pavement texture. In the following, a detailed description of the modified binary mask algorithm is presented in order to introduce the used steps in their entirety.

**Preparing Stage:** A statistical analysis is performed for most of the crack images to determine the range of crack area lengths, the range of crack area widths, and the minimum crack widths. These numbers are considered to meet the requirements for generating the binary mask shape of the latter step. In this thesis, the results of the statistical analysis are as follows: (1) the range of crack areas length is between 0.1 to 1 m on the ground, which equals 100-833 pixels on the image; and (2) the range of crack areas width is between 0.04 to 0.2 m on the ground, which equals 35-166 pixels on the image. The minimum crack width on the available case study is 3 mm (2.5 pixels). Based on the German regulations of the Road State Determination Manual (FGSV 2006), cracks thicker than 1 mm should be detected. This stage is done just once for most of the crack images in one case study. The results of the statistical analysis are used as pre-defined conditional statement values in all case studies of this thesis.

The overall modified binary mask detection algorithm (TEOMETE ET AL. 2005) is introduced as follows:

- (i) Define the binary ellipse mask based on the pre-defined conditional statement values mentioned above (results of preparing stage)
- (ii) Move the binary ellipse mask over the resultant image after applying the hole filling algorithm, as shown in Figure 4.4.

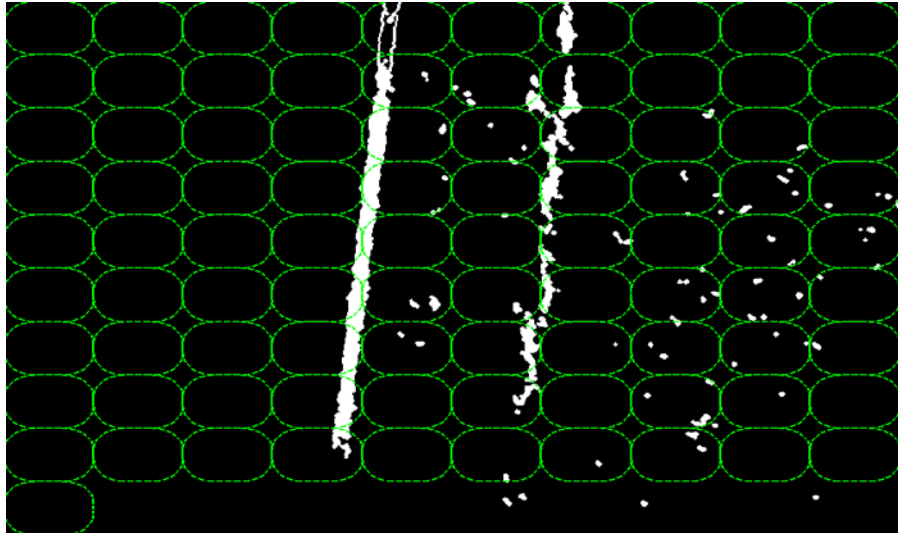


Figure 4.4: Moving binary ellipse mask over the image during the crack extraction and classification stage.

- (iii) When the pre-defined conditional statements values are satisfied, the ellipse will be printed over the contour on the image after applying the contouring algorithm (Figure 4.12, Section 4.4). This is done to define the region of interest. Until step (iii), the binary mask detection algorithm is utilized as in TEOMETE ET AL. (2005). After this, in order to fit the crack connectivity for the classification and filter out incorrect noise, this study modifies and extends the algorithm in the following steps:
- (iv) Some conditions must be checked as follows: (a) if there are different continuous ellipses (binary masks) printed over continuous contours; (b) and if these contours are corresponding with connected components (equivalence classes), having the same or nearly the same intensities and colours, the continuous binary ellipse masks will be merged around the continuous contour regions automatically. Otherwise, each binary ellipse mask will be drawn for each contour part alone automatically.



- (v) Draw the major axis and minor axis for each ellipse by a geometric method. This geometric method is done by generating two matrices. One matrix represents the  $x$ -coordinates for the starting and ending points of major and minor axes, respectively. On the other hand, the second matrix performs  $y$ -coordinates for the same points associated with major and minor axes, respectively. The two matrices are utilized mathematically in equations (4-1), and (4-2), respectively. Figure (4.5) shows how the major axis and minor axis are actually determined. The orientation angle of the binary ellipse shape  $\Omega$  is involved for calculating the coordinates of start and end points. The orientation angle value  $\Omega$  is assigned as the orientation of the major axis inside the binary ellipse mask region. This orientation angle value  $\Omega$  is obtained automatically from the region properties.

$$a_x = \begin{bmatrix} X_1 & X_3 \\ X_2 & X_4 \end{bmatrix}, \quad (4-1)$$

$$a_y = \begin{bmatrix} Y_1 & Y_3 \\ Y_2 & Y_4 \end{bmatrix}, \quad (4-2)$$

$$X_1 = (X_0 - d_{x1}) = \left( X_0 - \frac{r_a}{2} * \cos(\Omega) \right), \quad (4-3)$$

$$X_2 = (X_0 + d_{x2}) = \left( X_0 + \frac{r_a}{2} * \cos(\Omega) \right), \quad (4-4)$$

$$X_3 = (X_0 + d_{x3}) = \left( X_0 + \frac{r_b}{2} * \sin(\Omega) \right), \quad (4-5)$$

$$X_4 = (X_0 - d_{x4}) = \left( X_0 - \frac{r_b}{2} * \sin(\Omega) \right), \quad (4-6)$$

$$Y_1 = (Y_0 - d_{y1}) = \left( Y_0 - \frac{r_a}{2} * \sin(\Omega) \right), \quad (4-7)$$

$$Y_2 = (Y_0 + d_{y2}) = \left( Y_0 + \frac{r_a}{2} * \sin(\Omega) \right), \quad (4-8)$$

$$Y_3 = (Y_0 - d_{y3}) = \left( Y_0 - \frac{r_b}{2} * \cos(\Omega) \right), \quad (4-9)$$

$$Y_4 = (Y_0 + d_{y4}) = \left( Y_0 + \frac{r_b}{2} * \cos(\Omega) \right), \quad (4-10)$$

where

- $a_x$  : matrix represents the ( $x$ -coordinates) for the starting and ending points of major and minor axes, respectively,
- $X_1$  :  $x$ -coordinate for the start point of the major axis,
- $X_2$  :  $x$ -coordinate for the end point of the major axis,
- $X_3$  :  $x$ -coordinate for the start point of the minor axis,
- $X_4$  :  $x$ -coordinate for the end point of the minor axis,
- $a_y$  : matrix represents the ( $y$ -coordinates) for the starting and ending points of major and minor axes, respectively,
- $Y_1$  :  $y$ -coordinate for the start point of the major axis,
- $Y_2$  :  $y$ -coordinate for the end point of the major axis,
- $Y_3$  :  $y$ -coordinate for the start point of the minor axis,
- $Y_4$  :  $y$ -coordinate for the end point of the minor axis,
- $X_0$  :  $x$ -coordinate for the center of the ellipse shape (obtained automatically from region properties)(pixels),
- $Y_0$  :  $y$ -coordinate for the center of the ellipse shape (obtained automatically from region properties)(pixels),
- $r_a$  : major axis length (pixels),
- $r_b$  : minor axis length (pixels),

$\Omega$  : crack area orientation angle (degree).

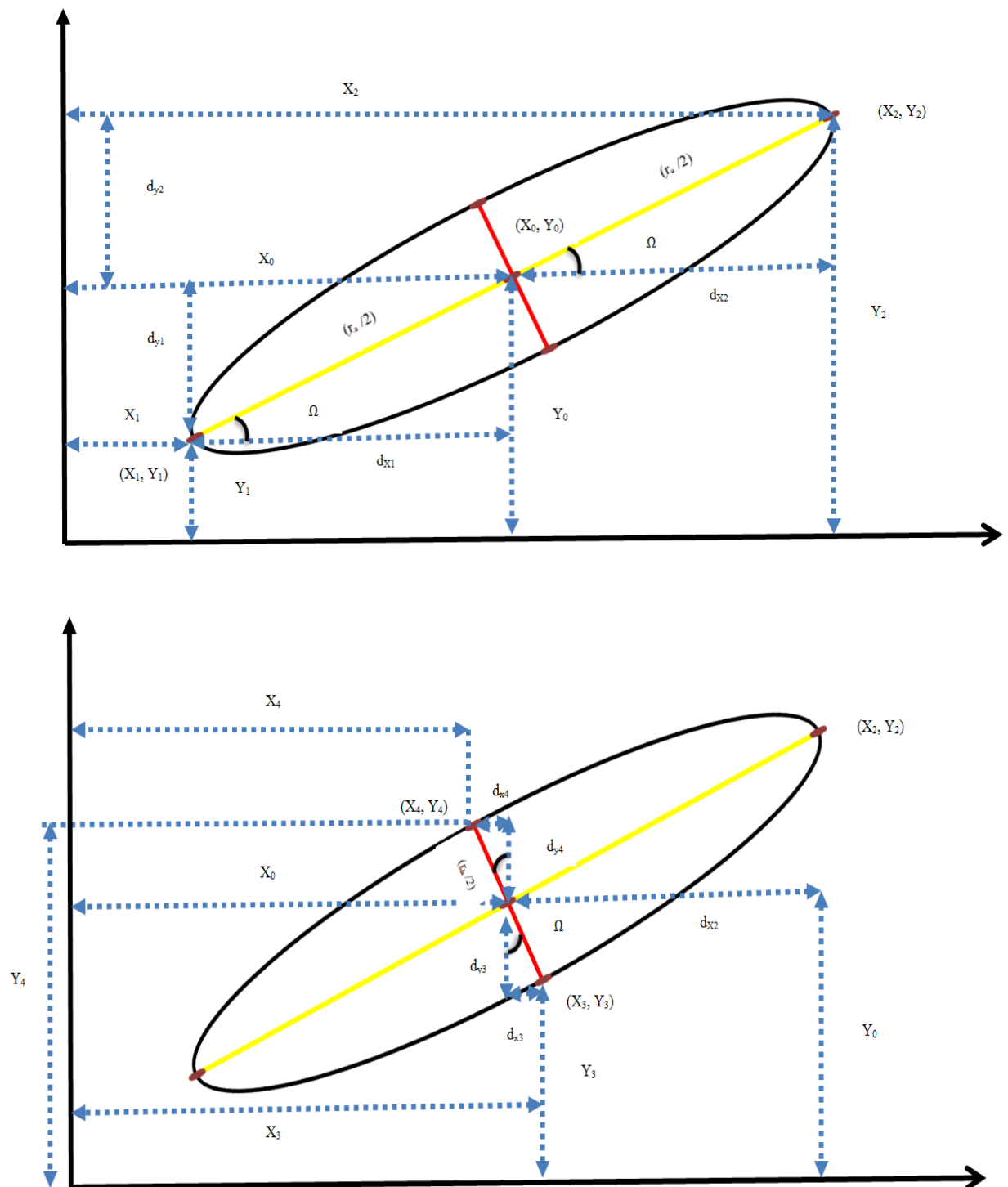


Figure 4.5: Masking ellipse definition; 1<sup>st</sup> line: explanation of the major axis; 2<sup>nd</sup> line: explanation of the minor axis.

- (vi) Detect cracks automatically, in which each contour region surrounded by an ellipse shape is automatically considered as a crack region (Figure 4.6). Otherwise, any other item (other green regions) is ignored automatically, as shown in Figure 4.13, Section 4.4.

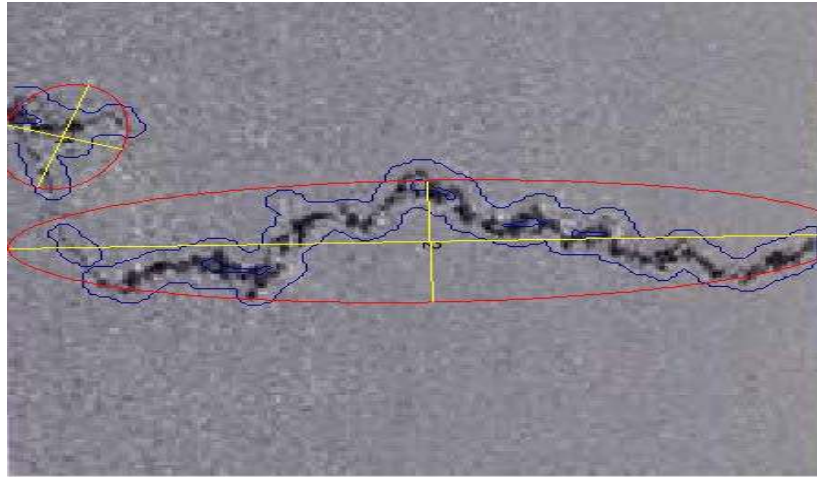


Figure 4.6: Ellipse around crack regions during the crack extraction and classification stage.

- (vii) Determine severity levels for each cracking region based on the state value  $ZG$  and the normalized state value  $ZW$  calculations that are described in Chapter 2, section (2.1.2).
- (viii) Extract crack characteristics automatically from the geometrical characteristics of the binary ellipse mask shape (region properties) as follows:
- Crack area length is represented by the length of the major axis given in pixels.
  - Crack area width is represented by the length of the minor axis given in pixels.
  - Crack area orientation  $\Omega$  is represented by the orientation of the major axis inside of the binary ellipse mask region. A virtual vertical axis ranging from  $-90^\circ$  to  $90^\circ$  is defined and passed through the ellipse shape centre. Then, the algorithm can move directly through a path within the range of  $-90^\circ$  to  $90^\circ$  from the positive horizontal axis to the major axis of the ellipse shape. The orientation angle will be generated from this movement either clockwise or counter-clockwise. The final orientation angle will be measured as a value in degrees with a positive or negative sign. The sign will represent the direction of the path from the positive horizontal axis to the major axis of the ellipse shape. The orientation angle is automatically realized from the region properties.
  - Area of crack region: In this thesis, the area of the crack region is determined by calculating the area of the ellipse surrounding each crack region by equation (4-11) below. This parameter is used in the case of network of cracks (block type). The modified algorithm generates a group of ellipse masks in the block type region. The affected areas by the block crack type are measured by summing-up the areas for all ellipses inside of the block crack region automatically (Figure 4.15, Section 4.4). The previous described overall modified binary mask algorithm is summarized in detail in Figure (4.7).

$$A = \pi \cdot 0.5^2 \cdot r_a \cdot r_b, \quad (4-11)$$

where

$r_a$  : major axis length (pixels),

$r_b$  : minor axis length (pixels),

A : area of the crack region that equals the ellipse area (pixels).

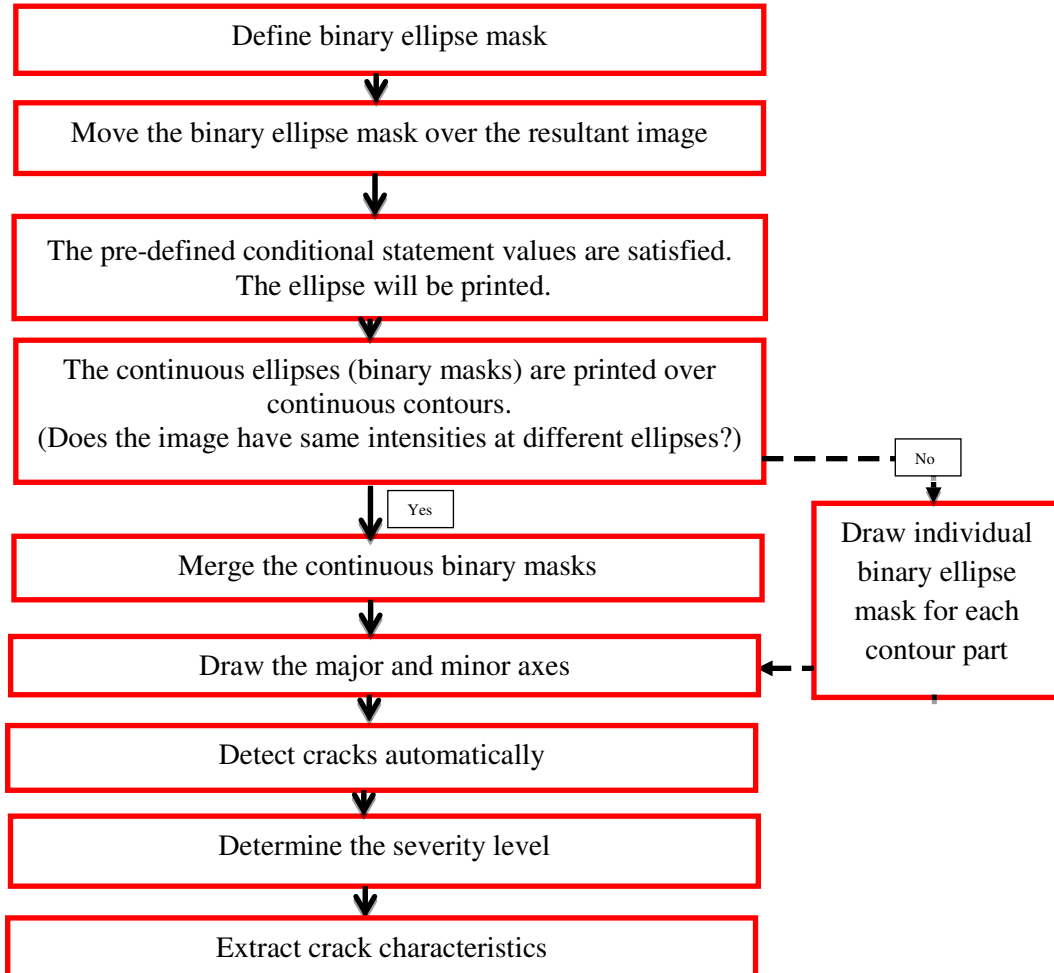


Figure 4.7: Workflow for the modified binary mask algorithm during the detection stage.

### 4.3 Classification Algorithm

The resultant image, after applying the modified binary mask algorithm, indicates the regions related to cracks only. A broad set of classification methods are introduced and investigated in the literature, for example (CHOU ET AL 1994). Generally, there is no standard method for classification, which indicates the capability of crack classification under different conditions, such as different pavement textures, different illuminations, and shadows. Furthermore, there are no standard specifications that can be used everywhere. The standard specifications are different from one country to another and sometimes from one state to another, within the same country. For example, in the U.S., there is a specification for each state. It is based on the pavement condition texture, the reflection of pavement materials, illumination and shadow conditions, and weather conditions (SHAHIN 2002). Every road authority has its own method for this classification. The author asserts that the differentiation between cracks types is considered as more of a challenge than detecting the cracks (GIRARDELLO 2002). In conclusion, the selection of the classification method is considered to be case-dependent.

GEORGOPOULOS ET AL. (1995) classifies cracks based on the orientation direction of their presence. Moreover, back propagation neural network is addressed for crack classification (CHOU ET AL. 1994, LE ET AL. 1990, HSU ET AL. 2001, CHOU/SALARI 2012). The projection histogram method is able to classify cracks by examining the peaks of the projection vectors (CHENG/MYOJIM 1998; RABABAAH ET AL. 2005; TEOMETE ET AL. 2005). JAVIDI ET AL. (2003) addressed the Hough Transform algorithm. Some other methods are based on predefined characteristics of each individual crack pattern (WANG/HARALICK 2002). SALARI ET AL. (2010) proposed a 2D-feature mapping method for crack classification. As described previously in Chapter 2, every classification method has its own problems and defects. The Hough Transform method (JAVIDI ET AL. 2003) suffers from two significant problems as follows: (i) it can be prone to failure to check pixel connectivity in the case of a large number sequence of pavement images; and (ii) although edge pixels are connected, the count of the accumulator cell cannot reflect the length of the crack segment. YING/SALARI (2009) state that the crack classification standard method significantly outperforms other methods, such as the Hough Transform method (JAVIDI ET AL. 2003). For example, the crack classification standard method classifies cracks based on predefined orientation angles and crack branch numbers. Moreover, it determines the crack length by taking pixel connectivity into consideration. While the Hough Transform method can classify cracks, it cannot detect their lengths exactly. Furthermore, YING/SALARI (2009) illustrate that the crack classification standard method is easier for realization than other methods (CHOU ET AL. 1994), because it is only based on the crack orientation and the number of crack branches. In the case of complex compound crack pavement images, the projection histogram method (TEOMETE ET AL. 2005), as well as other methods, fails while the crack classification standard method continues to work. Therefore, it is not very sensitive to noise and can deal with poor quality images. Thus, the crack classification standard method (YING/SALARI 2009) has been adapted, with some modifications and improvements, for this thesis application. In the following, a detailed description of the crack classification standard method is demonstrated in order to thoroughly introduce the steps.

Based on (YING/SALARI 2009), the orientation angle  $\Omega$  is defined as an angle between the horizontal axis to the start and end points of each crack. YING/SALARI (2009) introduced limits of the orientation angle  $\Omega$  with the horizontal axis, such as ( $30^\circ$ ,  $60^\circ$ ). These numbers (angles limits) are supposed as a specification for the control crack classification of either horizontal, vertical, or transverse. These numbers (angles limits) and crack types are selected based on YING/SALARI (2009) and available datasets. Therefore, the crack classification standard method (YING/SALARI 2009) is modified to meet the objectives of this thesis application as follows: (i) the orientation angle  $\Omega$  is defined as an angle between the horizontal (+x-axis) and the major axis of the region (ellipse shape), either clockwise or counter-clockwise. This orientation angle  $\Omega$  ranges from  $-90^\circ$  to  $90^\circ$ . It will be obtained automatically from applying the previous modified binary mask algorithm step. (ii) Based on the knowledge of the YING/SALARI (2009) algorithm, YING/SALARI (2009) created general specifications to connect between the crack type and its orientation, automatically. In this thesis, crack classification is done based on these general specifications. The classification of cracks (Figure 4.8) is implemented as follows (YING/SALARI 2009):

- 1- The vertical individual cracks have an orientation angle ( $\Omega \geq 60^\circ$ ),
- 2- The horizontal individual cracks have an orientation angle ( $\Omega \leq 30^\circ$ ),
- 3- The transverse individual cracks have an orientation angle ( $60^\circ > \Omega > 30^\circ$ ),
- 4- The network of cracks (block type) has different orientations associated to different branches. There is no specified range for its orientation.

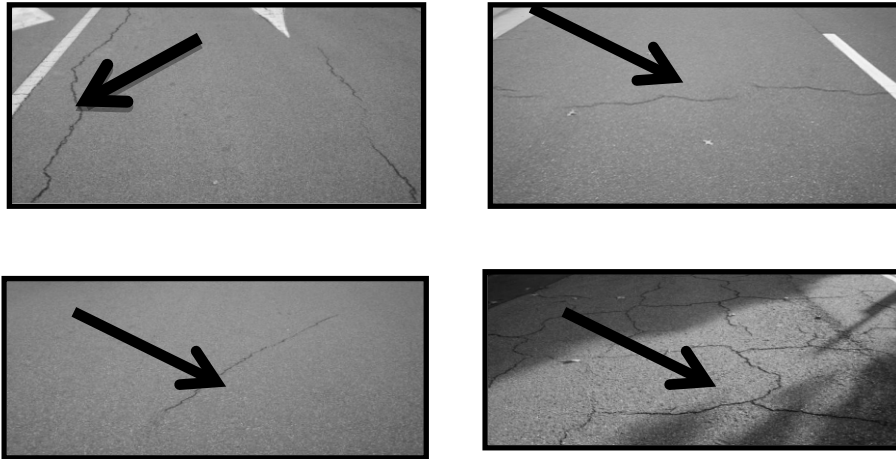


Figure 4.8: Types of cracking; 1<sup>st</sup> line: vertical individual cracks (left), Horizontal individual cracks (right); 2<sup>nd</sup> line: Transverse individual cracks (left), Network of cracks (Block type) (right) (YING/SALARI 2009).

Consequently, the algorithm for the determination of the number of branches is not explained in more detail by YING /SALARI (2009). Therefore, this study develops an algorithm for counting the number of block crack branches within an image as follows:

**Preparing Stage:** Statistical analysis is performed for most of the block crack images to determine the range of block crack branch area lengths and the range of block crack branch area widths. These numbers are considered to meet the requirements for generating the rectangle binary mask shape for (ii), the latter step. In this thesis, the results of the statistical analysis over most of the block crack branches are as follows: (1) the range of block crack branch area lengths is between 0.3 to 0.6 m on the ground, which equals 250-500 pixels on the image. (2) The range of block crack branch area widths is between 0.07 to 0.1 m on the ground, which equals 58-83 pixels on the image. This stage is done just once for most of the block crack images in one case study. The results of the statistical analysis are used as pre-defined conditional statement values in all case studies of this thesis.

The overall modified algorithm is introduced as follows:

- (i) If the resultant image, after applying the modified binary mask algorithm, has one ellipse region only, there are no branches and the algorithm should proceed to step (v) directly. Otherwise, if the answer is false, go to step (ii).
- (ii) Define the rectangular binary mask based on the pre-defined conditional statement values mentioned above in the preparing stage.
- (iii) Check each ellipse region inside of the image by moving the rectangular binary mask over it. If the rectangular binary mask fits with the ellipse shape, the ellipse shape is considered a block crack branch and one should go to step (iv) directly. Otherwise, it is considered to be a main crack and the algorithm should go to step (v) directly. This step must be repeated until the entire ellipse shapes inside the image are completed (Figure 4.9).
- (iv) Check if there is at least one branch in the image. The algorithm will count the total number of branches inside the images and classify them together as a network of cracks (block type), irrespective of the angles of the cracks. The classification procedure will now be completed. The algorithm will compute the area of the block cracks automatically by summation of the areas for all of the block branches inside of the image.

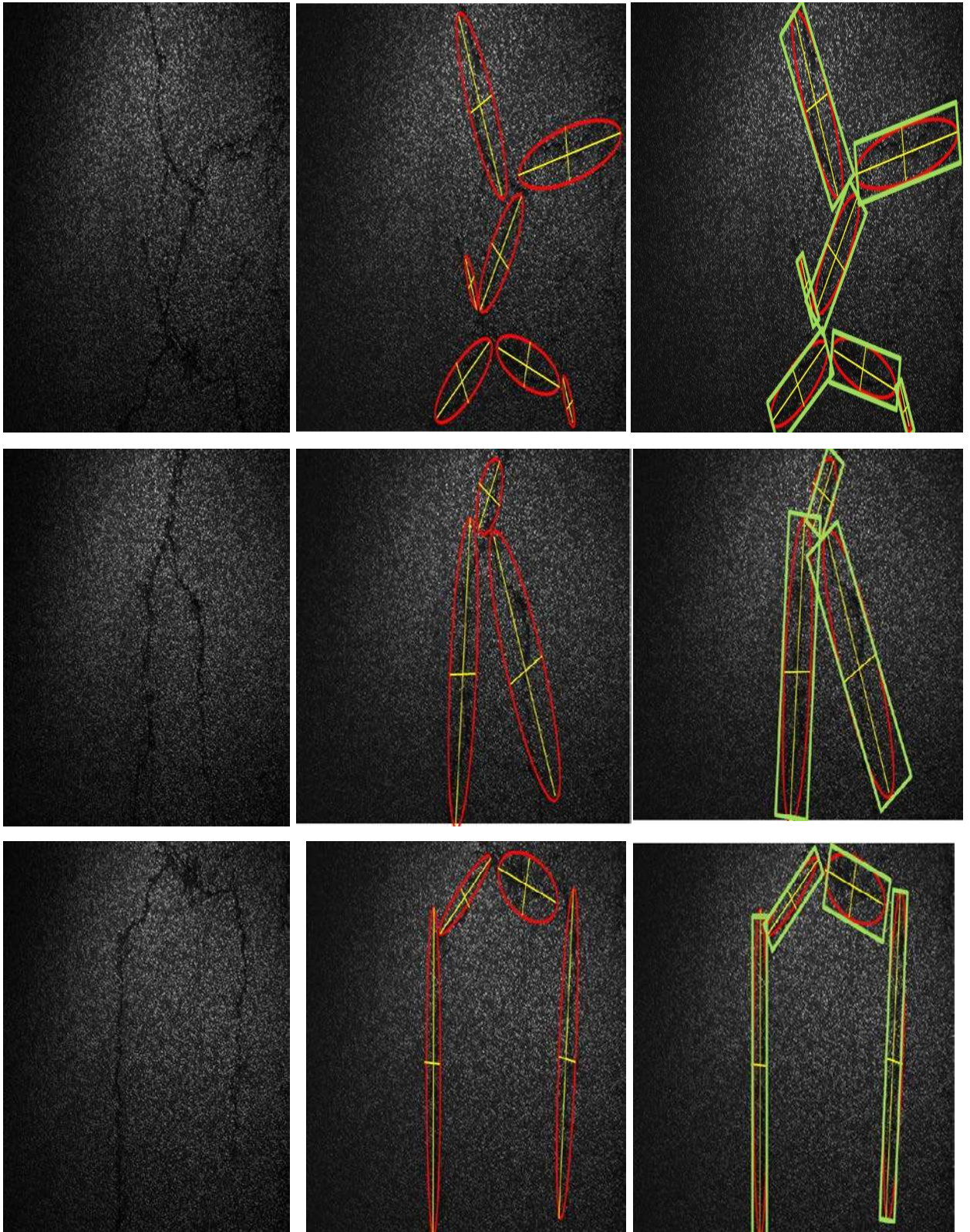


Figure 4.9: The modified algorithm for classification procedure; 1<sup>st</sup>line: first example of block crack shape with seven branches; 2<sup>nd</sup>line: second example of another block crack shape with three branches; 3<sup>rd</sup>line: third example of another block crack shape with four branches. (Note: green rectangle means that the rectangle binary mask determines the block crack branch).

- (v) If there are main cracks in the image, the cracks are classified as follows:
- If the orientation angle  $\Omega \geq 60^\circ$ , the crack is classified as a vertical individual crack.
  - If the orientation angle  $\Omega \leq 30^\circ$ , the crack is classified as a horizontal individual crack.
  - If the orientation angle  $60^\circ > \Omega > 30^\circ$ , the crack is classified as a transverse individual crack. The previously described overall modified classification method is summarized as shown in Figure (4.10).

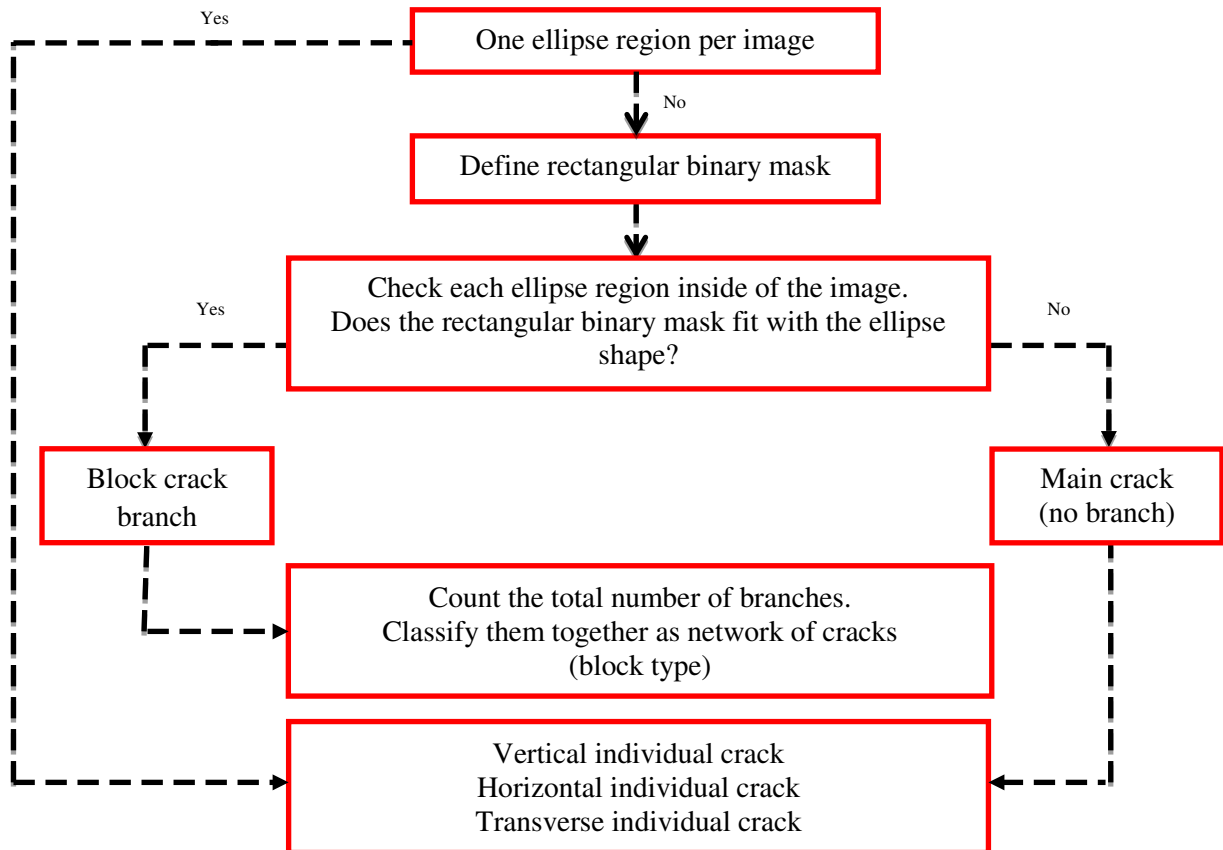


Figure 4.10: Workflow of the modified algorithm to count the number of block crack branches within the image and classify the cracks into different types during the detection stage.

Inspired by the positive results of using the modified classification algorithm (Figure 4.9), the latter figure shows that the modified algorithm can determine the block crack branches (marked by a green rectangular binary mask) accurately, despite of its different irregular shapes. This represents a key role to control the classification method. When the rectangle mask fits with the ellipse shape geometrically, the ellipse shape will be considered as a branch, automatically. Moreover, one branch is enough to classify cracks as a network of cracks (block type) without taking orientation into consideration. Otherwise, if the image contains just one ellipse, the block cracks will be excluded as unqualified. At that time, the orientation angle only is the main factor to classify cracks as either vertical individual cracks, horizontal individual cracks, or transverse individual cracks. This assumption is based on the fact that the block crack type must comprise different connected components (branches) with different intensities, colours, and orientations due to their irregular shapes. It is impossible to find block cracks that contain just one connected component (one branch equals one ellipse).



## 4.4 Experimental Results

To obtain the results, the algorithm of this thesis for crack extraction and classification was applied to the dataset of pavement images of different streets in Germany. The image (Figure 4.11) has the same characteristics as described previously in Chapter 3, section 3.1.2. In the following, a visualization of the crack extraction and classification steps is shown.

### Contouring Algorithm

The algorithm of this thesis successfully printed all of the probable crack locations automatically in the original image. This projection, for all coloured equivalence classes (probably crack regions), on the original image is done by the contouring algorithm. This algorithm is essential for the flow of the binary mask detection algorithm (Figure 4.11).

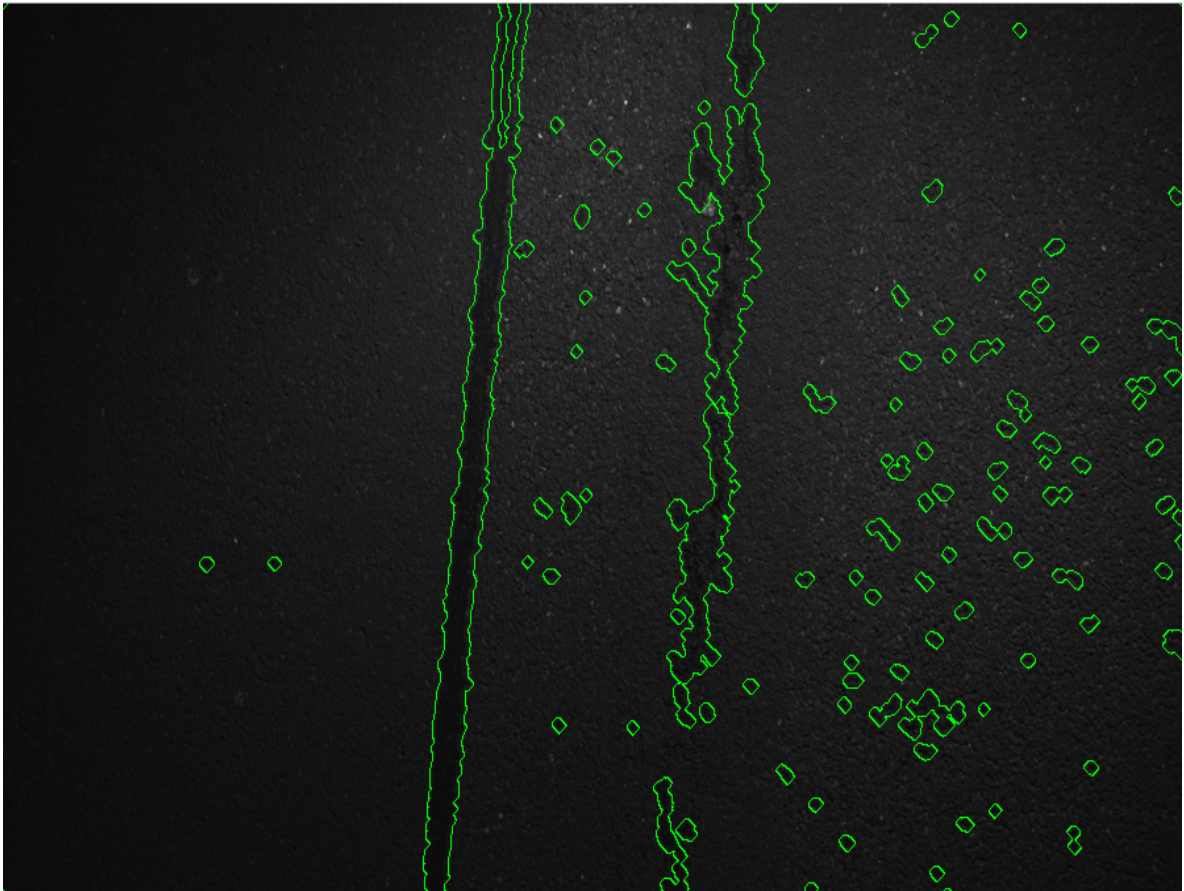


Figure 4.11: Results for applying the contouring algorithm.

### Binary Mask Detection Algorithm

The contouring algorithm image can be used as an input for the binary mask detection algorithm. The modified binary mask detection algorithm can generate a binary ellipse mask around the crack regions only, and ignore any other regions (noise). Moreover, this algorithm can extract crack characteristics, such as the crack area length, the crack area width, the crack area orientation, and the area of the crack regions, automatically. Figure 4.12 shows that the binary ellipse mask fits correctly around the crack region area, due to the accurately modified algorithm. Moreover, all of the noise regions (in green) are eliminated automatically, as presented in Figure 4.13 below. This algorithm is essential for the flow of the classification steps (AL-MISTAREHI/SCHWIEGER 2015).

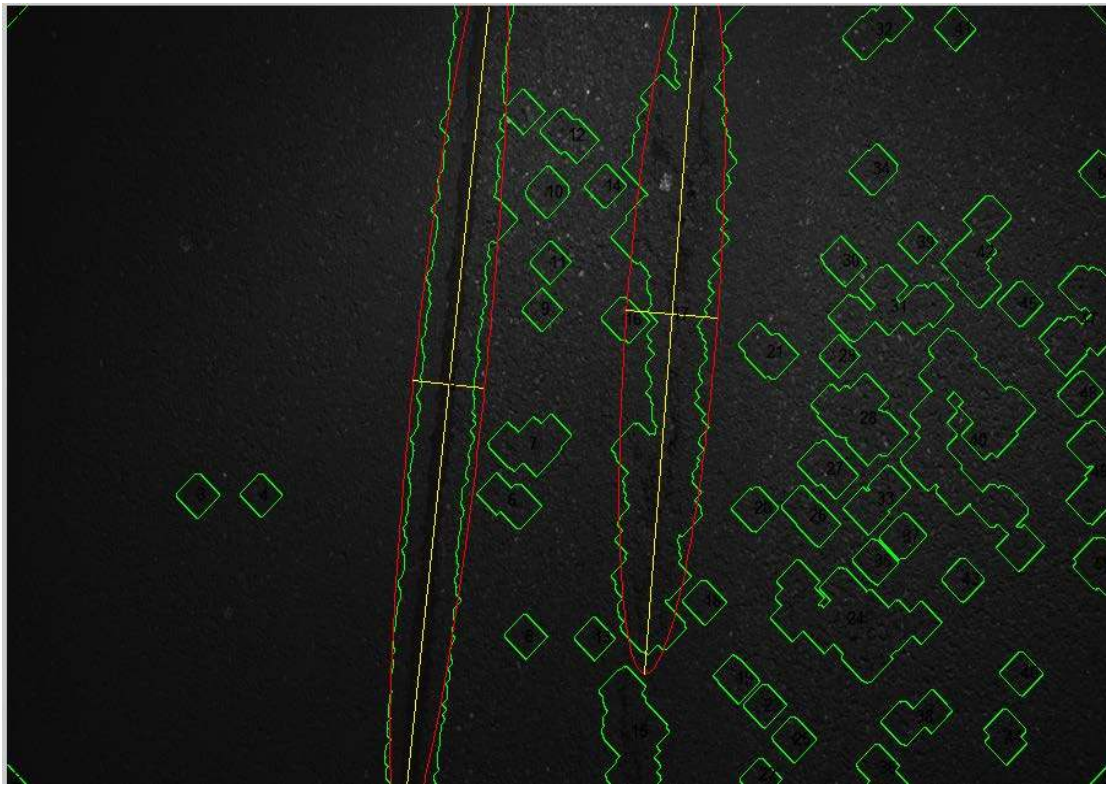


Figure 4.12: Final binary ellipse mask around the correctly detected crack regions, only during the detection stage. (Note: The green colour in the image means that there is a probability of cracks due to the texture of the street, and the ellipse shape is the correctly detected crack regions).

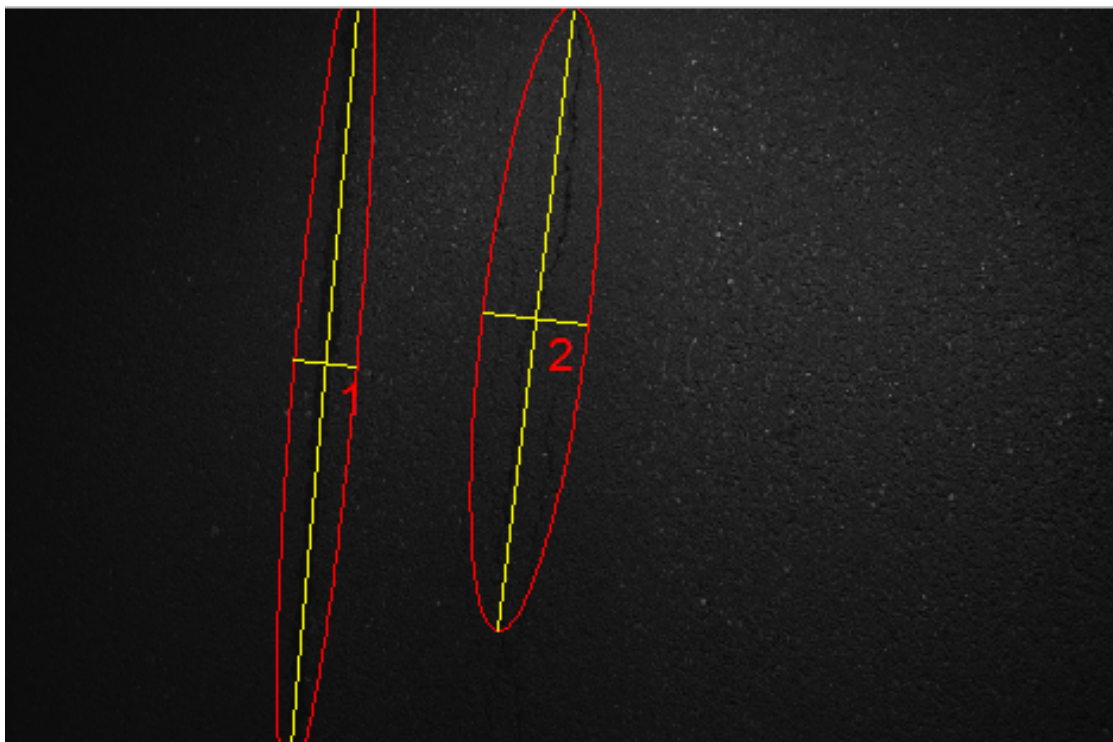


Figure 4.13: Final binary ellipse mask around the correctly detected crack regions, only after elimination of all of the noise regions.

## Classification Algorithm

Once the crack images are determined by the modified binary mask algorithm, the modified classification method can be easily applied using the stored crack orientation characteristics in the regions' properties. Moreover, the modified classification algorithm can determine whether or not the cracks have branches. Depending on the existence of the crack branches and crack orientations, a decision can be made to classify cracks automatically. Figure (4.14) shows an example of vertical individual cracks with their characteristics and severity levels. Furthermore, (Figure 4.15) demonstrates that the overall algorithm can generate a group of ellipse masks in the block crack type region. The area affected by the block cracks is measured by summing-up the areas for all the ellipses inside of the block crack region, automatically. This will help for further improvement, maintenance, and rehabilitation, such as patching, for all block crack regions (AL-MISTAREHI/SCHWIEGER 2015).

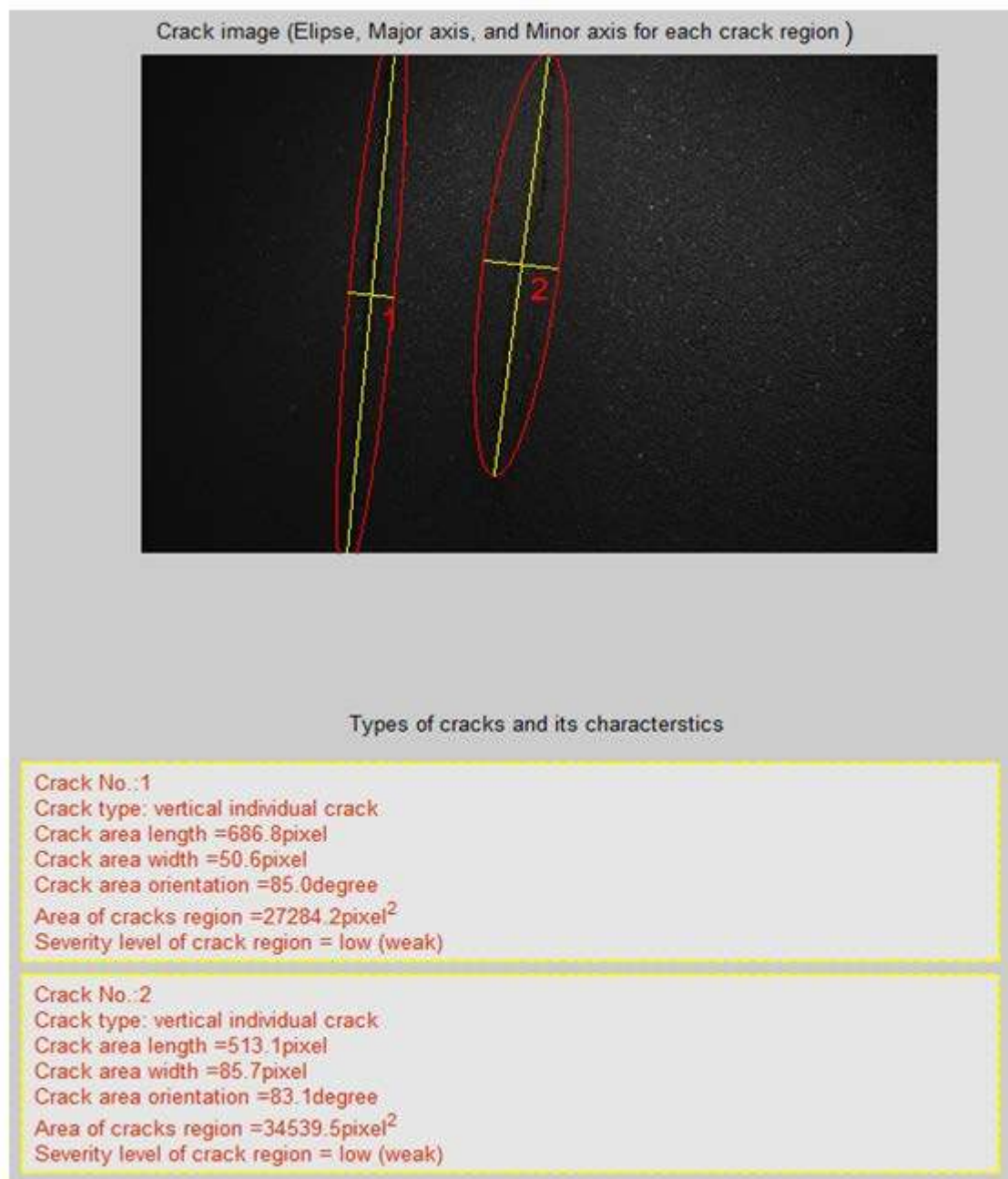


Figure 4.14: Final resultant image with vertical individual cracks and their characteristics.

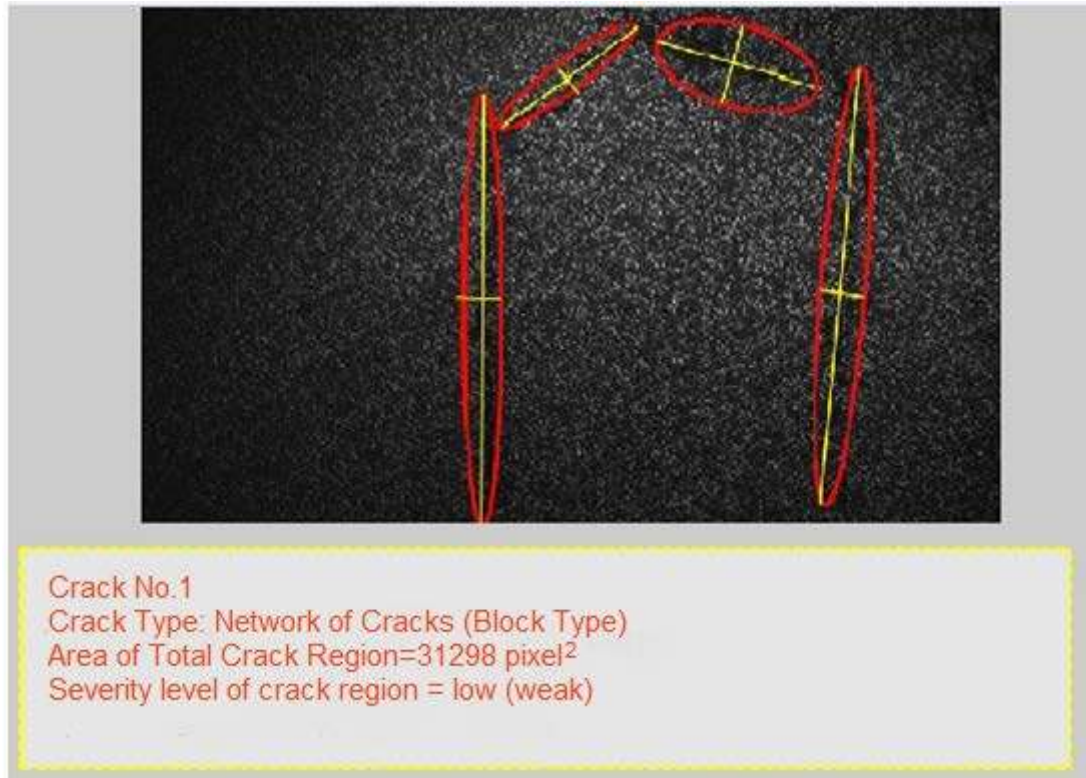


Figure 4.15: Final resultant image with network of cracks (block type) and their characteristics.

For example, (Figure 4.14) contains two cracks: (1) one vertical individual crack with a crack area length equals 686.8 pixel (0.82 m), crack area width equals 50.6 pixel (0.06 m), crack area orientation equals  $85.0^\circ$ , area of crack region equals 27284.2 pixel<sup>2</sup> (0.04 m<sup>2</sup>) and severity level of cracks region is low; (2) vertical individual cracks with crack area length equals 513.1 pixel (0.62 m), crack area width equals 85.7 pixel (0.10 m), crack area orientation equals  $83.1^\circ$ , area of crack region equals 34539.5 pixel<sup>2</sup> (0.05 m<sup>2</sup>), and severity level of cracks region is low (weak). The algorithm provides a good estimation of crack properties. This will be important for further maintenance.

As another example, (Figure 4.15) contains a network of cracks (block crack). The area of the total crack region equals 31298 pixel<sup>2</sup> (0.05 m<sup>2</sup>) and the severity level of crack region is low (weak). This will contribute to further improvements, maintenance, and rehabilitation, such as patching, for all block crack regions (AL-MISTAREHI/SCHWIEGER 2015). The decision for a network of cracks (block crack) is taken for this image because the rectangular binary mask fits with the ellipse shape (based on Figures 4.9 and 4.10, respectively).

## 5 Discussion of the Algorithm

### 5.1 Advantages of the Total Approach

This total approach is intended for combining and modifying various aspects of several individual techniques. Therefore, the major attempted refinements of this thesis's approach, regarding the four stages described in chapters 3 and 4, are introduced as follows:

#### Advantage 1: Ignoring linear extrinsic objects

Distinguishing between cracks and other linear extrinsic objects is still a problematic issue in the research community. Although several approaches have been developed and presented, these approaches are still unable to separate between cracks and other linear extrinsic objects. The linear extrinsic objects have some general characteristics. One of the most general characteristics is the linear geometrical shape. This common characteristic is shared between crack shapes and other linear extrinsic objects. Lane markings with different shapes, tire marks, paint, skid markings, railway tracks, sidewalks (curbs), and line stripping are considered to be the most popular examples of linear extrinsic objects.

The following explanation interprets how the algorithm behaves in order to separate linear extrinsic objects from cracks. The defined reasons for this advantage in the algorithm depend on the preparing stages before the cracks' detection stage. This explanation is summarized as follows:

- a. Change pixel intensities of the linear extrinsic objects to become background pixel intensities. This is done using a robust modified local adaptive (dynamic) thresholding algorithm. This modified algorithm takes into consideration the suitable window size  $ws$  and a correct constant  $c$ . The correct selection of these two values ( $ws$ ,  $c$ ) achieves a better result. These better results are visualized by using a white colour for all linear extrinsic objects, as a part of the background pixels. Furthermore, the intensity values of these linear extrinsic objects are changed to become similar to the background pixel intensity.
- b. Distort the linear extrinsic objects' geometrical shape by losing their linear geometrical properties. In other words, the linear extrinsic objects will lose any common denominator, such as linear geometrical shape or intensity values with the cracks' properties. The defined reason for this action in the algorithm depends on applying the hole pixel initial algorithm, accompanied by the dilation process, and the labelling connected components algorithm. This hole pixel initial algorithm and dilation process will enlarge the linear extrinsic objects to the maximum extent. Furthermore, it will distort their geometrical shapes by losing their geometrical linear properties. Every linear extrinsic object will have a different colour due to different intensity values. Finally, when the modified binary mask detection algorithm is moved over the connected component regions, the ellipse will not be drawn. This is because there are no cracks in the image, as shown in Figures (5.1 and 5.2), Appendix (B), Figure B.1, Figure B.2 and Figure B.8, respectively.

#### Advantage 2: Successful treatment of noisy pavement surfaces and lighting condition changes

This advantage focuses on the effect of lighting conditions and the texture of the pavement on the crack detection process. Crack identification within different noisy pavement textures is considered to be one of the most important drawbacks in several researches. Noisy pavement surfaces are defined as a change in pavement textures (low, moderate, and high). Lighting condition changes include shadows from road traffic, people, trees, reflectivity of paving materials, inter-reflected light, and different illumination conditions (low, moderate, and high).

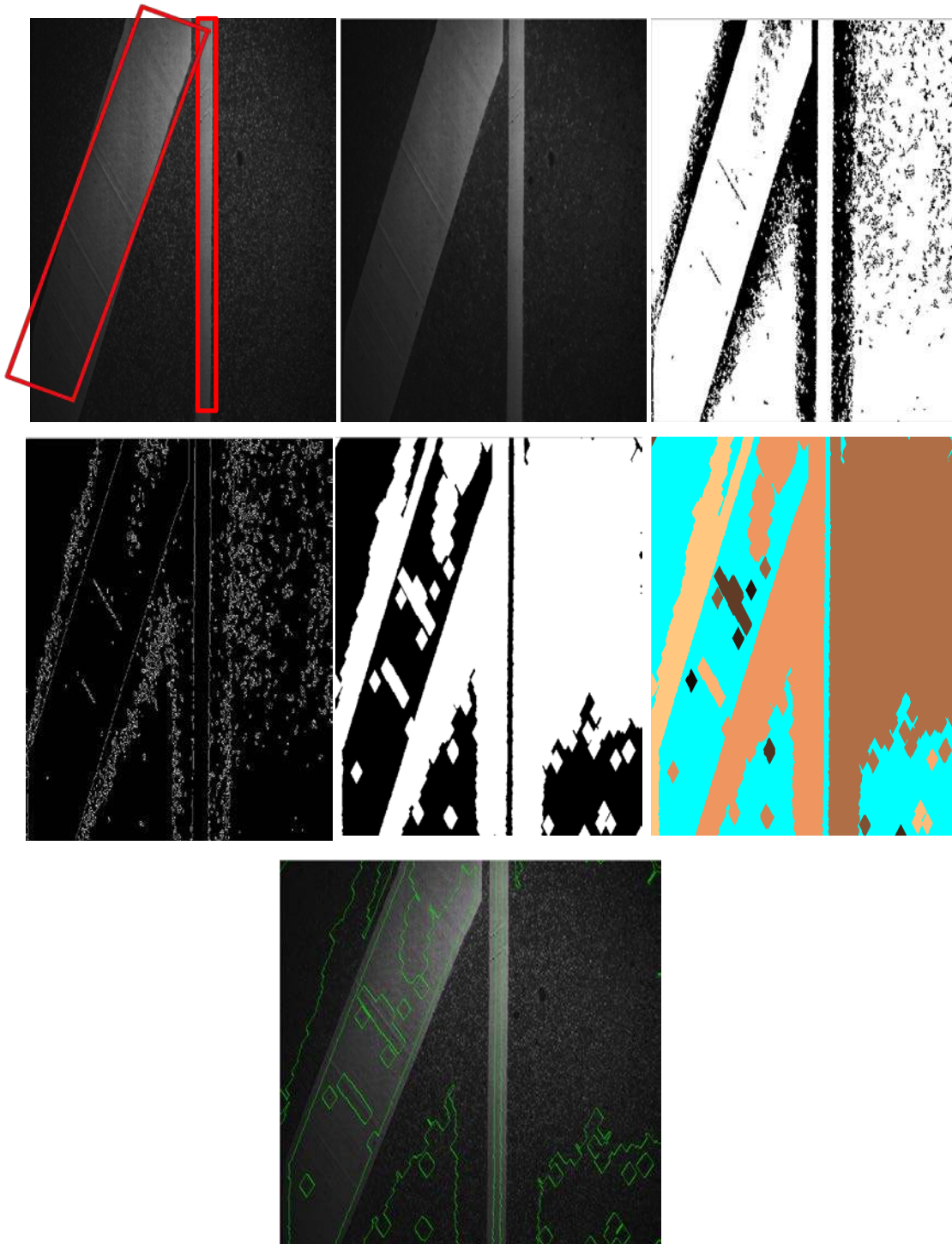


Figure 5.1: Behaviour of all of the overall algorithms to ignore lane markings within an image; 1<sup>st</sup> line: original image; image after applying the image enhancement stage (middle), image after applying the adaptive local threshold algorithm (right); 2<sup>nd</sup> line: image after applying the Sobel Edge Detector (left), image after applying the hole pixel initial algorithm, including several phases of the dilation process (middle), image after applying the labelling connected components algorithm (right); 3<sup>rd</sup> line: the final contouring image without an ellipse.

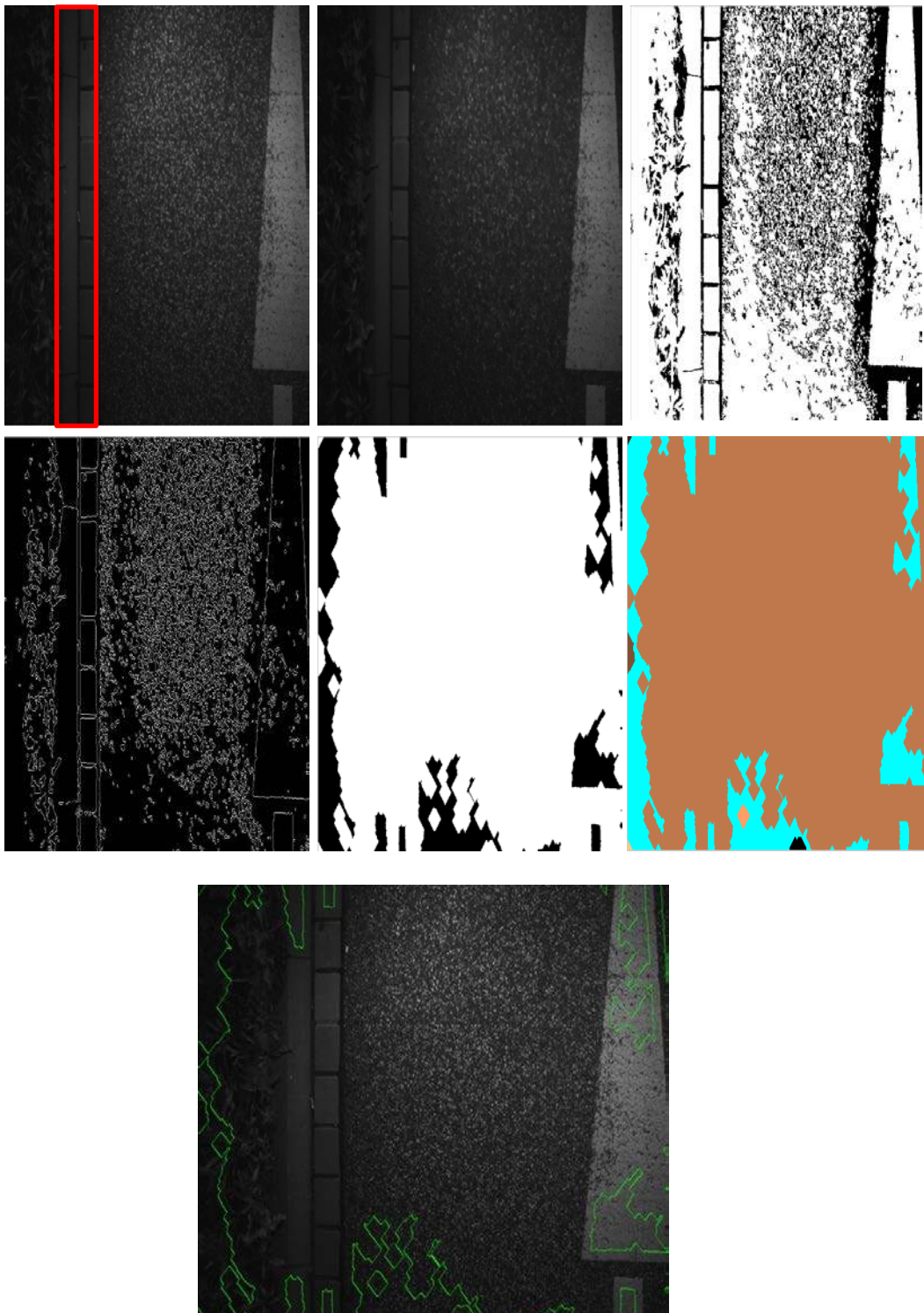


Figure 5.2: Behaviour of all of the overall algorithms to ignore sidewalks within an image; 1<sup>st</sup> line: original image (left), image after applying image enhancement (middle), image after applying the adaptive local threshold algorithm (right); 2<sup>nd</sup> line: image after applying the Sobel Edge Detector (left), image after applying the hole pixel initial algorithm, including several stages of the dilation process (middle), image after applying the labelling connected components algorithm (right); 3<sup>rd</sup> line: the final contouring image without an ellipse.

The defined reasons for this advantage in the algorithm depend on the following:

- a. A combination between different morphological operations during the pre-processing stage. This combination smoothes the image and reduces the jumps (peaks) of pixel intensities. This will reduce shadows, reflectivity of paving materials, and illumination effects.
- b. A kind of binarization is implemented during the thresholding stage. To some extent, shadows, reflectivity, and illumination effects will be omitted as a black pixel (background region) due to good binarization. Noise problems due to the different pavement textures are reduced. Good binarization is represented by applying the Sobel Edge Detector. The Sobel Edge Detector plays a critical role in extracting the outer edges of the crack in a white colour. Most of the noisy regions, due to the lighting and pavement texture changes, are filled with a black colour as a background.

Thus, the algorithm of this thesis provides a good solution for noisy pavement surfaces (low, medium, and high), lighting conditions, and shadows, as shown in Appendix (B) Figure B.5 and Chapter 6, section (6.4.4) (Figure 6.15 as an example of noisy high pavement texture) and section (6.4.2) (Figure 6.10 as an example of noisy moderate pavement texture, and Figure 6.9 as an example of noisy low pavement texture).

### **Advantage 3: Ignoring nonlinear extrinsic objects**

Differentiation between cracks and other nonlinear extrinsic objects is considered a difficult task in transportation research. Nonlinear extrinsic objects include manhole covers, signs on the ground, lighting columns, water pipelines, traffic loops, and bicycles. These nonlinear extrinsic objects have irregular and different shapes. They are considered a part of the noise problem. This advantage concentrates on the ability of the algorithm to ignore these nonlinear objects, even with their irregular and different shapes.

The defined reasons for this advantage in the algorithm depend on the following:

- a. The outer edges of these nonlinear extrinsic objects are extracted in a white colour by applying the Sobel Edge Detector. The Sobel Edge Detector paves the way to apply several post-processing steps.
- b. The hole pixel initial algorithm, accompanied by several phases of the dilation process as a filtering step, will attempt to fill all of the holes inside of the nonlinear extrinsic objects. This is done to cause its irregular geometrical shape to become larger. The labelling connected components algorithm is utilized to display different intensity values with different colours. Finally, the binary ellipse mask will not be generated for any of the nonlinear extrinsic object regions, as shown in Appendix (B) Figure B.4.

## **5.2 Disadvantages of the Total Approach**

The algorithm of this study demonstrates its ability to successfully detect and classify cracks for sequence images. However, this algorithm can be prone to failure in one situation only, as follows:

### **Problem: Oil spots on the ground**

Oil spots on the ground are considered as one part of the noise problem in pavement images. This is caused by some pits and holes in the pavement surface. These pavement holes can collect oil and other debris. By analysing these oil spot regions, the study concludes the following: (i) the brightness levels (intensity values) and the colour of the oil spot pixel regions are similar to the crack pixel regions, (Figure 5.3); and (ii) the geometric size and shape of the oil spot regions is the same as the geometric size and shape of narrow, small cracks.



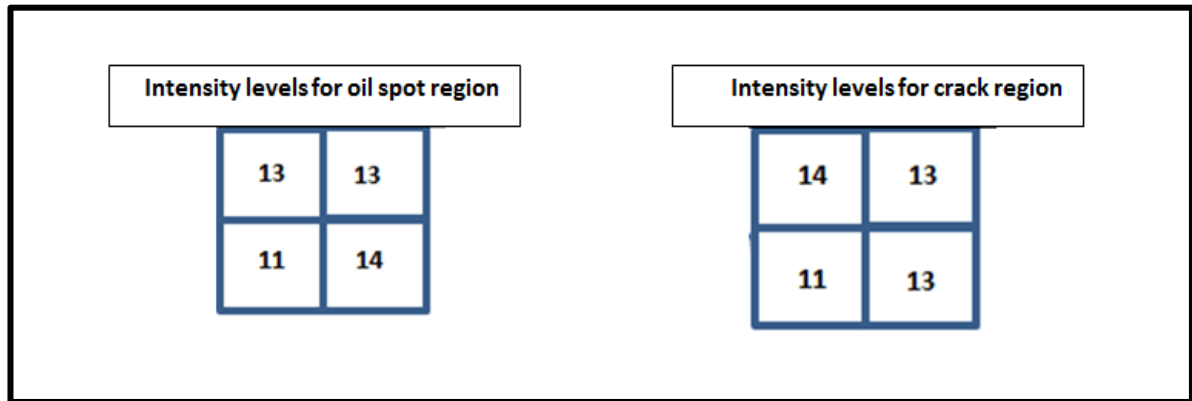


Figure 5.3: Comparison between brightness levels (intensities values) and the colour of oil spot pixel regions (left) and crack pixel regions (right).

The defined reasons for this disadvantage in the algorithm depend on the following explanation:

- a. The modified local adaptive (dynamic) thresholding algorithm gives a black colour for these oil spot regions, as part of the foreground pixels. Moreover, the thresholding algorithm cannot exclude oil spot pixels from the ranks of the foreground pixels. Therefore, if this process is completed, the small narrow cracks with the same brightness level and geometric size as the oil spots will be deleted. Consequently, the best decision is to keep these oil spot regions in the resultant image, after applying thresholding stage.
- b. The hole pixel initial algorithm and several phases of the dilation process will extend the oil spot regions and deform their geometric shapes. Every oil spot region will take a different colour during the labelling connected components step due to different intensity values. In conclusion, the deformation of the oil spots' geometric shapes will help to delete some oil spot regions. Nevertheless, the ellipse shape will be still drawn around each narrow, small oil spot region. This means that the geometric size and shape of the oil spot regions is still similar to the geometric size and shape of narrow, small cracks, even after the distortion during the post-processing stage.

This study concludes that the algorithm can be prone to failure in the case of oil spot existence on the pavement, due to the above mentioned reasons, as shown in Appendix (B) Figure B.3, Figure B.9, Figure B.10 and Figure B.11, respectively, and Chapter 6, section (6.4.1) (Figure 6.8) as different examples of false detection due to oil spots on the ground. This type of error is considered to be an error of the second type (based on Chapter 6, section 6.3).

## 6 Case Studies on Crack Extraction and Classification

An automated extraction and classification system for pavement cracks based on the level of severity and other distinguishing characteristics is an invaluable resource; facilitating our scientific understanding of pavement cracks for new research and development endeavours. An automated crack extraction and classification system is a more efficient and effective means of providing information about specific attributes of pavement cracks compared to the available manual system. In addition, an automated system serves as an accurate mean by which pavement evaluation, performance measurement, maintenance, rehabilitation, and road reconstruction issues can be determined (SHAHIN 2002). Furthermore, the automated records and archived crack measurements can be used to solve future pavement problems by searching through the automated digital images obtained from a variety of locations and environments. Therefore, a common digital technology should be used for the automated processing and analysis of images of cracked pavement in order to make them readily available to the public. There are three main advantages of automatic digital archiving of pavement cracks: 1) the precise location of a pavement crack can be identified; 2) it provides an opportunity for reconstruction using the correct maintenance procedures without the risks associated with manual surveying methods; and 3) it shares the knowledge of crack characteristics with the public in order to identify critical areas for future research.

Throughout this chapter, the results of automatic fusion will be highlighted, as well as combinations and modifications of digital image processing techniques for crack extraction and classification recording purposes. In particular, it aims to demonstrate the efficiency of the algorithm proposed in this thesis by presenting relevant case studies, in which the combinations and modifications for the outputs of digital image processing techniques are evaluated and assessed. In addition, the results of the algorithm are compared to other algorithms that have been previously used to successfully evaluate pavement images. This chapter refers to seven case studies that use a sequence of pavement crack images as input data, and one case study containing only individual pavement images. In the following section, this thesis provides a short overview of the data acquisition, as well as a detailed description of the obtained results.

### 6.1 Data Acquisition

Seven datasets have been utilized for investigation in this thesis: 1) four observed case studies that use a sequence of pavement crack images by LEHMANN + PARTNER GmbH, Germany; 2) one observed case study using a sequence of pavement crack images by 3D Mapping Solutions GmbH, Germany; and 3) two observed case studies of individual and sequenced pavement crack images provided by Unicom-Umap Company, Saudi Arabia. The data collection in the first four observed case studies was executed by LEHMANN + PARTNER GmbH, Germany, using a S.T.I.E.R. mobile mapping system. The primary goal of this work is to automatically extract and classify pavement cracks to create archiving datasets of comprehensive crack characteristics for an entire surveying site. (Note: S.T.I.E.R is not an abbreviation, it is an artificial name) (LEHMANN+PARTNER 2014).

3D Mapping Solutions GmbH in Germany has acquired data for one case study using the Mobile Strassen-Erfassungs-System (MoSES) mobile mapping system. Another case study obtained data in cooperation with the Unicom-Umap Company in Saudi Arabia. In addition, Video images, inertial navigation systems (INS), and global positioning system (GPS) satellites (VISAT™) were utilized for gathering images of either individual or sequences of pavement cracks. In addition, the dataset from Saudi Arabia is rich in diverse crack types. This work is aimed at automatically extracting and classifying cracks under a variety of conditions.

### 6.1.1 Data Acquisition System of LEHMANN + PARTNER GmbH

The sequence of pavement images (for the four case studies) observed by LEHMANN + PARTNER GmbH were obtained using the S.T.I.E.R. mobile mapping system. The S.T.I.E.R. measuring vehicle (Figure 6.1) is a system for surveying longitudinal and transverse evenness. Specifically, it measures the texture and 3D road surface and records the surface images, and is certified by the German Federal Highway Research Institute. The S.T.I.E.R. mobile mapping system stores geo-referenced digital images, with the system itself considered to be the basic unit, and combines an arbitrary number of image units. This system consists of different sensors, each with discrete specifications as follows: 1) panorama colour camera system which consists of several single cameras, tasked with taking panoramic images of the surroundings. Each of these colour cameras has a resolution with 1.44 MP. One of these cameras is arranged as a front camera; 2) macro picture cameras (surface cameras, with two in the rear) tasked with taking "nearly orthophotos of the road surface" with a very short overlap. The resolution of these surface cameras is 1920 x 1080 pixels, of which every image pixel equals 1.2 mm per ground point; 3) Fraunhofer Institute for Physical Measurement Techniques (IPM) laser scanning system, at 900 points per transverse profile. It functions to produce 3D profiles, transverse profiles, and record 3D surface images; 4) an Applanix POS LV 420 positioning system. The task for the combination of POS-LV positioning system and IPM laser scanner is to create a surface model with a grid size of up to 1 x 1 cm; and 5) the lighting unit to generate suitable lighting conditions for data collection. In this thesis, orthophoto images for the road surface (generated from surface cameras with a resolution of 1920 x 1080 pixels) are used to achieve the goals of this study. Further information regarding this system can be found in LEHMANN+PARTNER (2014).



Figure 6.1: S.T.I.E.R. mobile mapping system (LEHMANN+PARTNER 2014).

### 6.1.2 Data Acquisition System of 3D Mapping Solutions GmbH

This thesis also presents another type of pavement image (under different lighting conditions) in an attempt to improve the degree of automation. These sequences of pavement images (from one case study) were observed by 3D Mapping Solutions GmbH, using the Mobile Strassen-Erfassungssystem (MoSES). This system (Figure 6.2) integrates a cluster of digital cameras, a kinematic laser scanner, global positioning system receivers (GPS), an inertial navigation system (INS), and a distance-measuring instrument (DMI). Therefore, the system is able to collect panoramic views along roadways. The primary objective of this system is to obtain the specific information required. The detailed specifications of the Mobiles Strassen-Erfassungssystem (MoSES) are summarized as follows: 1) A single multi-camera module consists of up to four cameras. At present, MoSES is equipped with eight cameras from all types (color, grayscale, and infrared cameras), each with a different image resolution, resulting in images with different sizes. The task of this multi-camera system is to permit a complete survey of the traffic corridor; 2) two robust laser scanners for digitizing the traffic corridor and providing precise up-to-date 3D data for planning, tendering, construction work, and final inspection; 3) global positioning system receivers (GPS) for calculating geographical location by receiving information from global positioning system receivers, and an inertial navigation system (INS), for reporting velocity, orientation, and gravitational forces. In this thesis, color images of the road surface (generated from the multi-camera module, with a resolution

of 1178 x 1225 pixels) were used. Further information pertaining to this system can be found in 3D-MAPPING (2014).



Figure 6.2: MoSES mobile mapping system (3D-MAPPING 2014).

### 6.1.3 The Data Acquisition System of Unicom-Umap Company

Another type of individual and sequenced pavement image was tested using the algorithm of this study on two case studies utilizing the company Unicom-Umap and the VISAT™ mobile mapping system. These case studies represent sequences and individual images of circular pavement, as well as the King Fahd Expressway in Saudi Arabia. These images were obtained from a group of digital cameras, global positioning system receivers (GPS), and an inertial navigation system (INS), that were affixed to the Unicom-Umap Company vehicle (Figure 6.3). The specifications of the VISAT™ mobile mapping system of Unicom-Umap Company are as follows: 1) 6 to 12 cameras, with a resolution of 2058 x 2456 pixels. The primary task is to capture images of the traffic corridor; and 2) an integrated global positioning system receivers (GPS) and inertial navigation systems (INS), for generating a continuous stream of data on position and orientation. For the purpose of this thesis, color images of the traffic lane generated from the multi-camera system with a resolution of 2058 x 2456 pixels were used. Further information pertaining to this system can be found at UNICOM-UMAP (2014).



Figure 6.3: Unicom-Umap mobile mapping moving vehicle (UNICOM-UMAP 2014).

## 6.2 General Image Characteristics of the Case Studies

The algorithm for this study requires the following characteristics for its verification:

- (a) Noisy pavement surfaces (change in pavement textures: low, moderate, and high),

- (b) Distinctive types of cracking (vertical individual cracks, horizontal individual cracks, transverse individual cracks, and network of cracks (block type)),
- (c) Various linear extrinsic objects, such as lane marking with different shapes, tire marks, paint, skid markings, railways trucks, sidewalks (curbs), and line stripping,
- (d) Assorted nonlinear extrinsic objects, such as manhole covers, signs on the ground, lighting columns, water pipelines, traffic loops, and bicycles,
- (e) Oil spots on the ground,
- (f) Changes in lighting, such as shadows, shade from road traffic, persons, trees, and different illumination conditions (low, moderate, and high).

Table 6.1: General image characteristics of the case studies

Case Study No.	Source of Images	Noisy Pavement Surface	Characteristics				
			Crack Type	Linear Extrinsic Objects	Nonlinear Extrinsic Objects	Oil Spot on the Ground	Changes in Lighting Conditions
1	LEHMANN + PARTNER GmbH	Moderate pavement texture	Individual vertical, horizontal and transverse cracks	Yes	No	Yes	Low
2	LEHMANN + PARTNER GmbH	Mixture between moderate and low pavement texture	Individual vertical cracks	Yes	No	Yes	Low
3	LEHMANN + PARTNER GmbH	Mixture between high and low pavement texture	No cracks existing	Yes	Yes	Yes	Moderate
4	LEHMANN + PARTNER GmbH	Mixture between high and moderate pavement texture	Individual vertical, horizontal, transverse and block cracks	Yes	No	Yes	Moderate
5	3D Mapping Solutions GmbH	Low pavement texture	No cracks existing	Yes	Yes	Yes	High
6	Unicom-Umap	High pavement texture	Block cracks	No	No	Yes	Low
7	Unicom-Umap	Mixture between low, high, and moderate pavement texture	No cracks existing	Yes	Yes	Yes	High

Several different case studies of pavement images are required to test the algorithm presented in this thesis. Therefore, seven case studies with various pavement images from different countries were chosen in order to demonstrate the generality, efficiency, and the automation degree for the entire algorithm. Furthermore, the only means of creating a superior algorithm for crack detection and classification is by testing it on extensive sections of actual pavement (HEROLD ET AL. 2008). Thus, these seven case studies were chosen to evaluate the behaviour of the algorithm under the conditions (a) to (f) in Table 6.1 above.

### 6.3 Evaluation Criteria

The algorithm of this thesis needs a quality model for its evaluation. The quality concept is defined as the degree to which a set of inherent characteristics fulfils requirements (DIN EN ISO 9000 2005). In turn, a characteristic is defined as a distinguishable feature and it can generally be stated that quality is the fulfilment of requirements of data or processes. A quality model is defined as a part of the quality concept that contains a fixed set of inherent quality characteristics and variable quality parameters to describe the quality of information.

In general, a quality model should fulfill the following requirements. A fixed set of inherent quality characteristics is used to describe the quality of a phenomenon. It is essential to use the same quality characteristics throughout the process to obtain a uniform quality description. Concretization of the quality characteristics is effected by means of variable quality parameters. The quality parameters are needed to obtain flexibility for the description of heterogeneous data types. Each quality parameter is filled with a numerical value. On the one side it is the recent actual value that may be measured or obtained in another way. On the other side a target value has to be given for the respective parameter. The required quality is achieved, if the actual (measured) value fulfils the requirement (the target value) (SCHWIEGER ET AL. 2010). A general description of the terms quality characteristic and quality parameter is given as follows (SCHWEITZER/SCHWIEGER 2011):

- Quality characteristic: an inherent characteristic of a data or process, related to a requirements. The quality characteristics form the first hierarchy level. Each characteristic may be described by a number of sub-characteristics or parameters. A sub-characteristic has the same attributes as a characteristic. It forms the second hierarchy level.
- Quality parameters: the parameters substantiate the characteristics. Each parameter may be quantified with a specific (measured) value. Additional required quality values are defined on the parameter level.

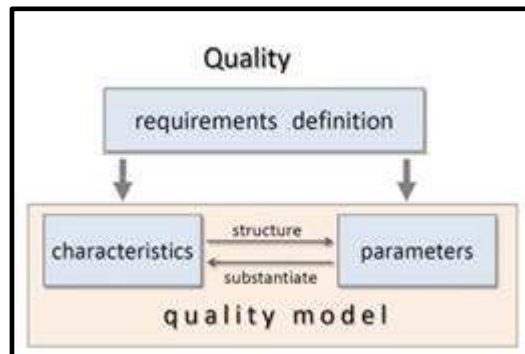


Figure 6.4: Definition of a quality model (SCHWEITZER/ SCHWIEGER 2011).

Figure 6.4 represents the relationship between characteristics and parameters, and the term quality is presented in conjunction with a quality model. The conclusion from this figure is that the characteristics and parameters are derivable from the requirements definition. Furthermore, the relationship between the characteristics and parameters is shown in a general way. The parameters substantiate the characteristics and the characteristics structure the parameters. There are different available quality models with respect to different fields. In the field of geodesy, quality is generally determined for measurements and evaluations based on these measurements. Most quality characteristics and parameters are related to accuracy; additional reliability and sensitivity parameters as product-related quality characteristics (geodetic nets) (SCHWIEGER ET AL. 2010) exist. In the geo-data as well as in the traffic telematics field, according to (WILTSCHKO/KAUFMANN 2005), the quality characteristics include availability, up-to-dateness, completeness, consistency, correctness and ac-

curacy. In civil engineering domain, quality is mainly defined and described by tolerances that are quality parameters for the quality characteristic “accuracy”. These tolerances are defined within norms, standards and general recognized codes of practice. E.g. in Germany more than 4000 DIN<sup>1</sup> standards are used in the construction of buildings. Despite the high number of accuracy parameters, no concluded quality model exists (SCHWIEGER ET AL. 2010).

The developed quality model of this thesis not only evaluates and judges the quality of the data but also optimizes the quality of the algorithm workflow (process). Therefore, the quality model of this thesis will distinguish between the quality of the process and the quality of the product. The following Figure 6.5 presents the structure of the quality model for the crack detection and classification.

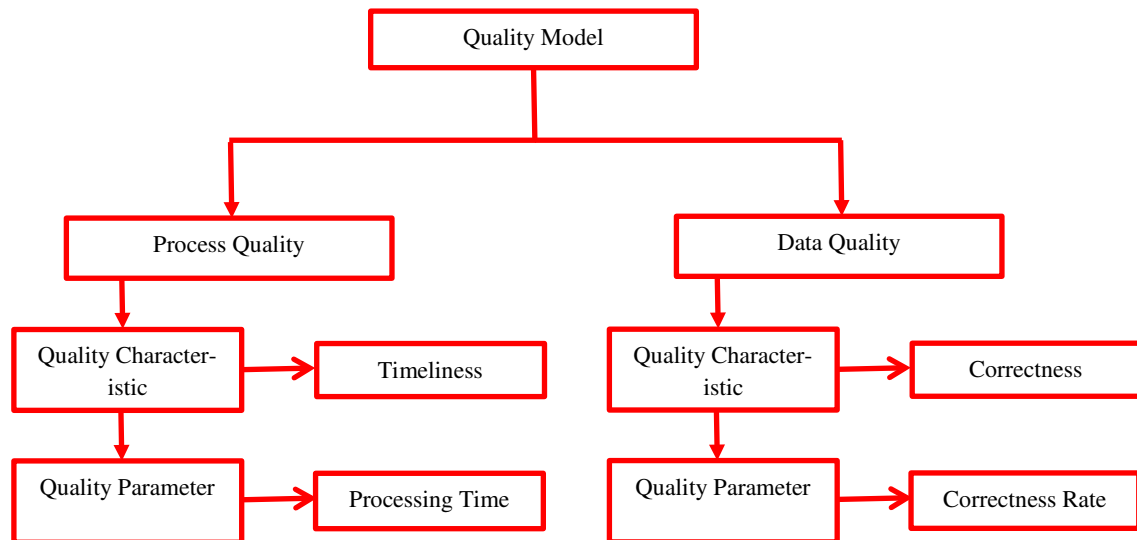


Figure 6.5: Structure of the quality model for the detection and classification of cracks.

**Data quality** in general is defined as the quality of incoming data (input), but in the case of this application, it is defined as the quality of outgoing results (output or product quality). **Product related quality characteristics** include among others correctness. The correctness is defined as degree of adherence of existence of information (feature(s), attributes, functions, relationships) to corresponding elements of the reality (WILTSCHKO/KAUFMANN 2005). This is judged by method of a statistical/hypothesis test.

**Statistical/Hypothesis Tests (General theory):** Two hypotheses are discussed in many hypothesis-testing problems. The first hypothesis is called the null hypothesis  $H_0$ . The second hypothesis is called the alternative hypothesis  $H_A$ . If the null hypothesis  $H_0$  is false, then the alternative hypothesis  $H_A$  is true, and vice versa. In general, statistical hypothesis is a rule or procedure, in which a random sample of  $y$  is used for deciding whether to reject or not reject null hypothesis  $H_0$ . A test of a statistical hypothesis is completely specified by the so-called critical region, which will be denoted by  $K$ . The critical region  $K$  of a test is the set of sample values of  $y$  for which  $H_0$  is to be rejected. Thus, the null hypothesis  $H_0$  is rejected if the sample value or observation of  $y$  falls in the critical region, if  $y \in K$ . Otherwise the null hypothesis  $H_0$  is accepted, if  $y \notin K$  (FÖRSTNER 1991). Two types of errors can be made:

1. Type I error (error of first type): rejection of  $H_0$  when in fact  $H_0$  is true.
  2. Type II error (error of second type): acceptance of  $H_0$  when in fact  $H_0$  is false.
- Table 6.2 shows the decision table with the type I and II errors.

<sup>1</sup>DIN: Deutsches Institut für Normung (German Institute for Standardization)

Table 6.2: Decision table with the type I error and II error (FÖRSTNER 1991)

	$H_0$ true	$H_0$ false
Reject $H_0$ $y \in K$	Wrong Type I error	Correct
Accept $H_0$ $y \notin K$	Correct	Wrong Type II error

The size of a type I error is defined as the probability that a sample value of  $y$  falls in the critical region when in fact  $H_0$  is true. This probability is denoted by  $\alpha$  and is called the level of significance. The size of the test,  $\alpha$ , can be computed once the critical region  $K$  and the probability density function of  $y$  is known under  $H_0$ . The size of a type II error is defined as the probability that a sample value of  $y$  falls outside the critical region when in fact  $H_0$  is false. This probability is denoted by  $\beta$ . The size of a type II error,  $\beta$ , can be computed once the critical region  $K$  and the probability density function of  $y$  is known under  $H_A$ . Figure 6.6 presents generally the errors types for statistical/hypothesis tests in the density distribution function (NIEMEIER 2008).

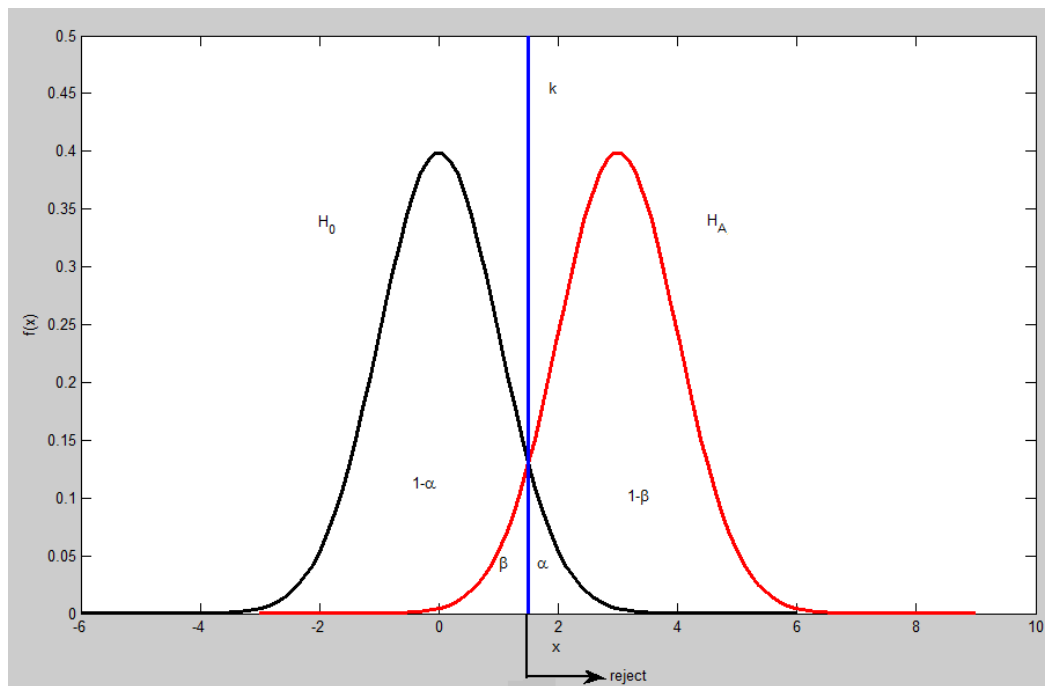


Figure 6.6: Errors types for statistical/hypothesis tests in the density distribution function.

In the case of crack detection and classification, correctness occurs in two cases as follows:

1. In reality there is no crack, and the algorithm does not detect any crack (case 1).
2. In reality there is a crack, and the real crack is detected and classified correctly by the algorithm (case 2).

Incorrectness occurs in two cases also as follows:

1. In reality there is a crack, but the algorithm can not detect it correctly; either no crack is identified or the existing crack is classified incorrectly (Type I error).
2. In reality there is no crack, but the algorithm detects crack (Type II error).



In this work, correctness and incorrectness cases are judged by using statistical/hypothesis tests (table 6.3, 6.4 and 6.5). **Product related quality parameters** include three parameters for correctness. These three parameters are the correctness rate for correct identified cracks, the correctness rate for correct identified crack types and the correctness rate for images where all cracks are classified correctly. The three parameters of correctness rates are defined and calculated using equation (6-1). Table (6.6) displays the indices for determining the correctness rates of equation (6-1).

Table 6.3: Statistical/hypothesis test for correct identified cracks  
( $H_{0_1}$ : crack is identified correctly;  $H_{A_1}$ : no crack)

	$H_{0_1}$ true	$H_{0_1}$ false $H_{A_1}$ true
Reject $H_{0_1}$ Accept $H_{A_1}$ $y \in K$	Special crack type is available $\Rightarrow$ but no crack is detected Type I error	No crack is available $\Rightarrow$ no crack is detected Correct (Case 1)
Accept $H_{0_1}$ $y \notin K$	There is a crack $\Rightarrow$ crack is detected correctly Correct (Part of Case 2)	No crack is available $\Rightarrow$ but crack is detected Type II error

Table 6.4: Statistical/hypothesis test for correct identified crack types  
( $H_{0_2}$ : crack type is identified correctly;  $H_{A_2}$ : crack type is not identified correctly)

	$H_{0_2}$ true	$H_{0_2}$ false $H_{A_2}$ true
Reject $H_{0_2}$ Accept $H_{A_2}$ $y \in K$	Crack is classified correctly $\Rightarrow$ but the examination gives a wrong result	Crack is classified incorrectly $\Rightarrow$ and it is recognized to be wrong
Accept $H_{0_2}$ $y \notin K$	There is a crack $\Rightarrow$ crack is classified correctly Correct (Part of Case 2)	The existing crack is classified incorrectly Type I error

Table 6.5: Statistical/hypothesis test for correct identified images  
( $H_{0_3}$ : image having crack is identified correctly;  $H_{A_3}$ : image having crack is not identified correctly)

	$H_{0_3}$ true	$H_{0_3}$ false $H_{A_3}$ true
Reject $H_{0_3}$ Accept $H_{A_3}$ $y \in K$	There is an image having cracks $\Rightarrow$ but it is identified as no crack image Type I error	There is no image having cracks $\Rightarrow$ and it is identified as no crack image Correct (Case 1)
Accept $H_{0_3}$ $y \notin K$	There is an image having cracks $\Rightarrow$ and it is identified as an image having cracks Correct (Part of Case 2)	There is no image having cracks $\Rightarrow$ but it is identified as a crack image Type II error

Theoretically, the complete statistical/hypothesis test should be implemented as described above in tables 6.3, 6.4 and 6.5 respectively. Actually, the first row in table 6.4 (gray colour) is not recognized by the algorithm of this thesis because it is impossible to check it automatically:

$$B_i = \left( \frac{M_i}{S_i} \cdot 100 \right), \quad (6-1)$$

where

- $B_i$  : correctness rate of the object entity (%),
- $M_i$  : number of correct identified object entities,
- $S_i$  : total number of the object entities (images, or crack type),
- $i$  : indices for determining the correctness rate ( $i=1, 2, 3, 4, 5, 6$ ).

Table 6.6: Indices for determining the correctness rate in equation (6-1)  
(Table No.\*\* represents every index belonging to a specific table)

Index (i)	Table No.**	Object	Entity
1	Table (6.3)	Cracks	Correct detected cracks in all images irrespective of type
2	Table (6.4)		Correct detected individual vertical cracks in all images
3	Table (6.4)		Correct detected individual horizontal cracks in all images
4	Table (6.4)		Correct detected individual transverse cracks in all images
5	Table (6.4)		Correct detected network of cracks (block) cracks in all images
6	Table (6.5)	Images	Correct detected images having cracks

Evaluation and judgement of the data quality is done based on the correctness quality characteristic only. The defined reason for this selection depends on the fact that the focus of this thesis is to get more correct results in crack detection and classification than previous algorithms. The correctness rate is important to show if the algorithm is able to detect and classify cracks correctly. The correctness rate will be displayed by percentage value.

**Process quality** is defined as the quality for the complete algorithm process. **Process related quality characteristics** include among other timeliness (WILTSCHKO 2004). In this work, the timeliness is defined as the time which the algorithm needs to detect and classify the cracks and its characteristics in the input images and provide the required output. It gives an indication about the algorithm effectiveness. The processing time to complete crack detection and classification is the **process related quality parameter**. It can be calculated using equation (6-2):

$$t_p = t_{end} - t_{beg} , \quad (6-2)$$

where

- $t_p$  : processing time for complete crack detection and classification [s],
- $t_{end}$  : time at the end of the algorithm process [s],
- $t_{beg}$  : time at the beginning of the algorithm process [s].

Timeliness is only selected for the evaluation and judgement of the process quality. The defined reasons for this selection depend on the goal of this thesis to detect and classify cracks for continuous mobile mapping images in a short period of time. The timeliness is the most important process quality characteristic to give an indication of the algorithm speed and effectiveness.

## 6.4 Evaluations

In the following section, a description of the obtained results and the completed evaluations is presented for seven case studies. The general image characteristics of these seven case studies are

explained in section (6.2), table (6.1). The general approach as introduced in Chapters 3 and 4 has been applied to these seven case studies. The obtained results are evaluated and judged based on the evaluation criteria described in section (6.3).

#### 6.4.1 Case Study 1: LEHMANN + PARTNER GmbH

This case study contains 96 pavement images with a length of 100 m on the street ground. Table 6.7 presents a description of the dataset for this case study. The acquired images for this case study have a moderate pavement texture. It is considered to be the main difference between this case study and the other case studies. The developed algorithm pertaining to each of the four stages was applied to this dataset with the aim of automatically extracting and classifying cracks for all images together, without human interaction. Moreover, some pavement images contained extrinsic objects, such as markings and oil spots on the ground. In situations which involve moderate pavement texture, it is challenging for the algorithm to detect cracks (marked in Figure 6.7, line 1, left) and ignore other objects at the same time.

Table 6.7: Description of the dataset for case study (1)

Category	Quality
Number of images	96 images
Number of crack images	70 images
Number of vertical crack images	60 images
Number of horizontal crack images	5 images
Number of transverse crack images	5 images
Number of network cracks (Block type)	0 images
Number of non-crack images	26 images
Length of vertical cracks for all images (m)	53.4 m
Length of horizontal cracks for all images (m)	0.5 m
Length of transverse cracks for all images (m)	5.4 m
Area of network cracks (Block type) for all images (m <sup>2</sup> )	0.0 m <sup>2</sup>

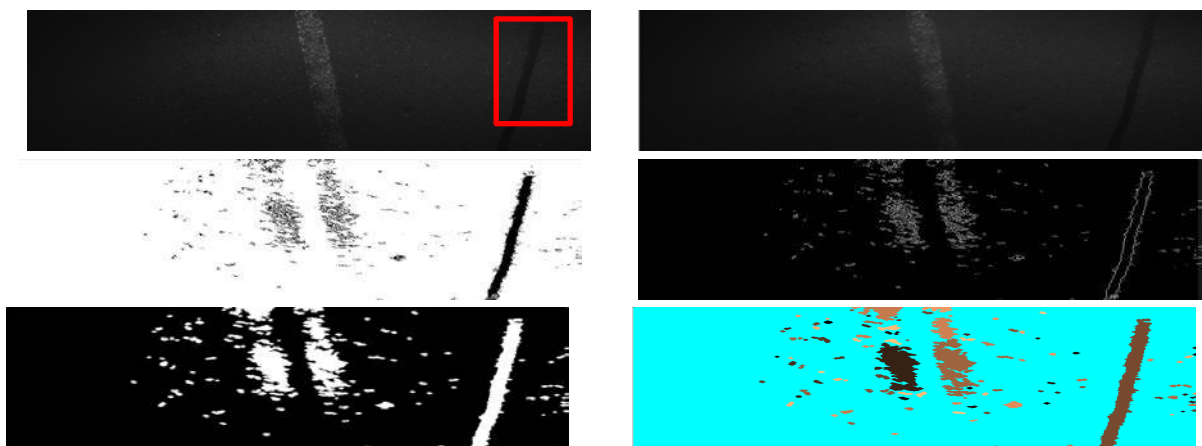


Figure 6.7: Behaviour of the algorithm for the preparation stages of crack extraction within the image: 1<sup>st</sup> line shows the original image (left), and the image after applying the pre-processing stage (right); 2<sup>nd</sup> line depicts the image after applying an adaptive local threshold algorithm (left), and the image after applying the sobel edge detector (right); 3<sup>rd</sup> line presents the image after applying the Hole Pixel Initial Algorithm including several dilation processes (left), and the image after applying the labeling connected components algorithm (right).

After the appearance of the coloured connected components, they will be printed on the original image during the contouring algorithm. The location of the cracks in the original image is defined successfully (Figure 6.8, left). Following this step, the modified binary mask detection algorithm, which is based on the geometric relationship for crack regions, is utilized for crack extraction, severity level, and characteristics. The image in Figure 6.8 (right) demonstrates that the modified ellipse binary mask fits correctly into the crack alignment, and the remaining noise (the other green regions) is ignored. In addition, the lane marking is deleted automatically, the characteristics of cracks are derived from the properties of the elliptical region, and the severity level is determined (Figure 6.8, right). Figure 6.8 (right) also shows that the image contains a vertical individual crack, with the crack area length equal to the major axis length (639.5 pixels = 0.77 m), width equal to the minor axis length (68.1 pixels = 0.01 m), an orientation of 83.6°, area of the crack region (29190.9 pixels<sup>2</sup> = 0.04 m<sup>2</sup>), and the severity level of crack region determined (low).

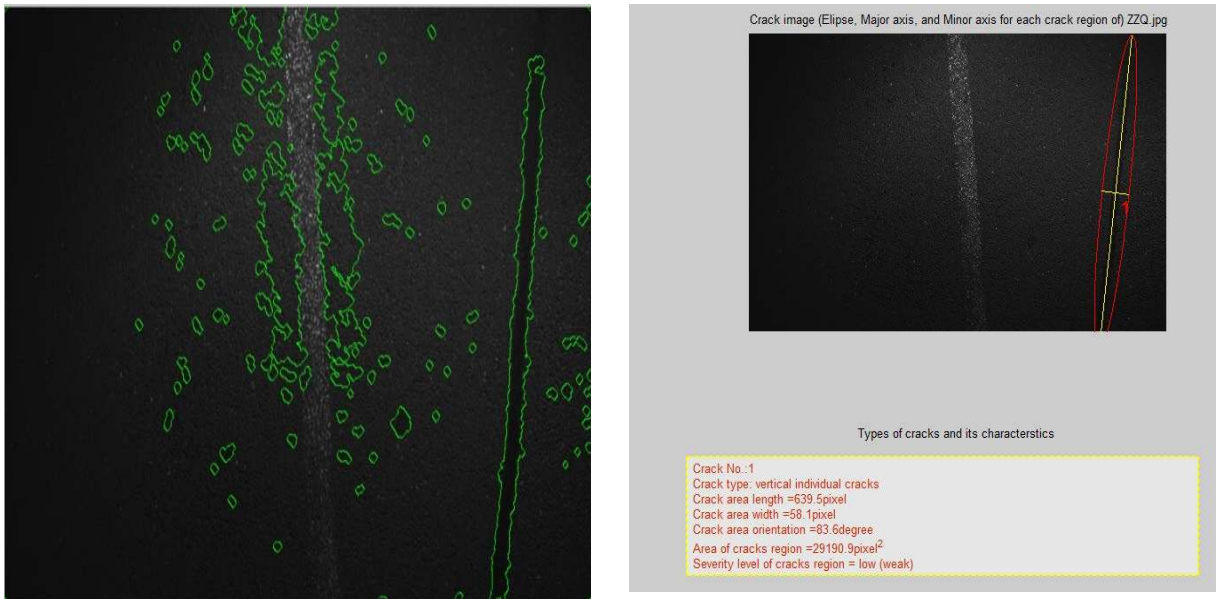


Figure 6.8: Behaviour of the algorithm for crack extraction and classification within the image shows the original image after applying a contouring algorithm (left), and the image after applying a modified binary mask algorithm, as well as the modified standard classification method (right).

Since the procedure described above has been successfully implemented, the correctness rate can be calculated using equation (6-1). A sample of the results will be displayed, as was shown in Figure 6.8 above. Table 6.8 summarizes that the crack evaluation and that an overall correctness rate for cracks ( $B_1$ ) of 98.9 % is achieved. The correctness rate for the image ( $B_6$ ) is 99%, with 98.7%, 100 %, 100%, and 100% achieved for the correctness rates for individual vertical ( $B_2$ ), horizontal ( $B_3$ ), and transverse cracks ( $B_4$ ), as well as network (block) cracks ( $B_5$ ), respectively. The severity level for most cracks is low. In conclusion, the algorithm succeeds in detecting different types of cracks for a moderate pavement texture. This is done for a sequence of 96 geo-referenced pavement images during a time period ( $t_p$ ) of only 3.6 min. In addition, the algorithm shows the ability to ignore markings and oil spots on the ground. Only one crack was falsely detected, and is considered as an error of the second type (based on section 6.3). This is because the main crack is detected from the image, in addition to other small crack regions that were falsely detected (marked in Figure 6.9). This occurs due to two reasons: 1) some oil spot regions have the same brightness level (intensity values) and color as narrow small crack pixel regions; and 2) the geometrical size and shape for oil spot regions is the same as the geometric size and shape of narrow small cracks. The explanation for this drawback is described in more detail in Chapter 5, section 5.2. An error of the first type (based on section 6.3) was not recorded in this case study. More details regarding other examples of the interface for a sample of sequence images with cracks and the resulting classification are reported in Appendix B.

Table 6.8: Results of the evaluation process  
(N1, N2, N3 and N4 represent a number of cracks having low, medium, high and very high severity levels)

Category	Quality
Falsely detected cracks	1 crack
Falsely detected images	1 image
$B_1$ (%)	98.9
$B_2$ (%)	98.7
$B_3$ (%)	100
$B_4$ (%)	100
$B_5$ (%)	100
$B_6$ (%)	99
N1	80
N2	10
N3	0.0
N4	0.0
$t_p$ [s]	212.7s $\approx$ 3.6 min

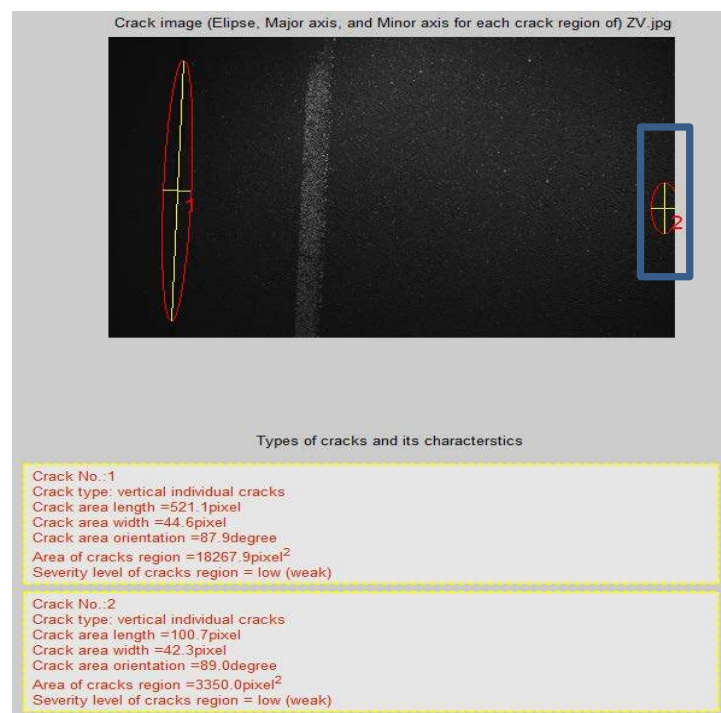


Figure 6.9: Example of a false detection (second type of error) in this case study.

## 6.4.2 Case Study 2: LEHMANN + PARTNER GmbH

This case study contains 94 pavement images, and represents 100 m of the street ground. Table 6.9 shows a description of the dataset for this case study. The acquired images for this case study are subjected to the same algorithm that was used in case study 1, and a mixture of moderate and low pavement texture is considered to be the main difference between the two studies (Figure 6.10 and Figure 6.11).

Table 6.9: Description of the dataset for case study (2)

Category	Quality
Number of images	94 images
Number of crack images	23 images
Number of vertical crack images	23 images
Number of horizontal crack images	0 images
Number of transverse crack images	0 images
Number of network cracks (Block type)	0 images
Number of non-crack images	71 images
Length of vertical cracks for all images (m)	24.2 m
Length of horizontal cracks for all images (m)	0.0 m
Length of transverse cracks for all images (m)	0.0 m
Area of network cracks (Block type) for all images (m <sup>2</sup> )	0.0 m <sup>2</sup>

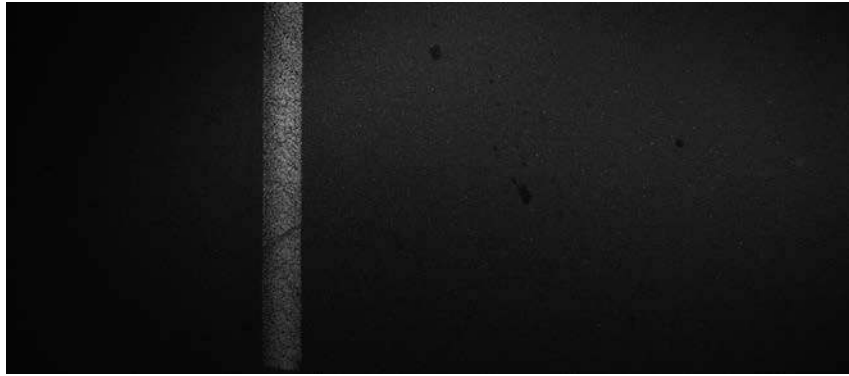


Figure 6.10: Image with low pavement texture, markings, and oil spots without cracks (LEHMANN+PARTNER 2014).

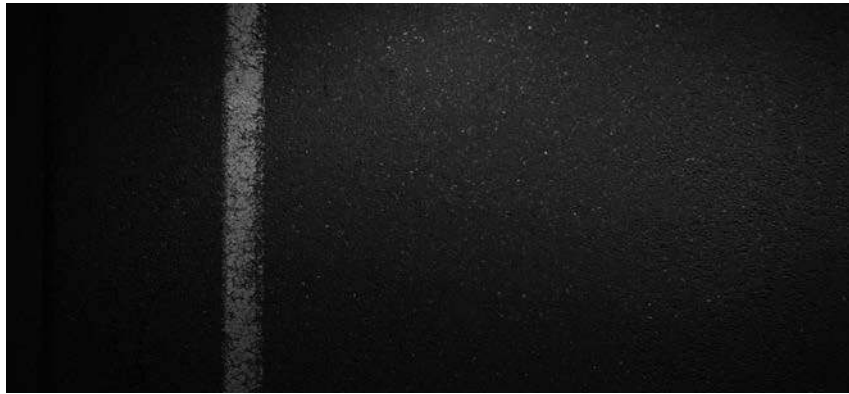


Figure 6.11: Image with moderate pavement texture, and markings with cracks (LEHMANN+PARTNER 2014).

In conclusion, the algorithm succeeds in detecting cracks in both the low and moderate pavement textures (Figure 6.12). Moreover, Table 6.10 depicts an overall correctness rate for the crack ( $B_1$ ) and image ( $B_6$ ) of 98.6% and 99%, respectively. The correctness rate for the crack ( $B_1$ ) is slightly lower when compared to the result of case study 1 where, 98.6%, 100%, 100%, and 100% are achieved as the correctness rates for individual vertical ( $B_2$ ), horizontal ( $B_3$ ), and transverse cracks ( $B_4$ ), as well as network (block) cracks ( $B_5$ ), respectively. The severity level for all cracks in this case study is low. The algorithm can complete the cracks detection and classification during a time period ( $t_p$ ) of only 3.8 min. The processing time is slightly higher when compared to the processing time of case study 1. Nevertheless, using this algorithm for narrow small oil spot regions was prone to failure as case study 1. One crack in this case study was falsely detected, and this error is considered to be the second type. An error of the

first type (based on section 6.3) was not recorded in this case study.

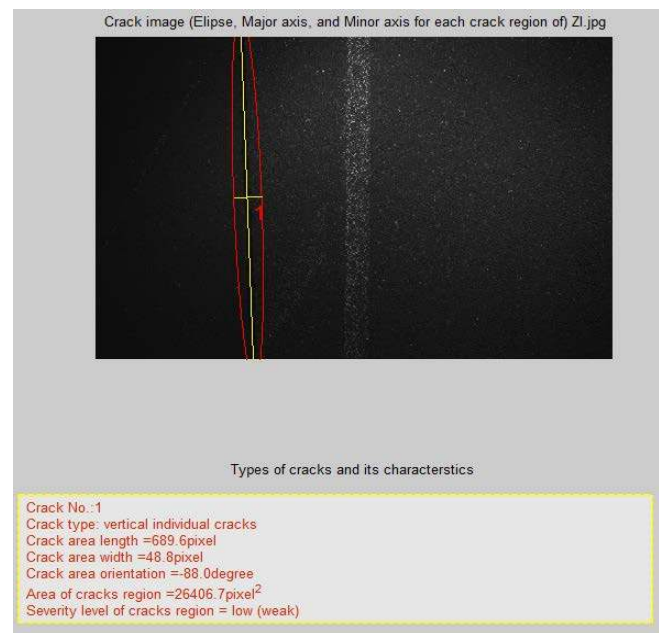


Figure 6.12: Final elliptical binary mask around crack regions only, its characteristics, and ignored markings on moderate pavement texture.

Table 6.10: Results of the evaluation process

(N1, N2, N3 and N4 represent a number of cracks having low, medium, high and very high severity levels)

Category	Quality
Falsely detected cracks	1 crack
Falsely detected images	1 image
$B_1$ (%)	98.6
$B_2$ (%)	98.6
$B_3$ (%)	100
$B_4$ (%)	100
$B_5$ (%)	100
$B_6$ (%)	99
N1	70
N2	0.0
N3	0.0
N4	0.0
$t_p$ [s]	280.80s≈3.8 min

### 6.4.3 Case Study 3: LEHMANN + PARTNER GmbH

Another dataset from LEHMANN + PARTNER GmbH was also tested by the algorithm. 95 pavement images are included in this case study, representing 100 m of the street ground. Table 6.11 shows a description of the dataset for this case study. A mixture of high and low pavement texture, moderate lighting conditions, and existing nonlinear extrinsic objects are considered to be the main differences between this case study and previous case studies (Figure 6.13, and Figure 6.14).

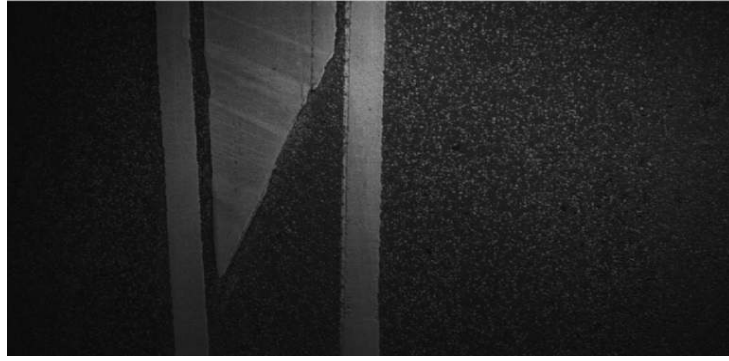


Figure 6.13: Image of high pavement texture, markings with different shapes, and oil spots without cracks (LEHMANN+PARTNER 2014).



Figure 6.14: Image with low pavement texture, shadows from vehicles, and oil spots without cracks (LEHMANN+PARTNER 2014).

Table 6.11: Description of the dataset for case study (3)

Category	Quality
Number of images	95 images
Number of crack images	0 images
Number of vertical crack images	0 images
Number of horizontal crack images	0 images
Number of transverse crack images	0 images
Number of network cracks (Block type)	0 images
Number of non-crack images	95 images
Length of vertical cracks for all images (m)	0.0 m
Length of horizontal cracks for all images (m)	0.0 m
Length of transverse cracks for all images (m)	0.0 m
Area of network cracks (Block type) for all images (m <sup>2</sup> )	0.0 m <sup>2</sup>

All images containing only different lane markings without cracks will be classified as “non-crack images” (Figure 6.15, line 2, right). Further details pertaining to the behaviour of the algorithm in the case of images with lane markings are described in Chapter 5, section 5.1.



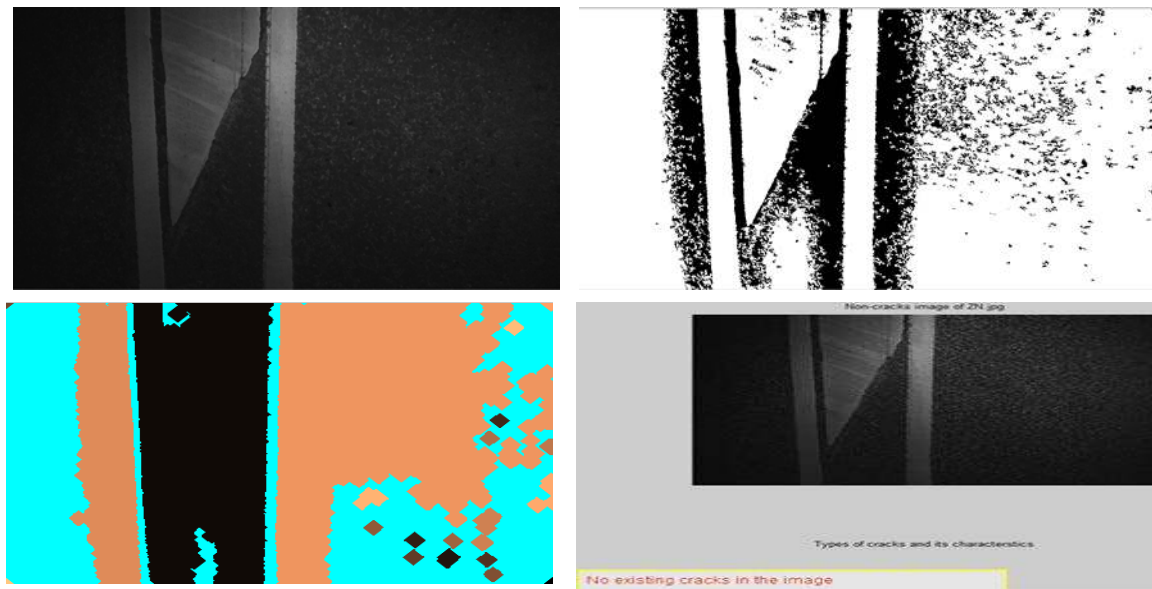


Figure 6.15: Non-crack images, and ignored markings with different shapes for high pavement texture: 1<sup>st</sup> line shows the image after applying the pre-processing stage (left), and the image after applying the adaptive local threshold algorithm (right); 2<sup>nd</sup> line shows the image after applying the labeling connected components algorithm (left), and the final image with no ellipse drawn inside it as a non-crack image (right).

Moreover, Table 6.12 shows that an overall correctness rate ( $B_6$ ) of 98.9 % is achieved for the image, an error higher compared to the results of the previous case studies. The correctness rate for the individual vertical ( $B_2$ ), horizontal ( $B_3$ ), and transverse cracks ( $B_4$ ), as well as network (block) cracks ( $B_5$ ) were not calculated due to the unavailability of any type of crack in this case study. In conclusion, this case study was tested to demonstrate the ability of the algorithm to cope with different marking shapes and oil spots for a mixture of pavement textures. A short period of only 3.8 min ( $t_p$ ) is required for processing 95 pavement images. Despite the strength of the algorithm, the problem of a small narrow oil spots still exists in this case study. The algorithm falsely detected only one crack, and is considered to be an error of the second type. An error of the first type (based on section 6.3) is not recorded in this case study. More details regarding other examples of false detection are reported in Appendix B.

Table 6.12: Results of the evaluation process

(N1, N2, N3 and N4 represent a number of cracks having low, medium, high and very high severity levels)

Category	Quality
Falsely detected cracks	1 crack
Falsely detected images	1 image
$B_1$ (%)	-
$B_2$ (%)	-
$B_3$ (%)	-
$B_4$ (%)	-
$B_5$ (%)	-
$B_6$ (%)	98.9
N1	0.0
N2	0.0
N3	0.0
N4	0.0
$t_p$ [s]	227.70s≈3.8 min

#### 6.4.4 Case Study 4: LEHMANN + PARTNER GmbH

The entire algorithm presented in Chapters 3 and 4 was also applied to another LEHMANN + PARTNER dataset. This dataset differs from other former datasets by having various network cracks (block crack types) and a mixture of high and moderate pavement textures (Figure 6.16 and Figure 6.17). 96 pavement images are included in this case study, representing 100 m on the street ground. Table 6.13 depicts a description of the dataset for this case study.



Figure 6.16: Image with high pavement texture and a sidewalk (curb) without cracks (LEHMANN+PARTNER 2014).

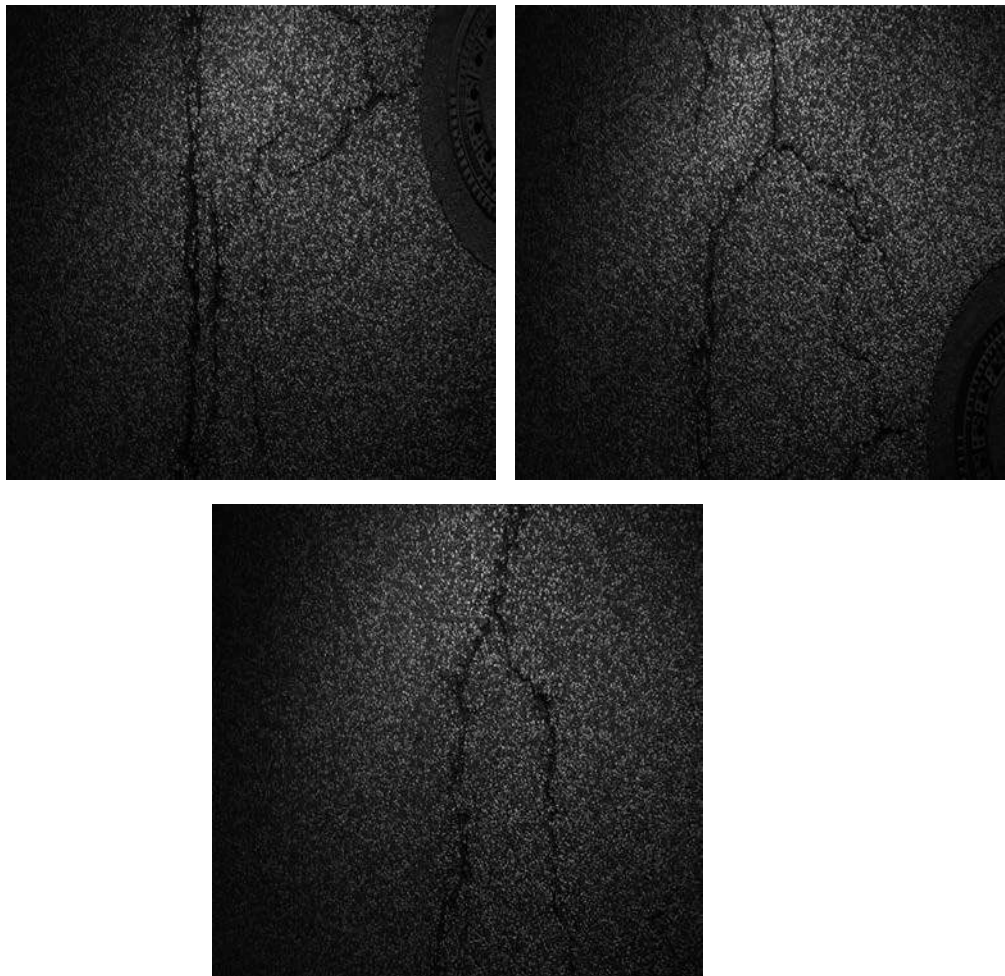


Figure 6.17: Different network cracks (block crack types) images with a high pavement texture (LEHMANN+PARTNER 2014).

Table 6.13: Description of the dataset for case study (4)

Category	Quality
Number of images	96 images
Number of crack images	50 images
Number of vertical crack images	18 images
Number of horizontal crack images	2 images
Number of transverse crack images	10 images
Number of network cracks (Block type)	20 images
Number of non-crack images	46 images
Length of vertical cracks for all images (m)	18.9 m
Length of horizontal cracks for all images (m)	1.7 m
Length of transverse cracks for all images (m)	7.3 m
Area of network cracks (Block type) for all images (m <sup>2</sup> )	0.57 m <sup>2</sup>

In conclusion, the algorithm succeeds in detecting and classifying network cracks (block type) (Figure 6.18). The behaviour of the algorithm in the case of network cracks (block type) is described in more detail in Chapter 4, section 4.3. The complete algorithm is successful for a sample from this case study that has sidewalks (curbs) with a mixture of high and moderate pavement textures. In addition, the algorithm does not detect sidewalks (curbs) as cracks, despite the linear shape. Further details pertaining to the algorithm behaviour with respect to sidewalk (curb) cancellation are presented in Chapter 5, section 5.1.

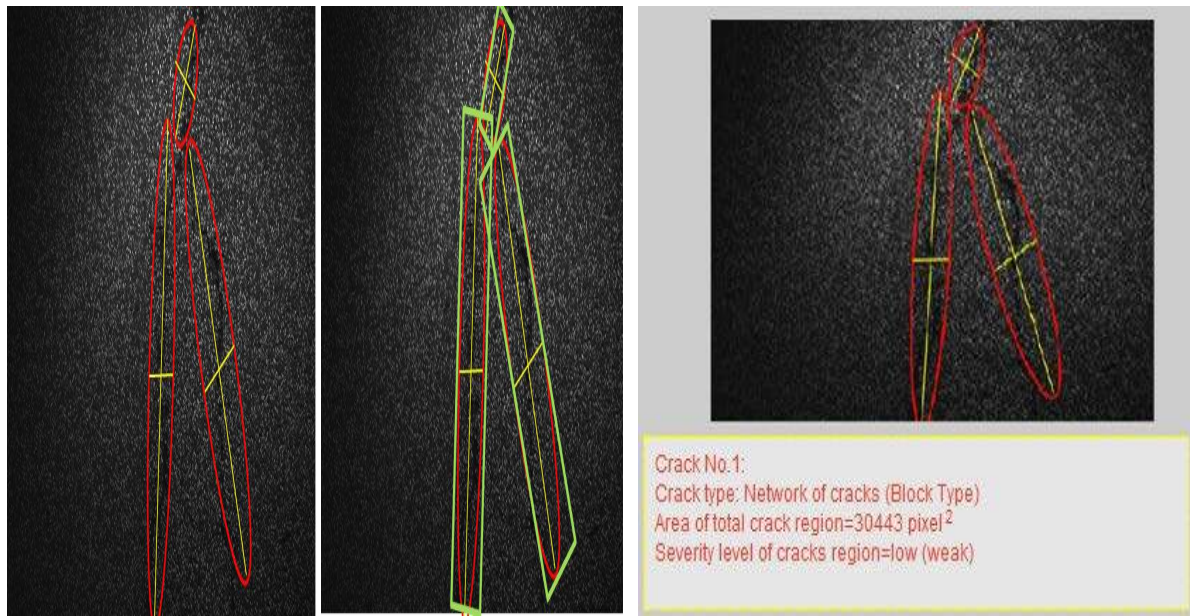


Figure 6.18: The behaviour of the algorithm in the case of crack network (block cracks types): a group of elliptical masks in the block type region (left); a group of rectangular binary masks for branch determination (middle); final classification as crack network (block type), its severity level, and characteristics (right).

The period of time ( $t_p$ ) for processing all the images is only 3.8 minutes, and the evaluation process is completed (Table 6.14). The processing time is slightly higher when compared to the processing time of case study 1 and equal to the results of case studies 2 and 3. The overall correctness rate for the crack ( $B_1$ ) is 98.9%, and is equal to the result of case study 1. The overall correctness rate achieved for the image ( $B_6$ ) is 99%, and is higher than the result of case study 3, and is equal to the results in case studies 1 and 2. Correctness rates of 98.2%, 100%, 100%, and 100% were achieved for the individual vertical ( $B_2$ ), horizontal ( $B_3$ ), and transverse cracks ( $B_4$ ), as well as the network (block) cracks ( $B_5$ ), respectively. The severity level for the majority of cracks in this case study was

low, with some of the cracks displaying a level of medium or high severity. However, although this algorithm performs well for network cracks (block type), the algorithm fails in the instance of small narrow oil spots on the ground as previous case studies. An error of the first type (based on section 6.3) is not recorded in this case study.

Table 6.14: Results of the evaluation process  
(N1, N2, N3 and N4 represent a number of cracks having low, medium, high and very high severity levels)

Category	Quality
Falsely detected cracks	1 crack
Falsely detected images	1 image
$B_1$ (%)	98.9
$B_2$ (%)	98.2
$B_3$ (%)	100
$B_4$ (%)	100
$B_5$ (%)	100
$B_6$ (%)	99
N1	70
N2	10
N3	10
N4	0.0
$t_p$ [s]	227.70s $\approx$ 3.8 min

#### 6.4.5 Case Study 5: 3D Mapping Solutions GmbH

This case study differs from the former datasets by having high lighting conditions and low pavement texture (Figure 6.19). 336 pavement images are included in this case study. Table 6.15 presents a description of the dataset used for this case study.



Figure 6.19: Image with a marking, sidewalks, and railways, without cracks (3D-MAPPING 2014).

Table 6.15: Description of the dataset for case study (5)

Category	Quality
Number of images	336 images
Number of crack images	0 images
Number of vertical crack images	0 images
Number of horizontal crack images	0 images
Number of transverse crack images	0 images
Number of network cracks (Block type)	0 images
Number of non-crack images	336 images
Length of vertical cracks for all images (m)	0.0 m
Length of horizontal cracks for all images (m)	0.0 m
Length of transverse cracks for all images (m)	0.0 m
Area of network cracks (Block type) for all images (m <sup>2</sup> )	0.0 m <sup>2</sup>

In conclusion, the entire algorithm can successfully process the images of this case study, and even with high lighting conditions and low pavement texture, it ignores sidewalks (curbs), markings, and railways (Figure 6.20).

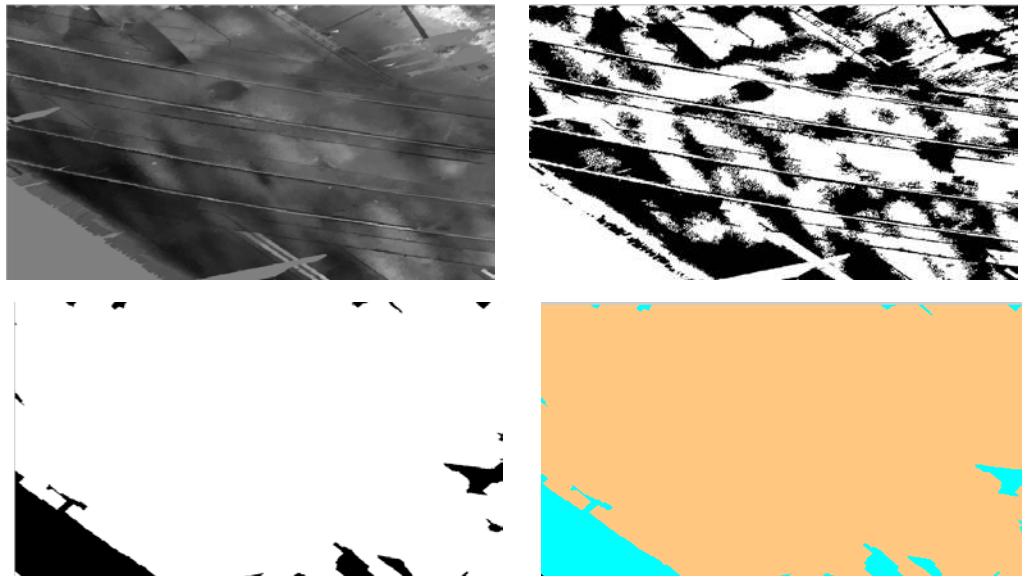


Figure 6.20: The behaviour of the algorithm during the processing stages for crack extraction from within an image; 1<sup>st</sup> line shows the image after the pre-processing stage (left), and the image after applying an adaptive local threshold algorithm (right); 2<sup>nd</sup> line shows the image after applying the HPIA, which included several applications of the dilation process (left), and the image after applying the labeling connected components algorithm (right).

Table 6.16 shows the results of the evaluation process. The overall correctness rate for the image ( $B_6$ ) was 100%, a value higher than in previous case studies. The correctness rate for individual vertical ( $B_2$ ), horizontal ( $B_3$ ), and transverse ( $B_4$ ) cracks, as well as the network (block) cracks ( $B_5$ ) were not calculated due to the lack of cracks in this case study. The period of time ( $t_p$ ) for completing the processing was 16.2 min, longer than the processing time for the LEHMANN + PARTNER GmbH images, because the 3D Mapping Solutions GmbH case study consists of a greater number of images than the LEHMANN + PARTNER case studies. Despite the higher image resolution obtained from 3D Mapping Solutions GmbH, there are several limitations. These limitations were mentioned previously, and include lighting conditions and disruptive surroundings. In conclusion, the algorithm ignores all of the disrupting surroundings, such as railways, sidewalks, and lighting conditions.

Table 6.16: Results of the evaluation process  
(N1, N2, N3 and N4 represent a number of cracks having low, medium, high and very high severity levels)

Category	Quality
Falsely detected cracks	0 crack
Falsely detected images	0 image
$B_1$ (%)	-
$B_2$ (%)	-
$B_3$ (%)	-
$B_4$ (%)	-
$B_5$ (%)	-
$B_6$ (%)	100
N1	0.0
N2	0.0
N3	0.0
N4	0.0
$t_p$ [s]	970.35s $\approx$ 16.2 min

#### 6.4.6 Case Study 6: Unicom-Umap

The next two case studies presented here are obtained from the company Unicom-Umap, using the VISAT™ mobile mapping system. The goals are to evaluate the algorithm, the usability under different lighting conditions, and to review whether the algorithm can detect and classify cracks with another type of pavement texture (different from the pavement texture found in Germany). Therefore, the properties of the Unicom-Umap images are different from the German case studies mentioned above. This dataset differs from the former datasets by having other crack shapes, crack images with a different resolution (2058x2456), a high pavement texture, and changes in lighting conditions. An evaluation using this thesis approach is introduced for each Unicom-Umap case study.

The first case study contains two individual pavement images for the circular street of Riyadh City in Saudi Arabia. These images are good representative examples of network cracks (block type) (Figure 6.21). A mixture of high pavement texture, and low lighting conditions are considered to be the main differences between this case study and previous case studies. Table 6.17 presents a description of the dataset for this case study.



Figure 6.21: Images of this case study: first example of network cracks (block type) (left); second example of network cracks (block type) (right) (UNICOM-UMAP 2014).

Table 6.17: Description of the dataset for case study (6)

Category	Quality
Number of images	2 images
Number of crack images	2 images
Number of vertical crack images	0 images
Number of horizontal crack images	0 images
Number of transverse crack images	0 images
Number of network cracks (Block type)	2 images
Number of non-crack images	0 images
Length of vertical cracks for all images (m)	0.0 m
Length of horizontal cracks for all images (m)	0.0 m
Length of transverse cracks for all images (m)	0.0 m
Area of network cracks (Block type) for the first image (m <sup>2</sup> )	90.6 m <sup>2</sup>
Area of network cracks (Block type) for the second image (m <sup>2</sup> )	36.5 m <sup>2</sup>

In conclusion, the overall algorithm succeeds in processing the images of this case study, despite the type of pavement texture (Figure 6.22). The results for the correctness rate were reviewed, and the evaluation process was utilized (Table 6.18). The overall correctness rate obtained for the image ( $B_6$ ) and crack ( $B_1$ ) was 100%, a superior value compared to all previous case studies. The correctness rate for individual vertical ( $B_2$ ), horizontal ( $B_3$ ) and transverse cracks ( $B_4$ ) were not calculated due to the lack of cracks in this case study. The severity level for the crack in the first image is very high, and also high in the second image. Errors of the first and second type (based on section 6.3) are not recorded in this case study.

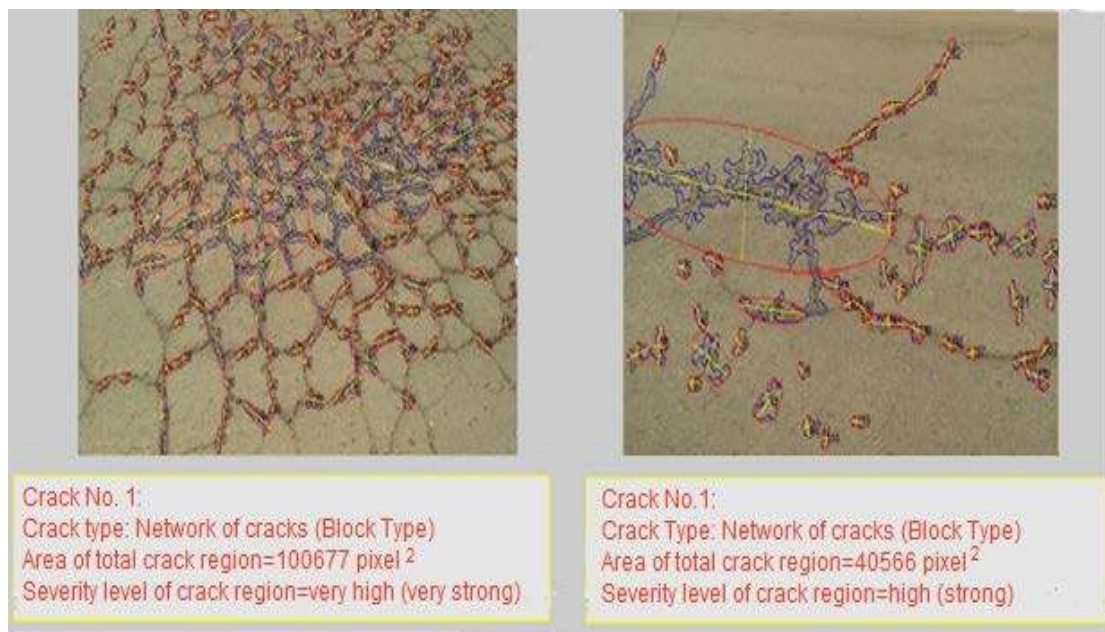


Figure 6.22: Behaviour of the modified standard classification method for two images in this case study shows the network of cracks (block type), its area, and severity level for the first and second image (left and right).

Table 6.18: Results of the evaluation process  
(N1, N2, N3 and N4 represent a number of cracks having low, medium, high and very high severity levels)

Category	Quality
Falsely detected cracks	0 crack
Falsely detected images	0 image
$B_1$ (%)	100
$B_2$ (%)	-
$B_3$ (%)	-
$B_4$ (%)	-
$B_5$ (%)	100
$B_6$ (%)	100
N1	0.0
N2	0.0
N3	1.0
N4	1.0
$t_p$ for for the first image[s]	16.8 min
$t_p$ for for first the image[s]	16.9 min

#### 6.4.7 Case Study 7: Unicom-Umap

This case study represents 200 pavement images for King Fahd Street of Riyadh city in Saudi Arabia. Image sequences for King Fahd Street differ from other former datasets by having mixture of low, moderate, and high pavement texture. This case study is used as a good example to determine if the algorithm can classify the images of Unicom-Umap Company as non-crack images and ignore any other limitations. Worthy of note, King Fahd Street is a main street in Saudi Arabia and does not have cracks (Figure 6.23). Table 6.19 shows a description of the dataset for this case study.



Figure 6.23: Example of the King Fahd Street images with markings, shadows (different lighting conditions), sidewalks (curbs), and extrinsic objects, such as trees, buildings, traffic, and lighting columns without cracks (left, middle, and right) (UNICOM-UMAP 2014).



Table 6.19: Description of the dataset for case study 7

Category	Quality
Number of images	200 images
Number of crack images	0 images
Number of vertical crack images	0 images
Number of horizontal crack images	0 images
Number of transverse crack images	0 images
Number of network cracks (Block type)	0 images
Number of non-crack images	200 images
Length of vertical cracks for all images (m)	0.0 m
Length of horizontal cracks for all images (m)	0.0 m
Length of transverse cracks for all images (m)	0.0 m
Area of network cracks (Block type) for all images (m <sup>2</sup> )	0.0 m <sup>2</sup>

To assess the correctness rate, the evaluation process results were computed (Table 6.20). This table indicates that there was improvement compared to the results for some German case studies. The overall correctness rate for the image ( $B_6$ ) was 100%, a value superior to that obtained in the previous case studies. The correctness rate for individual vertical ( $B_2$ ), horizontal ( $B_3$ ), and transverse cracks ( $B_4$ ), as well as network (block) cracks ( $B_5$ ) were not calculated due to the lack of cracks in this case study. The processing time ( $t_p$ ) for completing all analyses was 14.2 min, shorter than the processing time for the 3D Mapping Solutions GmbH images because the 3D Mapping Solutions GmbH case study consists of a greater number of images than the Unicom-Umap case studies. In conclusion, this case study provides an opportunity to test the empirical algorithm on another country's datasets with different pavement textures (Figure 6.24). Errors of the first type and second type (based on section 6.3) are not recorded in this case study.



Figure 6.24: Non-crack images: the algorithm ignores marking, extrinsic objects, and sidewalks (curbs) (left and right); the algorithm ignores shadows, oil spots, and escape of binder and sidewalks (curbs) (middle).

Table 6.20: Results of the evaluation process  
(N1, N2, N3 and N4 represent a number of cracks having low, medium, high and very high severity levels)

Category	Quality
Falsely detected cracks	0 crack
Falsely detected images	0 image
$B_1$ (%)	-
$B_2$ (%)	-
$B_3$ (%)	-
$B_4$ (%)	-
$B_5$ (%)	-
$B_6$ (%)	100
N1	0.0
N2	0.0
N3	0.0
N4	0.0
$t_p$ [s]	850.31s $\approx$ 14.2 min

## 6.5 Final Conclusion of the Case Studies

In the following section, this thesis will sum up the results of the seven case studies such as average correctness rate, average processing time, and average number of cracks having low, medium, high and very high severity levels, respectively (Table 6.21).

Table 6.21: Final Conclusion of the Case Studies

Case Study No.	Source of Images	Final Conclusion					
		Processing time $t_p$ [min]	Correctness Rate $B_6$ (%)	N1	N2	N3	N4
1	LEHMANN + PARTNER GmbH	3.6	99	80	10	0.0	0.0
2	LEHMANN + PARTNER GmbH	3.8	99	70	0.0	0.0	0.0
3	LEHMANN + PARTNER GmbH	3.8	98.9	0.0	0.0	0.0	0.0
4	LEHMANN + PARTNER GmbH	3.8	99	70	10	10	0.0
<b>Average (1 to 4)</b>		<b>3.8</b>	<b>98.9</b>	-	-	-	-
5	3D Mapping Solutions GmbH	16.2	100	0.0	0.0	0.0	0.0
<b>Average (5)</b>		<b>16.2</b>	<b>100</b>	-	-	-	-
6	Unicom-Umap	16.9	100	0.0	0.0	1.0	1.0
7	Unicom-Umap	14.2	100	0.0	0.0	0.0	0.0
<b>Average (6 to 7)</b>		<b>15.6</b>	<b>100</b>	-	-	-	-

The average processing time ( $t_p$ ) for processing all the images from LEHMANN + PARTNER GmbH is only 3.8 minutes, and the evaluation process is completed. Average correctness rates of 98.9%, 100%, and 100% were achieved for the case studies from LEHMANN + PARTNER GmbH, 3D Mapping Solutions GmbH, as well as Unicom-Umap, respectively. The severity level for the majority of cracks was low, with some of the cracks displaying a level of medium or high severity (Table 6.21).

This thesis shows that different case studies to evaluate various types of cracks are required to test an algorithm. Unfortunately, the available case studies from 3D Mapping Solutions and Unicom-Umap do not have cracks. In addition, obtaining other datasets was not possible. Therefore, the framework of this thesis is constrained to the seven case studies that were presented.

## 6.6 Performance Evaluations

In the following section, this study attempts to demonstrate the performance, efficiency, and credibility of the algorithm with regard to each of the four stages. A review of the current literature strongly confirms that none of the previous algorithms can detect and classify all cracks from continuous pavement images. In addition, several other common non-commercial methods in the literature have been used to test individual images for comparison. These methods include NIBLACK'S (1985), SAUVOLA/PIETIKAKINEN (2000), and Beamlet transformation for crack detection (YING/SALARI 2009). These methods are chosen over others as they have either been formerly utilized to evaluate individual pavement images efficiently, or they are used to separate textual information from its application. In this section, a comparative study is conducted between the algorithm of this thesis, and the three other common methods for individual images.

This comparative study has been conducted for 100 images from 3D Mapping Solutions GmbH (sample in Figure 6.25), another 100 images from LEHMANN + PARTNER GmbH (sample in Figure 6.26), and a set of 100 images from Unicom-Umap (sample in Figures 6.27). A kind of inversion is preformed for exemplary visualization (Figure 6.26). More details regarding other sample comparisons for different individual images are reported in Appendix C.

Moreover, some pavement images contained a high degree of noise (sample in Figure 6.26), and extrinsic objects, such as lane markings, sidewalks (curbs), shadows due to column lighting, and railroad crossing on the ground (samples in Figure 6.25, and 27). In situations that involve different pavement textures, it is challenging for the algorithm to detect cracks, and ignoring other objects at the same time.

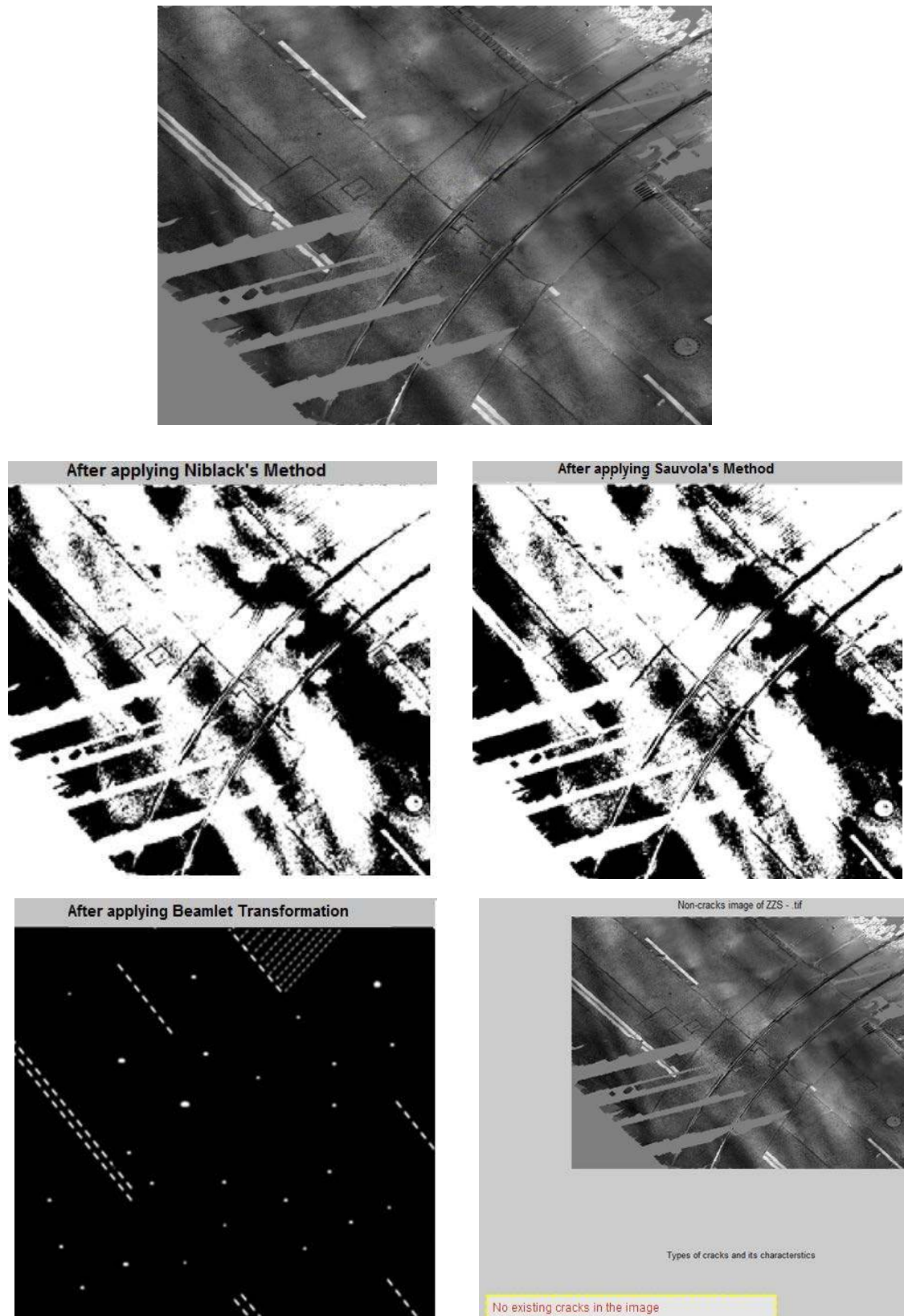


Figure 6.25: A comparison between the algorithm of this thesis and other methods: 1<sup>st</sup> line shows the original image for 3D-Mapping Solution; 2<sup>nd</sup> line shows the image after applying Niblack's method (left), and Sauvola's method (right); and 3<sup>rd</sup> line shows the image after applying the Beamlet transformation method (left), and the algorithm of this thesis (right).

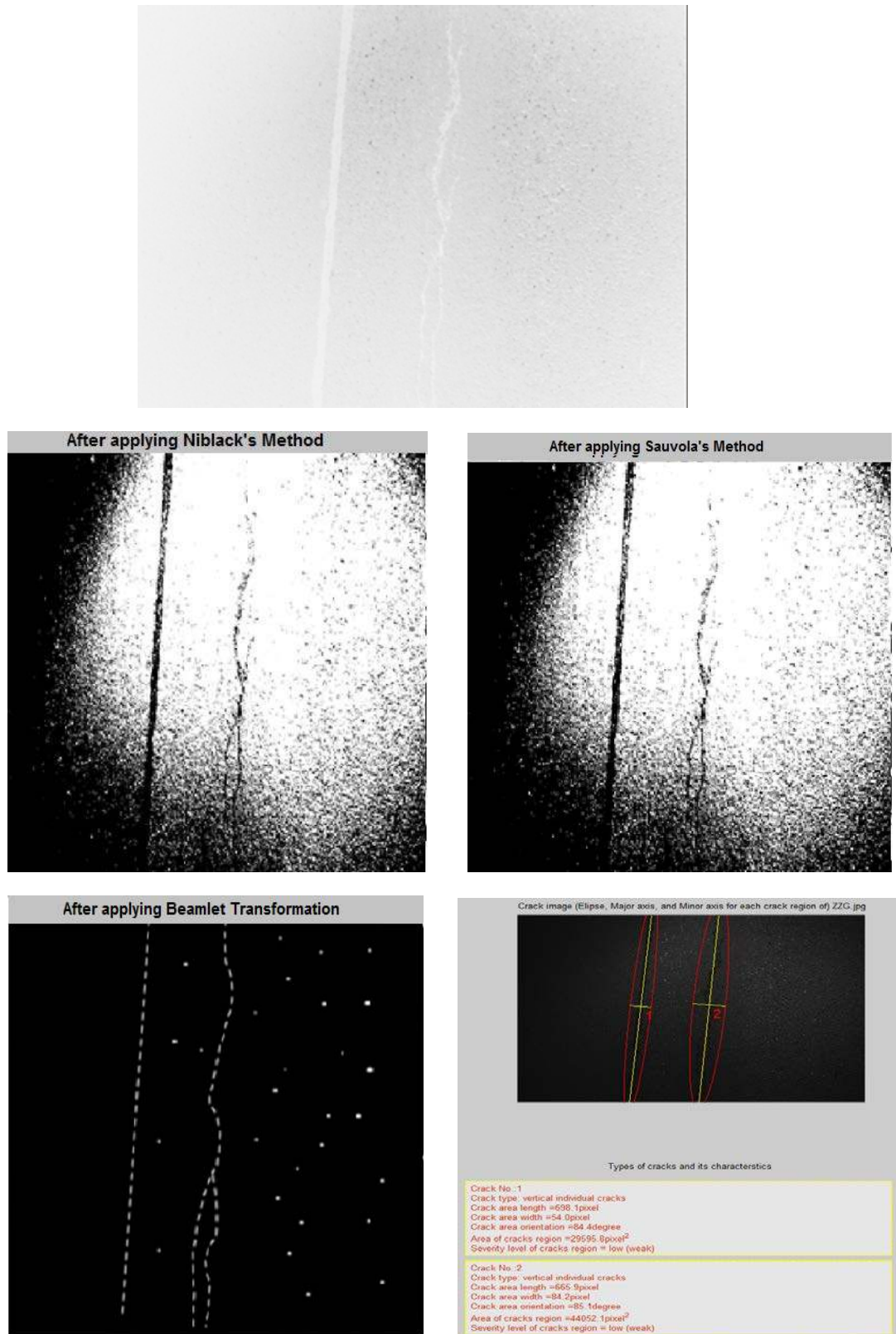


Figure 6.26: A comparison between the algorithm of this thesis and other methods: 1<sup>st</sup> line shows the original image (inverted illustration) from LEHMANN+PARTNER; 2<sup>nd</sup> line shows the image after applying Niblack's method (left), and Sauvola's method (right); and 3<sup>rd</sup> line shows the image applying Beamlet transformation method (left), and the algorithm of this thesis (right)

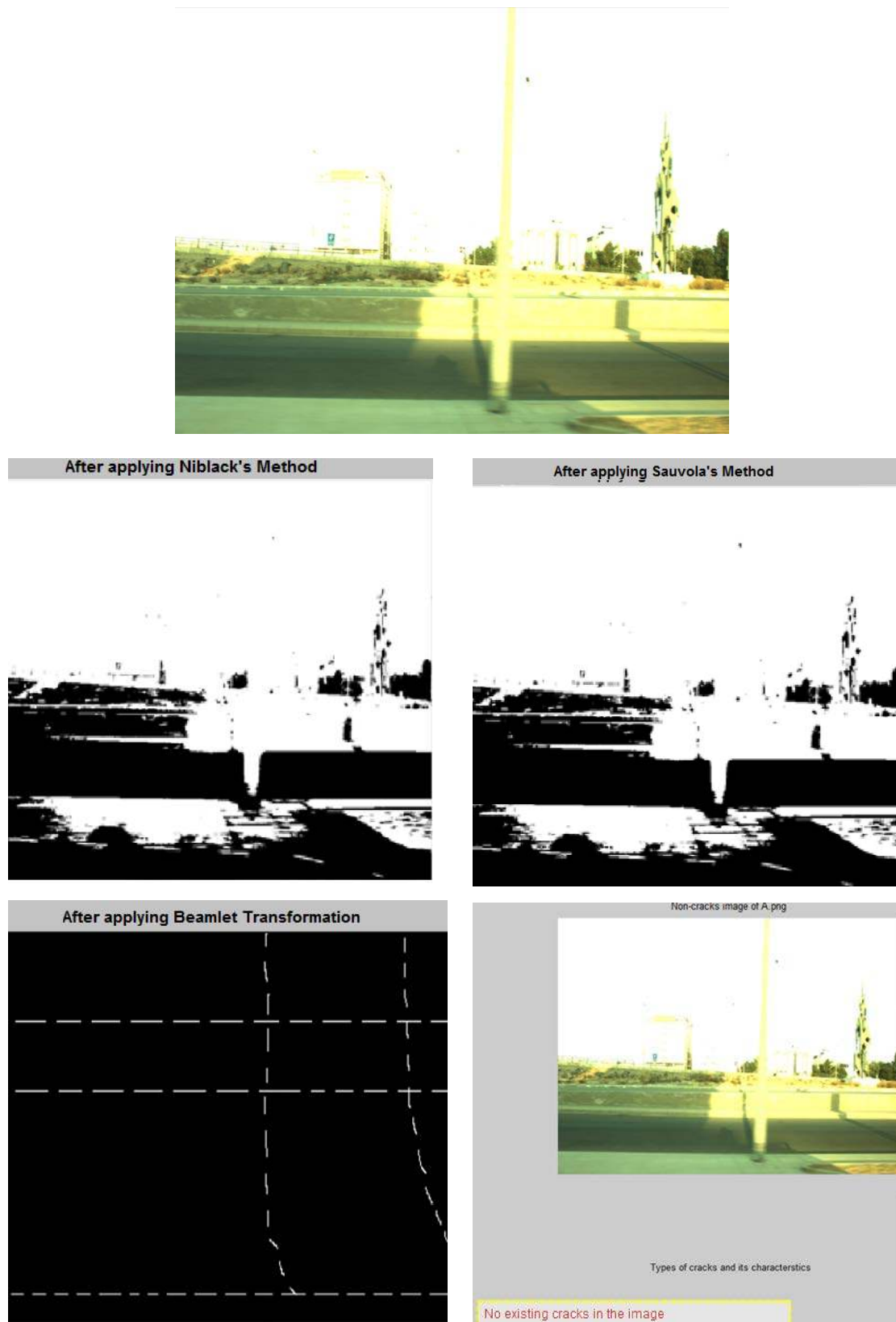


Figure 6.27: A comparison between the algorithm of this thesis and other methods: 1<sup>st</sup> line shows the original image for Unicom-Umap(King Fahd street); 2<sup>nd</sup> line shows the image after applying Niblack's method (left), and Sauvola's method (right); and 3<sup>rd</sup> line shows the image after applying the Beamlet transformation method (left), and the algorithm of this thesis (right).

The crack recognition results from the four different evaluation methods are presented in this section. The visual evaluation of the experimental results confirms that the algorithm of this thesis performs well above the other cited methods by exemplary visualization. However, from the analysis of the results, the following conclusions can be reached:

1. Results from Niblack's algorithm (NIBLACK'S 1985), with optimal parameters ( $w_s$  and  $v$ ), do not perform well around the region where the background is even, as the algorithm tries too hard to separate the pixels into two classes. However, the results revealed crack pixels in black as background pixels, in addition to the removal of some parts of the cracks. Moreover, regarding the Unicom-Umap case studies, Niblack's algorithm results appear to show a high degree of noise, and extrinsic objects, such as lane markings, sidewalks (curbs), shadows due to column lighting, and roads appear in white as a part of the foreground pixels.
2. Results from Sauvola's algorithm (SAUVOLA'S/PIETIKAKINEN 2000) are similar to the results from Niblack's algorithm in that they both out-perform the traditional method (Otsu's method), but not to the level of the algorithm in this thesis. In addition, these two methods could not perform well enough to binarize the crack images or achieve any overall improvement in recognition, and thus do not perform as well as the algorithm of this thesis. Since both the Niblack and Sauvola algorithms count the background information around the foreground texture as an important feature for local threshold calculation, the pixels for the cracks are considered part of the background pixels.
3. Results from the Beamlet transformation algorithm (YING/SALARI 2009) perform better than the Niblack (NIBLACK'S 1985) and Sauvola algorithms (SAUVOLA'S/PIETIKAKINEN2000). The Beamlet transform-based method is highly effective for the presence of cracks in pavement images, and can be applied to pavement images with a very high rate of detection, and a very high rate of correctness. However, the processing time in this method is higher than the processing time using the algorithm of this thesis (Table 6.22). Furthermore, this method detects cracks and noise surrounding the cracks, unlike the algorithm of this thesis. In addition, it is sensitive to different pavement textures (asphalt binder appears as noise), and it cannot distinguish between cracks and extrinsic objects, such as lane markings, sidewalks (curbs), column lighting, people, and roads (Figures 6.25, and 6.27).
4. The results of the algorithm of this thesis display an outstanding performance compared to the former methods, and have excellent preservation of the intended information after the evaluation. The primary advantage of the algorithm of this thesis is simplicity, since it does not require any further post-processing procedures. Moreover, it is based on a simple and robust technique, resulting in low computational cost, while allowing the user to achieve results on cracks without noise in an automatic fashion. Consequently, the processing time of this algorithm is lower and the correctness rate is higher than that of all the former methods of individual images (Table 6.22).

As presented in the previous sections, the processing time for crack detection and classification for sequences of mobile mapping images remains low and acceptable. For example, the average processing time is 3.8 min for completing the crack detection and classification when using approximately 96 mobile mapping (Lehmann+Partner GmbH) images sequences. In contrast, the average processing time is 16.2 min for 3D-Mapping Solutions GmbH images, while a sequence of 200 mobile mapping images by Unicom-Umap requires 15.6 min on average to complete all detections and classifications. Table 6.22 illustrates the processing time using each binarization to reveal the speed of the algorithm of this thesis for each individual image. Table 6.23 shows the processing time using each binarization method for 100 images obtained from 3D Mapping Solutions GmbH, LEHMANN + PARTNER GmbH, and Unicom-Umap. Table 6.24 shows the correctness rate using each binarization method for 100 images obtained from 3D Mapping Solutions GmbH, LEHMANN + PARTNER GmbH, and Unicom-Umap.

Table 6.22: Processing time [in sec] for one image using the algorithm of this thesis compared to other methods

Processing time [s]		Niblack's Method	Sauvola's Method	Beamlet Transformation Method	Algorithm of this thesis
Input image	Dimension [pixels]				
Figure 6.24	1178*1225	8.7	9	8.9	8.5
Figure 6.25	1920*1080	5	4	3.5	2.4
Figure 6.26	2058*2456	9.3	9	9	8.4

Table 6.23: Processing time [in min] for 100 images using the algorithm of this thesis compared to other methods

Processing Time [s]		Niblack's Method	Sauvola's Method	Beamlet Transformation Method	Algorithm of this thesis
Total Number of Input Images	Company Name				
100	3D-Mapping Solutions	9.2	9.1	8.0	6.4
100	LEHMANN + PARTNER	8.2	7.3	6.0	3.8
100	Unicom-Umap	8.1	8.1	7.3	5.2

Table 6.24: Correctness rate [in %] for 100 images using the algorithm of this thesis compared to other methods

Correctness Rate [%]		Niblack's Method	Sauvola's Method	Beamlet Transformation Method	Algorithm of this thesis
Total Number of Input Images	Company Name				
100	3D-Mapping Solutions	94.7	94.9	95.9	98.5
100	LEHMANN + PARTNER	94.1	95.1	96.5	98.9
100	Unicom-Umap	94.0	94.2	96.1	98.7

The algorithm can complete the crack detection and classification during a time period ( $t_p$ ) of only 2.4 sec (Table 6.22, Figure 6.25). The processing time is slightly lower when compared to the processing time of other binarization methods. The algorithm succeeds in detecting different types of cracks for different pavement textures. This is done for a sequence of 100 geo-referenced pavement images from LEHMANN + PARTNER Company during a time period ( $t_p$ ) of only 3.8 min (Table 6.23) and correctness rate of (98.9%) (Table 6.24). In conclusion, the algorithm of this thesis has higher correctness rate (Table 6.24), and lower processing time (Tables 6.22, and 6.23) compared to other binarization methods (Niblack's, Sauvola's, and Beamlet Transformation).



## 7. Conclusions and Future Directions

### 7.1 Conclusion

Within this thesis, the potential of combining and modifying digital image processing algorithms for road maintenance applications, such as crack extraction and classification, is discussed. The overall algorithm for crack extraction and classification is based on the use of improved images, created from the original digital images, in order to simplify the extraction and classification of cracks. This integration and combination between different preparation stages is directed at correcting background illumination, due to different occlusions and lighting conditions, weak reflectivity of the asphalt material, or inhomogeneous pavement textures. It also allows for the retrieval of more crack details by using a robust modified local adaptive threshold algorithm and distorting the geometrical size and shape of any extrinsic objects, especially in the case of noisy pavement images included partially by lane markings, sidewalks, railways, and other extrinsic objects. Furthermore, the overall method uses the labelling connected components algorithm. Moreover, this can be useful for coloured indicator existence, in which each crack region gives a unique colour based on its pixel intensity value.

In addition, the algorithm for crack extraction and classification, based on the modified binary mask detection algorithm and the geometric size and shape of common crack regions, is also investigated. A resultant image of the binary masks around the crack regions has been exploited for classifying cracks by a modified standard classification method. However, these methods are highly dependent on precise data acquisition and on the accurate resultant images, after applying all of the preparing stages. Therefore, using these methods in the case of some small, narrow oil spots, pits, and holes in the pavement surface, would be prone to failure. Moreover, the crack extraction and classifications are recorded, not only for archival purposes, but also for maintenance priorities, rehabilitation, and reconstruction, based on the severity level determined for each cracking region. For example, in Chapter 6, there are several case studies that have high and very high severity level cracks. These sections need maintenance priority over other sections.

The overall algorithm is used for testing real pavement crack images. Performance is checked by comparing the results with three well-known previous crack detection algorithms. Within the tests, four case studies contain 96, 94, 95, and 96 images, respectively, which were obtained by LEHMANN + PARTNER GmbH Company in Germany. The images of these four case studies have a resolution of 1920 x 1080 pixels. These images contain different types of cracks, lane markings, and lighting conditions. The developed algorithm delivers an average computation time of 3.8 min and the correctness detection rate for the images is 98.9% to complete crack detection and classification. In addition, one case study contains 336 different continuous crack images, which were captured by 3D Mapping Solutions GmbH Company in Germany too. The images of this case study have different resolutions with numerous extrinsic objects, such as railways, sidewalks, oil spots, and shadows. The developed algorithm exhibits a correctness detection rate for the images of 100% in 16.2 min processing time, and detects and classifies the cracks on around 336 continuous mobile mapping images. Another two case studies contain two images of a circular street, and 200 images of King Fahd Street, respectively, and were collected by Unicom-Umap Company in Saudi Arabia. The images of these two case studies have a resolution of 2058 x 2456 pixels. These images contain different types of cracks, different extrinsic objects, and other pavement textures (different from the abovementioned German case studies). The developed algorithm delivers an average computation time of 15.6 min, and the correctness detection rate for the images is 100% to complete crack detection and classification.

It is advantageous that the overall integration and combination approach of this thesis presents an effective solution by fusing together different modified algorithms for crack extraction and classification applications. Secondly, it achieves a complete automation, in order to meet the requirements of the end-user. Finally, it represents an automatic solution for different shortcomings in the previous crack extraction and classification algorithms.

## 7.2 Future Directions and Recommendations

There are still critical areas that need to be elucidated in further research studies. These critical areas can be summarized as follows:

- One of the advanced technologies that could be further investigated is the combination between laser scanner and photogrammetry. This technique could be utilized for registering the images captured by the mobile mapping vehicle cameras, with laser point clouds acquired by the mobile mapping vehicle laser scanner. This integration will be helpful for the crack extraction application and for severity level assessment of the out-breaks (potholes).
- The classification algorithm provides crack types, their severity level, and their geometric properties, such as width, length, and area. This motivates the development of more intelligent solutions for investigating the possibility of integrating these geometric properties for computing pavement indices for each crack type.
- The use of colour image segmentation could also be applied directly in the resultant image after applying the labelling connected components algorithm, which can detect cracks based on their colour. This is because colour is a strong indicator that often simplifies crack detection and identification; however, some noisy regions share the same colouring as the crack regions. Therefore, this motivates the development of novel approach for this problem through further research.
- The overall algorithms utilized throughout this thesis have been written as a proof of a concept. Further developments would include rewriting the code in a compiled language, instead of the MATLAB language. Furthermore, designing new data structures will make it more applicable. A graphical user interface (GUI) for crack detection applications should be designed for use in engineering departments in the municipalities of Germany or other countries, so that the end-user can make maintenance decisions with greater certainty.
- One of the techniques that could be investigated more thoroughly is that of unmanned aerial vehicles (UAV). This technique could be utilized for collecting aerial mobile mapping images for pavement sections. The images captured by the UAVs may be tested using the digital image processing algorithm of this thesis, especially in the case of crack clarity in the coverage of pavement surfaces.
- The algorithm provides a specification for crack extraction and classification. These specifications were acquired by labour-intensive statistical analysis, for most actual crack images due to the existing unavailability in crack extraction and classification specifications. To overcome this, the present study recommends that existing highway sections develop their specifications and create a general specification for all distress types.
- The correctness of the algorithm results is highly dependent on the image acquisition stage resolution. For this, this thesis recommends closely capturing high resolution (pixel values) images for pavement surfaces. This could lead to a higher correctness rate in the final detected cracks.

- The overall approach introduces a solution for crack extraction and classification in the case of different flexible pavement textures. This encourages improvement to the algorithm to detect other types of distress in the flexible pavement, such as outbreaks (potholes), binder enrichment, etc. This can be achieved by using pattern recognition techniques that geometrically cover the exact shape of other distresses.
- The overall approach presents a solution for crack extraction and classification in the case of flexible pavement. This encourages improvement to the algorithm to detect the types of distress in the other materials such as rigid pavement and stones.
- The overall approach is based on some hundred images only, so that the work is not 100 % representative. Therefore, this motivates that further work has to be done on a more general approach with more data and other materials, etc.

## Bibliography

- AASHTO. (2001): Standard practice for quantifying cracks in asphalt pavement surface - AASHTO Designation pp. 44-01. American Association of State Highway and Transportation Officials, Washington, DC, April, last accessed on October 15, 2014.
- ABUHADROUS, I.I, AMMOUN, S., NASHASHIBI, F. (2004): Digitizing and 3D Modeling of Urban Environments and Roads using Vehicle-Borne Laser Scanner System, IEE International Conference on Intelligent Robots and Systems (IROS'2004), Vol. 1, No. 28, pp. 76-81.
- ACHARYA, A., MEHRA, R., TAKHER, V.S. (2009): FPGA Based Non Uniform Illumination Correction in Image Processing Applications, IEE International Conference on Intelligent Systems, Vol.2, 349-358, ISSN: 2229-6093, pp. 40-55.
- AKIHITO, A., SAITO, K. (2005): Design and Prototype of a Support System for old pavement images, Proc. 13th Conference of the International Graphonomics Society (IGS), Salerno, Italy, pp. 54-58, (2005.6).
- ALBERTZ, J., WIGGENHAGEN, M. (2009): Taschenbuch zur Photogrammetrie und Fernerkundung, Guide for Photogrammetry and Remote Sensing, 5th-edition, Wichmann, Heidelberg.
- AL-MISTAREHI, B., SCHWIEGER, V., OBAIDAT, M.T. (2012): Cost Efficient Camera System to Acquire Data for Pavement Maintenance Management System. Proceeding on 3<sup>rd</sup> International Conference on Machine Control and Guidance, Stuttgart, Germany, March, 27-29, 2012, pp. 50-60.
- AL-MISTAREHI, B., SCHWIEGER, V. (2015): Automated Detection for Pavement Crack for Mobile Mapping Data. Proceeding on 2<sup>nd</sup> International Workshop on Integration of Point-and Area-wise Geodetic Monitoring for Structures and Natural Objects, Stuttgart, Germany, March, 23-24, 2015, pp. 70-83.
- ARAMINI, M.J. (1980): The Design and Implementation of Computer Algorithms for Contour Plotting, undergraduate thesis at Stevens Institute of Technology, Hoboken, NJ 07030.
- ARAN (2014): Automatic Road Analyzer company, Roadware Group, Inc. <http://www.roadware.com/aran.html/>, last accessed on October 15, 2014.
- ATKINSON, K.B. (1996): Close Range Photogrammetry and Machine Vision, Whittles Publishing, Caithness, Scotland, UK, pp. 355-387.
- BADEKAS, E., PAPAMARKOS, N. (2007): Binarization using Kohonen SOM, IET Image Process Journal., 2007, Vol. 1, No.1 pp. 67-85.
- BADEKAS, E., PAPAMARKOS, N. (2007): Optimal combination of binarization techniques using a self-organizing map neural network, Engineering Applications of Artificial Intelligence, Vol. 20 (2007), No.1, pp. 11-24, Xanthi, Greece.
- BARTOLO, A., CAMILLERI, K., BORG, J., FARRUGIA, P. (2004): Adaptation of Brensen's Thresholding Algorithm for Sketched Line Drawings, University of Malta, Malta, Department of Microelectronics, EUROGRAPHICS Workshop on Sketch-Based Interfaces and Modeling, pp. 40-60.
- BATCHA, J.P, REESE, J.R (1960): Surface Determination and Automatic Contouring for Exploration, Extraction, and Processing, IEE International Conference on Intelligent Systems, pp. 42-55.
- BATTIATO, S., GALLO, G., STANCO, F. (2002): A locally adaptive zooming algorithm for digital images, Dipartimento di Matematica ed Informatica, Università di Catania, Viale A. Doria 6, Catania 95125, Italy. Image and Vision Computing 20, pp. 805-812.
- BIENIECKI, W., GRABOWSKI, S. (2005): Multi-pass approach to adaptive thresholding based image segmentation, Computer Engineering Dpt., TU Lodz, Poland, CADSM'2005, February 23, Lviv- Slavske, Ukraine.
- BORMAN, S., STEVENSON, R. (1998): Spatial Resolution Enhancement of Low-Resolution Image Sequences, A comprehensive Review with Directions for Future Research Journal, Vol 3, No. 13, pp. 15-30.

- BOUKHAROUBA, S., REBORDAO, J.M, REBORDAO, J.M, WENDEL, P.L. (1985): An amplitude segmentation method based on the distribution function of an image, *Computer Vision Graphics Image Process*, Vol 4, No. 29 (1985) 47, 59, pp. 12-25.
- BRADLY, D., ROTH, G. (2007): Adaptive Thresholding Using the Integral Image, Carleton University, Canada, National Research Council of Canada, Vol 3, No.4, pp. 20-35.
- BRUSS, A.R. (1977): Extracting Topographic Features From Elevation Data Using Contour Lines, Working Paper 146, Artificial Intelligence Laboratory, Massachusetts Institute of Technology, Cambridge, MA 02139.
- BUGAO, X., YAXIONG, H. (2003): Automated Pavement Cracking Rating System: A Summary, center for transportation research, the university of Texas at Austin, Project Summary Report 7-4975-S Project 7-4975.
- BULEN, S., MEHMET, S. (2004): Survey over Image Thresholding Techniques & Quantitative Performance Evaluation - A Survey Over Categories, *Journal of Electronic Imaging*, Vol 13, No.1, pp. 146-165.
- BURGOYNE, J.A, LAURENT, G., PUGIN, L., EUSTACE, G., FUJINAGA, I. (2007): A comparative survey of image binarisation algorithms for optical recognition on degraded pavement images, *IEE International Conference on Intelligent Robots and Systems*, Vol 13, ISMIR2007, pp. 509-515.
- BURSANESCU, L., BLAIS, F. (1997): Automated pavement distress data collection and analysis: a 3-D approach. In: *Proceedings of the international conference on recent advances in 3-D digital imaging and modeling*, pp. 311-7. 2005.
- BYOUNG, L., HOSIN, D.L. (2003): A Robust Position Invariant Artificial Neural Network for Digital Pavement Crack Analysis. Technical Report TRB2003-000996. <http://www.ltrc.lsu.edu>.
- C&EE (2003): Automated Management of Pavement Inspection System (AMPIS), Department of Civil and Environmental Engineering, University of California, Irvine, CA.,pp. 12-65, <http://shino8.eng.uci.edu/AMPIS.html>, last accessed on October 15, 2014.
- CHANG, Y., FU, A., YAN, H. (2006): A Hierarchical Approach in Multilevel Thresholding Based on Maximum Entropy and Bayes Formula, *Workshop on Visual Information Processing (VIP2001)*, Sydney, Australia, October 2006.
- CHENG, H.D, CHEN, J.R, GLAZIER, C., HU, Y.G. (1999): Novel approach to pavement distress detection based on fuzzy set theory, *J. Comput. Civ. Eng.*, Vol 13, No. 4, pp. 270-280.
- CHENG, H.D, MYOJIM, M. (1998): Automated Pavement Distress Detection System *Journal of Information Sciences* 1998, Vol 10, No.2, pp. 219 - 240.
- CHENG, W., HASSAN, T., EL-SHEIMY, N., LAVIGNE, M. (2008): Automatic Road Vector Extraction For Mobile Mapping Systems, *the International Archives of the Photogrammetry, Remote Sensing and Spatial Information Sciences*. Vol. XXXVII. Part B3b. Beijing, No.1, pp. 200-225.
- CHEN, Y., LEEDHAM, G. (2005): Decompose algorithm for thresholding pavement images, *IEE Proc.-Vis. Image Signal Process.*, Vol. 152, No. 6, December, pp. 12-30.
- CHI, Z., YAN, H. (1993): Map Image Segmentation Based On Thresholding and Fuzzy Rules, *Electronics Letters Journal*, Vol 29, No.21, pp. 1841-1843, October.
- CHOU, E.Y, SALARI, J. (2012): Transportation Informatics: An Image Analysis System for Managing Transportation Facilities-Phase 2, final report, the University of Toledo-University Transportation Center, Vol 21, No. 12, pp. 255-288.
- CHOU, J., NEILL, O'W, CHENG, H.D (1994): Pavement distress classification using neural networks, *Systems, Man, and Cybernetics*, *IEEE international Conference*, pp. 397-401.

- CHOW, C.K, KANEKO, T. (1972): Automatic Boundary Detection of the Left Ventricle from Cineangiograms, *Comp. Biomed. Res.*(5), Vol 3, No.12, pp. 388-410.
- CLINE, G., SHAHIN, M., BURKHALTER, J. (2003): Automated Data Collection for Pavement Condition Index Survey. *TRB 2003*, Vol 5, No. 14, pp. 265-288. <http://www.pavementconsultants.com>.
- CORMEN, T.H, LEISERSON, C., CHARLES, E., RONALD, L. (2001): *Introduction to Algorithms*, 2<sup>nd</sup> Edition, MIT Press and McGraw-Hill. ISBN 0-262-03293-7, pp. 40-60.
- CORMEN, T.H, LEISERSON, C., CHARLES, E., RONALD, L. (2009): *Introduction to Algorithms*, 3<sup>rd</sup> Edition, MIT Press and McGraw-Hill. ISBN 0-262-03384-4, pp. 200-240.
- COTTAFAVA, G., LEMOLI, G. (1969): Automatic Contour Plotting, *Comm. ACM* 12, IEE International Conference on Intelligent Systems, pp. 386-391.
- DAVID, H.L, JOE, J.K (2005): Development of a Manual Crack Quantification and Automated Crack Measurement System, Project TR-457 report, Public Policy Center, Civil and Environmental Engineering, University of Iowa, pp. 222-240.
- DAVID, M. (2005): Image-based editing and image-based animation, *Proceedings of Graphics Interface 2005 Victoria*, British Columbia SESSIO, pp. 219 – 226.
- DAVID, T., MCQUEEN, J. (2004): A Study of Manual vs. Automated Pavement Condition Surveys, *IEE International Conference on Intelligent Systems*, pp. 60-85. <http://www.eng.auburn.edu/users>.
- DILLEN COURT, M.B., SAMET, H., TAMMINEN, M. (1992): A general approach to connected-component labeling for arbitrary image representations. *J. ACM. IEE International Conference on Intelligent Systems*, pp. 233-250.
- DIN EN ISO 9000 (2005): *Quality management systems- Fundamentals and vocabulary (ISO 9000:2005)*. Trilingual version EN ISO 9000:2005.
- 3D-MAPPING (2014): 3D-Mapping GmbH company. <http://www.3d-mapping.de/de/wir-ueber-uns/>, last accessed on October 15, 2014.
- DONOHO, D.L, HUO, X. (2001): Beamlets and Multiscale Image Analysis, *International Journal of Computer Science and Network Security*, Vol. 8, No. 1, pp. 213-216.
- DON, R.H., BILL, G.H (1993): Progress in Supervised Neural Networks. *IEEE Signal Processing Magazine*, Vol 20, No.4, pp. 25-40.
- DROOGENBROECK, M., TALBOT, H. (1996): Fast Computation of Morphological Operations with Arbitrary Structuring Elements, *Pattern Recognition Letters Journal, USA*, Vol. 17, No.14, pp. 1451-1460. Available: 10.1016/S0167-8655(96)00113-4.
- EFFORD, N. (2000): *Digital Image Processing: A Practical Introduction Using Java™*. Pearson Education. Chap. 11, "Morphological image processing", last accessed on October 15, 2014.
- EFTHIMIOS, B., NIKOLAOU, N., PAPAMARKOS, N. (2007): Binarization in Color images, *Electrical and Computer Engineering Dpt, Image Processing and Multimedia, Lab, Wiley Periodicals, Inc*, Vol. 16, No.2, pp. 262–274.
- EL-SHEIMY, N. (1996): A mobile Multi-Sensor System for GIS Application in Urban Centers, in *ISPRS Conference Proceedings, Vienna, Austria, 9-19 July*. Vienna: International Society for Photogrammetry and Remote Sensing, Vol 3, No. 13, pp. 15-30.
- EL-SHEIMY, N. (2005): An Overview of Mobile Mapping Systems, In *Proceedings of the FIG Working Week 2005 and GSDI-8, Cairo, Egypt*, pp. 16-21, May 2015.
- ERGINA, K. (2010): A Binarization Algorithm specialized on Images and Photos, *Analysis and Recognition, 2010. Proceedings. 8th Int Conf ICDAR*, 29 Aug.-1 Sept., pp. 463-470.

- ERMLER, W.C., GLASSER, F.D, KERN, C.W. (1976): Borine Carbonyl. Bonding and Properties in the Single-Determinant Approximation, IEE International Conference on Intelligent Systems J. Amer. Chem. Soc. 98, 3799 (1976), pp. 3799-3807.
- FAN, L., FAN, L., TAN, C.L. (2003): Wavelet Diffusion for Image Denoising, Proceedings of the Seventh International Conference on Document Analysis and Recognition (ICDAR), 0- 7695-1960-1/03, IEEE, pp. 3564-3589.
- FGSV (Ed.), (2006): ZTV ZEB-STB\_1- Zusätzliche Technische Vertragsbedingungen und Richtlinien zur Zustands-erfassung und -bewertung von Straßen\_1. FGSV Verlag-Nr. 489, Köln.
- FHWA (2003): US Department of Transportation, Federal Highway Administration. 2003. Distress Identification Manual. FHWA-03-031. Mclean, VA. <http://www.tfhr.gov>, last accessed on October 15, 2014.
- FINDLEY, D.J, CUNNINGHAM, C.M, HUMMER, J.E (2011): Comparison of mobile and manual collection for roadway components, Transportation Research Journal, Vol. 19, No 3, pp. 521 - 540.
- FISHER, D. (1981): Contouring Algorithms overview, IEE International Conference on Intelligent Systems, pp. 400-450.
- FISHER, R., PERKINS, S., WALKER, A., WOLFART, E. (1996): Hypermedia Image Processing J. Wiley & Sons Publishing, ISBN: 2229-6093, pp. 40-55.
- FISHER, R., PERKINS, S., WALKER, A., WOLFART, E. (2003): Connected Component Labeling. IEE International Conference on Intelligent Systems, pp. 300-350.
- FLORIANI, L.D, MAGILLO, P., PUPPO, E. (2000): VARIANT: A System for Terrain Modeling at Variable Resolution, Geoinformatica Journal, Vol. 4, No. 3, pp. 287-315.
- FÖRSTNER, W. (1991): Statistische Verfahren für die automatische Bildanalyse und ihre Bewertung bei der Objekterkennung und vermessung, ISBN: 3-7696-9417-1, München : Verl. d. Bayer. Akad. d. Wiss. No.2.
- FRANCESCHINI, R.A (2007): Sorting Stably, in Place, with  $O(n \log n)$  Comparisons and  $O(n)$  Moves. Theory of Computing Systems Journal, Vol 40, No (4), pp. 327–353. doi:10.1007/s00224-006-1311-1.
- FRYER, C.G, MITCHELL, H.L, CHANDLER, J.H (2006): Application of 3D Measurement from images, ISBN: 4-8896-8817-1, Whittles Publishing, Caithness, Scotland,UK., pp. 135-655.
- FU, K.S, MUI, J.K. (1981): A survey on image segmentation, Pattern Recognition Journal. Vol 13, No. 3, 1981, pp. 3-16.
- FUNDAKOWSKI, R.A., GRABER, R.K., FITCH, E.L., SKOK, E.L., LUKANEN, E.O. (1991): Video Image Processing for Evaluating Pavement Surface Distress, Final Report, National Cooperative Highway Research Program 1-27, September, Washington, D.C. Transportation research board: National Cooperative Highway research program. Vol 22, No.5, pp. 400-550.
- GANDOLFI, S., BARBARELLA, M., RONCI, E., BURCHI, A. (2007): Close photogrammetry and laser scanning using a mobile mapping system for the high detailed survey of a high density urban area, Italy, IEE International Conference on Intelligent Systems, pp. 200-215.
- GATOS, B.I, PRATIKAKIS, S., PERANTONIS, J. (2004): Locating objects in pavement Collection images, Lecture Notes in Computer Science Springer, Vol 3025 Methods and Applications of AI, ISBN 978- 540-21937-8, pp. 476-485.
- GEORGOPOULOS, A., LOZIOS, A., FLOUDA, A. (1995): Digital Image Processing as a tool for Pavement Distress Evaluation, ISPRS Journal of Photogrammetry and Remote Sensing 50(1) 23-33 0924-2716/95/\$09.50 © 2005 Elsevier Science B.V. ISPRS Journal of Photogrammetry and Remote Sensing, Vol. 50, issue 1, pp. 23-33.
- GEOVAN (2014): GEOVAN company from Geo-Span Corporation. <http://www.geospan.com4/>, last accessed on October 15, 2014.

- GERARDO, W.F, AL-QADI, I.L, LOULIZI, A., LA-HOUAR, S., MCGHEE, K., CLARK, T. (2004): Field Investigation of High Performance Pavements in Virginia, Report submitted to Virginia Department of Transportation. Report No., VTRC 05-CR9. Project No.: 70983. Contract No. 04-0627-10, pp. 300-350.
- GIE, (2014): Distressview, GIE Technologies Inc. <http://www.gietech.com/LVS.htm#Roughness4/>, last accessed on October 15, 2014.
- GILLIERON, P.Y, SKALOUD, J., LEVET, Y. (2001): A Mobile Mapping System for Automating Road Data Capture in Real Time, 5th Conference on Optical 3D Measurement Techniques, Vienna, Oct, pp. 54-58, (2001.6).
- GIRARDELLO, R. (2002): Automated Management of Pavement Inspection System (AMPIS), Universita Degli Studi Di Padova. Final Report, National Cooperative Highway Research Program 1-40, September, Washington, D.C. Transportation research board: National Cooperative Highway research program. Vol 12, No.5, pp. 300-450
- GONTRAN, H., SKALOUD, J., GILLIERON, P.Y. (2003): A Mobile Mapping System for Road Data Capture via Single Camera, 6th optical 3D Measurement Techniques Conference, Zurich, Switzerland, September 22-25, pp. 30-58, (2003.5).
- GONZALEZ, R., WOODS, R. (1992): Digital Image Processing, Pearson Prentice Hall, First Impression, Upper Saddle River, New Jersey, ISBN: 0-201-18075-8, pp. 665- 682.
- GONZALEZ, R., WOODS, R. (2002): Digital Image Processing, 2<sup>nd</sup> edition, Pearson Prentice Hall , 2002, Prentice-Hall Inc., Upper Saddle River, New Jersey, pp. 75-278.
- GONZALEZ, R., WOODS, R. (2008): Digital Image Processing, 3<sup>rd</sup> edition, Pearson Prentice Hall, Upper Saddle River, New Jersey, Upper Saddle River, New Jersey, pp. 100-250.
- GROEGER, J.L, STEPHANOS, P., DORSEY, P., CHAPMAN, M. (1960): Implementation of Automated Network-level Crack Detection Processes in Maryland, Transportation Research Record, Transportation Research Board, National Research Council, Washington, D.C. 2003, Vol.12, No.3, pp. 109-116.
- GUNARATNE, M., MRAZ, A., SOKOLIC, I. (2003): Study of the Feasibility of Video Logging with Pavement Condition Evaluation Florida Department of Transportation. Tallahassee, Florida. 2003. Report No. BC-965. Performing Organization code CEE/FDOT/168-LO. Final Report April, pp. 200-230.
- HARALICK, R.M, SHAPIRO, L.G (1985): Image Segmentation Techniques, Computer vision, graphics, and image processing Journal, Vol. 29, No.11, pp. 100-132.
- HECKMAN, A., MEYER, L. (1980): NICEPLOT Manual (Version 2), Materials Research Laboratory Computer Facility, University of Illinois, Urbana, IL 61801 (April), Vol 10, No.7, pp. 540-650.
- HE, G. (2002): Design and Application of the GPSVision Mobile Mapping System, ISPRS Congress, Commission II. China, August 20-23. Vol. XXXIV, Part 2, pp. 163-168.
- HE, L., CHAO, Y., SUZUKI, K. (2008): A Run-Based Two-Scan Labeling Algorithm. IEEE Transactions on Image Processing Journal, Vol 17, No 5: 749-756.doi:10.1109/TIP.2008.919369. PMID 18390379, pp. 43-55.
- HEROLD, M., ROBERTS, D., NORONHA, V., SMADI, O. (2008): Imaging Spectrometry and Asphalt Road Surveys, Transportation Research Emerging Technologies Journal, Vol 16, Issue 2, pp. 153-166 ,April.
- HISASHI, T., TATSUhide, N. (2000): Geo-Spatial Grasping of pavement with mobile mapping, Japan, International Archives of Photogrammetry and Remote Sensing Journal, Vol. XXXIII, Part B5. Amsterdam, No. 3, pp. 322-350.



- HOSIN, L. (1991): Application of Machine Vision Techniques for the Evaluation of Highway Pavements in Unstructured Environments. IEEE-91 ICAR, 7803-0078/91/0600- 1425, Vol 12, No. 7, pp. 155-170.
- HOWE, R., GLEMENA, G.G (1987): An Assessment of the Feasibility of Developing and Implementing an Automated Pavement Distress Survey System Incorporating Digital Image Processing, Final Report of Project, Virginia Transportation Research Council, November, pp. 366-455.
- HSU, C.J, CHEN, C.F, LEE, C., HUANG, S.M. (2001): Airport Pavement Distress Image Classification Using Moment Invariant Neural Network. 22<sup>nd</sup> Asian Conference on Remote Sensing and processing (CRISP), Singapore, pp. 200-250.
- HUNG, C.C, GIRARDELLO, R., SOELLER, T., SHINOZUKA, M. (2003): Automated Management for Pavement Inspection System, Proceedings of Spie's Smart Structures and Materials Conference, San Diego, CA, March, pp. 500-550.
- IC (2014): Digital Imaging System, International Cybernetics Corporation. <http://www.internationalcybernetics.com/imagingvehicle.html> last accessed on October 15, 2014.
- ISHIKAWA, K., AMANO, Y., HASHIZUME, T., TAKIUCHI, J., KAJIWARA, N. (2007): A Mobile Mapping System for Precise Road Line Localization Using a Single Camera and 3D Road Model,. Received October 20, 2006; accepted February 6, IEE International Conference on Intelligent Robots and Systems, pp. 41-55.
- JACHING, C., WENDE, O'N., CHENG, H.D. (1994): Pavement Distress Classification Using Neural Networks. IEEE-94, 0-7803-2129-4/94. Vol 35, No. 6, pp. 250-265.
- JAIN, A. (1986): Fundamentals of Digital Image Processing, prentice hall international edition, Prentice-Hall Inc., 1986, pp. 40-60.
- JAIN, R., KASTURI, R., SCHUNCK, B. (1995): Computer Vision, MIT Press and McGraw-Hill, San Diego.ISBN: 0-07-032018-7.
- JAMES, M. (1988): Pattern Recognition, John Wiley and Sons, New York.
- JAVIDI, B., STEPHENS, J., KISHK, S., NAUGHTON, T., MCDONALD, J., ISSAC, A. (2003): Pilot for Automated Detection and Classification of Road Surface Degradation Features, JHR 03-293, November. Vol 30, No. 4, pp. 31-55.
- JIAN, J.L. (2002): Development of a pavement crack detection method for measuring pavement crack depth on Florida Roadways University of South Florida Summary of Final Report, BB-884, March, pp. 300-450
- Ji, H., DO, Q.D.M., DOWNTON, A.C., KIM, J.H. (2005): A Comparison of Binarization Methods for pavement images, Proceeding of the 8th International Conference on Document Analysis and Recognition (ICDAR'05) 2005 IEEE. Vol 22, No.3, pp. 100-250
- JONES, R.L. (1971): A Generalized Digital Contouring Program, NASA Langley Research Center, Hampton, Virginia, NASA TN D-6022, pp. 78-99.
- KAMEL, M., ZHAO, A. (1993): Extraction of Binary objects from Grey Level Pavement Images, CVGIP: Graphical Models and Image Processing Journal, Vol.55, No.3, pp. 203-217.
- KAPUR, J.N, SAHOO, P.K, WONG, A.K.C. (1985): A new method for gray-level picture thresholding using the entropy of the histogram, Computer Vision Graphics Image Process Journal. 29 -273}28, Vol 9, No.2, pp. 150-165.
- KAVALLIERATOU, E., ANTONOPOULOU, H. (2005): Cleaning and Enhancing Images, ACIVS 2005, LNCS 3708, 2005. Springer-Verlag, Vol 26, No.9, pp. 681 – 688.
- KELVIN, C.P, QIANG, L., WEIGUO, G. (2007): Wavelet-Based Pavement Distress Image Edge Detection with a Trouis Algorithm, Transportation Research Record, Journal of the Transportation Research Board, Vol. 55, No. 2024, pp. 73-8.

- KELVIN, W., ROBERT, E. (1999): Investigation of Image Archiving for Pavement Surface Distress Survey. University of Arkansas, Department of Civil Engineering Fayetteville. <http://www.mackblackwell.org/research>. Transportation Research Record, Journal of the Transportation Research Board, Vol.1 40, No. 2035, pp. 18-40.
- KELVIN, W., WATKINS, W.Y.T.E, SUBASH, K. (2002): Digital Distress Survey of Airport Pavement Surface. Federal Aviation Administration Airport Technology Transfer Conference 2002. <http://www.airporttech.tc.faa.gov>, pp. 40-55.
- KHATTAK, J. A., HUMMER, J.A, KARIMI, H.A (2000): New and Existing Roadway Inventory Data Acquisition Methods, Journal of Transportation and statistics, December, 2000, Vol 3, No. 13, pp. 33-46.
- KITTLER, J., ILLINGWORTH, J. (1985): On threshold selection using clustering criteria, IEEE Trans. Systems, Man Cybernet. SMC-15, Vol 40, No. 54, pp. 652-655.
- KITTLER, J., ILLINGWORTH, J. (2006): Minimum error thresholding, Pattern Recognition Journal, Vol. 19, issue 1, pp. 41- 47.
- KITTLER, J., ILLINGWORTH, J., FÖGLEIN, J. (1985): Threshold selection based on a simple image statistic, Comput. J&& Graphics Image Process Journal. Vol 30, No.13, pp. 125-147.
- KLAIBER, M., ROCKSTROH, L., WANG, Z., BAROUD, Y., SIMON, S. (2012): A Memory-Efficient Parallel Single Pass Architecture for Connected Component Labeling of Streamed Images. IEE International Conference on Intelligent Robots and Systems, pp. 45-65.
- KOHLER, R. (1981): Image Segmentation by Adaptive Thresholding, 15 (1981). IEE International Conference on Intelligent Robots and Systems, pp. 30-55.
- KOUTSOPOULOS, H.N, DOWNEY, A.B. (2006): Primitive-based classification of pavement cracking images, Journal of Transportation Engineering, Vol. 19, issue 3, pp. 402-418.
- KUKKO, A., ANDREI, C.O, SALMINEN, V.M., KAARTINEN, I., CAPEK, K. (2007): Road Environment Mapping System of the Finnish Geodetic Institute – FGI Roamer. In Proceedings of the ISPRS Workshop Laser Scanning 2007 and SilviLaser 2007, Espoo, Finland; Rönnholm, P.; Hyypä, H.; Hyypä, J. Eds.; Vol. 40, No.6, pp. 241-247, Sept. 12-14.
- KUTZNER, A., KIM, P-S. (2008): Ratio Based Stable In-Place Merging. Lecture Notes in Computer Science 4978. Springer Berlin Heidelberg, pp. 246–257. Retrieved 2014-03-14.
- KWEON, I.S, KANADE, T. (1992): High-Resolution Terrain Map from Multiple Sensor Data, IEEE Transaction on Pattern Analysis and Machine Intelligence Journal, Vol. 14, No. 2, pp. 278-292.
- LAURENT, J., TALBOT, M., DOUCET, M. (1997): Road Surface Inspection Using Laser Scanners Adapted for the High Precision 3D Measurements of Large Flat Surfaces, 1<sup>st</sup> International Conference on Recent Advances in 3-D Digital Imaging and Modeling (3DIM '97), pp. 303-310.
- LEEDHAM, G. (2003): Comparison of Thresholding Algorithms for Background Segmentation in Difficult Images, Proc of 7th International Conference on Document Analysis and Recognition, ICDAR 2003, IEEE18. Vol 30, No. 15, pp. 203-210.
- LEE, H., KIM, J. (2005): Development of a Crack Type Index, Transportation Research Record: Journal of the Transportation Research Board, Vol. 70, No. 1940, pp. 99–109.
- LEE, H., WEISSMAN, M.A, POWELL, J.P (1991): Highway Inventory Features Using Stereoscopic Imaging System, in Application of Advance Technologies in Transportation Engineering, Minneapolis, MN, 18-21 August. Vol 3, No. 13, pp. 15-30.
- LEE, S.Y, CHOI, K.H, JOO, I.H., CHO, S.I., PARK, J.H (2006): Design and Implementation of 4S-Van: A Mobile Mapping System,.ETRI Journal, Vol. 28, No. 3, June, pp. 463-480.

- LE, S.U, CHUNG, S.Y, PARK, R.H. (1990): A comparative performance study of several global thresholding techniques for segmentation, *Computer Vision Graphics Image Process Journal*. 29-273}28. Vol. 29, No. 3, pp. 250-266.
- LEVINE, M.D, NAZIF, A.M (1985): Dynamic measurement of computer generated image segmentations, *IEEE Trans. Pattern Anal Journal. Mach. Intell. PAMI-7*, Vol.22, No.9, pp. 155-164
- LIAPIS, S., SIFAKIS, E., TZIRITAS, G. (2004): Color and Texture Segmentation using Wavelet Frame Analysis Deterministic Relaxation and Fast Marching Algorithms *Journal of Visual Communication and Image Representation*, Vol. 15 (2004), No. 5, pp. 1–26.
- LI, H., LIU, S., WANG, H. (2011): Separation of Objects with Unclear Edges from the Non-uniform Background, *Chinese Journal of Electronics*, Vol.20, No. 1, January, pp. 1-40.
- LI, L., CHAN, P., RAO, A., LYTTON, R.L. (1991): Flexible pavement distress evaluation using image analysis, *Proceedings of the Second International Conference on Applications of Advanced Technologies in Transportation Engineer*, August, pp. 473-477.
- LIU, J., GAO, J., SHEN, Q (2009): A background separation method of nonuniform image segmentation, *school of mechanical and electronics engineering, China*, 978-1-4244-2800-7/09, *IEE International Conference on Intelligent Robots and Systems*, Vol 25, No. 9, pp. 30-55.
- LEHMANN+PARTNER (2014): Lahmann+Partner GmbH company. <http://vectragermany.com/technologie/system-stier>, last accessed on October 15, 2014.
- LUHMANN, T. (2003): *Nahbereichsphotogrammetrie, Grundlagen, Methoden und Anwendungen*, 2. Auflage Book ISBN (3-87907-398-8). Herbert Wichmann Verlag. Heidelberg, Germany.
- LUHMANN, T., ROBSON, S., KYLE, S., HARLEY, L. (2006): *Close Range Photogrammetry, Principles, Methods, and Application*, Institute for Applied Photogrammetry and Geoinformatics, University for Applied Sciences, Oldenburg, Germany, and University College London, UK, Whittles Publishing, Caithness, Scotland, UK, ISBN (1-870325-50-8).
- LYNCH, J.J (2012): Development of a Computer Interface and Database for the Evaluation of Pavement by the PASER Method, Report No: MIOH UTC TS43 2012-Final, Department of Civil and Environmental Engineering, University of Detroit Mercy, Detroit. Transportation research board: National Cooperative Highway research program, pp. 250-450.
- MADEIRA, S., GONCALVES, J., BASTOS, L. (2008): Low Cost Mobile Mapping System For Urban Surveys, 13th FIG Symposium on Deformation Measurement and Analysis, 14th IAG Symposium on Geodesy for Geotechnical and Structural Engineering, LNEC, LISBON May 12-15, pp. 150-450
- MANDLI (2014): Mandli communications, Inc., <http://www.mandli.com/home.html>, last accessed on October 15, 2014.
- MARTIN, H., ROBERTS, D., NORONHA, V., SMADI, O. (2008): Imaging Spectrometry and Asphalt Road Surveys, *Transportation Research Emerging Technologies Journal*, Vol. 16, Issue 2, April 2008, pp. 153-166.
- MASER, K.R. (1987): Computational techniques for automating visual inspection. Department of Civil Engineering, MIT, Cambridge, Mass. *Transportation Research Emerging Technologies Journal*, Vol. 29, No.18, pp. 373-577.
- MASTANDREA, A., SWINDALL, B., KLASSEN, G. (1995): Development and Implementation of an Automated Facility Inventory System, *Transportation Research Record 1500*: 127-33.
- MATLAB (2014): Matlab Help- (2012) Mathworks knowledge <http://www.mathworks.com/help/matlab/>, last accessed on October 15, 2014.

- MCGHEE, K.H. (2004): Automated pavement distress collection techniques—a synthesis of highway practice. Report for national cooperative highway research program (synthesis 334), transportation research board of the national academies. National Cooperative Highway research program, pp. 300-450
- MEHMET, S., SANKUR, B. (2004): Survey over image thresholding techniques and quantitative performance evaluation, *Journal of Electronic Imaging*, January, Vol. 13, No.1, pp. 146– 165.
- MEIGNEN, D., BERNADET, M., BRIAND, H. (1997): One application of neural networks for detection of defects using video data bases: identification of road distresses. In: *Proceedings of the eighth international workshop on database and expert systems applications (DEXA '97)*, pp. 459–64.
- MICHAEL, B.W. (1992): The PAVUE real-time automated pavement distress analyzer, paper presented in the pavements section of the 1992 TAC Annual conference in Quebec City-Canda, September, pp. 14-17.
- MILSTEIN, N. (1998): *Image Segmentation by Adaptive Thresholding*, Technion – Israel Institute of Technology, the Faculty for Computer Sciences, Spring, last accessed on October 15, 2014.
- MOHAJERI, M.H, MANNING, P.J (1991): ARIA™, An Operating System of Pavement Distress Diagnosis by Image Processing. *Transportation Research Record* 1311, TRB, National Research Council, Washington, D.C., Vol. 40, No. 12, pp. 120-130.
- MOHIDEEN, S.K, PERUMAL, S.A, SATHIK, M.M. (2008): Image De-noising Using Discrete Wavelet Transform, *International Journal of Computer Science and Network Security*, Vol. 8, No. 1, pp. 213-216.
- MOTWANI, M.C, GADIYA, M.C, FREDERICH, C. (2004): Survey of Image Denoising Techniques, *Proceedings of GSPx*, Santa Clara Convention Center, Santa Clara, CA., pp. 219-225.
- MRAZ, A., GUNARATNE, M., NAZEF, A. (2008): Guidelines for Performance Assessment of Digital Imaging Systems Used in Highway Applications, doi: 10.1061/~ASCE!0733-947X~2005!131:6(429), *Journal of Transportation Engineering*, ASCE, , Vol. 25, No. 10, pp. 140-250.
- NIBLACK'S, W. (1985): *An Introduction to Digital Image Processing*, 1<sup>st</sup> Edition, Strandberg Publishing Company Birkeroed,Denmark, ISBN: 87-872-0055-4.
- NIEMEIER, W. (2008): *Ausgleichsrechnungsrechnung, Statistische Auswertemethoden*, ISBN: 978-3-11-019055-7, copyright 2008 by Walter de Gruyter GmbH & Co. KG, Berlin.
- NIKOLAOS, N., DIMITRIOS, V. (2008): *A Binarization Alogrithms*, Department of Computer Science Technology & Telecommunications, TEI of Larisa, Greece, 12th WSEAS International Conference on COMMUNICATIONS, Heraklion, Greece, July 23-25, pp. 55-70.
- NWPMAM (1992): *SHARP Distress Identification Field Rating Manual for Asphalt Pavement*. NorthWest Pavement Management Association. <http://www.wsdot.wa.gov/ta/T2Center/Mgt.Systems/PavementTechnology/PavementBook.pdf>, last accessed on October 15, 2014.
- O'GORMAN, L. (1994): Binarization and Multi-thresholding of Images Using Connectivity, *CVGIP: Graphical Models Image Process Journal*, November, Vol.56, No.6, pp. 494-506.
- OISHI, T., YAMADA, K., TAKEDA, H., KAWAI, T. (2008): Development of Simple Mobile Mapping System for the Construction of Road Foundation Data, Japan. *IEE International Conference on Intelligent Robots and Systems*, pp.30-55.
- OSTU'S, N. (1979): A thresholding selection method from gray-level histogram, *IEEE Trans. Systems Man Cybernet Journal*, Vol. 22, No.7, pp. 62-66.
- PAPAMARKOS, N. (2001): *Digital Processing and Image Analysis*, Pearson Prentice Hall, Athens, Giourdas.

- PAPAMARKOS, N., GATOS, B. (1994): A new approach for multilevel threshold selection CVGIP: Graphical Models Image Process Journal. Vol. 56, No. 5, pp. 357-370.
- PATHVIEW (2014): Pathway Services, Inc. <http://www.pathwayservices.com/>, last accessed on October 15, 2014.
- PAVLIDIS, T. (1977): Structural Pattern Recognition, Springer-Verlag, Heidelberg/New York.
- PAVLIDIS, T. (1982): Algorithms for Graphics and Image Processing, Computer Science Press Journal, Rockville, Maryland. Vol. 44, No. 8, pp. 357-370.
- PETRIE, G. (2010): An Introduction to the Technology Mobile Mapping Systems, GEOInformatics Journal, Vol. 13, No. 2 January/February, pp. 444-466.
- PETROU, M., BOSDOGIANNI, P. (1999): Image Processing, The Fundamentals, 1<sup>st</sup> Edition. John Wiley & Sons.Ltd, Online ISBN: 9780470841907.
- PING, W., XIANG, L., FANG, H. (2004): Research on Mobile Mapping System and its Application, Map Asia Conference GIS development.net, pp. 290-296.
- PRATT, W.K (1978): Digital Image Processing, 3<sup>rd</sup> Edition, John Wiley & Sons. Ltd, New York, ISBN 0-471-22132-5.
- RABABAAH, H., WOLFER, J., VRAJITORU, D. (2005): Asphalt Pavement Crack Classification: a Comparison of GA, MLP, and SOM. Proceedings of the Genetic and Evolutionary Computation Conference (GECOCO'05 and SIGEVO 1), Washington, DC, late breaking papers. Computer and Information Sciences, Indiana University South Bend, pp. 300-326.
- RADIM, k., ODSTRCILIK, J., JIRI, J., VRATISLAV, H. (2011): Illumination correction and contrast equalization in color fundus images, 19th european signal processing conference, Barcelona, Spain, August-September, pp. 111-121.
- RALUCA, B. (2010): Computer Vision Group, TUC-N. <http://users.utcluj.ro/~raluca/ip2014/ipl07e.pdf>, last accessed on October 27, 2014.
- RANDOLPH, T., SMITH, M. (2008): Enhancement of images using a binary angular representation, Proceedings of, Int Symp on Intelligent Multimedia, Video and Speech Processing, 2008. Hong Kong, China, ISBN: 962-85766-2-3, pp. 111-121.
- REITERER, A., DAMBACHER, M., MAINDOEFER, I., HÖFLER, H., EBERSBACH, D., FREY, C., SCHELLER, S., KLOSE, D. (2012): Neue Laserscanner-Technologie zur Ebenheitsmessung von Straßenbelägen. VDV-Magazin, 63/2012, Nr.5, pp. 376-379.
- ROSENFELD, A., KAK, A.C. (1982): Picture Processing, 2<sup>nd</sup> Edition, Vol. 2, Academic Press, New York/London.
- RUKUHARA, T., TERADA, k., NAGAO, M. (1990): Automatic Pavement-Distress-Survey System, Journal of Transportation Engineering, Vol. 116, No.1, pp. 280-286.
- SAHOO, P.K, SOLTANI, S., WONG, A.K.C., CHEN, Y.C. (1988): A survey of thresholding technique, Comput. Vision Graphics Image Process Journal. Vol. 41, No,2, pp. 233-260.
- SALARI, E. (2012): Pavement Distress Evaluation using 3D Depth Information from Stereo Vision., Report No: MIOH UTC TS43 2012-Final, Department of Electrical Engineering and Computer Science, University of Toledo, Toledo, OHIO. Transportation research board: National Cooperative Highway research program, pp. 200-430
- SALARI, E., CHOU, E.Y-J., LYNCH, J., DUTTA, U. (2010): Transportation Informatics: Advanced Image Processing Techniques for Automated Pavement Distress Evaluation, Report No: MIOH UTC TS18p2 2010-Final, Department of Electrical Engineering and Computer Science, University of Toledo, Toledo, OHIO, and Department of Civil and Environmental Engineering, University of Detroit Mercy, Detroit. Transportation research board: National Cooperative Highway research program, pp. 255-450

- SALVATORE, C., ALESSANDRO, D.G, BATTIATO, S. (2006): Evaluation of Pavement Distress Surface Analysis Using Digital Image Collection Analysis, Seventh International Congress on Advances in Civil Engineering, October 11-13, Yildiz Technical University, Istanbul, Turkey, pp. 114-134.
- SAMET, H., TAMMINEN, M. (1988): Efficient Component Labeling of Images of Arbitrary Dimension Represented by Linear Bintree. *IEEE Transactions on Pattern Analysis and Machine Intelligence* 10: 579. doi:10.1109/34.3918. Vol 22, No.1, pp. 40-60.
- SANKUR, B., SEZGIN, M. (2004): A Survey Over Image Thresholding Techniques And Quantitative Performance Evaluation, *Journal of Electronic Imaging* January., Vol.13, No. 1, pp. 146- 165.
- SAUVOLA, J., PIETIKAKINEN, M. (2000): Adaptive pavement image binarization Machine Vision and Media Processing Group, Infotech Oulu, University of Oulu, P.O. BOX 4500, FIN-90401 Oulu, Finland, *Pattern Recognition Journal*, Vol. 33, No.4, pp. 225-236.
- SCHWARZ, K.P, MARTELL, H.E, EL-SHEIMY, N., LI, R., CHAPMAN, M.A., COSANDIER, D. (1993): VIASAT—a mobile highway survey system of high accuracy. In: *Proceedings of the IEEE vehicle navigation and information systems conference*, pp. 476–811.
- SCHWEITZER, J., SCHWIEGER, V. (2011): Modeling of Quality for Engineering Geodesy Processes in Civil Engineering, *Journal of Applied Geodesy* (2011), Vol. 5, No.1, pp. 13-22 @ de Gruyter 2011.
- SCHWIEGER, V., WENGERT, M., ZHANG, L. (2010): A Quality Model for Residential Houses Construction Processes, TS 10D-Building Measurement and Modelling, *Proceedings of the XXIV FIG International Congress 2010*, Sydney, Australia, 11-16 April, published on CD only.
- SEAN, B., STEVENSON, R. (1998): Spatial Resolution Enhancement of Low-Resolution Image Sequences, A comprehensive Review with Directions for Future Research, University of Notre Dame, Technology. *IEE International Conference on Intelligent Robots and Systems*, pp. 40-55.
- SEO, J.D, LEE, J.C, LEE, Y.D. (2004): Development of Road Information System Using Digital Photogrammetry, XXth ISPRS Congress, Commission II, July 12- 23 July, Istanbul, Turkey, pp. 30-44.
- SHAHIN, M.Y. (2002): *Pavement Management for Airports, Roads, and Parking Lots*, 2<sup>nd</sup> edition, K; uwer Academic Publishers Group, 101 Philip Drive, Assinippi Park, Norwell, Massachusetts 02061.
- SHAHIN, M.Y, WALTHER, J.A. (1990): *Pavement Maintenance Management for Roads and Streets Using the PAVER System*, USACERL Technical Report project, M-90/05, Vol 12, No. 6, pp. 280-290.
- SINGH, P., GARG, A.K. (2011): Non Uniform Background Removal using Morphology based Structuring Element for pavement images, *International Journal of Computer Applications* (0975-8887), Vol. 33, No.6, Novemeber, pp. 256-276.
- SOLIHIN, Y., LEEDHAM, C. (1999): Integral Ratio: A New Class of Thresholding Techniques for Images, *IEEE Transactions on Pattern Analysis and Machine Intelligence Journal*, Vol. 21, No.8, pp. 761-768.
- SOSS, M. (2003): Proof of correctness of Square Tracing algorithm when both pattern and background are 4-connected, [www.imageprocessingplace.com/countouring\\_tracing.pdf](http://www.imageprocessingplace.com/countouring_tracing.pdf), last accessed on October 15, 2014.
- SUZUKI, K., HORIBA, I., SUGIE, N. (2003): Linear-time connected-component labeling based on sequential local operations. *Computer Vision and Image Understanding Journal (Comput. Vis. Image Underst.)* 89: 1. doi:10.1016/S1077-3142(02)00030-9, Vol 12, No. 3, pp. 30-45.

- TALAYA, J., BOSCH, E., ALMUS, R., SERRA, A., BARON, A. (2004): GEOVAN: The Mobile Mapping System from the ICC. In Proceedings of the 4th International Symposium on Mobile Mapping Technology (MMT' 2004), Kunming, pp. 12-22.
- TAO, C. (2000): Mobile mapping technology for road network data acquisition. *Journal of Geospatial Engineering*; Vol. 2, No. 2, pp. 1– 14.
- TAO, C.V. (1998): A Review of Mobile Mapping Technology for Road Network Data Acquisition, *Journal of Geospatial Engineering*, Vol. 2, No.2, pp. 30-43.
- TAO, C.V. (1999): Innovations on Multi-Sensor and Multi-Platform Integrated Data Acquisition, Dept. of Geomatics Engineering, The University of Calgary 2500 University Drive, NW, Calgary, Alberta, Canada T2N 1N4. *Journal of Geospatial Engineering*, Vol. 2, No.2, pp. 2-26.
- TAREK, A., MONEM, A., OLOUFA, A., MAHGOUB, H. (2005): Asphalt Crack Detection Using Thermography, University of Central Florida Center for Advanced Transportation Systems Simulation (CATSS) Inframation Proceedings 2005 ITC 108 A 2005-06-01, pp. 400-555.
- TEOMETE, E., VIREN, R.A., HALIL, C., SMADI, O. (2005): Digital Image Processing for Pavement Distress Analysis, Proceedings of the 2005 Mid-Continent Transportation Research Symposium, Ames, Iowa, © 2005 Iowa State University, pp. 6-36.
- TIMOTHY, E. (2004): Semi-automated detection of defects in road surfaces, Master thesis at Monash University, Australia Clayton Campus, <http://www.csse.monash.edu.au/hons/projects/2004/Timothy.Evans/Research.pdf>.
- TOUSSAINT, G. (1997): Course Notes: Grids, connectivity and contour tracing [www.imageprocessingplace.com/countouring\\_tracing.pdf](http://www.imageprocessingplace.com/countouring_tracing.pdf), last accessed on October 15, 2014.
- TRIER, O.D, JAIN, A.K. (1995): Goal Directed Evaluation of Binarisation Methods, Workshop on Performance versus Methodology in Computer Vision 17, 3 (Aug. 1995), Proc. NSP/ARPA 95, pp. 209-217.
- TRIER, O., TAXT, T. (1995): Improvement of Integrated Function Algorithm for Binarization of Images, *Pattern Recognition Letters Journal*, March., Vol. 16, No. 3, pp. 277-283.
- TSAI, W.H. (1985): Moment-preserving thresholding: A new approach, *Computer. Vision, Graphics and Image Process Journal*. 29, 1985, Vol 3, No.1, pp. 377-393
- TSAO, S., KEHTARNAVAZ, N., CHAN, P., LYTON, R. (1994): Image-based expert-system approach to distress detection on CRC pavement, *Journal of Transportation. Engineering*, Vol. 120, No. (1), pp. 52– 64.
- UNICOM-UMAP (2014): Unicom-Umap compay. [www.saudiunicom.com](http://www.saudiunicom.com), last accessed on October 15, 2014.\_
- VENTZAS, D. (1994): Edge Detection Techniques in the Industry, *Journal of Advances in Modelling & Analysis Series B, AMSE*, Vol. 29, No. 2, pp. 57-64.
- VERA, I., THENOUX, G., SOLMINIHAX, H.D, ECHAVEGUREN, T. (2010): Technical assessment model for the performance of flexible pavement maintenance, *Journal of Revista de la Construcción*, Vol. 9, No. 2, pp. 76 – 88.
- VERNON, D. (1991): *Machine Vision*, 1<sup>st</sup> Edition, Prentice-Hall, Wiley, NewYork.
- VINCENT, L. (1993): Morphological Grayscale Reconstruction in Image Analysis: Applications and Efficient Algorithms, *IEEE Transactions on Image Processing Journal*, April, pp. 176-201.
- WALDEN, A.R (1972): Quantitative Comparison of Automatic Contouring Algorithms, Kansas Geological Survey, K.O.X. Technical Report, The University of Kansas, Lawrence, Kansas, pp. 276-290.
- WALKER, D. (2004): Pavement Surface Evaluation and Rating-Asphalt Airfield Pavements, Manual for PSERA, Federal Aviation Administration, pp. 300-320.

- WANG, K., ELLIOT, R. (1999): Investigation of Image Archiving for Pavement Surface Distress Survey, University of Arkansas, Department of Civil Engineering Fayetteville. <http://www.mackblackwell.org/research.pdf>, Transportation research board, pp. 200-220.
- WANG, S., HARALICK, R.M. (2002): A segmentation system based on thresholding, Computer Vision Graphics Image Process Journal. Vol. 25, No.3, pp. 46-67.
- WELLNER, P.D. (1993): Adaptive thresholding for the digitaldesk, Tech. Rep. EPC-93-110, EuroPARC. Transportation research board: National Cooperative Highway research program, pp. 666-688.
- WESZKA, J.S. (1978): A survey of threshold selection techniques, Computer Vision Graphics Image Process Journal. Vol. 7, No.2, pp. 259-265.
- WILLIAM, K.P. (1991): Digital Image Processing, 2<sup>nd</sup> edition, John Wiley & Sons, 1991 Image Processing Toolbox, User's guide, Version 3, The Mathworks [http://www.mathworks.com/access/helpdesk/help/pdf\\_doc/images/images\\_tb.pdf](http://www.mathworks.com/access/helpdesk/help/pdf_doc/images/images_tb.pdf), pp. 233-280.
- WILTSCHKO, T. (2004): Sichere Information durch infrastrukturgestützte Fahrerassistenzsysteme zur Steigerung der Verkehrssicherheit an Straßenknotenpunkten, PhD thesis, University of Stuttgart, 2004, available at [http://elib.uni-stuttgart.de/opus/volltexte/2004/1929/pdf/Dissertation\\_Thomas\\_Wiltschko.pdf](http://elib.uni-stuttgart.de/opus/volltexte/2004/1929/pdf/Dissertation_Thomas_Wiltschko.pdf), last accessed on October 2, 2015.
- WILTSCHKO, T., KAUFMANN, T. (2005): Probabilistic Model to describe and evaluate information Quality, Final Project EDC-11145 EURORoads/28646, Version 1.
- WU, A.Y, HONG, T.H, ROSENFELD, A (1982): Threshold selection using quadtrees, IEEE Transportation Pattern Analysis Journal. Mach. Intell. PAMI-4, 1982, Vol.2, No.1, pp. 90-94.
- WU, S., AMIN, A. (2003): Automatic Thresholding of Gray-level Using Multi-stage Approach, Proceedings of the 7th International Conference on Document Analysis and Recognition (ICDAR 2003), 0-7695-1960-1/03, IEEE, pp. 60-80.
- WU, V., MANMATHA, R., RISEMAN, EM. (2005): An Automatic System to Detect and Recognize Objects In Images, IEEE Transactions on Pattern Analysis and Machine Intelligence Journal, November, Vol. 21, No. 11, pp. 1224-1229.
- XIAOLEI, H., KIM, E., HEFLIN, J. (2011): Finding VIPS - A Visual Image Persons Search Using a Content Property Reasoner and WeBontology, Proceeding. of IEEE International Conf. on Multimedia & Expo (ICME), pp. 1260-1280.
- YANG, J.D, CHEN, Y.S, HSU, W.H. (1994): Adaptive Thresholding Algorithm And Its Hardware Implementation, Pattern Recognition Letters Journal 1994, Vol. 15, No. 2, pp. 141-150.
- YANG, Y., YAN, H. (2000): An adaptive logical method for binarization of pavement images, Pattern Recognition Journal, Pattern Recognition Society, Elsevier Science, Vol. 33, Issue 5, May, pp. 787-807.
- YANOWITZ, D.L, BRUCKSTEIN, A.M (1989): A new Method for image segmentation, Computer Vision Graphics and Image Processing Journal, 1989, Vol.46, No. 1, pp. 82-95.
- YING, L., SALARI, E. (2009): Beamlet Transform Based Technique for Pavement Image Processing and Classification, Master thesis at Department of Electrical Engineering and Computer Science, University of Toledo, Toledo, Ohio 43606.
- YOUNG, S.K, CARL, T.H (2002): A man-machine balanced rapid object model for automation of pavement crack sealing and maintenance, Canadian Journal of Civil Engineering., doi:10.1139/l02-018 | © 2002 NRC. Vol. 29, No. 3, pp. 522-542.
- YUJIE, H., ROBERT, A.W. (1990): An efficient and fast parallel-connected component algorithm. J. ACM. IEEE Transactions on Pattern Analysis and Machine Intelligence Journal, November, Vol. 22, No. 2, pp. 1300-1325.



YU, S-J (2005): Digitizing and 3D Modeling of Road Surface using an Integrated Multisensory Approach. Project in Lieu of Thesis presented for the Masters of Science Degree, university of Tennessee, Knoxville, November.

YU, S.J, SUKUMAR, S.R, KOSCHAN, A.F., PAGE, D.L., ABIDI, M.A (2007): 3D Reconstruction of Road Surfaces Using an Integrated Multi-Sensory Approach. Opt. Laser. Engineering Journal, Vol. 45, No.2, pp. 808-828.

ZHOU, J., HUANG, P., CHIANG, S.F. (2003): Wavelet-aided pavement distress image processing, Wavelets: Applications in Signal and Image Processing X. Proceedings of the SPIE, pp. 728-73



## Appendix A: Introducing overview of Pavement Distress Data Capturing Systems being used worldwide

No	Company/Institution	System	Equipments	Web-link/Reference
1	ARRB Group 'Australian Road Research Board'	Network Survey Vehicles (NSV)	GPS ( DGPS); Digital Laser Profiler; Digital Imaging System; GIPSI-Track geometry; Rotorpulser Data Acquisition system	<a href="http://www.arrb.com.au/Equipment-services/Hawkeye-2000-Series.aspx">http://www.arrb.com.au/Equipment-services/Hawkeye-2000-Series.aspx</a>
2	CSIRO's crack tracker	CSIRO's System	Series of line scan camera; GNSS; Lighting system	<a href="http://www.csiro.au/promos/ozadvances/Series3CrackMovB.html">http://www.csiro.au/promos/ozadvances/Series3CrackMovB.html</a>
3	3D Mapping Solutions GmbH, Munich, Germany	Mobiles Strassen-Erfassungs-System (MoSES)	3D Mapping multi camera module; powerful high performance laser scanners; GNSS	<a href="http://www.3d-mapping.de/dynasite.cfm?dssid=4324">http://www.3d-mapping.de/dynasite.cfm?dssid=4324</a>
4	Eagle Eye Technologies, Hamburg, Germany	Eagle Eye Technologies MMS	Stereo camera; GPS; INS; Georader (X-ray)	<a href="http://www.ee-t.de">http://www.ee-t.de</a>
5	EarthEye, Orlando, Florida (USA)	EarthEye's Mobile Asset Collection (MAC) Vehicle	Mobile LiDAR Solutions; GNSS	<a href="http://www.eartheye.com/Services/Mobile">http://www.eartheye.com/Services/Mobile</a>
6	Earth Technology Corporation, Canada	Pavement Condition Evaluation Services (PCES)	Line scan camera; GNSS	<a href="http://www.earthcanada.com/">http://www.earthcanada.com/</a>
7	GeoAutomation company, Belgium	GeoAutomation™ MMS Van (Image-based mobile mapping)	Set of cameras; GNSS	<a href="http://www.geoautomation.com/">http://www.geoautomation.com/</a>
8	GeoVISAT company, Belgium	VISAT™ MMS Van	GPS; INS; DMI; panoramic cameras	<a href="http://www.geovisat.eu">http://www.geovisat.eu</a>
9	G.I.E. Technology, Canada	LaserVision System	Laser; camera; GNSS	<a href="http://www.gietech.com/LVS">http://www.gietech.com/LVS</a>
10	GIE Technology, Inc.	LaserVersion System	Laser; DGPS; camera	<a href="http://www.gietech.com/LVS">http://www.gietech.com/LVS</a>
11	GISPRO mapping company, Szczecin, Poland	UltraCammapping system	Digital aerial camera system; GNSS	<a href="http://www.microsoft.com/ultracam/en-us/AUG10Gispro.aspx">http://www.microsoft.com/ultracam/en-us/AUG10Gispro.aspx</a>

No	Company/Institution	System	Equipments	Web-link/Reference
12	Infrastructure Management Services (IMS), Swiss	PAVUE System	Video camera; video cassette recorders; GNSS	<a href="http://www.imsrst.com">http://www.imsrst.com</a>
13	International Cybernetics Corporation	Digital Imaging System	Progressive Scan CCD camera; GPS; IMU; inclination odometer; barometer	<a href="http://www.internationalcybernetics.com/imagingvehicle.html">http://www.internationalcybernetics.com/imagingvehicle.html</a>
14	Komatsu, Japan	Komatsu System	2D laser; video camera with special light system; GPS	RUKUHARA ET AL. (1990)
15	Lambda Tech. International, Fort Wayne, USA	GPSVision™ MMS	GPS; INS; four high-speed digital color stereo cameras	<a href="http://www.lambdatech.com/">http://www.lambdatech.com/</a>
16	Lehmann+Partner GmbH company	S.T.I.E.R Mobile Mapper System	Laser scanner, Fraunhofer (IPM); surface cameras; panorama cameras; Applanix POS LV; lighting Unit; GNSS	<a href="http://www.ipm.fraunhofer.de">http://www.ipm.fraunhofer.de</a> . <a href="http://www.vvertragermany.com/system-stier">http://www.vvertragermany.com/system-stier</a>
17	Mandli Communications, Inc., Madison, Wisconsin	Pavement Scanner Profile System (PPS) [roadview]	Laser; Camera; GPS	<a href="http://www.mandli.com/systems">http://www.mandli.com/systems</a>
18	National Optics Institute, Canada	Road Inspection System	Laser; GNSS	LAURENT ET AL. (1997)
19	Omnicom Engineering, York, U.K.	OmniInspector System	Camera; GPS	<a href="http://www.omnieng.co.uk/index.php?id=47">http://www.omnieng.co.uk/index.php?id=47,</a>
20	Pathway Services, Inc.	Pathrunner Video inspection vehicle (VIV)	Pathrunner: camera; GPS; (VIV): 5 LASERS+4 cameras	<a href="http://www.pathwayservices.com">http://www.pathwayservices.com</a>
21	Road Radar Ltd., Canada	Road Radar system™	GPS; Ground Penetrating Radar; video camera	<a href="http://www.rrl.com">www.rrl.com</a>
22	Roadware Group, Inc.	Automatic Road Analyzer (ARAN); Canada	Video camera; Laser SDP; Laser XVP; 2 or more CCD; GPS; IMU; accelerometers	<a href="http://www.roadware.com">http://www.roadware.com</a>

No	Company/Institution	System	Equipments	Web-link/Reference
23	'ROMDAS' (ROad Measurement Data Acquisition System) Data Collection Ltd. (DCL), New Zealand	ROMDAS® (Road Measurement Data Acquisition System)	GPS; digital video camera; Laser crack measurement system; Laser rutting measurement system; Laser profilometers (IRI)	<a href="http://www.romdas.com">http://www.romdas.com</a>
24	Siteco -company incorporated with Parma university and Bologna university; Italy	Road-Scanner System	2 GPS; IMU; Laser Scanner Faro; LS880	<a href="http://www.sparpointgroup.com">http://www.sparpointgroup.com</a> .
25	Surface Engineer and Software, Inc. (SES)	Road Surface Analyzers (ROSAN)	Laser; accelerometer; GNSS	GERARDO ET AL. (2004)
26	Swiss Federal Institute of Technology (EPFL)	Crack Recognition Holographic System (CREHOS)	Laser; GNSS	MOTWANI ET AL. (2004)
27	Transmap Corporation, Columbus, Ohio and Tampa, Florida (USA)	ON-SIGHT™ van	GPS; IMU; DMI; 4 or more digital color CCD cameras; Sick LiDAR scanner	<a href="http://www.transmap.com/?page_id=1312">http://www.transmap.com/?page_id=1312</a>
28	Triple Vision.	National Cooperative Highway Research Program (NCHRP)	Camera; GNSS	FUNDAKOWSKI ET AL. (1991)
29	University of California	Automated Road Inspection System	Camera with special light system; GNSS	<a href="http://shino8.eng.uci.edu/AMPIS.html">http://shino8.eng.uci.edu/AMPIS.html</a>
30	WayLink Systems Corporation	Digital Highway Vehicle	Camera; GPS; gyroscope	<a href="http://www.waylink.com">http://www.waylink.com</a>

## Appendix B: Overview of Some Case Studies

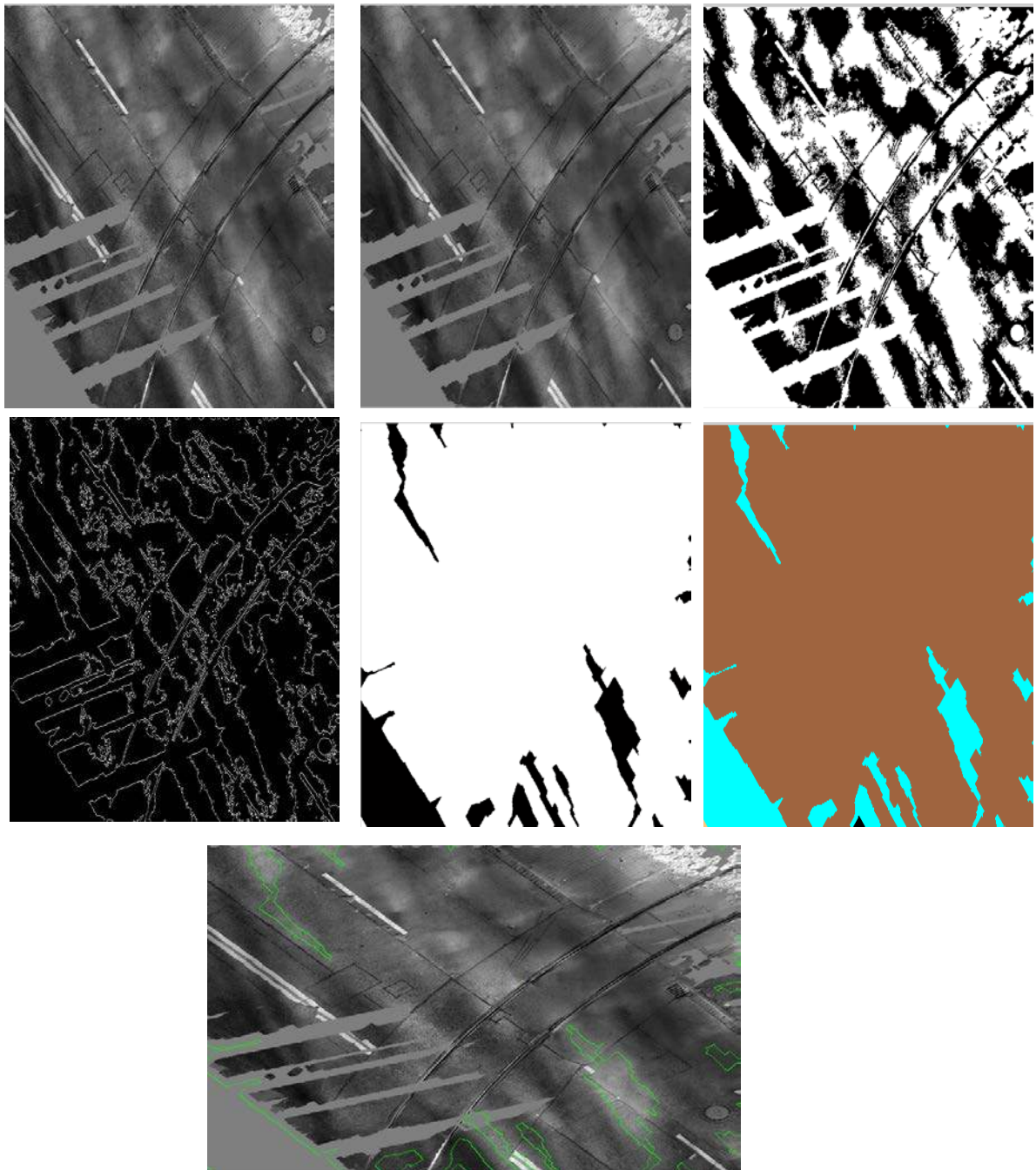


Figure B.1: Behaviour of all the overall algorithms of this thesis to ignore railways, sidewalks, manholes and lane markings within an image; 1<sup>st</sup> line: 3D-Mapping Solution original image (left), the image after applying image enhancement stage (middle), the image after applying adaptive local threshold algorithm (right); 2<sup>nd</sup> line: image after applying sobel edge detector (left), the image after applying hole pixel initial algorithm including several times of dilation process (middle), the image after applying labelling connected components algorithm (right); 3<sup>rd</sup> line-right: the final contouring image without an ellipse.

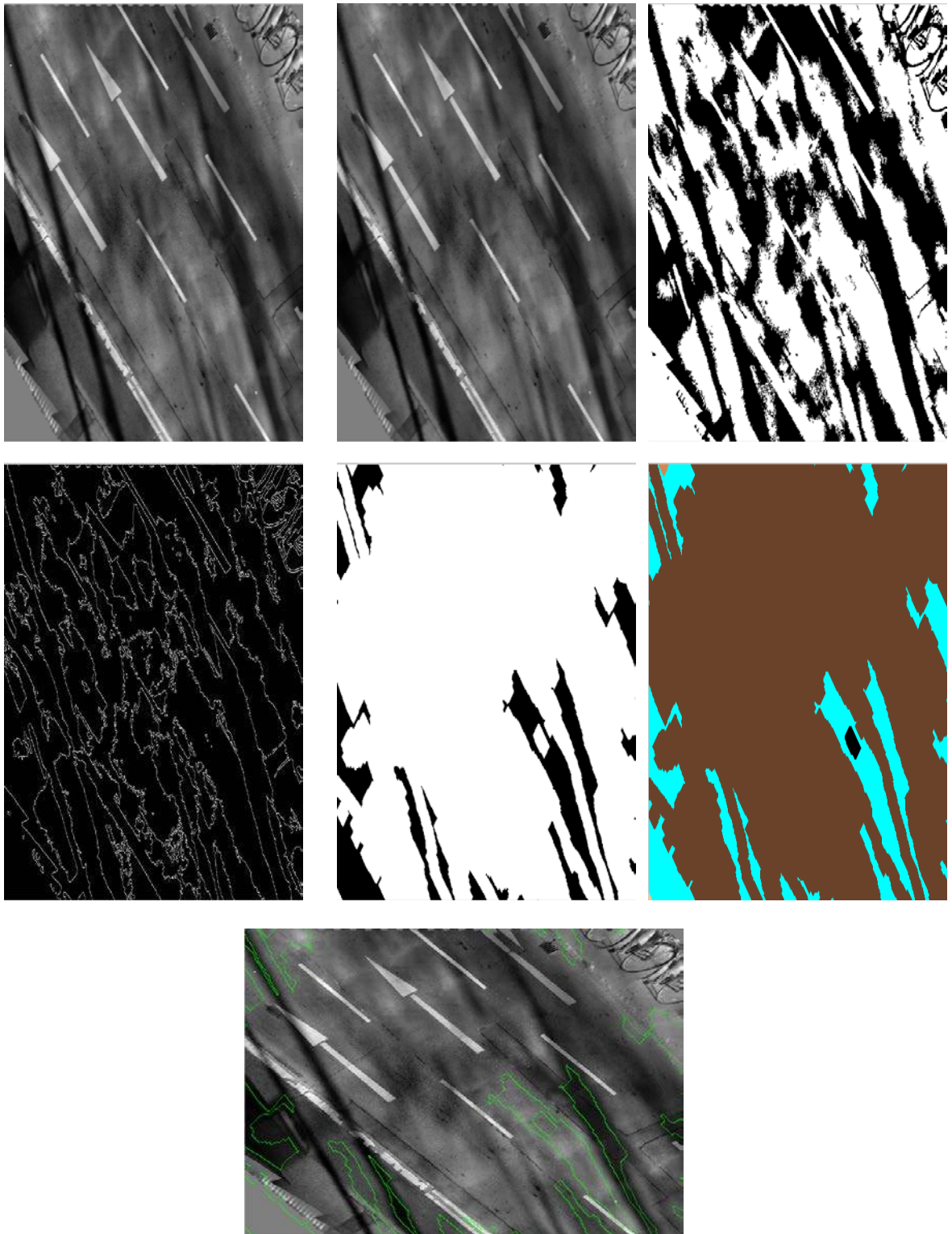


Figure B.2: Behaviour of all the overall algorithms of this thesis to ignore sidewalks, shades of road traffic, shadows and lane markings within an image; 1<sup>st</sup> line: 3D-Mapping Solution original image (left), the image after applying image enhancement stage (middle), the image after applying adaptive local threshold algorithm (right); 2<sup>nd</sup> line: image after applying sobel edge detector (left), the image after applying hole pixel initial algorithm including several times of dilation process (middle), the image after applying labelling connected components algorithm (right); 3<sup>rd</sup> line-right: the final contouring image without an ellipse.

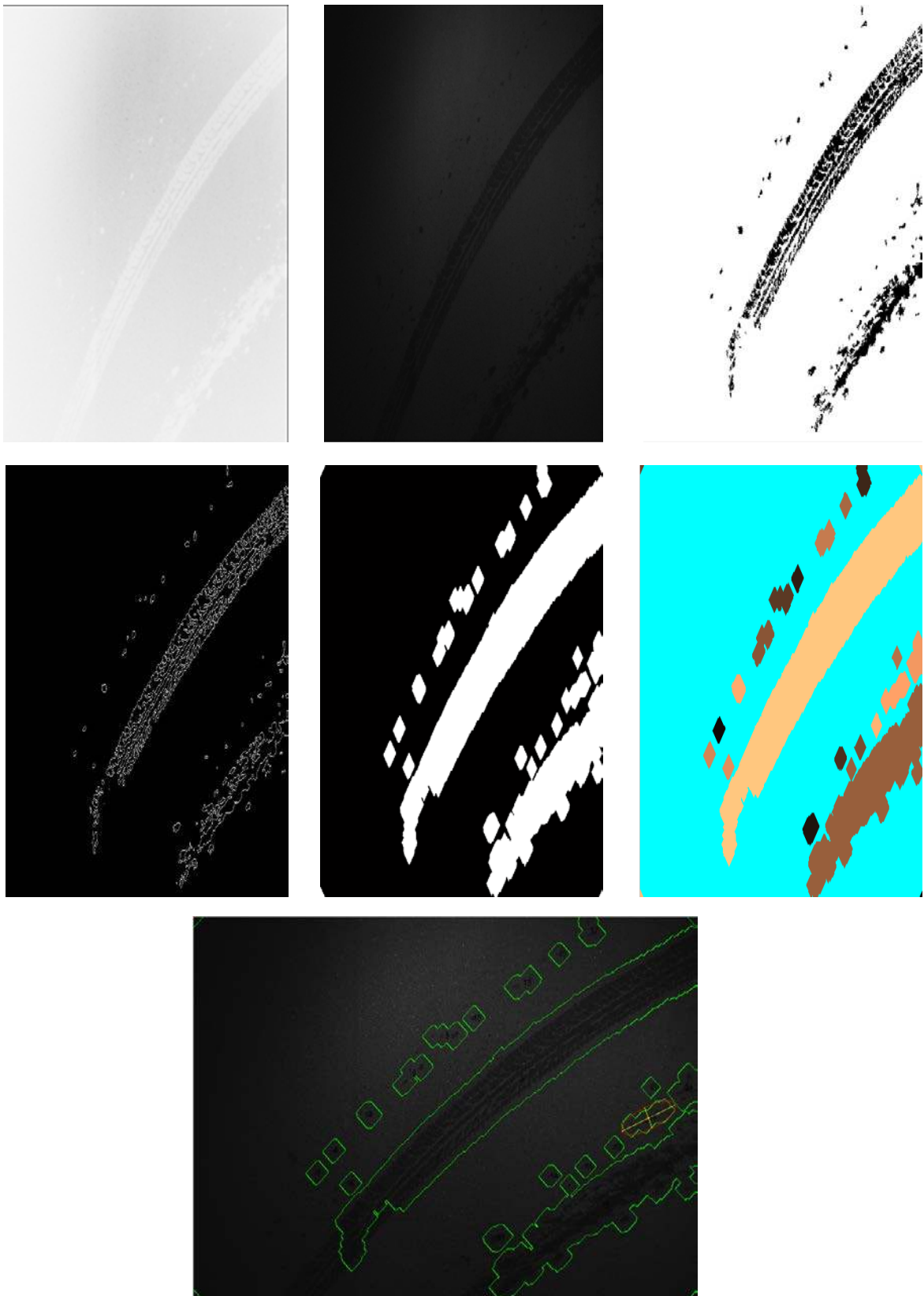


Figure B.3: Behaviour of all the overall algorithms of this thesis fails to delete small narrow spot oil within an image; 1<sup>st</sup> line: (LAHMANN+PARTNER) original image (inverted illustration)(left), the image after applying image enhancement stage (middle), the image after applying adaptive local threshold algorithm (right); 2<sup>nd</sup> line: image after applying sobel edge detector (left), the image after applying hole pixel initial algorithm including several times of dilation process (middle), the image after applying labelling connected components algorithm (right); 3<sup>rd</sup> line-right: the final contouring image with drawn ellipse inside it as a false detection.



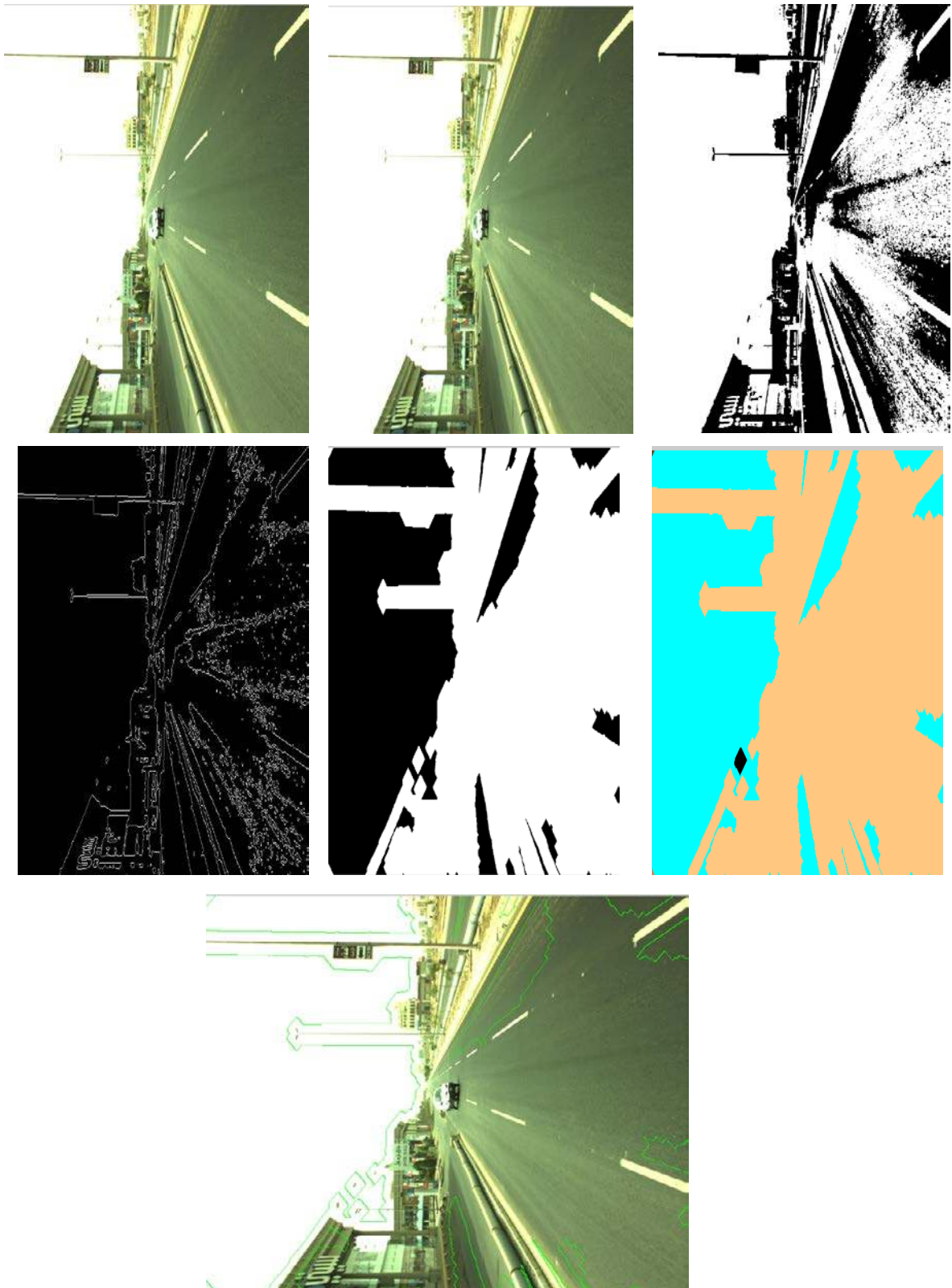


Figure B.4: Behaviour of all the overall algorithms of this thesis to ignore lane markings, sidewalks, and other extrinsic objects within an image; 1<sup>st</sup> line: Unicom-Umap original image of king Fahd Street (left), the image after applying image enhancement stage (middle), the image after applying adaptive local threshold algorithm (right); 2<sup>nd</sup> line: image after applying sobel edge detector (left), the image after applying hole pixel initial algorithm including several times of dilation process (middle), the image after applying labelling connected components algorithm (right); 3<sup>st</sup> line-right: the final contouring image without an ellipse.

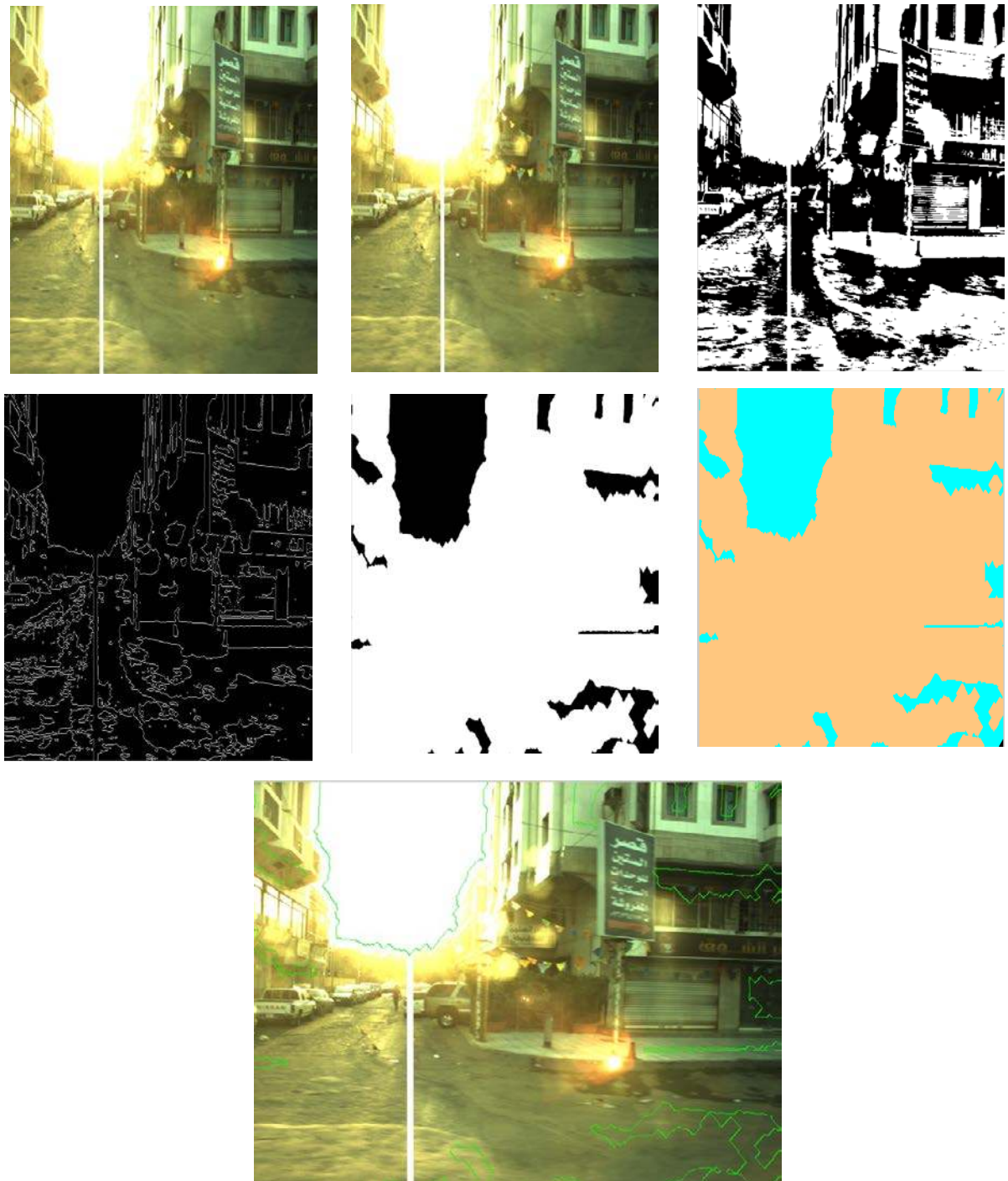


Figure B.5: Behaviour of all the overall algorithms of this thesis to ignore shades (different light conditions and different pavement textures(escape of binder)), sidewalk (curbs) and extrinsic objects such as buildings, and traffic within an image; 1<sup>st</sup> line: Unicom-Umap original image of Muktar street (left), the image after applying image enhancement stage (middle), the image after applying adaptive local threshold algorithm (right); 2<sup>nd</sup> line: image after applying sobel edge detector (left), the image after applying hole pixel initial algorithm including several times of dilation process (middle), the image after applying labelling connected components algorithm (right); 3<sup>rd</sup> line-right: the final contouring image without an ellipse.

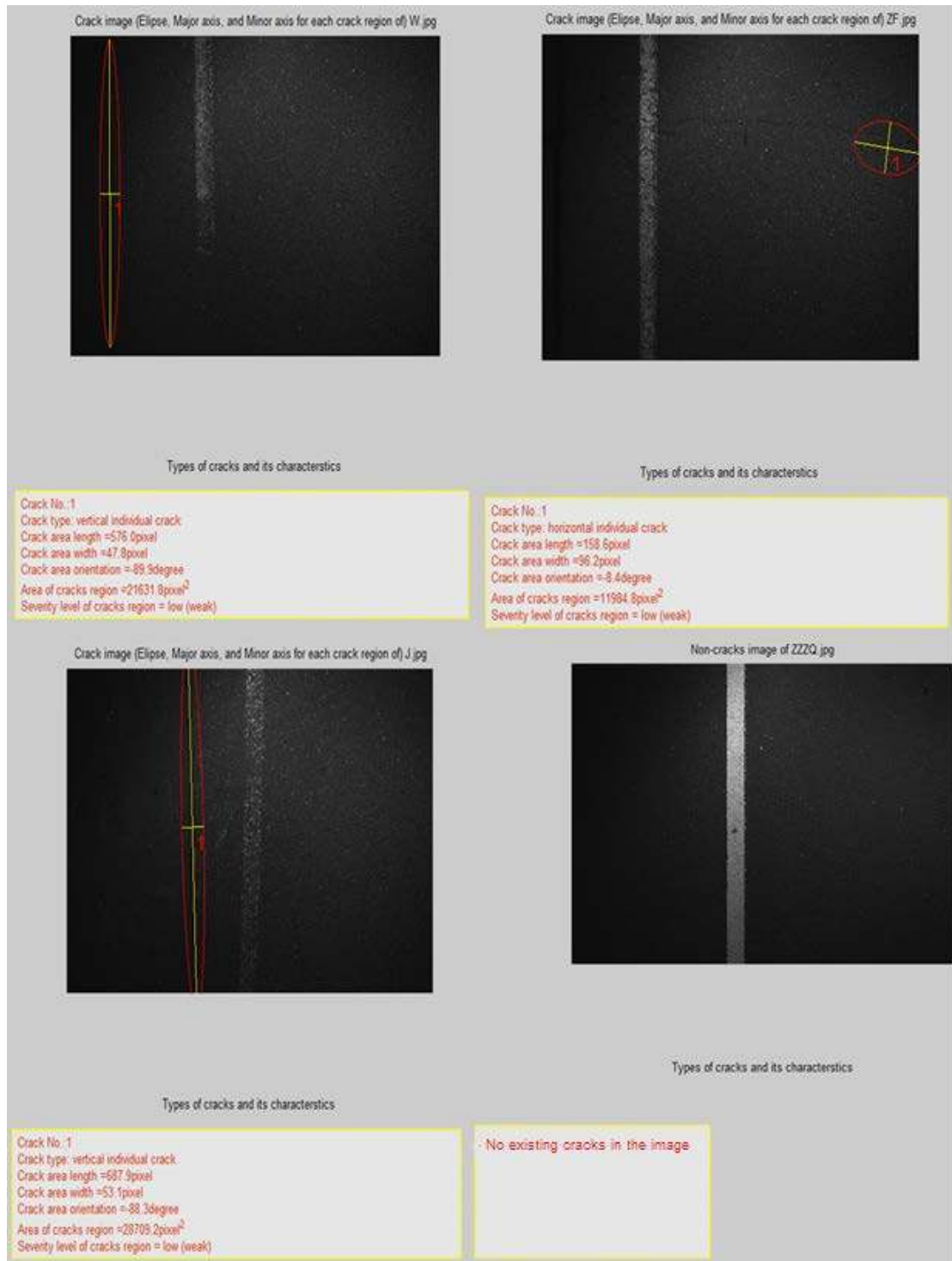


Figure B.6: Example of the interface for a sample of sequence images with cracks and the resulting classification (case study 1).

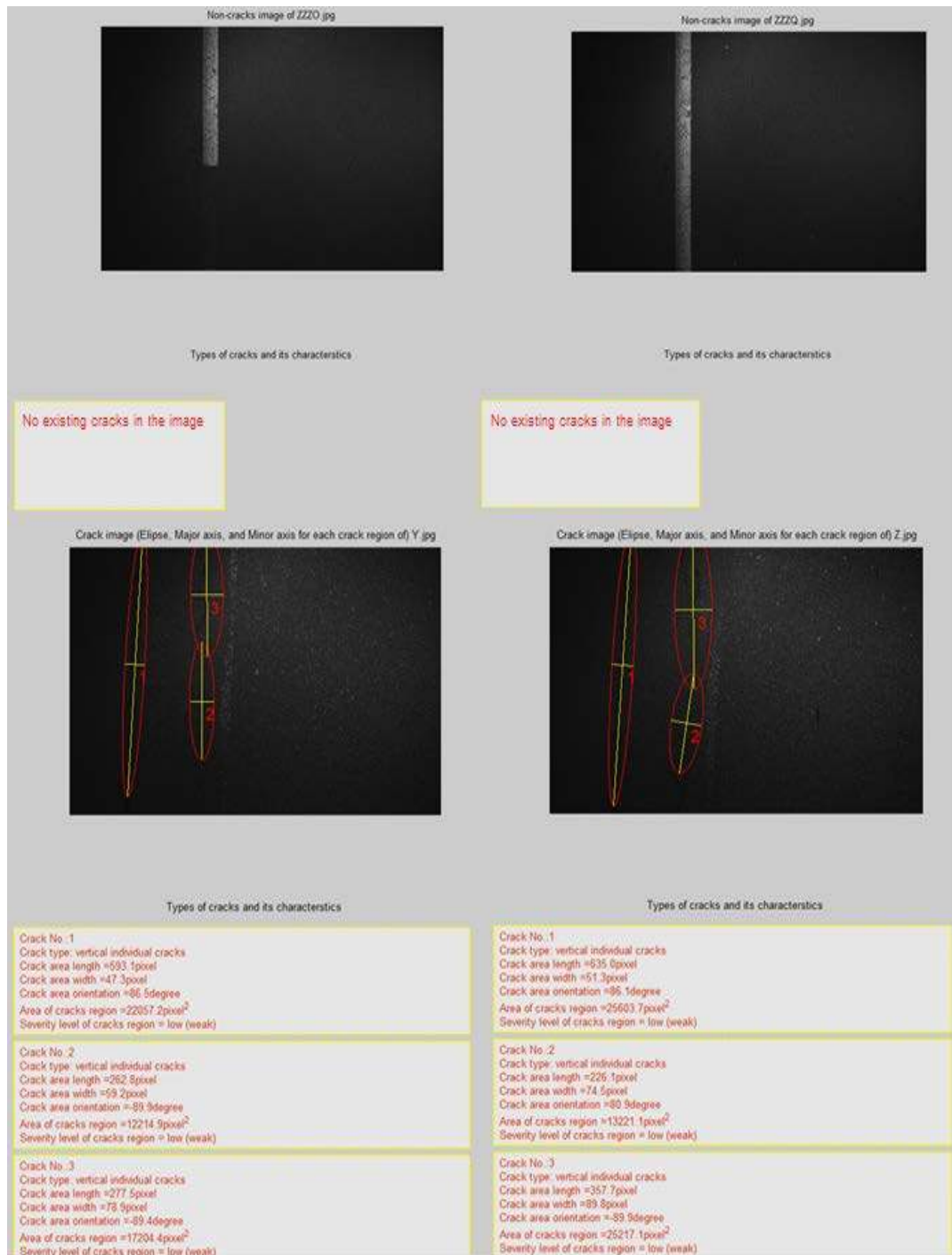


Figure B.7: An example of the interface for a sample of image sequences with cracks, and their classification (case study 2).

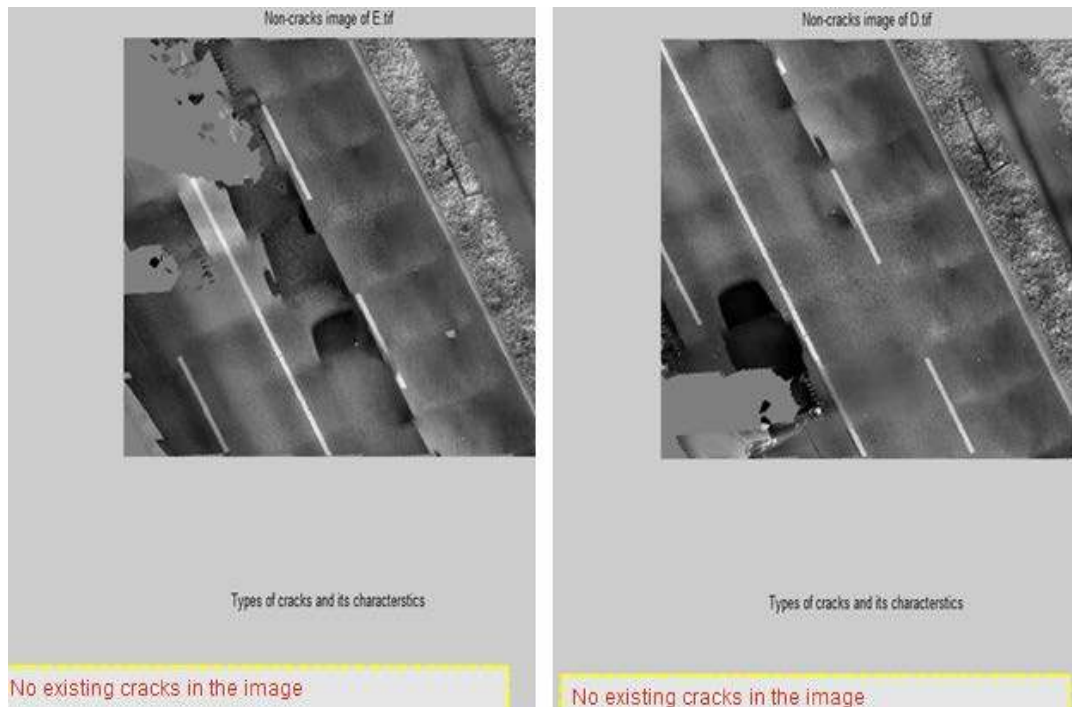


Figure B.8: An example of the interface for a sample of image sequences without cracks, and their classification (case study 5).



Figure B.9: A sample of false detection (second type of error) in case study (2).



Figure B.10: A sample of a false detection (second type of error) for case study (3).



Figure B.11: An example of a false detection (second type of error) for case study (4).

## Appendix C: Some Comparative studies for Performance Evaluation

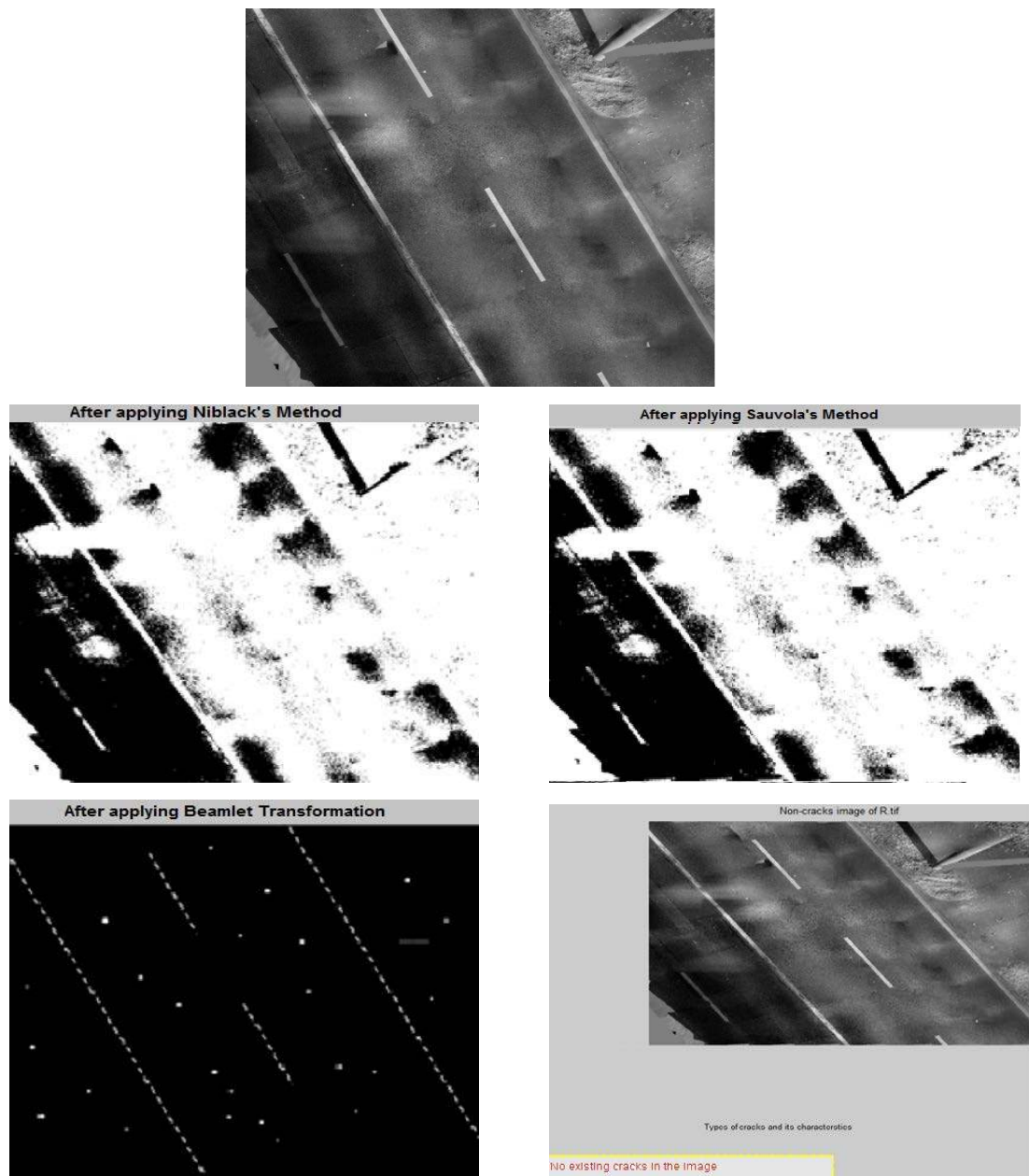


Figure C.1: Comparative study between the algorithm of this thesis and other methods; 1<sup>st</sup> line: 3D-Mapping Solution original image ; 2<sup>nd</sup> line: the image after applying Niblack's method (left), the image after applying Sauvola's method (right); 3<sup>rd</sup> line: the image after applying Beamlet transformation method (left), the image after applying the algorithm of this thesis (right).

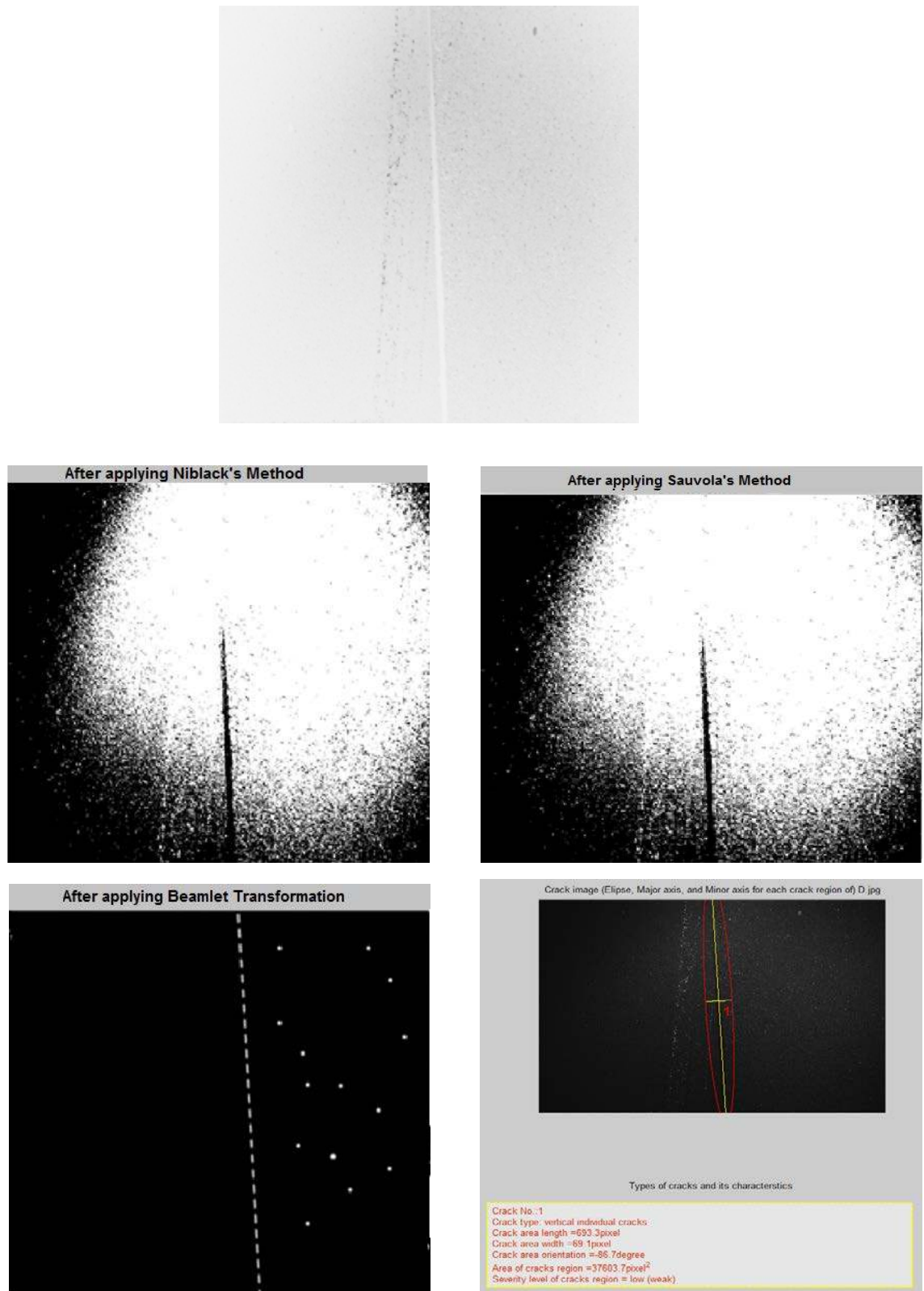


Figure C.2: Comparative study between the algorithm of this thesis and other methods; 1<sup>st</sup> line: LEH-MANN+PARTNER original image (inverted illustration); 2<sup>nd</sup> line: explains the image after applying Niblack's method (left), the image after applying Sauvola's method (right); 3<sup>rd</sup> line: the image after applying Beamlet transformation method (left), the image after applying the algorithm of this thesis (right).



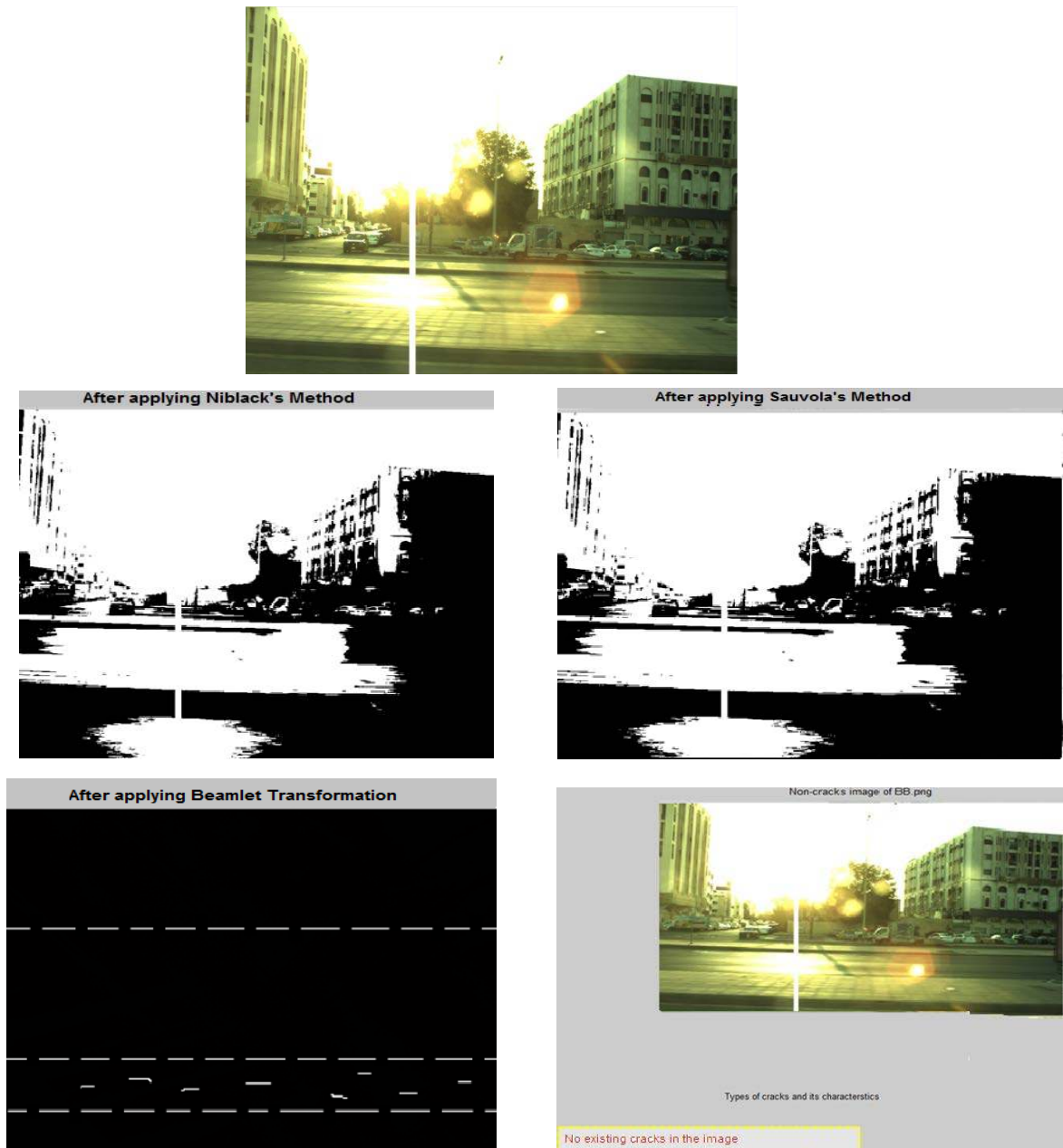


Figure C.3: Comparative study between the algorithm of this thesis and other methods; 1<sup>st</sup> line: Unicom-Umap of original image (King Fahd street) ; 2<sup>nd</sup> line: the image after applying Niblack's method (left), the image after applying Sauvola's method (right); 3<sup>rd</sup> line: the image after applying Beamlet transformation method (left), the image after applying the algorithm of this thesis (right).

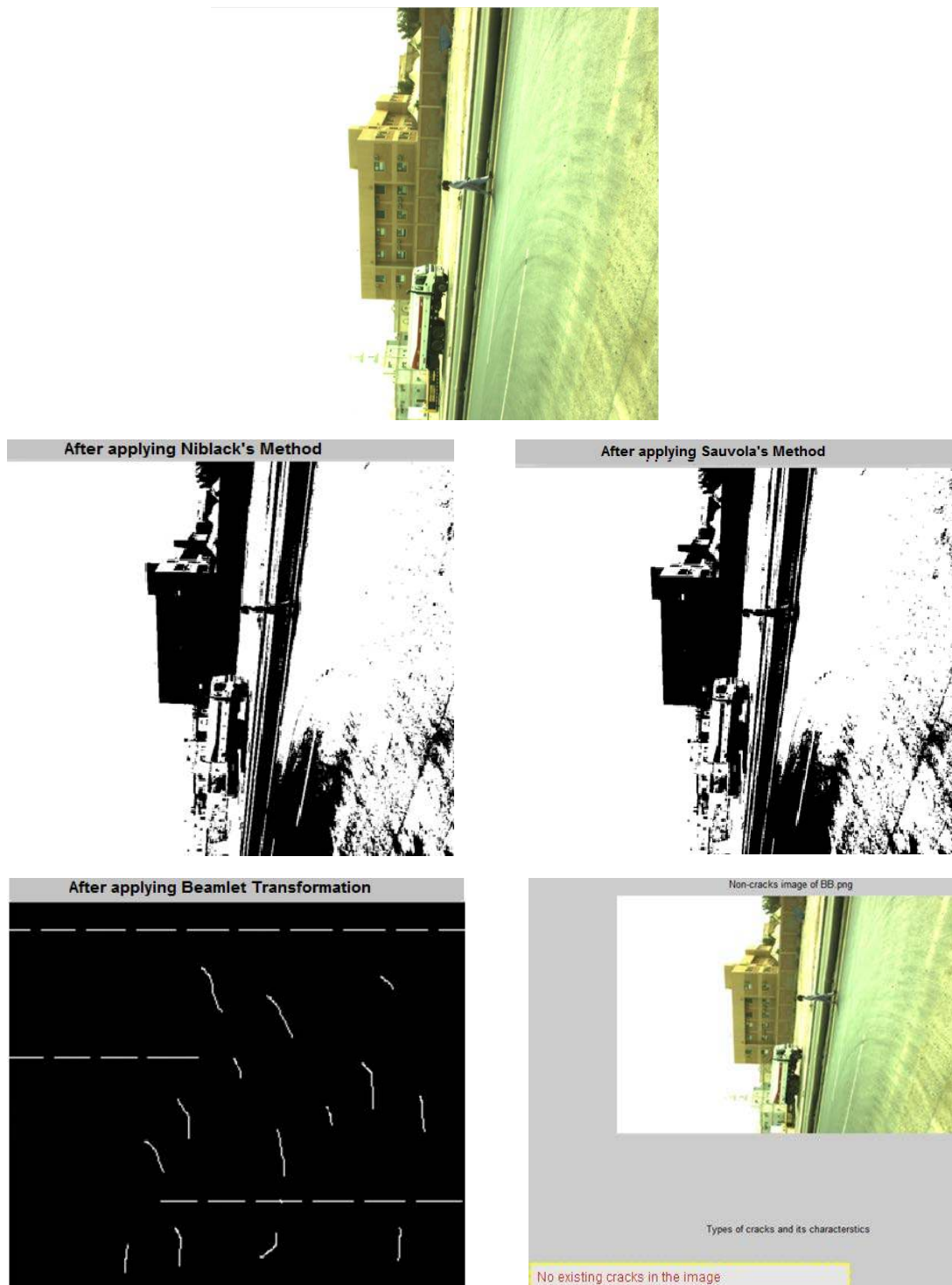


Figure C.4: Comparative study between the algorithm of this thesis and other methods; 1<sup>st</sup> line: Uni-com-Umap of original image (King Fahd street) ; 2<sup>nd</sup> line: the image after applying Niblack's method (left), the image after applying Sauvola's method (right); 3<sup>rd</sup> line: the image after applying Beamlet transformation method (left), the image after applying the algorithm of this thesis (right).

## Acknowledgements

On the completion of this dissertation, I feel highly excited to express my gratitude to all those who have inspired, encouraged, guided me in preparing and presenting my research work.

First of all I would like to thank Allah, for all gifts and blessings I have and for giving me the ability and the courage to proceed and finish my work. I take the opportunity and honour to express my deep sense of gratitude to my supervisor, Prof. Volker Schwieger, Institute of Engineering Geodesy (IIGS), Stuttgart. I am deeply indebted for his immeasurable guidance and help throughout the tenure of this work. He has been subtle meticulous in correcting and improving the standard issues in those critical moments when I could possibly deflect and deviate. He not only gave me his able, experienced and scholarly guidance but also sanctified my liberty in the treatment of the subject. I am deeply indebted to him for his immense patience with the invaluable suggestions he made without which this work would not have come to this shape. My sincere thanks are extended to PD Dr.-Ing. Alexander Reiterer, my co-advisor, and Prof. Dr.-Ing. habil. Dieter Fritsch for their interest in my work. I would like to convey my heartfelt thanks to Mr. Dirk Ebersbach, for his cooperation.

I owe special thanks to all IIGS (Institute of Engineering Geodesy) members, especially Dipl.-Ing. Annette Scheider for her friendship, her scientific help in solving different programming issues which absolutely had an effect on my study.

I would like to convey my gratitude to my colleagues: Ashraf Abdallah for his brotherhood, his friendship and persistent help during the entire time of my stay at the IIGS, and Dr.-Ing. Martin Metzner for his kindness and encouragement.

Also I would like to express my gratitude to my great father (God bless his soul), my loving mother, my loving husband (Dr. Ali K.Qtaishat) for his immense patience and his moral and financial support, my small daughter (Mna), my small baby (Khaled) whose consistent encouragement and support was always pushing me ahead and giving me enthusiasm.

Last but not the least, I would like to express my warmest gratitude to my husband's father, my husband's mother and Attorney at Law Naji K Quteishat for their encouragement and immense cooperation. And I like to thank my dear siblings (Dr. ALaa, Dr. Mohammed, Dooa, Dr. Abed el-hameed,) for their inspiration and encouragement.

Stuttgart, November 2015

Bara' Al-Mistarehi



---

## Curriculum Vita

### Personal Information:

Name: Bara Wasfi Al-Mistarehi

Date of birth: January 26, 1984

Place of birth: Irbid, Jordan

Nationality: Jordanian

Marital status: married

### Education:

Since 10/2011: doctoral candidate and research associate at the Institute of Engineering Geodesy (IIGS), University of Stuttgart, Germany

10/2007 – 10/2009: M. Sc. in Highway and Transportation Engineering, Jordan University of Science and Technology (JUST), Jordan

2002 – 2007: B. Sc. in Civil Engineering / Highway and Transportation, Jordan University of Science and Technology (JUST), Irbid, Jordan

2001 – 2002: High school education / scientific section, Irbid, Jordan